PrP^{Sc} complexity in different forms of Creutzfeldt-Jakob disease identified using biochemical approaches

Young Pyo Choi

Doctor of Philosophy
University of Edinburgh
2010

Declaration

I declare that this thesis has been composed by myself and that the work presented herein is my own, except where otherwise stated. No part of this thesis has been, or will be, submitted for any other degree or professional qualification.

Young Pyo Choi

2010

Acknowledgements

I would like to express my sincere thanks to my supervisors Dr. Mark Head and Professor James Ironside for their support and guidance. Thanks to Drs. Alex Peden and Lynne McGuire for their advice and comments during thesis preparation. Thanks to Linda McCardle for her assistance in neuropathology. Thanks to Mags Le Grice and Suzzane Lowrie for preparing tissue sections for neuropathological analysis. Thanks to Dr. Alex Peden for labelling europium to antibody 3F4.

Abstract

Transmissible spongiform encephalopathies (TSEs) or prion diseases are a group of fatal neurodegenerative diseases affecting humans and animal species. Prion diseases are characterized by the conversion of the host encoded prion protein (PrP^{C}) into a disease-associated isoform (PrP^{Sc}), which (according to the prion hypothesis) is thought to be the main component of the infectious agent. PrP^{Sc} has been traditionally distinguished from PrP^{C} by its biochemical properties, such as partial resistance to proteolysis and detergent-insolubility. In the absence of a foreign nucleic acid genome associated with prion diseases, efforts to provide a molecular basis for the biological diversity of prions have focused on biochemical characterization of PrP^{Sc}. In Creutzfeldt-Jakob disease (CJD) and other forms of human prion disease, the biochemical characterization of PrP^{Sc} has been largely restricted to the analysis of PK-resistant fragments of PrP^{Sc} (PrP^{res}) by Western blot. However, given recent findings on the complexity of PrP^{Sc} identified in laboratory prion strains, PrP^{res} analysis alone may not provide a complete description of PrP^{Sc} present in CJD brains. For a more complete characterization of PrP^{Sc} in human prion diseases, this study investigated biochemical properties of PrP^{Sc} in different forms of CJD by employing approaches that differ in principle from conventional Western blot analysis of PrP^{res}. The novel biochemical approaches used in this study have identified further complexity of PrP^{Sc} accumulated in CJD brains, not only between different forms of CJD but also within single cases of individual disease entities. In this study, the two biochemical criteria most frequently used to define PrP^{Sc} (3F4 epitope accessibility *versus* resistance to limited proteolysis) did not always correlate, indicating probable non-uniform distribution of PK-sensitive isoform of PrP^{Sc} within the same CJD brains. In variant CJD (vCJD) brains, the thalamic region, which is characterized by distinct neuropathological features, could also be distinguished from frontal cortex and cerebellum by the sedimentation profiles of PrP^{C} and PrP^{Sc} on sucrose step gradients. Moreover, the conformational stability of PrP^{Sc} was found not to be uniform among human prion diseases and did not correlate with PrP^{res} type or

prion protein genotype. Taken together, the results from this study provide a more complete description of PrP^{Sc} species occurring in CJD brains and contribute to a fuller understanding of the agents and the disease processes involved in humans.

Abbreviations

A117V	Alanine (A) to valine (V) mutation at *PRNP* codon 117
ACDP	Advisory committee on dangerous pathogens
BASE	Bovine amyloidotic spongiform encephalopathy
BSA	Bovine serum albumin
BSE	Bovine spongiform encephalopathy
Cb	Cerebellum
CD	Circular dichroism
CDI	Conformation-dependent immunoassay
CJD	Creutzfeldt-Jakob disease
CNS	Central nervous system
cps	counts per second
CSA	Conformation stability assay
CWD	Chronic wasting disease
cyPrP	PrP that is localized in the cytosol as a result of inefficient translocation into the endoplasmic reticulum
^{ctm}PrP	a transmembrane form of PrP in which central hydrophobic domain spans the membrane with its N-terminus exposed to the cytosol
D178N	Aspartic acid (D) to asparagine (N) mutation at *PRNP* codon 178
E200K	Glutamic acid (E) to lysine (K) mutation at *PRNP* codon 200
E219K	Glutamic acid (E) to lysine (K) mutation at *PRNP* codon 219
ELISA	Enzyme-linked immunosorbent assay
ER	Endoplasmic reticulum
F198S	Phenylalanine (F) to serine (S) mutation at *PRNP* codon 198
FC	Frontal cortex
fCJD	Familial Creutzfeldt-Jakob disease
FFI	Fatal familial insomnia
FTIR	Fourier transform infrared spectroscopy
GABA	Gamma-aminobutyric acid
GdnHCl	Guanidine hydrochloride
GPI	Glycosylphosphatidylinositol
GSS	Gerstmann-Straussler-Scheinker Disease
iCJD	Iatrogenic Creutzfeldt-Jakob disease
kDa	Kilo Dalton
LDS	Lithium dodecyl sulfate
mAb	monoclonal antibody
MM	Methionine homozygote at *PRNP* codon 129
MM1	MM1 subtype of sporadic CJD
MM2	MM2 subtype of sporadic CJD
MRI	Magnetic resonance imaging (MRI)
MV	Methionine/Valine heterozygote at *PRNP* codon 129
MV1	MV1 subtype of sporadic CJD

MV2	MV2 subtype of sporadic CJD
NaPTA	Sodium phosphotungstic acid
NCJDSU	National CJD Surveillance Unit
NMR	Nuclear magnetic resonance
NOG	n-octyl-β-D-glucopyranoside
OD	Optical density
ORF	Open reading frame
P102L	Proline (P) to leucine (L) mutation at *PRNP* codon 102
P105L	Proline (P) to leucine (L) mutation at *PRNP* codon 105
PBS	Phosphate buffered saline
PIPLC	Phosphatidylinositol-specific phospholipase C
PMCA	Protein misfolding cyclic amplification
PMI	Post mortem interval
PK	Proteinase K
PRNP	Human prion protein gene
PrP	prion protein
PrP^{c}	Normal cellular form of prion protein
PrP^{res}	Protease-resistant prion protein
PrP^{Sc}	Disease-associated form of prion protein
PSPr	Protease-sensitive prionopathy
PVDF	Polyvinylidene fluoride
rpm	Revolutions per minute
sCJD	Sporadic Creutzfeldt-Jakob disease
sFI	Sporadic fatal insomnia
T183A	Theronine (T) to alanine (A) mutation at *PRNP* codon 183
TBS	Tris buffered saline
TBST	Tris buffered saline + 0.1% Tween 20
Th	Thalamus
TME	Transmissible mink encephalopathy
TRF	Time-resolved fluorescence
TSE	Transmissible spongiform encephalopathy
UK	United Kingdom
vCJD	Variant Creutzfeldt-Jakob disease
V180I	Valine (P) to isoleucine (L) mutation at *PRNP* codon 180
V210I	Valine (P) to isoleucine (L) mutation at *PRNP* codon 210
VV	Valine homozygote at *PRNP* codon 129
VV2	VV2 subtype of sporadic CJD
WB	Western blot
Y145TOP	Stop mutation causing termination of *PRNP* translation at codon 145 tyrosine

Table of contents

Declaration ……ii

Acknowledgements……iii

Abstract……iv

Abbreviations……vi

Table of contents……viii

List of figures……xiv

List of tables……xvii

Chapter 1

General introduction……1

1.1 Overview……2

1.2 Prion protein gene……3

1.3 Prion protein……6

1.3.1 Cellular prion protein (PrP^{C}) ……6

1.3.2 Disease-associated prion protein (PrP^{Sc}) ……8

1.3.3 Two models describing the self-propagation of PrP^{Sc} ……10

1.4 Strain variation in prion diseases……11

1.5 Biochemical analysis of PrP^{Sc} for prion strain/phenotype discrimination……13

1.5.1 TME prion strains……13

1.5.2 Human prion diseases……14

1.5.3 BSE in cattle and other species ……16

1.5.4 Atypical/Nor98 scrapie in small ruminants……17

1.5.5 Atypical bovine prion diseases……17

1.6 Human prion diseases……19

1.6.1 Sporadic prion disease: sCJD and sFI……20

1.6.2 Variant CJD……25

1.6.3 Other forms of acquired human prion disease: Kuru and iCJD ……27

1.6.4 Familial (genetic) forms of human prion disease……28

1.7 Complicated biochemical properties of PrP^{Sc}……32

1.7.1 PK-sensitive isoform of PrP^{Sc}……32

1.7.2 Various sizes of PrP^{Sc}……..…..……...……..…..…….....34
1.7.3 Conformational stability of PrP^{Sc}……..…..……...……..…….....35
1.8 Biochemical approaches for PrP^{Sc} analysis.....….…..…….....37
1.9 Aims.....…….…..……..…..…….....,.40

Chapter 2

Abnormal prion protein in CJD brains: comparison of a conformation change with resistance to limited proteolysis.....…….…….....41
2.1 Introduction…...……..…...…....……..…..…….....42
2.2 Materials and methods..…..…...……....…..…..……....44
2.2.1 Laboratory requirement in handling human TSE material.....….....44
2.2.2 Human brain materials……..…..….....….....44
2.2.2.1 Case selection criteria.....…..…….....44
2.2.2.2 Case details.....……..…..…….....45
2.2.2.3 Brain samples for analysis.....…..…….....46
2.2.3 Methods ……..……..……..…….....…..……..….....51
2.2.3.1 Conformation-dependent immunoassay (CDI).....51
2.2.3.1.1 History and methodological speculation.....51
2.2.3.1.2 CDI procedures.....……..…..…….....53
2.2.3.2 Other methods.....….....…..…….....57
2.3 Results.....…….…..……..…..…….....….....60
2.3.1 Analysis of brain homogenates by CDI without additional pre-treatment.....60
2.3.1.1 Non-CJD (neurological control) cases...……..…..…….....60
2.3.1.2 vCJD cases.....……..…..…….....63
2.3.1.3 sCJD cases.....……..…..…….....66
2.3.2 PrP^{C} and PrP^{Sc} in CJD brains with different disease phenotypes.....69
2.3.2.1 PrP^{C} in CJD brains with different disease phenotypes…...….....70
2.3.2.2 PrP^{Sc} in CJD brains: comparison of a conformational change (CDI) with resistance to limited proteolysis(WB)...…..…..…….....73
2.3.2.2.1 vCJD.....……..…..…….....73
2.3.2.2.2 MM1 sCJD.....……..…..…….....77
2.3.2.2.3 MM2 sCJD.....……..…..…….....81
2.3.2.2.4 MV1 sCJD.....……..…..…….....85

2.3.2.2.5 MV2 sCJD.....89
2.3.3 Further analysis of CJD brains: comparison before and after proteolysis.....94
2.3.3.1 Non-CJD brains.....94
2.3.3.2 CJD brains.....96
2.3.4 Further characterization of proteolytic fragments of PrP^{Sc} in Western blot.....101
2.3.4.1 PrP^{res} type analysis.....101
2.3.4.2 A small proteolytic fragment of PrP^{Sc} in MV2-2.....105
2.3.5 Supplementary data.....107
2.3.5.1 Liner range investigation in CDI.....107
2.3.5.2 Liner range investigation in Western blot analysis of PrP^{res}.....110
2.3.5.3 Analytical precision.....112
2.4 Discussion.....114
2.4.1 PrP^{C} in CJD brains.....114
2.4.2 CDI-based distinction between non-CJD and CJD brains: FC tissue analysis.....116
2.4.3 PrP^{Sc} in CJD brains determined by CDI or resistance to limited proteolysis (WB)...118
2.4.3.1 Analysis of multiple samples from different brain regions.....118
2.4.3.2 A conformational change (CDI) *versus* resistance to limited proteolysis (WB)....119
2.4.3.3 CDI analysis following limited proteolysis.....120
2.4.3.4 Speculation on the distribution profiles of PrP^{Sc}/PrP^{res} in CJD brains.....122
2.4.4 PK-resistant fragments of PrP^{Sc} (PrP^{res}).....124
2.4.4.1 Mixed PrP^{res} types.....124
2.4.4.2 PrP^{res} migrating between type 1 and type 2 standards.....125
2.4.4.3 PK-resistant fragment of PrP^{Sc} with low molecular mass comparable to that of GSS.....126
2.4.5 Speculation on potential limitation associated case selection.....127
2.4.6 Analytical sensitivity of CDI.....128
2.4.7 Mixed phenotypes in neuropathology: implication for sCJD classification.....129
2.4.8 Summary.....130

Chapter 3

Distribution profiles of different PrP conformers after fractionation in sucrose step gradient........131
3.1 Introduction.....132

3.2 Materials and methods.....134
3.2.1 Human brain materials.....134
3.2.2 Methods 134
3.3 Results.....137
3.3.1 Distribution profiles of PrP^{C}, total PrP and PrP^{Sc} in sucrose gradient.....137
3.3.1.1 Distribution profiles of PrP^{C} in sucrose gradient.....137
3.3.1.2 Distribution profiles of total PrP in sucrose gradient.....144
3.3.1.3 Distribution profiles of PrP^{Sc} in sucrose gradient.....148
3.3.2 Distribution profiles of PrP^{Sc} in sucrose gradient after mild proteolysis.....157
3.3.2.1 Effect of PK treatment to PrP conformers in fractionated samples.....157
3.3.2.2 Distribution of PrP^{Sc} after digestion with 2.5μg/ml PK.....161
3.3.3 Distribution of PrP^{res} in sucrose gradient.....163
3.3.4 Supplementary data: total protein distribution in sucrose gradient.....167
3.4 Discussion.....170
3.4.1 PrP^{C}: sedimentation profiles in sucrose gradient.....170
3.4.1.1 Non-CJD control brains.....170
3.4.1.2 CJD brains.....171
3.4.2 Total PrP in CJD brains: sedimentation profiles in sucrose gradient.....172
3.4.3 PrP^{Sc}/PrP^{res} in CJD brains: sedimentation profiles in sucrose gradient.....173
3.4.3.1 Two possible indicators for PrP^{Sc} in CDI D/N ratio and [D-N] values.....173
3.4.3.2 PK digestion of sucrose fractions.....173
3.4.3.3 PrP^{Sc}/PrP^{res} sedimentation profiles in sucrose gradient: between size and density.....175
3.4.3.4 Further speculations on regional difference of vCJD brains.....177
3.4.4 Considerable additional experiments using fractionated samples.....179

Chapter 4

Conformational stability states of PrP^{Sc} measured by CDI in different forms of human prion disease.....182
4.1 Introduction.....183
4.2 Materials and methods.....185
4.2.1 Human brain materials.....185
4.2.2 Methods 185

4.3 Results.....189
4.3.1 GdnHCl-induced denaturation of PrP^{Sc} in brain homogenates.....189
4.3.2 Enrichment of PrP^{Sc} by Sarcosyl extraction and centrifugation.....195
4.3.3 Conformational stability of PrP^{Sc}: comparison between vCJD and sCJD.....199
4.3.4 Conformational stability of PrP^{Sc}: variation between samples.....202
4.3.5 Analysis of additional cases at concentrations of 1.5M and 2M GdnHCl.....206
4.3.6 Conformational stability of vCJD PrP^{Sc}: comparison between brain regions.....208
4.3.7 Conformational stability of PrP^{res}.....210
4.3.8 Conformational stability of PrP^{Sc} in GSS cases with P102L mutation.....212
4.4 Discussion.....214
4.4.1 GdnHCl-induced denaturation of brain homogenate containing mixed PrP conformers.....214
4.4.2 Conformational stability of PrP^{Sc}: analysis of detergent insoluble fraction of PrP.....214
4.4.3 Conformational stability of PrP^{res}.....216
4.4.4 Conformational stability of PrP^{res}: importance in determining disease incubation periods.....217
4.4.5 Conformational stability of PrP^{Sc}/PrP^{res}: limitation in inferring the conformational state.....218
4.4.6 Speculation on effects of the detergent in protein conformation.....219
4.4.7 Speculation on the mechanism of PrP^{Sc} denaturation by GdnHCl.....219
4.4.8 Summary.....220

Chapter 5

Discussion.....222
5.1 Summary of findings.....223
5.1.1 PrP^{C} in CJD brains.....223
5.1.2 PrP^{Sc} in CJD brains: comparison between 3F4-based CDI and resistance to limited proteolysis.....224
5.1.3 Distribution profiles of PrP^{Sc} between the three brain regions in CJD brains.....225
5.1.4 PrP^{Sc} in CJD brains: sedimentation profiles in the sucrose step gradient.....226
5.1.5 Conformational stability of PrP^{Sc} in CJD brains.....228
5.1.6 A proteolytic fragment of ~8 KDa fragment in MV2 sCJD.....229

5.2 Outstanding questions and future research.....230
5.2.1 Further analysis of size distribution of PrP^{Sc} in the thalamus of vCJD brains.....230
5.2.2 Further analysis of conformational stability of PrP^{Sc}.....231
5.2.3 Abnormal PrP species in FFI.....232
5.3 Implications of this study.....234

References.....236

Appendix

1. Neuropathology of CJD brains.....270
1.1 vCJD.....270
1.2 MM1 sCJD.....272
1.3 MM2 sCJD.....274
1.4 MV1 sCJD.....276
1.5 MV2 sCJD.....278
1.6 Summary.....282
2. Papers submitted for publication.....284

List of figures

Chapter 1

1.1 Primary structure of human cellular prion protein (PrP^{C})…….....8

1.2 Two models depicting the conformational conversion of PrP^{C} into PrP^{Sc}…….....10

1.3 Lesion profiles in RIII mice infected with BSE or vCJD…….....12

1.4 Various PK-resistant core fragments of PrP^{Sc} observed in human prion diseases…….....15

1.5 Western blot analysis of types 1 and 2 PrP^{res}…….....16

Chapter 2

2.1 Diagram of conformation-dependent immunoassay.....….....56

2.2 Comparison of CDI results between native and denatured states in non-CJD brains…….....62

2.3 Comparison of CDI results between native and denatured states in vCJD brains…….....65

2.4 Comparison of CDI results between native and denatured states in MM1 sCJD brains.....68

2.5 PrP^{C} in CJD brains with MM genotype at codon 129…….....71

2.6 PrP^{C} in CJD brains with MV genotype at codon 129…….....72

2.7 CDI [D-N] values for tissues of FC, Cb and Th from vCJD brains…….....75

2.8 Distribution of PrP^{res} in three regions of vCJD brains…….....76

2.9 CDI [D-N] values for tissues of FC, Cb and Th from MM1 sCJD brains…….....….79

2.10 Distribution of PrP^{res} in three regions of MM1 sCJD brains…….....80

2.11 CDI [D-N] values for tissues of FC, Cb and Th from MM2 sCJD brains…….....83

2.12 Distribution of PrP^{res} in three regions of MM2 sCJD brains…….....84

2.13 CDI [D-N] values for tissues of FC, Cb and Th from MV1 sCJD brains.....87

2.14 Distribution of PrP^{res} in three regions of MV1 sCJD brains.....88

2.15 CDI [D-N] values for tissues of FC, Cb and Th from MV2 sCJD brains…….....92

2.16 Distribution of PrP^{res} in three regions of MV2 sCJD brains…….....93

2.17 High susceptibility of PrP^{C} to proteolytic treatment in non-CJD brains…….....95

2.18 Comparison of CDI results before and after proteolysis…….....98

2.19 Comparison of CDI D/N ratios before and after proteolysis…….....99

2.20 Comparison of CDI [D-N] values before and after proteolysis…….....100

2.21 Analysis of PrP^{res} type in MM2 sCJD brains…….....103

2.22 Analysis of PrP^{res} type in MV2 sCJD brains…….....104

2.23 A proteolytic fragment of PrP^{Sc} with low molecular weight in a case of MV2 sCJD.....106

2.24 Investigation of linear range in CDI.....109
2.25 Investigation of linear range in Western blot analysis of PrP^{res}.....111
2.26 Intra-assay variation in CDI.....113

Chapter 3

3.1 Distribution profiles of PrP^{C} from FC of non-CJD brains after fractionation in sucrose step gradient.....140
3.2 Distribution profiles of PrP^{C} from FC of vCJD brains after fractionation in sucrose step gradient.....141
3.3 Distribution profiles of PrP^{C} from FC of MM1 sCJD brains after fractionation in sucrose step gradient.....142
3.4 Comparison of PrP^{C} distribution in sucrose step gradient between non-CJD and CJD brains 143
3.5 Distribution of total PrP in sucrose step gradient.....146
3.6 Comparison of the distribution profiles of total PrP in sucrose step gradient.....147
3.7 CDI D/N ratios for fractions from FC of non-CJD brains.....152
3.8 CDI D/N ratios for fractions from FC of vCJD brains.....153
3.9 Comparison CDI D/N ratios between fractions derived from different regions of a vCJD brain.....154
3.10 CDI D/N ratios for fractions from FC of MM1 sCJD brains.....155
3.11 Comparison of CDI D/N ratios for fractions derived from different regions of vCJD brains and FC of MM1 sCJD brains.....156
3.12 Absence of detectable PrP in the fractionated samples from FC of non-CJD1 (a) or non-CJD3 (b) after digestion with 2.5μg/ml PK.....159
3.13 Effects of PK treatment to different PrP conformers in fractionated samples from different regions of a vCJD brain.....160
3.14 Comparison of CDI D/N ratios for PK-treated fractions between vCJD FC, vCJD Th and MM1 sCJD FC.....162
3.15 PrP distribution after fractionation in sucrose step gradient.....165
3.16 PrP distribution after fractionation in sucrose step gradient.....166
3.17 Total protein distribution after fractionation in sucrose step gradient.....168
3.18 A standard curve generated using BSA.....169
3.19 Total protein distribution after fractionation in sucrose step gradient.....169

Chapter 4

4.1 Comparison of CDI results between native (N) and denatured (D) states.....192
4.2 Change of CDI TRF counts with exposure to increasing concentrations of GdnHCl.....193
4.3 Change of CDI D/N ratio with exposure to increasing concentrations of GdnHCl.....194
4.4 Distribution of PrP^{C} and PrP^{Sc} after Sarcosyl extraction and centrifugation.....197
4.5 Enrichment of PrP^{res} in pellets after Sarcosyl extraction and centrifugation.....198
4.6 GdnHCl-induced denaturation of PrP^{Sc}.....201
4.7 Comparison of GdnHCl-induced denaturation of PrP^{Sc} between samples.....204
4.8 Denatured fraction of PrP^{Sc} after treatment with 1.5M or 2M GdnHCl.....207
4.9 GdnHCl-induced denaturation of PrP^{Sc} from cerebellum or thalamus of vCJD brains.....209
4.10 Conformational stability of PrP^{res} from frontal cortex of vCJD and MM1 sCJD brains.....211
4.11 Comparison of denaturation profiles of PrP^{Sc} between two GSS cases with different PrP^{res} patterns.....213

Appendix 1

A1.1 Neuropathology in vCJD.....271
A1.2 Neuropathology in MM1 sCJD.....273
A1.3 Neuropathology in MM2 sCJD.....275
A1.4 Neuropathology in MV1 sCJD.....277
A1.5 Neuropathology in MV2 sCJD.....280
A1.6 Neuropathology in a MV2 sCJD case with atypical pathological features.....281

List of tables

Chapter 1

1.1 Codon 129 genotype frequencies in normal and CJD populations in the UK (%)…..5

1.2 Classification of human prion disease.....19

1.3 Classification of sCJD based on genotype at codon 129 and PrP^{res} type.....24

Chapter 2

2.1 Clinical, genetic and biochemical information for vCJD cases.....47

2.2 Clinical, genetic and biochemical information for sCJD cases.....48

2.3 Clinical, genetic and biochemical information for GSS cases with P102L mutation.....49

2.4 Clinical, genetic and biochemical information for neurological control cases.....49

2.5 Variables of neurological control and CJD cases as a group.....50

Chapter 4

4.1 $GdnHCl_{1/2}$ values for PrP^{Sc} from frontal cortex of vCJD.....205

4.2 $GdnHCl_{1/2}$ values for PrP^{Sc} from frontal cortex of MM1 sCJD.....205

4.3 $GdnHCl_{1/2}$ values for PrP^{Sc} from cerebellum and thalamus of vCJD.....209

4.4 Comparison of $GdnHCl_{1/2}$ values between relevant studies.....221

Appendix 1

A1.1 Neuropathological features in different subtypes of sporadic CJD.....283

CHAPTER 1

General introduction

1.1 Overview

Transmissible spongiform Encephalopathies (TSEs) or prion diseases are a group of fatal neurodegenerative diseases affecting humans and animal species. The prion diseases in humans include Creutzfeldt-Jakob disease (CJD), Gertsmann-Straussler-Scheinker Syndrome (GSS) and fatal familial insomnia (FFI). The prion diseases in animals include bovine spongiform encephalopathy (BSE) in cattle, scrapie in sheep and goats and chronic wasting disease (CWD) in elk and deer. Prion diseases are characterized clinically by neurological symptoms such as dementia and ataxia, and pathologically by brain lesions showing spongiform degeneration, neuronal loss and gliosis (Ironside *et al.* 2008). More distinctively, an abnormally folded isoform of a host encoded protein, the prion protein (PrP) accumulates in the central nervous system (CNS) of affected individuals in most forms of prion diseases (Budka 2003; Prusiner 1998).

Prion diseases appear to share some pathophysiological features with other neurodegenerative diseases such as Alzheimer's and Parkinson's diseases (Aguzzi and Calella 2009; Aguzzi and Haass 2003). However, prion diseases are unique in that they are transmissible within species and occasionally between species by inoculation or by ingestion of infected materials. Although the infectious agent that causes TSEs is not fully understood, a wealth of experimental evidence strongly supports the "protein-only" or prion hypothesis (Prusiner 1998). Prions can be defined as "small proteinaceous infectious particles that are resistant to inactivation by most procedures that modify nucleic acids" (Prusiner 1982; Prusiner 1998). The misfolded conformer (PrP^{Sc}) of cellular PrP (PrP^{C}) is the only known component of prion (Bolton *et al.* 1982; McKinley *et al.* 1983) and propagates in an autocatalytic manner by inducing PrP^{C} to adopt a disease-associated conformation (Caughey 2003; Caughey and Raymond 1991; Prusiner 1998). PrP^{C} was shown to be essential for prion invasion through the study using mice devoid of PrP^{C} (Bueler *et al.* 1993; Sailer *et al.* 1994). Since the first discovery of a linkage between GSS and a mutation in PrP gene (Hsiao *et al.* 1989), more than 30 pathogenic mutations in PrP gene have

been identified in humans with inherited forms prion disease (Kovacs *et al.* 2005; Mead 2006). No nucleic acids genome has been identified as a constituent component of prions (Meyer *et al.* 1991; Safar *et al.* 2005b), which make prions distinct from all other conventional infectious pathogens such as viruses and bacteria. More compelling evidence supporting the prion hypothesis has come from *in vitro* generation of infectious prions. In 2004, Prusiner and co-workers firstly reported the generation of synthetic mammalian prions, which were produced by polymerizing recombinant mouse PrP into amyloid fibrils (Legname *et al.* 2004). In the following year, Soto and colleagues reported the successful generation of infectious prions by amplifying PrP^{Sc} in vitro using the methods named protein misfolding cyclic amplification (PMCA) (Castilla *et al.* 2005a). Since then, the successful generation of prion infectivity has been reported in various studies from different groups (Castilla *et al.* 2008a; Castilla *et al.* 2008b; Colby *et al.* 2009; Colby *et al.* 2010; Deleault *et al.* 2007; Kim *et al.* 2010; Makarava *et al.* 2010; Wang *et al.* 2010).

1.2 Prion protein gene

The genes encoding PrP of various species was fully sequenced in 1986 (Basler *et al.* 1986; Liao *et al.* 1986; Locht *et al.* 1986). The entire open reading frame (ORF) of PrP gene was found to be located within a single exon in all examined mammalian and avian species (Prusiner 1998). The human PrP gene (*PRNP*) located on the short arm of chromosome 20 is composed of two exons with the ORF in exon 2 (Sparkes *et al.* 1986). In animals including sheep, cattle and mice, the PrP genes contain three exons with the ORF in exon 3 that is analogous to exon 2 of the human PrP gene (Prusiner 1998). The PrP gene is highly conserved across many mammalian and avian species, suggesting the functional importance of PrP (Lee *et al.* 1998; Wopfner *et al.* 1999).

Genetic variation in the PrP gene can be directly associated with prion diseases (pathogenic mutation) or can influence the disease susceptibility and phenotypes (polymorphism). In humans, there are more than 30 pathogenic mutations including

point mutations resulting in an amino-acid substitution and insertion of additional octapeptide repeats (Mead 2006). Additionally, non-pathogenic polymorphisms in human *PRNP* have a profound influence on disease susceptibility and phenotype (Collinge *et al.* 1991; Goldfarb *et al.* 1992b; Palmer *et al.* 1991; Parchi *et al.* 1999b; Windl *et al.* 1996; Zeidler *et al.* 1997). A polymorphism at codon 129 that encodes methionine (M) or valine (V) is a particularly important factor in determining disease susceptibility and phenotype. In variant CJD, the effect of polymorphism at codon 129 is dramatic (Table 1.1). All pathologically confirmed cases of variant CJD (vCJD) have been homozygous for methionine at position 129 (Table 1.1)(Brandel *et al.* 2009). In sporadic CJD (sCJD), about 65% of patients are methionine homozygotes at *PRNP* codon 129 (Table 1.1)(Bishop *et al.* 2009; Head *et al.* 2004a; Parchi *et al.* 1999b). In comparison, the proportion of methionine homozygotes at this position is about 40% in general white population (Bishop *et al.* 2009; Nurmi *et al.* 2003; Parchi *et al.* 1999b). Individuals who have a heterozygous MV genotype at codon 129 have shown longer incubation periods in acquired forms of prion disease such as kuru and iatrogenic CJD (Brown *et al.* 2000; Cervenakova *et al.* 1998; Lee *et al.* 2001). Another polymorphism at codon 219 (E219K) is also proposed to be associated with susceptibility to sCJD in Japan (Shibuya *et al.* 1998).

The polymorphic effects of the PrP gene are also well known in sheep scrapie. In sheep, the three polymorphic sites of the PrP gene at codons 136, 154 and 171 have profound effects on the disease susceptibility and pathogenesis (Hunter 2003; Hunter 2007). Animals carrying the genotype of $V_{136}R_{154}Q_{171}/V_{136}R_{154}Q_{171}$ are known to most susceptible to classical scrapie (Belt *et al.* 1995; Hunter *et al.* 1996); in comparison, the presence of the $A_{136}R_{154}R_{171}$ allele is known to confer a level of resistance to scrapie (Houston *et al.* 2002). In mice, two polymorphic sites of the PrP gene at codons 108 and 189 are known to be closely associated with disease progression (Moore *et al.* 1998; Westaway *et al.* 1987).

Table 1.1 Codon 129 genotype frequencies in normal and CJD populations in the UK (%)

Codon 129 genotype	MM	MV	VV	Reference
Normal population	42	47	11	(Nurmi *et al.* 2003)
sCJD population	67	19	14	(Head *et al.* 2004a)
vCJD population[a]	100	0	0	(Brandel *et al.* 2009)

Note a. One individual with MV genotype at codon 129 was diagnosed as a possible vCJD on the basis of ante-mortem examination. Post-mortem examination was not performed for this patient (Kaski *et al.* 2009). Additionally, one case of preclinical vCJD was reported in an individual with MV genotype at codon 129 (Peden *et al.* 2004); this patient who had received blood transfusion from a donor later found to incubate vCJD died without neuorological symptoms, but the accumulation of PrP^{res} was identified in the spleen.

1.3 Prion protein

1.3.1 Cellular prion protein (PrP^C)

The cellular prion protein (PrP^C) is a cell-surface glycoprotein which is attached to the outer membrane by its glycosylphosphatidylinositol (GPI) anchor (Stahl *et al.* 1987). In the CNS, PrP^C is expressed at high levels in neurons but also found in glial cells (Kretzschmar *et al.* 1986; Manson *et al.* 1992; Moser *et al.* 1995). PrP^C is also expressed at lower levels in a variety of peripheral tissues including immune cells, kidney, heart and skeletal muscle (Caughey *et al.* 1988; Ford *et al.* 2002; Mabbott and MacPherson 2006). Like other membrane and secreted proteins, PrP^C is synthesized in the rough endoplasmic reticulum (ER)-attached ribosome, enters ER concurrent with its synthesis and is transported along the secretary pathway to the cell surface (Hegde and Rane 2003; Westergard *et al.* 2007). Nascent PrP^C undergoes post-translational modifications including cleavage of the ER signal peptide and cleavage of GPI signal peptide followed by attachment of the GPI anchor (Kang *et al.* 2006; Stahl *et al.* 1987). In humans, a mature form of PrP^C consists of 208 amino acids (aa) containing the GPI anchor at serine 230.

The structure of PrP^C determined by nuclear magnetic resonance (NMR) spectroscopy is very similar among various mammalian species; the N-terminal tail of the molecule is largely unstructured whereas the C-terminal domain is globular and contains three α-helices and two β-sheets (Donne *et al.* 1997; Lysek *et al.* 2005; Riek *et al.* 1996; Riek *et al.* 1997; Zahn *et al.* 2000). The flexible amino-terminal domain of PrP^C contains octapeptide repeat region, which is known to play an important role in copper binding through its histidine residues (Brown 2001; Viles *et al.* 1999). The insertional mutations of this octapeptide repeat region cause inherited forms of prion disease in humans (Mead 2006; Owen *et al.* 1989). The amino-terminal portion of PrP^C also contains a conserved hydrophobic segment (residues 111 - 134) that can span the membrane (Hegde *et al.* 1998; Kim *et al.* 2001; Stewart *et al.* 2001). The carboxyl-terminal globular domain of PrP^C has two glycosylation sites at asparagine (N) residues 181 and 197 in the human PrP (Haraguchi *et al.*

1989); thus PrP^C can be present in three different glycoforms (di-, mono- and un-glycosylated PrP) according to the degree of the occupancy of the two potential N-linked glycosylation sites. Additionally, a disulphide bridge between cysteine residues 179 and 214 (in the human protein) is present in the C-terminal domain (Turk *et al.* 1988).

The physiological function remains still unclear, although more than two decades has passed since the identification of PrP^C as an endogenous cellular protein (Aguzzi and Calella 2009; Solomon *et al.* 2009). A variety of lines of mice that are devoid of PrP^C develop normally without showing any severe pathology (Weissmann and Flechsig 2003), although subtle abnormalities were reported in several lines of PrP-deficient mice (Collinge *et al.* 1994; Nishida *et al.* 1999; Tobler *et al.* 1996). Even the postnatal deletion of neuronal PrP^C does not elicit neurodegeneration in mice (Mallucci *et al.* 2002). One very recent study reported that neuronal expression of PrP^C is essential for long-term peripheral myelin maintenance (Bremer *et al.* 2010). Significantly, PrP-deficient mice were shown to be fully resistant to prion infection (Bueler *et al.* 1993). Several proposed functions of PrP^C include an anti-apoptotic activity, protection against oxidative stress, copper transport, a role in synaptic formation and function and participation in transmembrane signalling processes involved in neuronal survival and neurite outgrowth (Aguzzi *et al.* 2008; Watts and Westaway 2007).

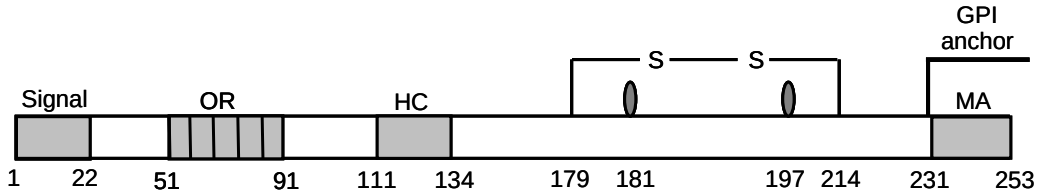

Figure 1.1 Primary structure of human cellular prion protein (PrP^{C}). The secretory signal peptide (1 - 22) is present at the extreme N-terminus. The membrane anchor region (MA; 231 - 253) is cleaved when the GPI anchor is attached at serine 230. The mature form of human PrP^{C} contains 208 amino acids (23 - 230) and has two potential sites for N-linked glycosylation at residues 181 and 197 and one disulphide bond (S-S) between cysteine residues 179 and 214. OR: octapeptide repeats; HC: hydrophobic core. The numbers represent the position of respective amino acids. Modified from reference (Aguzzi and Calella 2009).

1.3.2 Disease-associated prion protein (PrP^{Sc})

According to the prion hypothesis the central phenomenon that characterizes prion disease is the conformational conversion of PrP^{C} into a pathogenic conformer of PrP (PrP^{Sc}), which is thought to be the main constituent of infectious prions (Prusiner 1998). PrP^{Sc} replicates its pathogenic conformation at the expense of PrP^{C} (Bessen *et al.* 1995; Horiuchi *et al.* 2000; Kocisko *et al.* 1994) and accumulates in the CNS of affected individuals. Demonstration of PrP^{Sc} is currently the most reliable diagnostic marker of prion propagation. The formation of PrP^{Sc} is a post-translation process that happens after mature PrP^{C} reaches the cell surface (Caughey 1993; Caughey and Raymond 1991); nonetheless, post-translational modifications that distinguish the two conformers of PrP remains largely elusive except for few recent findings (Canello *et al.* 2008; Colombo *et al.* 2009; Stahl *et al.* 1993).

The distinction between PrP^{C} and PrP^{Sc} has been largely achieved based on the difference in biochemical properties. While PrP^{C} exists as monomers or dimers with α-helix-rich structure, PrP^{Sc} is present as ß-sheet-rich polymers that often form amyloid plaques in the brain (Caughey *et al.* 1991; Meyer *et al.* 2000; Pan *et al.* 1993; Pergami *et al.* 1996). The conversion of PrP^{C} into PrP^{Sc} accompanies the change of biochemical properties such as proteinase-K (PK) resistance or detergent solubility. In contrast to PrP^{C}, PrP^{Sc} is insoluble to non-denaturing detergents and partially resistant to proteolytic digestion (Meyer *et al.* 1986). Proteolytic treatment of PrP^{Sc} leaves PK-resistant fragments of PrP^{Sc} (PrP^{res}) as a result of the cleavage of 60 - 70 amino terminal residues (Bolton *et al.* 1982). This PK-resistant core fragment with molecular weight of 27 - 30 KDa (PrP 27-30) in dissociating and denaturing condition has been a useful surrogate marker for the diagnosis of prion disease (Grassi *et al.* 2000; Schaller *et al.* 1999; Wadsworth *et al.* 2001).

The difference in the secondary structure between PrP^{C} and PrP^{Sc} was revealed in early studies employing circular dichroism (CD) and/or Fourier transform infrared (FTIR) spectroscopy (Pan *et al.* 1993; Safar *et al.* 1993). PrP^{C} is predominantly composed of α-helices (~40%) with little ß-sheet content (3%), whereas PrP^{Sc} has greatly increased ß-sheet contents (~40%) and slightly lower amounts of α-helices (30%) (Pan *et al.* 1993). In contrast to PrP^{C}, high-resolution structure is poorly determined for PrP^{Sc} because of its insolubility (Aguzzi and Polymenidou 2004; Riesner 2003). A highly ordered structure of PrP^{res} shown by Wille and colleagues is the highest resolution information for PrP^{Sc} structure (Caughey *et al.* 2009; Wille *et al.* 2002). A trimeric arrangement of PrP^{Sc} was proposed as a minimal assembly of PrP^{Sc} in two different models (DeMarco and Daggett 2004; Govaerts *et al.* 2004).

1.3.3 Two models describing the self-propagation of PrP^{Sc}

Currently, the exact mechanism in which PrP^{C} is converted into PrP^{Sc} remains unclear. Two models have been proposed in order to explain the propagation of PrP^{Sc} (Figure 1.2). In the "template-directed refolding" model, a spontaneous conversion of PrP^{C} into PrP^{Sc} is a rare event or may be prevented by a high energy barrier between the two conformers of PrP (Aguzzi and Polymenidou 2004; Caughey *et al.* 2009). The pre-existing PrP^{Sc} acts as a template for the cellular conformer of PrP to be refolded into a pathogenic conformation. In the "seeded nucleation" model, the two isoforms of PrP are supposed to co-exist in a balance which is heavily shifted toward PrP^{C} in a non-disease condition (Aguzzi and Polymenidou 2004; Caughey *et al.* 2009). In this model, a monomeric form of PrP^{Sc} is harmless and what is infectious is a small oligomeric form of PrP^{Sc} that propagates by recruiting PrP^{Sc} monomers.

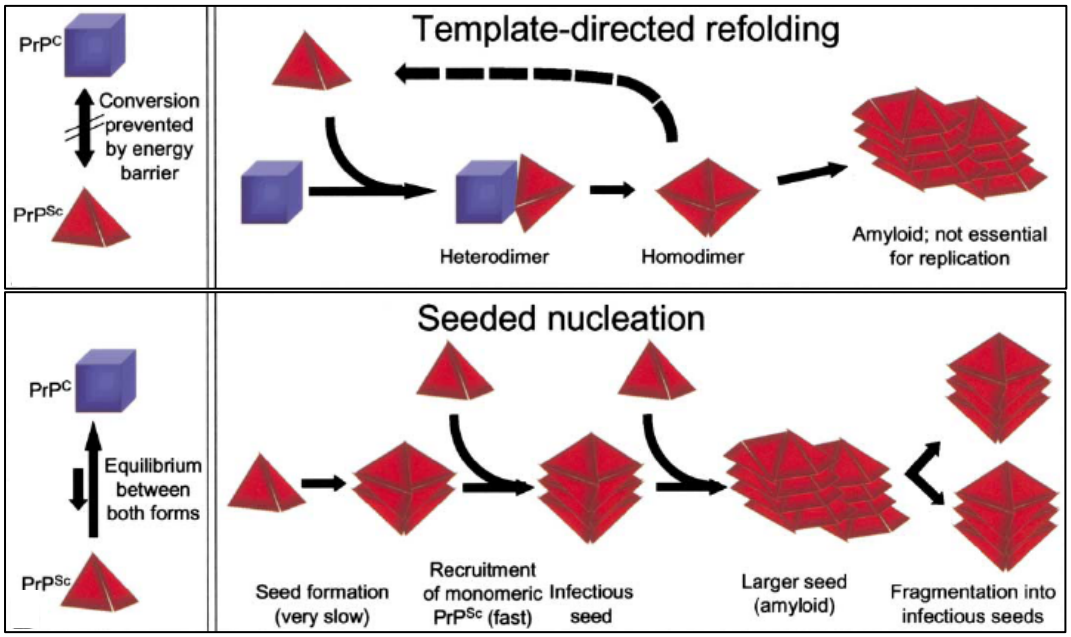

Figure 1.2 Two models depicting the conformational conversion of PrP^{C} into PrP^{Sc}. Upper row describes the template-directed refolding model and bottom row explains the seeded nucleation model. Taken from reference (Aguzzi and Polymenidou 2004).

1.4 Strain variation in prion diseases

Prion strains can be defined as infectious isolates which cause distinct disease phenotypes when experimentally inoculated into identical hosts (Aguzzi *et al.* 2007). The presence of prion strains was first recognized by Pattison and Misslon in 1961 (Pattison and Millson 1961). In this study, scrapie-infected goats were classified into two groups according to their clinical manifestation:"drowsy" goats *versus* "scratch" goats. The successful transmission of scrapie to rodents became an important milestone in the study of prion diseases (Chandler 1961; Kimberlin and Walker 1977), which made possible larger scale of transmission studies that had been impractical in sheep and goats. Prion strains that have been identified until now are mostly based on the disease characteristics obtained by bioassay in rodents (particularly in mice). Most commonly used parameters to distinguish prion strains are the length of incubation period between the initial infection and development of clinical symptoms, and profile of neuropathological changes in the brains of infected mice (lesion profile)(Bruce 2003). For the generation of lesion profile, the severity of vacuolation is semi-quantitatively scored in defined brain areas (nine grey matter and three white matter areas) (Bruce *et al.* 1991; Fraser and Dickinson 1968). Clinical features in laboratory animals may be an additional useful parameter to distinguish prion strains, as is the case in the two TME prion strains isolated in hamsters (Bessen and Marsh 1992b). Once prion strains are isolated by serial passage, they can retain their identities indefinitely on further passages as long as the conditions of passage remain constant (Bruce 2003).

The transmission studies of scrapie from a wide range of natural and experimental sources into inbred mice revealed the existence of multiple strains of prions (Dickinson 1976). About 20 strains of scrapie have been isolated in mice by serial passage of scrapie materials, each with phenotypically distinct disease characteristics (Bruce 1993; Bruce and Fraser 1991). In transmissible mink encephalopathy (TME), two strains termed DY (drowsy) and HY (hyper) were isolated in hamsters by serial passage of TME brain materials (Bessen and Marsh 1992b). Transmission studies in

wild-type and transgenic mice revealed that cattle BSE, human vCJD and TSEs in cats and exotic ungulates were caused by the same prion strain (Figure 1.3)(Bruce *et al.* 1994; Bruce *et al.* 1997; Hill *et al.* 1997; Scott *et al.* 1999). Therefore, vCJD is definitely an independent prion strain isolated from prion-infected human brains. Except for vCJD, it appears largely elusive how many strains are present in human prion diseases (Aguzzi *et al.* 2007). For example, six subtypes of sCJD were suggested to exist on the basis of clinico-pathological phenotype and these were proposed to correlate with the combination of *PRNP* genotype at codon 129 and PrP^{res} type (Parchi *et al.* 1999b). However, each subtype of sCJD has not yet been shown to result from an independent prion strain, which would require evidence of persistence of strain characteristics on serial passage in experimental animals (Aguzzi *et al.* 2007). Nonetheless, one transmission study using bank voles proposed the existence of at least two prion strains in sCJD (Nonno *et al.* 2006). Additionally, another transmission study using transgenic mice suggested that the prion strain associated with FFI is identical to that of sporadic form of fatal insomnia (Mastrianni *et al.* 1999).

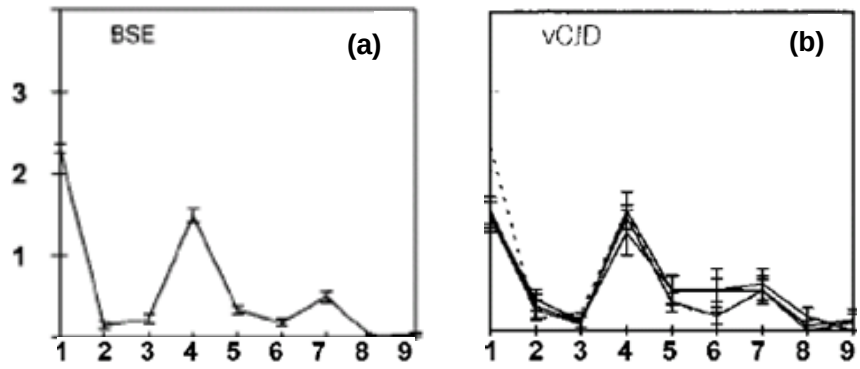

Figure 1.3 Lesion profiles in RIII mice infected with BSE or vCJD. Picture (a) represents the pooled lesion profile from four cases of cattle BSE and picture (b) shows the lesion profiles from three cases of vCJD. Dotted line in (b) represents the pooled BSE profile shown in (a). Vacuolar degeneration is semi-quantified on a scale of 0 - 5 (vertical axis) in the nine grey matter areas (horizontal axis). Modified from reference (Bruce *et al.* 1997).

1.5 Biochemical analysis of PrP^{Sc} for prion strain/phenotype discrimination

Unlike conventional pathogens such as viruses, the existence of multiple strains in prion diseases cannot be explained in terms of genetic variants. The strain phenomenon in prion diseases appeared to be difficult to be explained within the framework of the prion hypothesis, and was once a powerful argument against the protein-only hypothesis (Chesebro 1998; Soto and Castilla 2004). In order to explain the strain phenomenon seen in prion diseases, conformational variation of PrP^{Sc} has been proposed as a main strain determinant (Prusiner 1998). According to this concept, each prion strain represents a specific disease-associated conformation of PrP^{Sc} that can propagate faithfully by imposing the same conformation on new host PrP^{C} (Prusiner 1998). The conformational difference of PrP^{Sc} between biologically distinct prion strains (and between distinct disease phenotypes) has been largely inferred from differing biochemical properties of PrP^{Sc} including: gel mobility and/or glycoform ratio of PrP^{res} (Bessen and Marsh 1994; Collinge *et al.* 1996; Hill *et al.* 2006; Monari *et al.* 1994; Parchi *et al.* 1996), the ratio between PK-sensitive form and PK-resistant form of PrP^{Sc} (Safar *et al.* 1998) and conformational stability of PrP^{res} (Peretz *et al.* 2001; Peretz *et al.* 2002). Despite the substantial evidence, however, it remains still largely uncertain whether such conformational difference of PrP^{Sc} is the cause of prion strain phenomenon or simply another pathological phenotype of prion diseases (Soto and Castilla 2004). In this context, one exception is a recent study performed by Colby and colleagues (Colby *et al.* 2009), which has shown the incubation periods of synthetic prions can be directly modulated by varying the conformational stability of recombinant PrP amyloids.

1.5.1 TME prion strains

The most convincing evidence that biologically distinct prion strains can be distinguished by biochemical properties of PrP^{Sc} has come from studies that examined the HY and DY TME strains isolated in hamsters. When PK-resistant core fragments of PrP^{Sc} were analysed by Western blot, the unglycosylated fragment of DY PrP^{res} migrated faster than that of HY PrP^{res} with the difference of ~2 KDa in

molecular weight (Bessen and Marsh 1992a). This difference was shown to result from the differential accessibility of PK to the N-terminus of PrP^{Sc} (Bessen and Marsh 1994), which has been interpreted as indirect evidence of conformational difference between HY PrP^{Sc} and DY PrP^{Sc}. Additionally, the two TME strains were distinguishable by the extent of PK resistance and sedimentation profiles (Bessen and Marsh 1992a). More directly, structural analysis employing FTIR spectroscopy revealed the difference in ß-sheet secondary structure between HY PrP^{Sc} and DY PrP^{Sc} (Caughey *et al.* 1998).

1.5.2 Human prion diseases

In human prion diseases, much evidence supporting conformation-based strain diversity has been gathered by Western blot analysis of PK-resistant core fragments of PrP^{Sc}. Two major PrP^{res} types (termed type 1 and type 2) have been recognized (Parchi *et al.* 1996; Parchi *et al.* 1997). These two PrP^{res} types differ in the degrees of their N-terminal truncation following treatment with PK (Figures 1.4 and 1.5). Type 1 PrP^{res} has a main cleavage site at glycine 82, whereas type 2 PrP^{res} is predominantly truncated at serine 97 (Parchi *et al.* 2000b). In addition to the two major variants of PrP^{res}, smaller C-terminal fragments (CTF) of 12 - 13 KDa were recently identified in some forms of sCJD (Notari *et al.* 2008; Zou *et al.* 2003) and internal small fragments of 7 - 8 KDa were found in GSS associated with various pathogenic mutations (Parchi *et al.* 1998; Piccardo *et al.* 1998; Piccardo *et al.* 2001). A further distinction of PrP^{res} can be achieved on the basis of glycosylation site occupancy (referred to type A or type B; Figure 1.5) (Head *et al.* 2004a; Parchi *et al.* 1997). Type B PrP^{res} is characterized by the high occupancy of both potential glycosylation sites, whereas type A PrP^{res} has a prominent monoglycosylated (or rarely unglycosylated) PrP^{res} species (Head *et al.* 2004a; Parchi *et al.* 1997). Variation in these parameters has been identified in association with different phenotypes of human prion disease (Collinge *et al.* 1996; Hill *et al.* 2006; Monari *et al.* 1994; Parchi *et al.* 1997; Parchi *et al.* 1996). PrP^{res} types in concert with *PRNP* status at codon 129 have formed a molecular basis in the subclassification of sCJD

(Hill *et al.* 2003; Parchi *et al.* 1999b). When brain extracts from FFI with D178N mutation (with type 2 PrP^{res}) or from familial CJD with E200K (with type 1 PrP^{res}) were inoculated into transgenic mice expressing a chimeric human-mouse PrP, distinct PrP^{res} types remained unchanged in recipient mice implying that conformational variation of PrP^{Sc} is independent of amino acid sequence of PrP (Telling *et al.* 1996).

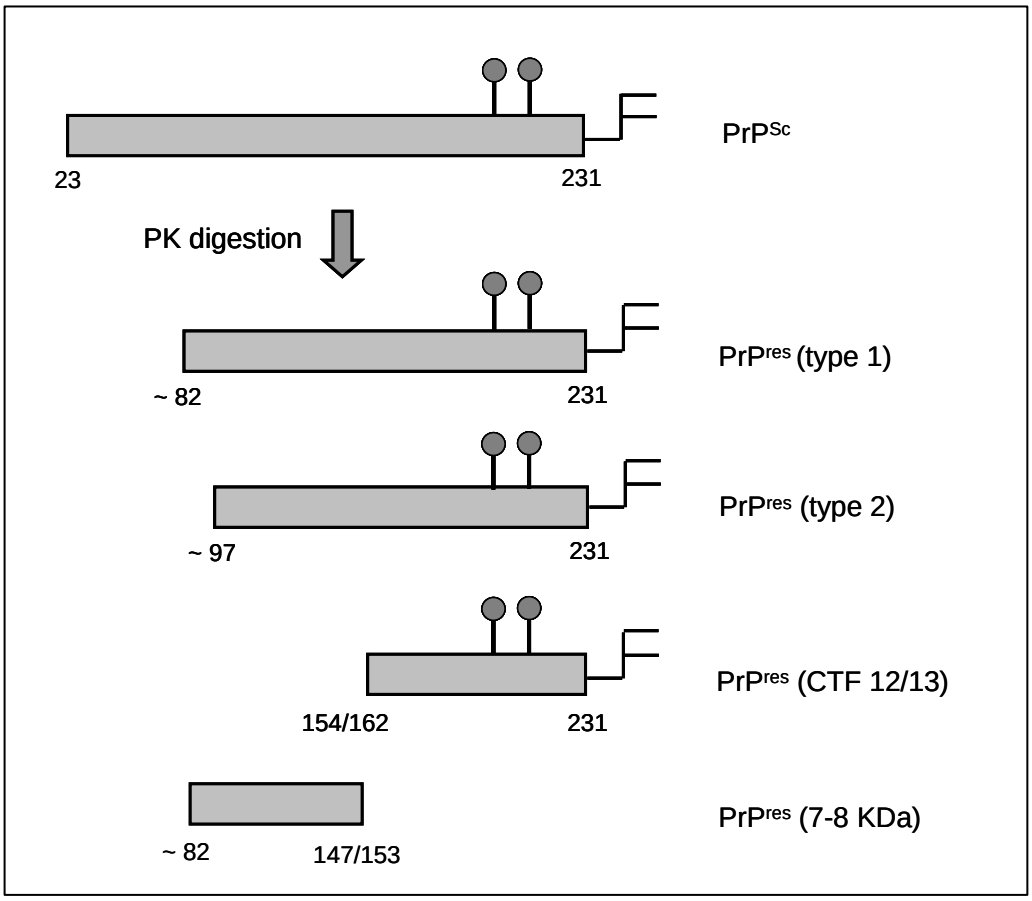

Figure 1.4 Various PK-resistant core fragments of PrP^{Sc} observed in human prion diseases. Following proteolysis, several forms of PK-resistant core fragment of PrP^{Sc} can be detected from human brains affected by prions. They include types 1 and 2 PrP^{res}, a smaller C-terminal fragment of 12 or 13 KDa (CTF 12/13) and an internal fragment of 7-8 KDa. Modified from reference (Gambetti *et al.* 2003).

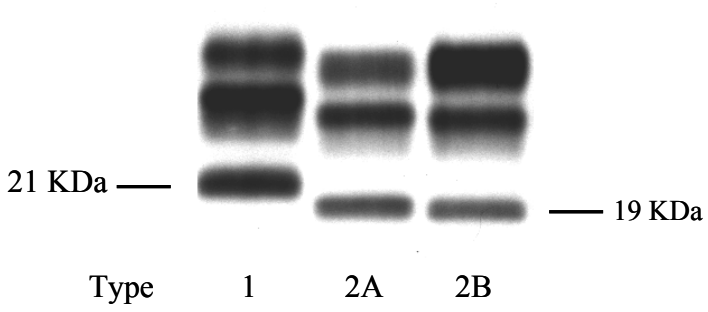

Figure 1.5 Western blot analysis of types 1 and 2 PrP^{res}. Type 1 and type 2A PrP^{res} are associated with various forms of sCJD, whereas type 2B PrP^{res} is observed in vCJD. Type 1 and type 2 PrP^{res} can be distinguished by their difference in migration of unglycosylated species of PrP^{res}. In comparison with type 2A PrP^{res}, type 2B PrP^{res} which is characteristic molecular signature of vCJD-affected brains is characterized by high occupancy of both potential glycosylation sites. Image is taken from (Head *et al.* 2004a).

1.5.3 BSE in cattle and other species

The BSE agent can retain its biological identity after crossing between species naturally or experimentally (Bruce *et al.* 1994; Bruce *et al.* 1997). In transmission studies to mice, the strain properties of cattle BSE were found to be closely similar to those of human vCJD or TSEs in cats and exotic ungulate species (Bruce *et al.* 1994; Bruce *et al.* 1997). Moreover, the BSE strain properties remained unchanged in experimentally infected domestic species such as sheep and pigs (Bruce *et al.* 1994; Green *et al.* 2005). Similarly, molecular signature of PrP^{Sc} seen in cattle BSE is also maintained after transmission to other species. In western blot analysis, PrP^{res} in cattle BSE is characterized by a faster migrating unglycosylated moiety and the abundance of diglycosylated form (Baron *et al.* 2007). The molecular properties of PrP^{res} in cattle BSE was similar to those found in human vCJD, indicating a possible linkage between the two (Collinge *et al.* 1996). The molecular signature in cattle

BSE was also retained in sheep experimentally infected with BSE (Hope *et al.* 1999; Stack *et al.* 2002).

1.5.4 Atypical/Nor98 scrapie in small ruminants

Active surveillance of TSEs in small ruminants such as sheep and goats has shown that atypical/Nor98 scrapie is present not only in many European countries but also in other parts of the world (Benestad *et al.* 2003; Buschmann *et al.* 2004; Cook 2007; Epstein *et al.* 2005; Everest *et al.* 2006). These atypical scrapie cases are characterized by lower molecular weight fragments of PrP^{Sc} following treatment with PK. While all classical scrapie cases have shown typical triplet bands migrating between 18 and 30 KDa (Benestad *et al.* 2008), the atypical/Nor98 scarpie cases can be characterized by lower molecular weight fragments of PrP^{Sc} migrating at 11 - 12 KDa (Arsac *et al.* 2007; Benestad *et al.* 2003) or at 7 - 8 KDa (Klingeborn *et al.* 2006). In a transmission study to transgenic mice expressing ovine PrP (Le *et al.* 2005), the atypical scrapie isolates were found to share unique biological and biochemical features which are different from those of classical scrapie. Currently, atypical/Nor98 scrapie is considered as a prion strain affecting small ruminants that is distinct from classical scrapie or BSE in sheep (Benestad *et al.* 2008).

1.5.5 Atypical bovine prion diseases

Similar to the finding of atypical/Nor98 scrapie in small ruminants, large scale of active BSE surveillance has identified two novel forms of TSE in cattle. These atypical forms of TSE cases in cattle were distinguishable from classical BSE by the Western blot molecular features of PrP^{res}. A French study identified three cattle showing a higher molecular weight of unglycosylated form of PrP^{res} when compared to classical BSE (H-type)(Biacabe *et al.* 2004). Another form of bovine prion disease was first described in two cattle in Italy in which an unglycosylated PrP^{res} migrated slightly faster than that of classical BSE and monoglycosylated form of PrP^{res} predominated (L-type)(Casalone *et al.* 2004); these L-type cases were also characterized by the presence of amyloid plaques leading to the term bovine

amyloidotic spongiform encephalopathy (BASE). Since then, cases of the two novel forms of prion diseases in cattle have also been found in other European countries and in North America (Buschmann *et al.* 2006; Nicholson *et al.* 2008; Polak *et al.* 2008). Prions in the brains of cattle affected by BASE could be efficiently transmitted to transgenic mice expressing human PrP (Kong *et al.* 2008). When BASE strain was serially passaged in wild-type mice, lesion profile and PrP^{res} signature in the recipient mice was indistinguishable from those of BSE-infected mice (Capobianco *et al.* 2007).

1.6 Human prion diseases

Human prion diseases are a group of fatal neurodegenerative disorders including a wide spectrum of clinical and neuropathological phenotypes and can occur as sporadic, acquired and familial (genetic) forms (Table 1.2)(Gambetti *et al.* 2003; Ironside and Head 2004; Wadsworth *et al.* 2003). The sporadic form of human prion diseases encompasses two phenotypes: sporadic CJD and sporadic fatal insomnia (sFI). Additionally, a new phenotype of prion disease named protease-sensitive prionopathy (PSPr) was identified recently (Gambetti *et al.* 2008). Acquired forms of human prion disease can be caused by human-to-human transmission (iatrogenic CJD and kuru) or animal-to-human transmission (vCJD) of the infectious agent. Familial (or genetic) forms of prion diseases are associated with pathogenic and insertional mutations in the *PRNP* and include familial CJD (fCJD), GSS and FFI.

Table 1.2 Classification of human prion disease

Aetiology	Disease	Remarks
Idiopathic	Sporadic CJD	
	Sporadic fatal insomnia	
	Protease sensitive prionopathy	
Acquired	Variant CJD	Bovine source
	Iatrogenic CJD	Human source
	Kuru	Human source
Familial (Genetic)	Familial CJD	E200K, D178N-129V
	Fatal familial insomnia	D178N-129M
	Gerstmann-Straussler-Scheinker disease	P102L, A117V, F198S

1.6.1 Sporadic prion disease: sCJD and sFI

sCJD is the most common form of human prion disease, accounting for around 85% of cases of human prion disease (Brown *et al.* 1987). sCJD occurs worldwide with an incidence of approximately one to two cases per million of the population per annum (Ladogana *et al.* 2005). This incidence rate is even across a wide range of countries, although slightly higher incidence of sCJD was reported in Switzerland in recent years (Glatzel *et al.* 2002; Glatzel *et al.* 2003). sCJD is an idiopathic disorder in which its aetiology remains unknown, although somatic mutation or the spontaneous conversion of PrP^{C} into PrP^{Sc} as a rare stochastic event were proposed as a possible cause (Collinge 1997; Wadsworth *et al.* 2003).

sCJD is not a uniform disorder but exhibits a wide spectrum of clinical and neuropathological phenotype. The majority of sCJD cases are clinically characterized by a rapidly progressive dementia and myoclonus with disease duration of several months (Brown *et al.* 1994; Pocchiari *et al.* 2004). Atypical forms of sCJD include cases characterized by ataxia and longer disease duration (Gomori *et al.* 1973). sFI is characterized by insomnia and clinically indistinguishable from FFI (Parchi *et al.* 1999a). Spongiform change can be observed in most cases of sCJD with variability in its nature, regional distribution and degree of severity (Parchi *et al.* 1999b). While spongiform degeneration is made of fine vacuoles in the majority of cases, spongiform change composed of larger, occasionally confluent vacuoles characterize a small group of cases (Gambetti *et al.* 2003). Amyloid plaques are found usually in the cerebellum in a less common subtype of sCJD cases (Kovacs and Budka 2009). sFI exhibits major pathology in the thalamus that is characterized by severe neuronal loss and astrogliosis without spongiform change (Parchi *et al.* 1999a). The immunostaining of PrP^{Sc} after specific treatment of sections shows several deposition patterns of PrP^{Sc} including: synaptic deposition, perivacuolar deposition, plaques and perineuronal staining (Ironside *et al.* 2005; Kovacs *et al.* 2002a). Perivacuolar staining of PrP is usually observed in the rim of larger, confluent type of vacuoles (Parchi *et al.* 1996). Perineuronal staining of PrP is detected in a minority of cases of

sCJD (Kovacs *et al.* 2002a). In sFI, the PrP^{Sc} level is much lower than in sCJD cases and immunostaining for PrP is either negative or minimal in limited brain areas (Gambetti *et al.* 2003; Parchi *et al.* 1999b).

The direct role of codon 129 of *PRNP* in determining disease phenotype was firstly recognized in the study of two inherited forms of prion disease which share a pathogenic mutation, but differ significantly in their clinical and pathological phenotypes (FFI: D178N-129M; fCJD: D178N-129V) (Goldfarb *et al.* 1992b). Individuals who are homozygotes at *PRNP* codon 129 were found to be over-presented in sporadic and acquired forms of CJD (Collinge *et al.* 1991; Palmer *et al.* 1991; Will *et al.* 1996; Windl *et al.* 1996). Heterozygosity at the polymorphic site codon 129 was shown to be associated with a particular pathological change - formation of amyloid plaques - in the cerebellum (Schulz-Schaeffer *et al.* 1996). Distinct PrP^{res} types were also associated with distinct disease phenotypes. PrP^{res} in the brains affected by FFI is of type 2, whereas PrP^{res} in fCJD with D178N is of type 1 (Monari *et al.* 1994). vCJD was able to be distinguished from various forms of sCJD on the basis of PrP^{res} type (Collinge *et al.* 1996).

Based on these findings, attempts were made to relate distinct phenotypes of sCJD with the *PRNP* codon 129 polymorphism (MM, MV, VV) and PrP^{res} type (type 1 and type 2). Parchi and colleagues classified 300 sCJD cases according to the PrP^{res} type and the codon 129 genotype, which results in six possible combinations: MM1, MM2, MV1, MV2, VV1 and VV2 (Table 1.3)(Parchi *et al.* 1999b). The individuals who are MM homozygous or MV heterozygous and carry type 1 PrP^{res} are combined into one subtype due to their similarity in clinical and neuropathological features (Gambetti *et al.* 2003; Parchi *et al.* 1999b); in comparison, the patients who are MM homozygous and carry type 2 PrP^{res} are classified into two subtypes according to distinct disease phenotypes: MM2 and sFI. Accordingly, sCJD is classified into six subtypes in the classification system proposed by Parchi and Gambetti. Another group of investigators have proposed an alternative classification system (Hill *et al.*

2003). When compared to that proposed by Parchi et al., the classification system proposed by Collinge and colleagues is based on three (rather than two) PrP^{res} types distinguished by electrophoretic mobility (Collinge *et al.* 1996; Hill *et al.* 2006; Wadsworth *et al.* 2008b). Despite this difference, however, both systems are in substance identical in that they classify sCJD cases based on the M/V polymorphism at codon 129 and the PrP^{res} type (Head and Ironside 2009). This study refers to as type 1 or type 2 PrP^{res} as defined by Parchi and Gambetti and accordingly follows their classification system.

One important issue in classifying sCJD cases is the presence of cases showing both PrP^{res} types. This phenomenon was initially identified in about 5% of patients affected by sCJD (Parchi *et al.* 1999b). The subsequent studies have confirmed that the co-occurrence of both PrP^{res} types is present in a substantial proportion of patients affected by sCJD (Head *et al.* 2004a; Puoti *et al.* 1999; Schoch *et al.* 2006; Uro-Coste *et al.* 2008). It was proposed that all sCJD cases associated with type 2 PrP^{res} as well as vCJD cases could contain type 1 PrP^{res} on the basis of mAbs specifically recognizing type 1 PrP^{res} only (Polymenidou *et al.* 2005; Yull *et al.* 2006). However, this finding was contested in a later study on a methodological background (Notari *et al.* 2007). Two recent studies that carried out an extensive investigation of this phenomenon has shown that the co-existence of PrP^{res} type is present in 30 ~ 40% of sCJD cases and can be associated with patients who are clinically and/or neuropathologically distinguishable from those showing pure PrP^{res} types (Cali *et al.* 2009; Parchi *et al.* 2009b).

Recently, Gambetti et al. reported a novel form of human prion disease referred to as protease-sensitive prionopathy (PSPr)(Gambetti *et al.* 2008). The PSPr cases have shown distinct clinical and neuropathological features (Gambetti *et al.* 2008); all cases were homozygous for valine at codon 129 and did not have any pathogenic mutation in *PRNP*. Abnormal PrP associated with PSPr was found to be largely sensitive to PK digestion and less highly aggregated (Gambetti *et al.* 2008). More

interestingly, proteolytic treatment of PrP^{Sc} produced a "ladder-like" electrophoretic migration profile of PrP^{res} ranging from approximately 6 to 29KDa (Gambetti *et al.* 2008). Additional PSPr cases have been identified in the UK and in the Netherlands (Head *et al.* 2009a). The aetiology of this novel form of human prion disease is not known.

Table 1.3 Classification of sCJD based on genotype at codon 129 and PrP^{res} type (Parchi *et al.* 1999b)

sCJD subtype (codon 129 genotype /PrP^{res} type)	Previous classification	% of cases	Age at onset	Duration (months)	Clinical Features	Neuropathological Features
MM1, MV1	Classical CJD	70	65	4	Rapidly progressive dementia, early and prominent myoclonus	"Classical CJD" distribution of pathology; often prominent involvement of occipital cortex; "synaptic type" PrP staining
VV2	Ataxic variant	16	61.3	6.5	Ataxia at onset, late dementia	Prominent involvement of subcortical, including brain stem nuclei; in neocortex, spongiosis is often limited to deep layers; PrP staining shows plaque-like, focal deposits, as well as prominent perineuronal staining
MV2	Kuru-plaque variant	9	59.4	17.1	Ataxia in addition to progressive dementia, long duration (> 2 yr) in some cases	Similar to VV2 but with presence of amyloid-kuru plaques in the cerebellum, and more consistent plaque-like focal PrP deposits
MM2	Not established	2	64.3	15.7	Progressive dementia	Large confluent vacuoles with perivacuolar PrP staining in all cortical layers; cerebellum is relatively spared
VV1	Not established	1	39.3	15.3	Progressive dementia	Severe pathology in the cerebral cortex and striatum with sparing of brain stem nuclei and cerebellum; no large confluent vacuoles, and very faint synaptic PrP staining
sFI (MM2)	Thalamic variant of CJD	2	52.3	15.6	Insomnia and psychomotor hyperreactivity, in addition to ataxia and cognitive impairment	Prominent atrophy of the thalamus and inferior olive (no spongiosis) with little pathology in other areas; spongiosis may be absent or focal, and PrP^{Sc} is detected in lower amount than in the other variant

1.6.2 Variant CJD

In 1996, a new variant form of CJD (vCJD) was identified in 10 patients in the UK, raising a possibility that they might be causally linked to BSE (Will *et al.* 1996). Subsequent studies based on biological strain typing and biochemical analysis of PrP^{Sc} strongly supported this possibility (Bruce *et al.* 1997; Collinge *et al.* 1996; Hill *et al.* 1997; Lasmezas *et al.* 1996; Scott *et al.* 1999). Additionally, the highly characteristic neuropathological features seen in vCJD was not identified in the retrospective study of archived brain materials (Budka *et al.* 2002). It is now widely accepted that vCJD and BSE are caused by the same prion strain, most likely resulting from the consumption of BSE-contaminated meat products (Ward *et al.* 2006; Will 2003). So far, vCJD is the only known example of zoonotic human prion disease. As of March 2010, 172 cases of vCJD have been identified in the UK and 47 cases in other countries (http://www.cjd.ed.ac.uk).

vCJD has been identified mostly in young individuals. The mean age at onset is 28 years with a mean duration of illness of 15 months (Brandel *et al.* 2009; Will *et al.* 2000). All vCJD cases identified in the UK and France have been homozygous for methionine at *PRNP* codon 129 (Bishop *et al.* 2009; Brandel *et al.* 2009; Peden *et al.* 2010). One case of pre- or sub-clinical vCJD was identified in a patient with MV genotype at codon 129 (Peden *et al.* 2004). This patient had received a blood transfusion from a donor later found to be incubating vCJD, died from a non-neurological disorder, but infection with the vCJD agent was inferred from the accumulation of PrP^{res} in the spleen and lymph node (Peden *et al.* 2004). In 2009, a possible vCJD case was reported in a MV heterozygotes on the basis of ante-mortem examination (Kaski *et al.* 2009). In a large scale-study using anonymized human lymphoid samples, the accumulation of abnormal PrP was identified in the appendix of three individuals, two of which were later found to be homozygous for VV at *PRNP* codon 129 (Hilton *et al.* 2004; Ironside *et al.* 2006). Since the accumulation of abnormal PrP in lymphoreticular system is a consistent feature of vCJD in comparison with other forms of human prion diseases (Bruce *et al.* 2001; Head *et al.*

2004b; Hilton *et al.* 1998), this finding indicated the presence of asymptomatic carriers of vCJD, particularly individuals with MV or VV genotypes at codon 129 (Hilton 2006; Ironside *et al.* 2006). This possibility was further supported by a recent transmission study using gene-targeted human transgenic mice (Bishop *et al.* 2006). Collectively, individuals who are heterozygous or homozygous for valine at *PRNP* codon 129 appears to susceptible to vCJD/BSE prions, but may have more prolonged incubation periods compared to MM individuals (Ironside *et al.* 2006; Kaski *et al.* 2009). In kuru, another form of acquired prion disease in humans, individuals with MV or VV genotype were found to frequently have a longer incubation period (up to decades) and to develop disease at a later stage of the epidemic (Collinge *et al.* 2006; Collinge *et al.* 2008; Goldfarb *et al.* 2004).

The principal pathological change observed in vCJD-affected brains is the formation of florid plaques which can be readily identified on hematoxylin-eosin stains (Ironside *et al.* 2000). Florid plaques have an dense core with radiating fibrils in the periphery of the plaque which are surrounded by a rim of vacuoles (Ironside 1998; Will *et al.* 1996). Spongiform degeneration can be observed in various regions, but particularly severe in caudate nucleus and putamen (Ironside *et al.* 2000). Marked astrocytosis and neuronal loss in the thalamus is another diagnostic feature of vCJD (Ironside *et al.* 2000); interestingly, this region (pulvinar of the thalamus) is also characterized by bilateral high signal on magnetic resonance imaging (MRI) brain scans (Zeidler *et al.* 2000).

In Western blot analysis, the unglycosylated species of PrP^{res} from vCJD-affected brains migrates at ~ 19 KDa with its N-terminus predominantly at serine 97 (type 2 PrP^{res})(Parchi *et al.* 2000b). Additionally, PrP^{res} in vCJD is characterized by the predominance of diglycosylated form of PrP^{res}, which has been used as a molecular marker to distinguish vCJD from some forms of sCJD with type 2 PrP^{res} (Collinge *et al.* 1996; Head *et al.* 2004a). Recent studies employing an antibody whose epitope lies between type 1 and type 2 N-termini have shown that type 1 PrP^{res} is present at

low levels in vCJD brains (Yull *et al.* 2006; Yull *et al.* 2009), although technical validity of this kind of approach was questioned by Notari et al. (Notari *et al.* 2007).

BSE in sheep and scrapie were found to be efficiently transmitted to sheep by blood transfusion even when donor sheep were in preclinical stage of infection, raising concerns about the potential risk of iatrogenic transmission associated with preclinical vCJD carriers (Houston *et al.* 2000; Houston *et al.* 2008; Hunter *et al.* 2002). To date, four cases of secondary (human-to-human) infection of vCJD via blood transfusion have been identified. While three of the four patients with MM genotype at codon 129 developed clinical symptoms and died of vCJD (Health Protection Agency. 2007; Llewelyn *et al.* 2004; Wroe *et al.* 2006), one patient with MV genotype died in a preclinical phase without any evidence of a neurological disorder (Peden *et al.* 2004). Three donors developed vCJD signs after 17 months to three and a half years of their blood donation; two secondary vCJD patients were associated with a common donor (Health Protection Agency. 2007). The biological strain properties of the vCJD (or BSE) agent were found not to be altered in the secondary human-to-human transmission (Bishop *et al.* 2008). Similarly, neuropathological features and PrP^{res} profiles in the secondary cases were indistinguishable from those of primary cases (Head *et al.* 2009b; Wroe *et al.* 2006).

1.6.3 Other forms of acquired human prion disease: kuru and iCJD

Kuru is an epidemic prion disease which affected the Fore population and its neighbouring population in the Eastern Highlands of Papua New Guinea (Gajdusek and ZIGAS 1957; Gajdusek and ZIGAS 1959). More than 3,000 cases of kuru are thought to have occurred (Goldfarb 2002); the majority of kuru cases have been detected in women and children. The most probable route of spread of kuru is the ritual cannibalistic consumption of dead relatives (Gajdusek 1977). Kuru epidemic is presumably believed to be initiated by the cannibalistic consumption of an individual who died of sCJD (Gajdusek 1977). This proposition is strengthened by a recent study showing similar transmission properties between kuru and sCJD (Wadsworth

et al. 2008b). Since cannibalism was outlawed in the late 1950s, the occurrence has declined gradually and the age of onset has increased progressively (Gajdusek 1977; Goldfarb *et al.* 2004). Kuru is the first form of human prion disease whose transmissibility was experimentally proven (Gajdusek *et al.* 1967; Gajdusek *et al.* 1968; Gajdusek *et al.* 1966), followed by success in transmitting other members of human prion disease (Gibbs, Jr. *et al.* 1968; Masters *et al.* 1981; Tateishi *et al.* 1995). Kuru is characterized clinically by a progressive cerebellum disease (Gajdusek and ZIGAS 1957; Gajdusek and ZIGAS 1959), and its incubation period may reach five decades given that small number of cases (mostly MV genotype) are still occurring (Collinge *et al.* 2006).

Iatrogenic CJD (iCJD) is an acquired form of human prion disease which is accidentally transmitted during the course of medical or surgical procedures (Aguzzi *et al.* 2008). The first case of iCJD was reported in 1974 in association with transplantation of a cornea derived from a donor who had died of CJD (Duffy *et al.* 1974). Since then more than 400 cases of iCJD have been globally identified in association with accidental transmission of CJD prions (Will 2003). The majority of iCJD cases are associated with implantation of contaminated dura mater grafts (196 cases) or contaminated growth hormones derived from human cadavers (194 cases)(Brown *et al.* 2006). The mean incubation period is 11 years (range: 1.5 - 23 years) in dura mater-associated cases and 15 years (range: 4 - 36 years) in growth hormone-associated cases (Brown *et al.* 2006).

1.6.4 Familial (genetic) forms of human prion disease

About 10 - 15% of cases of human prion disease are associated with disease-specific mutations (Kovacs *et al.* 2005; Windl *et al.* 1996; Windl *et al.* 1999). So far, more than 30 pathogenic mutations in the *PRNP* have been identified, which can be divided into three types: point mutations resulting in an amino-acid substitution or premature stop codon, and insertion of additional octapeptide repeats (Mead 2006). They can be inherited in an autosomal-dominant manner, many of which show high

penetrance (the proportion of carriers who will eventually develop the disease)(Gambetti *et al.* 2003; Kovacs *et al.* 2005). Although it remains uncertain how pathogenic mutations in the *PRNP* lead to the development of prion disease, one possible explanation is that they may make it easier for PrP^{C} to be spontaneously converted into PrP^{Sc} (Wadsworth *et al.* 2003). It remains questionable whether all forms of familial prion disease are transmissible since some less frequent forms of GSS lack the evidence of transmissibility (Brown *et al.* 1994; Tateishi *et al.* 1996). Familial prion diseases present clinically with marked variability even between individuals carrying the same *PRNP* mutation (Barbanti *et al.* 1996; Collinge *et al.* 1992; Zarranz *et al.* 2005; Zerr *et al.* 1998). It is well known that polymorphism at codon 129 contribute to the phenotypic diversity of familial prion disease (Gambetti *et al.* 2003). Familial prion diseases can be classified into three phenotypes according to their clinical and pathological features: CJD, GSS and FFI.

In a sCJD-like phenotype called familial CJD (fCJD), clinical and pathological features are overall within the range of those of sCJD although marked variability between and within family groups carrying different mutations are also evident. The substitution of lysine (K) for glutamic acid (E) at codon 200 (E200K) in the *PRNP* is the most frequently observed pathogenic mutation in association with fCJD (Gambetti *et al.* 2003; Kovacs *et al.* 2005). The patients carrying the E200K mutation have been identified in various countries including: Chile, Italy, Slovakia and Jews of Israel (Chapman *et al.* 1994; D'Alessandro *et al.* 1998; Goldfarb *et al.* 1991; Lee *et al.* 1999; Spudich *et al.* 1995). Other point mutations in the *PRNP* associated with fCJD include D178N, V180I, T183A and V210I (Gambetti *et al.* 2003). While the patients who have the D178N mutation with valine at codon 129 on the mutant allele develop the disease phenotype of CJD, those who share this mutation but with methionine at codon 129 on the mutant allele develop the phenotype of FFI (Goldfarb *et al.* 1992b).

The phenotype of Gertsmann-Straussler-Scheinker Syndrome (GSS) was first described in 1936 in a large Austrian family, which was later found to be associated with proline-to-leucine substitution (P102L) in the *PRNP* (Kretzschmar *et al.* 1991). The disease onset occurs from the third to seventh decade of life with average disease duration of five to six years (Collins *et al.* 2001; Piccardo *et al.* 1998). The majority of patients with GSS phenotype present with slowly progressive cerebellar ataxia, accompanied by cognitive decline at a later stage of the disease progress (Collins *et al.* 2001); however, variation in clinical phenotype between family members carrying the same mutation can range from that of typical CJD to that of classic GSS (Goldfarb *et al.* 1992a; Hainfellner *et al.* 1995). On microscopic examination, GSS is characterized by the presence of multicenteric amyloid plaques (Kovacs and Budka 2009). Protease treatment of brain extracts from individuals affected with GSS yields proteolytic fragments of PrP^{Sc} of lower molecular weight (Parchi *et al.* 1998; Piccardo *et al.* 1998; Tagliavini *et al.* 2001). The P102L substitution is the commonest mutation associated with the GSS phenotype (Doh-ura *et al.* 1989; Hsiao *et al.* 1989). Other associated mutations include: P105L, A117V, Y145STOP, F198S (Collins *et al.* 2001).

The phenotype of fatal familial insomnia (FFI) was first described in 1986 (Lugaresi *et al.* 1986), which was later found to be a member of prion diseases (Medori *et al.* 1992). Patients with FFI present with progressive untreatable insomnia, autonomic dysfunction and motor signs (Almer *et al.* 1999; Medori *et al.* 1992). Thalamic degeneration accompanying marked neuronal loss and astrogliosis is prominent pathological changes in FFI (Gambetti *et al.* 2003). The unglycosylated species of PrP^{res} from brains affected with FFI migrates at ~ 19 KDa (type 2 PrP^{res}) in Western blot analysis (Monari *et al.* 1994). Additionally, PrP^{res} associated with FFI is characterized by a marked under-representation of the unglycosylated form (Parchi *et al.* 1995; Parchi *et al.* 1999a). The only known *PRNP* mutation linked to FFI is the D178N with methionine at codon 129 on the mutant allele (Goldfarb *et al.* 1992b); as described above, the patients with this mutation but valine at codon 129 on the

mutant allele develops the phenotype of fCJD. However, it has been questioned by several studies whether the phenotype determination of patients with D178N is fully relying on the codon 129 allelic polymorphism (McLean *et al.* 1997; Zerr *et al.* 1998).

1.7 Complicated biochemical properties of PrP^{Sc}

1.7.1 PK-sensitive isoform of PrP^{Sc}

Currently, the identification of PrP^{Sc} is the only unambiguous marker of prion infection. In the absence of a definitive PrP^{Sc}-specific antibody and given the poor understanding of PrP^{Sc} structure (Aguzzi and Calella 2009; Aguzzi and Polymenidou 2004), PrP^{Sc} has been most commonly distinguished from PrP^{C} by its partial resistance to proteolysis. In most forms of prion disease, PrP^{Sc} leaves an N-terminally truncated core fragments of PrP^{Sc} (PrP^{res}) under the condition in which PrP^{C} is fully degraded by PK (Bolton *et al.* 1982; Meyer *et al.* 1986); both N-terminally and C-terminally truncated smaller fragments of PrP^{Sc} are also detectable in several forms of prion disease including GSS and PSPr in humans and atypical scrapie in sheep (Gambetti *et al.* 2008; Klingeborn *et al.* 2006; Piccardo *et al.* 1998). For decades, the demonstration of PrP^{res} by immunological methods has been the basis of diagnosis of prion diseases.

However, recent studies have revealed that PK-sensitive isoform of PrP^{Sc} is present at substantial levels in the brains affected with prions. This unnoticed fraction of PrP^{Sc} was first argued for in a report describing conformation-dependent immunoassay (CDI)(Safar *et al.* 1998). It was found that the conformational rearrangement of PrP^{C} into PrP^{Sc} accompanies the burial of epitopes toward the N-terminal region of PrP (Peretz *et al.* 1997). It was found that the epitope of mAb 3F4 recognizing amino acids 108-111 of hamster PrP is not accessible in native PrP^{Sc} in contrast to PrP^{C} and becomes exposed after denaturation (Safar *et al.* 1998); Safar's CDI was developed in the form of direct ELISA employing this mAb as a detector antibody. In the CDI, time-resolved fluorescence (TRF) signals were similar between native and denatured samples of normal hamster brains containing only PrP^{C} (Safar *et al.* 1998). In contrast, CDI signals greatly increased after denaturation in the analysis of hamster brains infected with various laboratory prion strains (Safar *et al.* 1998); newly detected CDI signals after denaturation was thought to be mostly derived from PrP^{Sc}. Strikingly, when scrapie-infected hamster brains were assayed

by CDI following proteolysis, the newly detected signals after denaturation were greatly reduced implying the presence of PK-susceptible fraction of PrP^{Sc} (Safar *et al.* 1998). Moreover, eight prion strains could be distinguished by the ratio of PK-sensitive PrP^{Sc} to PK-resistant PrP^{Sc} (Safar *et al.* 1998).

Subsequently, Safar's CDI was improved into a sandwich format by incorporating a capture antibody named Mar-1 (Bellon *et al.* 2003). When PrP^{Sc} in CJD brain homogenates were enriched by precipitation with sodium phosphotungstate (NaPTA) and then assayed by the sandwich CDI, its sensitivity was similar to that of infectivity bioassay measured in transgenic mice (Bellon *et al.* 2003; Safar *et al.* 2005a). Furthermore, as much as 90% of PrP^{Sc} in brains affected with sCJD was found to be susceptible to PK digestion (Safar *et al.* 2005a). Similarly, a significant proportion of PrP^{Sc} in natural isolates of sheep scrapie was also found to be susceptible to PK in CDI analysis (Thackray *et al.* 2007a).

The biological significance of this PK-susceptible fraction of PrP^{Sc} was revealed in a recent study (Colby *et al.* 2010). Synthetic prions which were generated by polymerizing recombinant mouse PrP into amyloid fibers were shown to transmit disease without generating detectable PK-resistant PrP^{Sc} when inoculated into transgenic mice (Colby *et al.* 2010); intriguingly, serial transmission of these synthetic prion strains did not generate PK-resistant form of PrP^{Sc}. Moreover, spongiform degeneration in mice infected with synthetic prions containing only PK-susceptible PrP^{Sc} was more severe than those infected with synthetic prions associated with PK-resistant PrP^{Sc} (Colby *et al.* 2010). Nevertheless, in naturally occurring prion strains, it remains largely uncertain how much (or whether) PK-sensitive fraction of PrP^{Sc} contributes to the determination of biological disease properties such as infectivity, strain phenomenon and neurotoxicity. In several laboratory prion strains, PK-susceptible fraction of PrP^{Sc} was found not to be required in maintaining biological strain properties and biochemical properties of PrP^{Sc} (Bessen and Marsh 1994; Deleault *et al.* 2008). Additionally, the majority of

PK-sensitive fraction of PrP^{Sc} in the RML prion strain was not associated with prion infectivity when measured by scrapie cell assay (Cronier *et al.* 2008). In comparison, the incubation period of the Chandler prion strain was prolonged to some degree following proteolytic removal of PK-sensitive fraction of PrP^{Sc} (Shindoh *et al.* 2009).

1.7.2 Various sizes of PrP^{Sc} aggregates

In contrast to monomeric or dimeric PrP^{C} (Meyer *et al.* 2000; Pergami *et al.* 1996), PrP^{Sc} is present as polymers that often form amyloid plaques in the brain. A recent study has shown that PrP^{Sc} in scrapie-infected hamster brains constitutes a spectrum of aggregate sizes, ranging from small oligomers to large polymers (Tzaban *et al.* 2002). When the brain homogenates from prion-infected hamsters were fractionated by ultracentrifugation in 10 - 60% sucrose step gradient, PrP molecules spread throughout the sucrose gradient (Tzaban *et al.* 2002); in contrast, PrP molecules from the brains of normal hamsters were mostly found in the top few fractions. In an additional analysis using size exclusion chromatography, PrP^{Sc} was shown to form a spectrum of aggregation sizes ranging from smaller than 600 KDa to that of prion rods, which are known to be composed of as many as 1,000 PrP molecules (Prusiner *et al.* 1983; Tzaban *et al.* 2002). Interestingly, PrP^{Sc} species of lower molecular mass which were recovered in the intermediate fractions of the sucrose gradient were found to be susceptible to protease digestion (Tzaban *et al.* 2002). Similarly, PrP^{Sc} molecules in mouse-adapted scrapie strains also dispersed throughout the 10 - 60% gradient after ultracentrifugation (Pan *et al.* 2004; Pan *et al.* 2005a; Pan *et al.* 2005c). A significant proportion of PrP molecules in various subtypes of sCJD was recovered in the bottom heavy fractions of the 10 - 60% gradient after ultracentrifugation, whereas the majority of PrP molecules in GSS associated with A117V mutation and in PSPr failed to sediment in the same condition of velocity sedimentation (Cali *et al.* 2006; Gambetti *et al.* 2008; Yuan *et al.* 2006).

The biological significance of size of PrP^{Sc} aggregates in prion disease was revealed by Caughey and colleagues in a recent study (Silveira *et al.* 2005). In this study,

highly purified PrP^{res} molecules from scrapie-infected hamster brains was first sonicated to generate various sizes of PrP^{res} and then fractionated according to their size. The analysis of these fractions revealed that, in respect to PrP content, prion infectivity and converting activity of PrP^{res} peaked in small oligomeric species of PrP^{res} of 300 - 600 KDa (Silveira *et al.* 2005); in comparison, these activities were substantially lower in smaller particles or larger aggregates of PrP^{res}.

1.7.3 Conformational stability of PrP^{Sc}

Protein conformation can be investigated by measurements of conformational stability after exposure to a denaturant (such as GdnHCl) in an appropriate range of concentrations (Shirley 1995). Based on this concept, Prusiner and co-workers developed the conformation stability assay (CSA) in order to investigate the conformation of PrP^{Sc} from different laboratory prion strains (Peretz *et al.* 2001; Peretz *et al.* 2002). In CSA, aliquots of brain homogenates containing PrP^{Sc} are first exposed to increasing concentrations of GdnHCl and then digested with PK. A fraction of PrP^{Sc} which becomes susceptible to proteolytic degradation following incubation with GdnHCl at a particular concentration is considered to be denatured by the concentration of GdnHCl (Peretz *et al.* 2001); the relative conformational stability of PrP^{Sc} is expressed as the concentration of GdnHCl required to render half of PrP^{Sc} molecules susceptible to PK ($GdnHCl_{1/2}$ value).

Prion strains which were indistinguishable by electrophoretical mobility of PrP^{res} in Western blot analysis could be discriminated by the conformational stability of PrP^{Sc} (or PrP^{res})(Peretz *et al.* 2001; Peretz *et al.* 2002). PrP^{Sc} in transgenic mice propagating synthetic prions was found to be conformationally far more stable than that of commonly used RML strain (Legname *et al.* 2005). In a subsequent study, a positive correlation between higher stability (as judged by $GdnHCl_{1/2}$ values measured by CSA) and longer incubation periods was found (Legname *et al.* 2006). The hypothesis that incubation time is a function of PrP^{Sc} stability was further tested by artificially producing an array of synthetic PrP amyloids differing in their

conformational stability and then testing their biological properties (Colby *et al.* 2009). The results confirmed that a more labile PrP^{Sc} conformation correlated with faster replication, shorter incubation periods and a degree of strain instability (Colby *et al.* 2009).

1.8 Biochemical approaches for PrP^{Sc} analysis

In the absence of a foreign nucleic acid genome associated with prion diseases, efforts to provide a molecular basis for the biological diversity of prions have focused on the biochemical characterization of disease-associated prion protein (PrP^{Sc}). PrP^{Sc} has been traditionally analysed by conventional Western blot (WB) following limited proteolysis. The WB analysis of proteolytic fragments of PrP^{Sc} produces information on electrophoretic mobility and glycoform ratio of PrP^{res}. Occasionally, two-dimensional (2D) gel electrophoresis in which proteins are separated based on their size and charge has been used to characterize PrP^{Sc} (Pan *et al.* 2005b; Pan *et al.* 2001; Zanusso *et al.* 2002). 2D gel electrophoresis was reported to differentiate between MM2 subtype of sCJD and sporadic form of fatal insomnia, which is not distinguishable based on conventional one-dimensional gel electrophoresis (Pan *et al.* 2001). However, variation between gels remains a problematic issue in the 2D gel electrophoresis (Huzarewich *et al.* 2010). The precise proteolytic cleavage sites of PrP^{Sc} can be determined using mass spectrometry (Dagdanova *et al.* 2010; Tagliavini *et al.* 2001) or by automated Edman degradation (Parchi *et al.* 2000b; Xie *et al.* 2006). Despite its diagnostic usefulness, however, protease-resistant core fragment size is at best a surrogate marker of conformation of PrP^{Sc} and size classes present in this polydispersed material is not taken account. Another important limitation in the analysis of PK-resistant PrP^{Sc} is the failure to take account of PK-sensitive of PrP^{Sc}.

The key event that occurs in prion-affected individuals is the conversion of PrP^{C} into PrP^{Sc}, which mainly accumulates in the brain of affected individuals. Conformational variation of PrP^{Sc} has been proposed as a main strain determinant in order to explain strain phenomenon in prion diseases. A conformation-based assay was first reported by Safar and colleagues using hamster prion strains (Safar *et al.* 1998). Safar's conformation-dependent immunoassay (CDI) was further improved by introducing a capture antibody and NaPTA precipitation (Bellon *et al.* 2003; Safar *et al.* 2005a). Similar conformation-based immunoassays have been reported by other groups

(McCutcheon *et al.* 2005; Thackray *et al.* 2007a). Conformational variation of PrP^{Sc} between different prion strains has been investigated by measuring its stability (Peretz *et al.* 2001; Peretz *et al.* 2002). This assay named conformational stability assay (CSA) is able to distinguish some prion strains which are not distinguishable based on gel mobility of PrP^{res} (Peretz *et al.* 2001; Peretz *et al.* 2002).

Since PrP^{Sc} is a polydispersed aggregated molecule, its sedimentation property and size can be exploited not only to separate PrP^{Sc} from PrP^{C} but to understand biological properties of prions. Two hamster-adapted TME strains (HY and DY strains) showed distinct sedimentation properties after ultracentrifugation (Bessen and Marsh 1992a). Various traditional sizing methods such as size exclusion chromatography (Tzaban *et al.* 2002; Yuan *et al.* 2006), filtration (Caughey *et al.* 1995), ultracentrifugation in sucrose step gradient (Pastrana *et al.* 2006; Tzaban *et al.* 2002) have been used to investigate size class of PrP^{Sc}. Silveira and colleagues recently tried another kind of separation method named field flow fractionation (FFF) to overcome the pitfalls of these sizing methods in analysing large, insoluble protein aggregates (Silveira *et al.* 2006; Silveira *et al.* 2005). Given the recent findings regarding biological influence of PrP^{Sc} size (Kristiansen *et al.* 2007; Silveira *et al.* 2005; Simoneau *et al.* 2007; Tixador *et al.* 2010), it would be important to measure precise size classes of PrP^{Sc} in various prion strains and disease phenotypes

Prion propagation *in vivo* can be modelled using *in vitro* converting assay. Successful cell-free formation of protease-resistant prion protein was first reported by Caughey and colleagues (Kocisko *et al.* 1994). This conversion assay employing partially purified PrP^{res} and ^{35}S-labelled recombinant PrP^{C} has made a substantial contribution to our understanding of various issues including polymorphic effect in sheep scrapie (Bossers *et al.* 1997), molecular basis of prion strain (Bessen *et al.* 1995) and species barrier (Raymond *et al.* 1997; Raymond *et al.* 2000). More recently, another kind of *in vitro* converting assay named protein misfolding cyclic amplification (PMCA) was introduced by Soto and colleagues (Saborio *et al.* 2001). In PMCA, PrP^{Sc} in diseased

brain is diluted in normal brain homogenates and then subjected to repeated cycle of incubation and sonication (Castilla *et al.* 2006). PMCA has shown much higher conversion efficiency when compared to Caughey's assay and is thought to more closely mimic *in vivo* prion propagation (Jones *et al.* 2010). Newly generated PrP^{Sc} by PMCA was found to be infectious (Castilla *et al.* 2005a) and to retain biological and biochemical strain properties (Castilla *et al.* 2008b; Soto *et al.* 2005). PrP^{Sc} in body fluids such as blood and urine can be successfully detected using PMCA (Castilla *et al.* 2005b; Chen *et al.* 2010; Gonzalez-Romero *et al.* 2008). Furthermore, PMCA can spontaneously generate PrP^{Sc} from normal brains of various species including humans (Barria *et al.* 2009). PMCA technique was successfully applied to human prion diseases such as vCJD (Jones *et al.* 2007; Jones *et al.* 2009b). In an assay named quaking induced conversion (QuIC), recombinant PrP was used as substrate instead of normal brain material and automated shaking replaced sonication (Atarashi *et al.* 2008; Orru *et al.* 2009).

Human prion agents are classified as Hazard Group 3 pathogen and required to be handled in Containment Level 3 (CL3) facility by Advisory Committee on Dangerous Pathogens classify (www.dh.gov.uk/ab/ACDP/index.htm). The requirement of CL3 can act as a substantial technical constraining factor in analysing human prion disease, as was the case in this study. In this study, conformational (CDI and CSA) and sizing (sucrose density gradient) methods in addition to conventional WB, which are available in CL3 laboratory within NSCJDU, were employed for the biochemical analysis of PrP^{Sc}.

1.9 Aims

In CJD, the biochemical characterization of PrP^{Sc} is currently largely based on the Western blot analysis of PK-resistant core fragments of PrP^{Sc} (PrP^{res}). Given the recent progress toward a better biochemical characterization of PrP^{Sc} (as described in section 1.7), it becomes evident that the Western blot analysis of PrP^{res} is an incomplete description of biochemical diversity of PrP^{Sc} present in CJD brains.

This study aims to investigate the biochemical properties of PrP^{Sc} in CJD brains by employing approaches that differ in principle from conventional Western blot analysis of PrP^{res}, and thus to provide a more complete description of PrP^{Sc} species occurring in the human brains affected by prions. These biochemical assays include conformation-dependent immunoassay (CDI), velocity sedimentation in sucrose step gradients, gradual unfolding of PrP^{Sc} mediated by exposure to a wide range of concentration of GdnHCl. This thesis addresses the following three specific aims:

1. To compare abnormal PrP defined by a conformation change (CDI) with that defined by resistance to limited proteolysis (WB) (Chapter 2).

2. To investigate the distribution profiles of different PrP (PrP^{C}, PrP^{Sc} and PrP^{res}) conformers after velocity sedimentation in sucrose step gradients (Chapter 3).

3. To measure the conformational stability of PrP^{Sc} to GdnHCl-induced denaturation using conformation-sensitive mAb 3F4 in CDI (Chapter 4).

CHAPTER 2

Abnormal prion protein in CJD brains: comparison of a conformational change with resistance to limited proteolysis

2.1 Introduction

Prion diseases are characterized by the conversion of the host-encoded prion protein (PrP^{C}) into a disease-associated isoform (PrP^{Sc}), which is thought to be the main component of the infectious agent or prion (Bolton *et al.* 1982; Prusiner 1982; Prusiner 1998). The conversion of α-helical PrP^{C} into ß-sheet-rich PrP^{Sc} accompanies the change of biochemical properties such as protease resistance or detergent solubility (Caughey *et al.* 1991; Meyer *et al.* 1986; Pan *et al.* 1993). In the absence of a definitive PrP^{Sc}-specific antibody, PrP^{Sc} has been distinguished from PrP^{C} based on these biochemical properties. The proteolytic treatment of PrP^{Sc} leaves N-terminally truncated, PK-resistant core fragments of PrP^{Sc} (PrP^{res})(Oesch *et al.* 1985). The presence of PrP^{Sc} in a sample has been most commonly demonstrated by detecting PrP^{res}, usually in Western blot after limited proteolysis. In CJD, two distinct types of PrP^{res} have been identified on the basis of the sizes of PK-resistant fragments (type 1 and type 2); a nonglycosylated fragment of type 1 PrP^{res} migrates at 21 KDa, whereas that of type 2 PrP^{res} migrates at 19 KDa (Parchi *et al.* 1996). Additionally, PrP^{res} can be classified into two types based on the proportion of the three possible glycoforms (type A and type B)(Parchi *et al.* 1997; Parchi *et al.* 2000b). All vCJD cases can be characterized by the type 2 PrP^{res} with high glycosylation site occupancy (type 2B), which can be distinguished from type 2 PrP^{res} in sCJD cases usually predominated by the monoglycosylated form (Collinge *et al.* 1996; Head *et al.* 2004a; Parchi *et al.* 1999b; Parchi *et al.* 1996). The type of PrP^{res} in combination with genotype at *PRNP* codon 129 have been the molecular basis in the classification of sCJD (Parchi *et al.* 1999b).

Another biochemical method that distinguishes PrP^{Sc} from PrP^{C} is conformation-dependent immunoassay (CDI), which is based on a conformational transition in the N-terminus of PrP during the formation of PrP^{Sc} (Peretz *et al.* 1997). CDI was initially developed in the form of direct ELISA using the mAb 3F4 that binds to amino acids 109 -112 of human PrP (Safar *et al.* 1998). The introduction of NaPTA

precipitation and incorporation of a capture antibody into CDI greatly increased the sensitivity in detecting PrP^{Sc} (Bellon *et al.* 2003; Safar *et al.* 2002; Safar *et al.* 2005a). Interestingly, CDI has revealed that a significant portion of PrP^{Sc} in the brains of scrapie-infected hamsters is susceptible to PK digestion (Safar *et al.* 1998); in a subsequent study, as much as 90% of PrP^{Sc} present in the brains of humans affected with CJD was estimated to be PK-sensitive (Safar *et al.* 2005a). Moreover, CDI was reportedly able to distinguish various prion strains propagated in hamsters based on the ratio of PK-resistant PrP^{Sc} to PK-sensitive PrP^{Sc} (Safar *et al.* 1998).

In this chapter, multiple samples from various CJD phenotypes were comparatively examined by CDI or WB following limited proteolysis, in order to investigate the relation between the inaccessibility of the 3F4 binding site and resistance to limited proteolysis, both of which define PrP^{Sc} biochemically. Three vCJD cases and 12 sCJD cases (three cases each from MM1, MM2, MV1 and MV2 subtypes) were investigated by the two biochemical methods; in each case, three samples (each of ~100mg) were taken each from the frontal cortex, cerebellum and thalamus and analysed separately (i.e. nine brain specimens in individual cases). The abnormal form of PrP determined by the two aforementioned biochemical methods were compared between CJD phenotypes, cases and regions (For clarity, hereafter, abnormal PrP with a hidden 3F4 epitope is termed "PrP^{Sc}" and abnormal PrP leaving PK-resistant core fragments after limited proteolysis is referred to as "PrP^{res}"). Additionally, adjacent samples of the three brain regions in individual cases were examined by histology to assess the correlation with the biochemical results.

2.2 Materials and methods

2.2.1 Laboratory requirement in handling human TSE material

The Advisory Committee on Dangerous Pathogens (ACDP) classifies TSE agents in various species as hazard group 3 (www.dh.gov.uk/ab/ACDP/index.htm). In prion-infected individuals, a high titre of prion infectivity is found in central nervous system (brain and spinal cord) and a lower level of infectivity is also present in peripheral nerve and/or in lymphoid tissue such as tonsil and spleen. The prion agents are not inactivated by conventional chemical and physical decontamination methods and exhibit exceptional stability against such treatments. The effective ways of prion decontamination recommended by the ACDP is to incubate infective material with 2M sodium hydroxide (NaOH) for 1 hour or with 20,000ppm sodium hypochlorite (NaClO) for 1 hour.

In this study, human brain material from diseased individuals of different phenotypes was analysed using various biochemical methods. The overall containment measures recommended by the ACDP when working with human prion agents are Containment Level 3 (CL3, with derogations). All laboratory work described in this thesis were performed in CL3 laboratory, which is located within the National CJD surveillance unit (NCJDSU). As required by the Lab code of Practice in NCJDSU, all laboratory procedures involving human TSE material was performed within a microbiological cabinet and decontamination of infective material was achieved by incubation with 2M NaOH for the minimum of one hour.

2.2.2 Human brain materials

2.2.2.1 Case selection criteria

In this study, brain material was obtained by submission of a tissue request to the National CJD Surveillance Unit Brain & Tissue Bank under the name of the primary supervisor (Dr. Mark W. Head).

Cases of human prion disease were selected based on the following criteria: 1) whether half-frozen brain is available; 2) whether consent for research use of brain material was obtained; 3) typical clinical and neuropathological presentation of disease phenotype of interest; 4) excluding CJD cases with mixed PrP^{res} type. Under these selection criteria, if available, priority was given to relatively recent cases which have presumably experienced fewer freezing/thawing cycles. When selecting cases, other parameters such as sex and post mortem interval were not usually considered due to the limited number of available cases.

2.2.2.2 Case details

Brain materials from 12 variant CJD (vCJD) cases, 22 sporadic cases (sCJD) cases and one GSS case with the *PRNP* P102L mutation were used in this chapter. Five non-CJD cases with other neurological disorders were used as controls. These cases were selected based on the availability of autopsy-collected frozen half brain specimens with consent for research use. Appropriate ethical approval was obtained for the research use of these brain materials. A definite diagnosis for these cases had been made by established criteria (Budka *et al.* 1995; Ironside *et al.* 2000). The codon 129 polymorphism of the *PRNP* of each case was determined by restriction fragment length polymorphism (Nurmi *et al.* 2003). The protease-resistant core fragments of PrP^{Sc} (PrP^{res}) found in brains were classified as type 1, 2A or 2B according to the nomenclature of Parchi and colleagues (Parchi *et al.* 1999b). All 13 vCJD cases were homozygous for methionine at the *PRNP* codon 129 genotype and had a type 2B PrP^{res} isotype in brain tissue (Table 2.1). The 22 sCJD cases comprised of 13 sCJD cases with MM genotype at codon 129 and a type 1 PrP^{res}, three cases with MM genotype and a type 2A PrP^{res}, three cases with MV genotype and a type 1 PrP^{res}, and three cases with MV genotype and a type 2A PrP^{res} (Table 2.2). One GSS case was homozygous for methionine at codon 129 with P102L mutation and had only small fragments of PrP^{res} (Table 2.3). The five non-CJD control cases were referred to the National CJD surveillance Unit suspected to be CJD, but received an alternative diagnosis, such as vascular dementia or Alzheimer's disease. Their final

diagnosis and genotype at *PRNP* codon 129 are described in Table 2.4. Variables such as sex, disease duration and post mortem interval were compared as a group between neurological controls, sCJD and vCJD cases (Table 2.5).

2.2.2.3 Brain samples for analysis

For CDI analysis, initially, around 100mg of frozen tissue was taken from grey matter-enriched frontal cortex (FC). In a group of CJD cases, triplicate samples were taken from frontal cortex, cerebellar cortex (Cb) and thalamus (Th). For the CJD cases in which multiple frozen tissues were taken from several brain regions, sections were taken from formalin-fixed, paraffin-embedded tissue blocks from the corresponding regions for immunohistochemistry.

Table 2.1 Clinical, genetic and biochemical information for vCJD cases

ID in this study	Sex	Age at onset	Duration (months)	codon 129 genotype	PrP^{res} type	Post mortem interval (days)
vCJD1	M	25	10	MM	2B	2
vCJD2	F	29	10	MM	2B	1
vCJD3	F	51	13	MM	2B	2
vCJD4[a]	M	18	13	MM	2B	2
vCJD5	M	25	10	MM	2B	2
vCJD6	F	28	9	MM	2B	3
vCJD7	M	26	11	MM	2B	4
vCJD8	M	32	17	MM	2B	2
vCJD9	F	17	13	MM	2B	1
vCJD10	M	19	11	MM	2B	3
vCJD11	M	35	15	MM	2B	4
vCJD12	M	33	12	MM	2B	5
vCJD13	M	29	7	MM	2B	4

Note a. This case was used only for stability study (Chapter 4).

Table 2.2 Clinical, genetic and biochemical information for sCJD cases

ID in this study	Sex	Age at onset	Duration (months)	codon 129 genotype	PrP^{res} type	Post mortem interval (days)
MM1-1	M	67	1	MM	1	5
MM1-2	M	79	4	MM	1	2
MM1-3[a]	F	57	24	MM	1	1
MM1-4	M	61	1	MM	1	5
MM1-5	F	78	3	MM	1	6
MM1-6	M	79	3	MM	1	2
MM1-7	M	77	1	MM	1	3
MM1-8	M	63	4	MM	1	4
MM1-9	M	74	2	MM	1	2
MM1-10	F	74	4	MM	1	10
MM1-11	F	74	3	MM	1	3
MM1-12	M	61	3	MM	1	3
MM1-13	M	73	3	MM	1	3
MM2-1	F	44	17	MM	2A	1
MM2-2	M	37	23	MM	2A	2
MM2-3	F	60	8	MM	2A	3
MV1-1	M	77	4	MV	1	4
MV1-2	M	74	3	MV	1	4
MV1-3	M	38	8	MV	1	4
MV2-1	F	60	14	MV	2A	4
MV2-2	M	72	7	MV	2A	7
MV2-3	M	65	9	MV	2A	4
VV2-1[b]	M	52	6	VV	2A	not available

Note a. This case is classified as the panencephalopathic variant of sporadic CJD.
b. This case was used only for stability study (Chapter 4).

Table 2.3 Clinical, genetic and biochemical information for GSS cases with P102L mutation

ID in this study	Sex	Age at onset	Duration (months)	codon 129 genotype	PrP^{res} type	Post mortem interval (days)
GSS1[a]	F	44	8	MM	1	3
GSS2	F	37	89	MM	small fragments only	9

Note a. This case was used only for stability study (Chapter 4).

Table 2.4 Clinical, genetic and biochemical information for neurological control cases

ID in this study	Sex	Age at onset	Duration (months)	codon 129 genotype	PrP^{res} type	Final diagnosis	Post mortem interval (days)
non-CJD1	F	70	2	MM	---	Vascular dementia.	1
non-CJD2	F	65	4	MV	---	Vascular dementia.	3
non-CJD3	M	69	13	VV	---	Lewy body dementia	4
non-CJD4	M	72	14	MM	---	Motor neurone disease	3
non-CJD5	F	80	4	MM	---	B cell lymphoma	4

Table 2.5 Variables of neurological control and CJD cases as a group

		Sex (M:F)	Age at onset[a] (years)	Disease duration[a] (months)	Post mortem interval[a] (days)
Neurological control (n=5)		2:3	71.2 ± 5.5 (65 - 80)	7.4 ± 5.6 (2 - 14)	3.0 ± 1.2 (1 - 4)
vCJD (n=13)		9:4	28.2 ± 8.9 (17 - 51)	8.9 ± 2.6 (7 - 17)	2.7 ± 1.3 (1 - 5)
sCJD	MM1 only[b] (n=12)	9:3	71.7 ± 6.9 (61 - 79)	2.7 ± 1.2 (1 - 4)	4.0 ± 2.3 (2 - 10)
	All sCJD cases (n=23)	16:7	65.0 ± 12.7 (37 - 79)	6.7 ± 6.6 (1 - 24)	3.7 ± 2.1 (1 - 10)

Note a. Values are mean ± S.D. with range in parentheses.

b. One MM1 sCJD case (MM1-3 in Table 2.2) which is also classified as the panencephalopathic variant of sporadic CJD is not included.

2.2.3 Methods

2.2.3.1 Conformation-dependent immunoassay (CDI)

2.2.3.1.1 History and methodological speculation

Conformation-dependent immunoassay (CDI) was first described by Safar and colleagues in 1998 (Safar *et al.* 1998). Based on the conformational rearrangement that occurs in the N-terminus of PrP during the conversion of PrP^{C} into PrP^{Sc}, Safar's CDI was in the form of direct ELISA using dissociation-enhanced time-resolved fluorescence (TRF) system (Safar *et al.* 1998). This CDI measured the immunoreactivity of an antibody named 3F4 whose epitope is accessible in PrP^{C}, but masked in native PrP^{Sc}; after denaturation PrP^{Sc} becomes accessible by mAb 3F4. While normal hamster brains containing only PrP^{C} showed similar level of TRF signals before and after denaturation, diseased brains exhibited great increase of fluorescence signals after denaturation (Safar *et al.* 1998); newly detected CDI signals after denaturation were thought to be mostly derived from PrP^{Sc}. Safar's CDI revealed that a proteinase K (PK)-sensitive isoform of PrP^{Sc} is present at a substantial level in scrapie-affected hamster brains. Interestingly, various hamster prion strains were distinguishable based on the ratio of PK-sensitive PrP^{Sc} to PK-resistant PrP^{Sc} (Safar *et al.* 1998). In addition, Safar and colleagues also identified selective precipitation of PrP^{Sc} by NaPTA, which increased the diagnostic sensitivity of CDI by being incorporated into the sample processing procedure (Safar *et al.* 1998).

Since the first description of CDI using hamster prion strains in 1998, various groups have reported improved versions of CDI with a similar format as follows: sandwich formatted ELISA, semi-purification of PrP^{Sc} using NaPTA precipitation and time-resolved fluorescence (TRF) detection system. In 2002, CDI was successfully applied as a diagnostic test for BSE with sensitivity being similar to that of animal bioassay measured in transgenic mice (Safar *et al.* 2002); since the mAb 3F4 recognizes only human and hamster prion protein (PrP), Safar *et al*. employed high-affinity recombinant antibody fragments reacting with bovine PrP. In the following year, human PrP^{Sc} in vCJD and sCJD brains were successfully detected by CDI

incorporating NaPTA precipitation in sample treatment (Bellon *et al.* 2003). Subsequently, using the same format of CDI as Bellon's, Safar *et al*. reported that as much as 90% of PrP^{Sc} in sCJD brain was susceptible to proteolysis (Safar *et al.* 2005a). More recently, CDI successfully detected vCJD PrP^{Sc} newly generated by PMCA (Jones *et al.* 2007). The existence of a substantial level of PK-sensitive PrP^{Sc} in natural sheep scrapie was also revealed by CDI (Thackray *et al.* 2007a).

Because CDI does not require proteolytic treatment to differentiate between PrP^{C} and PrP^{Sc}, a major advantage of this kind of assay is that both PK-sensitive and PK-resistant species of PrP^{Sc} can be measured. Given that the ratio of PK-sensitive PrP^{Sc} to PK-resistant PrP^{Sc} was found to be distinct between hamster prion strains and that PK-sensitive isoform of PrP^{Sc} may constitute as much as ~ 90% of PrP^{Sc} in sCJD, it would seem to be imperative to investigate both isoforms of PrP^{Sc} for a fuller understanding of prion disease. Another potential advantage that CDI has is that this assay allows the separate investigation of PrP^{C} from PrP^{Sc} in diseased brain. Although PrP^{C} has received relatively less attention when compared to PrP^{Sc}, its possible contribution to the pathologic effect of PrP^{Sc} raises the necessity for the investigation of PrP^{C} (Brandner *et al.* 1996; Mallucci *et al.* 2003; Rambold *et al.* 2008). One limitation of CDI is that this assay does not produce information on PrP^{res} such as its size or glycoform ratio. This limitation may be more pronounced in human prion disease given the importance of PrP^{res} type in distinguishing various disease phenotypes (Collinge *et al.* 1996; Hill *et al.* 2003; Parchi *et al.* 1999b)

Although CDI was initially developed based on the conformational difference between PrP^{C} and PrP^{Sc}, the selective precipitation of PrP^{Sc} using NaPTA has been widely employed in CDI as a sample treatment step in order to increase its diagnostic sensitivity. For the same reason, this semi-purification step of PrP^{Sc} has been occasionally performed in diagnostic Western blot, particularly in the test using peripheral tissue (Peden *et al.* 2010; Peden *et al.* 2006; Peden *et al.* 2007; Wadsworth *et al.* 2001). In this study, CDI was performed without NaPTA semi-purification step

for the following reasons: 1) this study is not designed for diagnostic purpose; 2) this study is intended to look at both PrP^{C} and PrP^{Sc} simultaneously; 3) only a small proportion of PrP^{C} is reported to be recovered by NaPTA precipitation (Wadsworth *et al.* 2001); 4) it is questionable whether NaPTA can precipitate all species of PrP^{Sc}, for example oligomeric species (Sasaki *et al.* 2009). Despite close similarity in CDI format between this study and previous studies (Bellon *et al.* 2003; Safar *et al.* 2005a), direct comparison of results (for example, the proportion of PK-sensitive PrP^{Sc}) between them may be limited given the above-stated points. Nonetheless, the composition of two PrP conformers present in CJD brains is believed to be more accurately measured using brain homogenates rather than using a particular fraction such as a NaPTA-precipitated one.

2.2.3.1.2 CDI procedures

Preparation of brain tissue

Brain homogenates were prepared in nine volumes (w/v) of phosphate-buffered saline (PBS), pH 7.4, containing 2% Sarcosyl by two cycles of homogenization in the FastPrep instrument (Qbiogene). Each cycle was run for 45 seconds at the speed of $6.5ms^{-1}$ with the interval of 10 minutes between the runs. The 10% brain homogenates were further diluted to 5% (w/v) using PBS containing 2% Sarcosyl (w/v) and were incubated for 10 minutes at room temperature on a shaking platform. The samples were then cleared by centrifugation at 500 × g for 5 minutes at 20°C and the supernatants were collected. The cleared samples were aliquoted and stored at -80°C until use. In some cases, the 5% brain homogenates were serially diluted by a factor of two before analysis.

Preparation of microtitre plate

A 96-well black microtitre plate (Fisher, DIS-942-010H) was incubated overnight at room temperature with 200µl/well 10µg/ml anti-PrP antibody MAR-1 (CSL Behring, Marburg, Germany) in bicarbonate-carbonate coating buffer. MAR-1 recognizes specifically human PrP with a correctly formed disulphide bridge. After overnight

incubation, the plate was washed four times with wash buffer (PerkinElmer) and then saturated with 0.5% (w/v) bovine serum albumin (BSA) and 6% Sorbitol (w/v) in wash buffer for 1 hour at room temperature on a plate shaker. Plates were washed four times with wash buffer immediately before loading samples.

Conformation-dependent immunoassay (CDI)

The conformation-dependent immunoassay (CDI) was performed as described previously with a few modifications (Bellon *et al.* 2003; Safar *et al.* 2005a). The 5% brain homogenates prepared in 2% Sarcosyl in PBS were split into two parts for CDI application. One part was mixed with the same volume of PBS containing Complete EDTA-free® protease inhibitors (native sample, N) and the other part was mixed with the same volume of 8M GdnHCl and incubated for 6 minutes at 81°C (denatured sample, D). Both N and D samples were adjusted using distilled water containing EDTA-free protease inhibitors to a final concentration of GdnHCl of 0.35M in 435µl final volume. Samples were then loaded in duplicate into the plate (200µl/well) coated with MAR-1. After incubating the plate for 2 hours at room temperature with shaking, the plate was washed four times with wash buffer. The detection of bound PrP was achieved by the europium $(Eu)^{3+}$ -labelled mAb 3F4 recognizing amino acids 109-112 of human PrP. The detector antibody diluted in assay buffer (PerkinElmer) at 50ng/ml was added to each well, followed by incubation for 2 hours at room temperature on a plate shaker. The plate was developed after six times washes followed by 5 minutes incubation in enhancement solution (PerkinElmer) at room temperature. The low pH of enhancement solution allows Eu^{3+} to become free from its chelation with the mAb 3F4. Subsequently, a highly fluorescent chelation is formed between the free Eu^{3+} and ligand in enhancement solution. The time-resolved fluorescent (TRF) signals, measured as cps (counts per seconds), were counted using a Victor 2 fluorometer (PerkinElmer). The flowchart of CDI is illustrated in Figure 2.1.

CDI D/N ratio and [D-N] value

TRF counts obtained from CDI were used to generate a D/N ratio and a [D-N] value (Safar *et al.* 1998; Safar *et al.* 2005a). The D/N ratios were obtained by dividing TRF counts of denatured samples (D) by the counts of the corresponding native samples (N). For the generation of [D-N] values, TRF counts measured in the native state were subtracted from those measured in the denatured state.

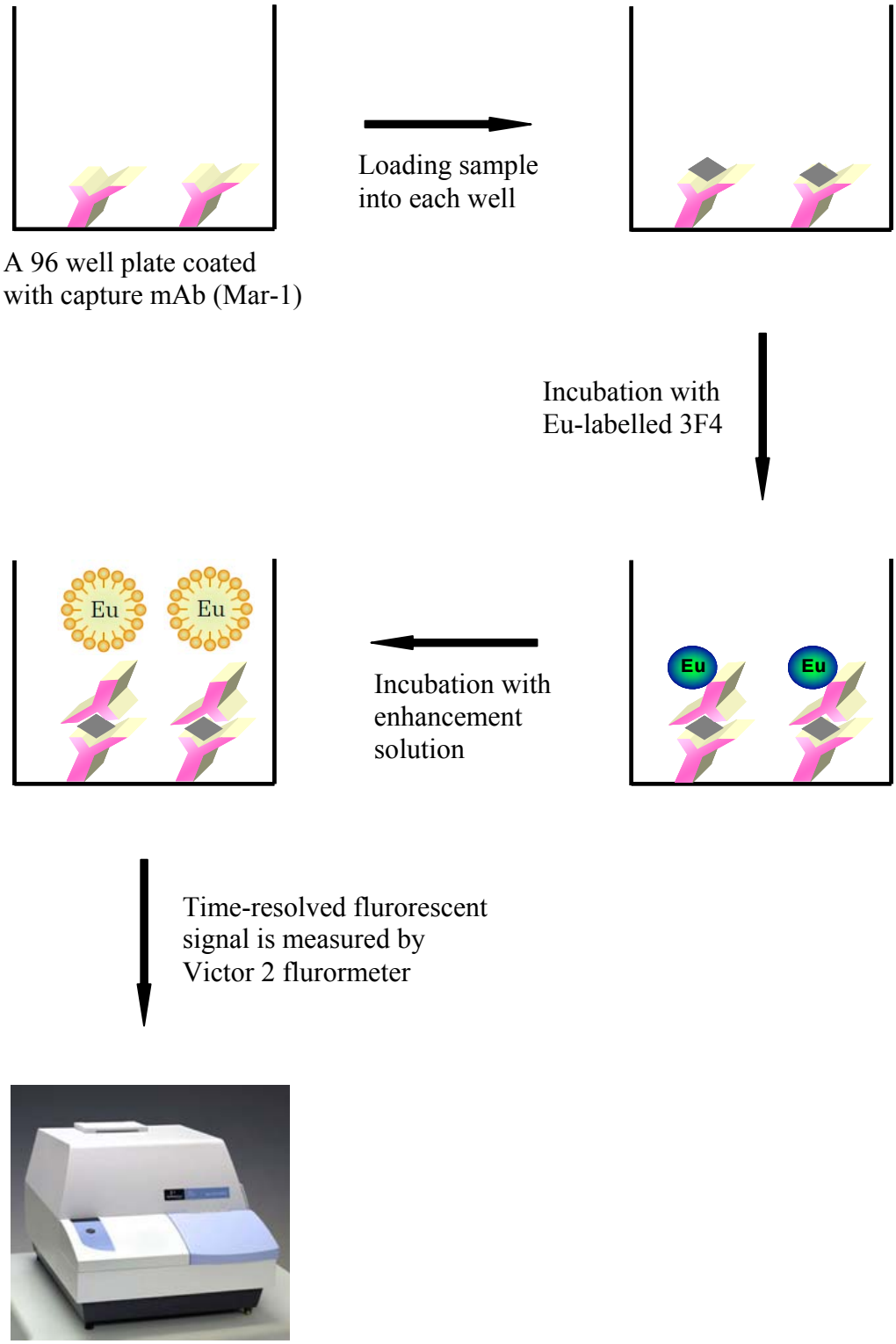

Figure 2.1 Diagram of conformation-dependent immunoassay.

2.2.3.2 Other methods

Western blot (WB) analysis of PrP^{res}

The analysis of PrP^{res} in brain tissue was conducted as described previously (Yull *et al.* 2009). The cleared 5% brain homogenates was digested with 50µg/ml PK for 1 hour at 37°C unless specified. PK activity was terminated by the addition of Pefabloc SC (Roche) to a final concentration of 1mM. Samples were mixed with NuPAGE LDS 4X sample buffer to a final concentration of 1X and then incubated for 10 minutes at 100°C. For the pellets obtained after methanol precipitation or centrifugation at 20,800 × g for 1 hour, proteins were resuspended with 25µl of 2X LDS sample buffer and boiled for 10 minutes. Samples were loaded onto a 10% Bis-Tris NuPAGE gel (Invitrogen) and then electrophoresed in MES buffer (Invitrogen) for 50 minutes at 200 volts. The separated proteins on the gel were transferred to polyvinylidene difluoride (PVDF) membrane (Hybond-P; Amersham) for 1 hour at 30 volts. The membrane was then blocked for 1 hour with 5% (w/v) non-fat dry milk in TBST (20mM Tris/HCl, pH 7.4, 150mM NaCl and 0.1% Tween 20). After three washes with TBST, the membrane was incubated with anti-PrP antibody 3F4 (Dako) at a final concentration of 75ng/ml IgG for 1 hour. The membrane was again washed three times with TBST and then incubated with horseradish peroxidase-conjugated anti-mouse IgG $F(ab')_2$ fragment (Amersham) at a dilution of 1 in 40,000 for 1 hour. Following five washes in TBST, blots were developed with ECL plus reagent (Amersham) and then exposed to X-ray film (Hyperfilm ECL; Amersham) for the periods of 30 seconds to 30 minutes. The molecular weight of PrP was determined by reference to IgG-binding MagicMark XP Western protein standards (Invitrogen). Films showing suitable exposures were scanned using a Bio-Rad GS-800 densitometer and quantitative analysis of the blots was performed using Quantity One Software (Bio-Rad Laboratories).

Protein precipitation by methanol

Samples left undigested or digested with various concentrations of PK were mixed with nine volumes of pre-chilled methanol followed by overnight incubation at

-80°C. Samples were then centrifuged at 16,000 × g for 30 minutes and the supernatants were carefully aspirated. Proteins in the pellet fractions were resuspended in sample buffer and analysed by Western blot as described above.

Enrichment of PrP^{res} by centrifugation

For the enrichment of PK-resistant fragments of PrP^{Sc}, samples of various volumes digested with 50µg/ml were centrifuged at 20,800 × g for 1 hour at 4°C as described previously (Head *et al.* 2004b). After careful aspiration of the supernatants, pellets were analysed by Western blot as described above.

Neuropathology

Serial sections were cut at 5µm from formalin-fixed, paraffin-embedded tissue blocks and then mounted onto Superfrost glass slides (Thermo Scientific). The sections were dried overnight in a 56°C incubator and then deparaffinised and were taken down to water followed by immersion into picric acid to remove formalin pigment. For routine staining, sections were stained with hematoxylin and eosin.

For PrP immunohistochemistry, sections treated with picric acid were blocked with 3% hydrogen peroxide in methanol for 30 minutes to prevent endogenous peroxidase from acting. Sections were then autoclaved at 121°C in distilled water for 10 minutes, followed by immersion in 96% formic acid for 5 minutes and then digestion with 10µg/ml PK for 5 minutes at room temperature. For PrP labelling, duplicate sections were incubated for 1 hour with the mAbs 3F4 (Dako) or KG9 (TSE Resource Center, Roslin institute) diluted in Novocastra IHC Diluent (Novocastra Laboratories Ltd). The mAb 3F4 was used at a dilution of 1:15 (final concentration: 5 µg/ml) and the mAb KG9 was used at a dilution of 1:1,000 (The mAb KG9 is not a commercial antibody and was obtained in the form of culture fluid. The dilution factors of both mAbs were in-house titrations in NSCJDU). The detection system used was the Novolink™ polymer kit from Leica Microsystems. Sections were incubated for 30 minutes with Post Primary Block, followed by incubation with Polymer Link for 30

minutes. PrP immunolabelling on the section was visualized using diaminobenzidine (DAB) followed by light counterstaining with hematoxylin.

* Note: The results on neuropathology were described in Appendix 1 (page 270 - 283).

2.3 Results

2.3.1 Analysis of brain homogenates by CDI without additional pre-treatment

The CDI in this study employed the mAb 3F4 recognizing amino acids 109-112 of human PrP as a detector. The epitope of the mAb 3F4, which is exposed in PrP^{C}, is hidden in PrP^{Sc} and becomes accessible upon denaturation (Kascsak *et al.* 1987; Peretz *et al.* 1997; Safar *et al.* 1998). Therefore, CDI signals obtained from native samples represent PrP^{C} and those obtained from denatured samples represent total PrP irrespective of their conformations (Safar *et al.* 1998). Since the newly detected PrP signals after denaturation are thought to be mainly derived from PrP^{Sc}, the difference of CDI signals between native and denatured aliquots (D-N) and/or the ratio of CDI signals between the two folding states (D/N) have been used as indicators for the presence of PrP^{Sc} (Bellon *et al.* 2003; Safar *et al.* 1998; Safar *et al.* 2005a). In this section, samples from CJD and control brains were assayed by CDI without additional treatment like NaPTA precipitation, and [D-N] values and D/N ratios were compared between CJD and non-CJD groups.

2.3.1.1 Non-CJD (neurological control) cases

Tissues of frontal cortex from five non-CJD control cases were investigated by CDI in the native and denatured states. The 5% brain homogenate was prepared as described in section 2.2.3 and split into two parts. While one part was mixed with same volume of PBS containing protease inhibitors and left without further treatment (native sample), the other part was heated at 81°C for 6 minutes after mixing with same volume of 8M GdnHCl (denatured sample). Both aliquots were diluted and adjusted to a final concentration of 0.35M GdnHCl and assayed by CDI.

The TRF counts obtained in the native state from neurological control brains were variable between cases, implying variable amounts of PrP^{C} between them (white bars in Figure 2.2a); after denaturation, slight increase of fluorescence signals was

observed in all cases (black bars in Figure 2.2a). The difference of TRF counts between the two different folding states ([D-N] value) was in the range of 13,000 ~ 46,000 with the average of 25,900 (Figure 2.1b). When the ratios of the TRF counts between native and denatured aliquots were generated (D/N ratios), they were in the range of 1.2 ~ 1.5 and were similar between cases (Figure 2.1c). The higher [D-N] values do not always mean higher D/N ratios because the levels of PrP^C were variable between cases. The D/N ratio was highest in non-CJD1(1) sample among those investigated in this study, whereas the [D-N] value was highest in the non-CJD2 sample (Figures 2.2b and 2.2c).

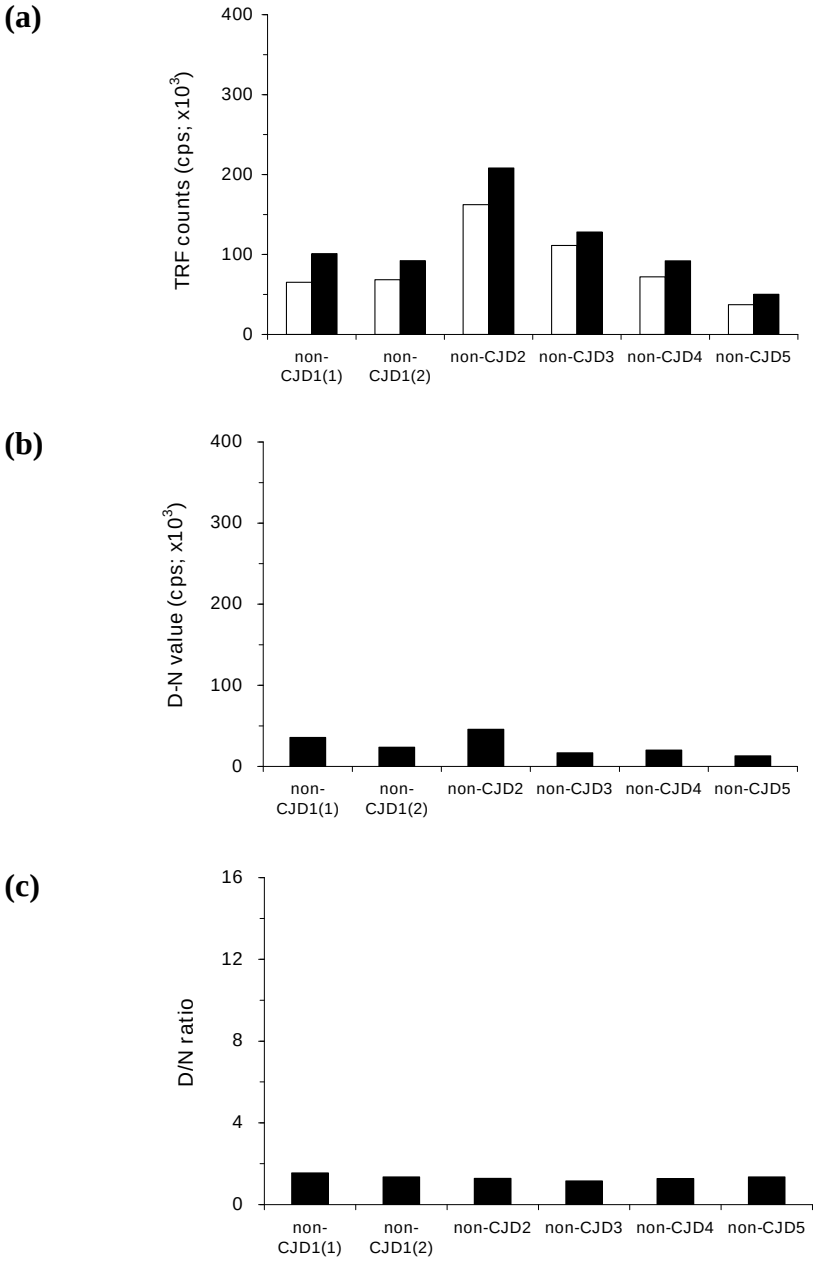

Figure 2.2 Comparison of CDI results between native and denatured states in non-CJD brains. Five cases of neurological controls were analysed by CDI using brain homogenates from tissues of frontal cortex. (a) Comparison of TRF counts measured in the native (white bars) and the denatured states (black bars) (b) [D-N] values in non-CJD brains. TRF counts of native samples were subtracted from those of corresponding denatured samples to give [D-N] values. (c) D/N ratios in non-CJD brains. TRF counts of denatured samples were divided by those of corresponding native samples to give D/N ratios. Data shown represent the average for duplicate wells.

2.3.1.2 vCJD cases

Tissues of frontal cortex from 12 vCJD cases were assayed by CDI in the native and denatured states. When the vCJD samples were analysed by CDI in the native state, the fluorescence signals were readily detectable in all vCJD cases and were broadly similar between cases (white bars in Figure 2.3a). Given that CDI fluorescence counts obtained from native samples represent PrP^C (Safar *et al.* 1998), readily detectable amounts of PrP^C were present in the vCJD-affected brains. The amounts of PrP^C were roughly similar between cases, accounting for a significant portion of total PrP. The levels of PrP^C in vCJD cases were largely within the range of those of neurological controls (Figure 2.2), despite great difference in the age of disease onset between the two groups (Table 2.5). Individuals that differ in other factors such as sex, disease duration and/or post mortem interval did not show any readily recognizable distinction in PrP^C levels.

Upon denaturation, significant increase of CDI TRF counts was observed in all 12 cases (black bars in Figure 2.3a). Although the differences of CDI signals between the native and denatured states were variable between cases, they can be easily distinguishable from those of non-CJD brains (Figure 2.3b). The [D-N] values were in the range of 100,000 ~ 260,000, except for two cases whose values were 62,000 (vCJD13) and 74,000 (vCJD10), respectively; even [D-N] values from these two cases were much higher than the average of those of neurological controls (average: 25,900). Since the increase of CDI TRF counts after denaturation in CJD brains was considered to be mainly derived from PrP^{Sc}, the variation in the [D-N] values between these vCJD samples appeared to reflect differences in the levels of PrP^{Sc}.

When the ratios of the TRF counts between native and denatured aliquots were generated (D/N ratios), they were in the range of 2.0 ~ 5.0, except for two cases whose ratios were 1.6 (vCJD13) and 1.9 (vCJD3), respectively (Figure 2.4c). The D/N ratios in all 12 cases including the two cases with low values were higher than those of control brains (average: 1.3). The samples with higher [D-N] values had

usually higher D/N ratios, but the difference in the D/N ratios between vCJD and neurological controls did not seem as distinct as that observed in the [D-N] values.

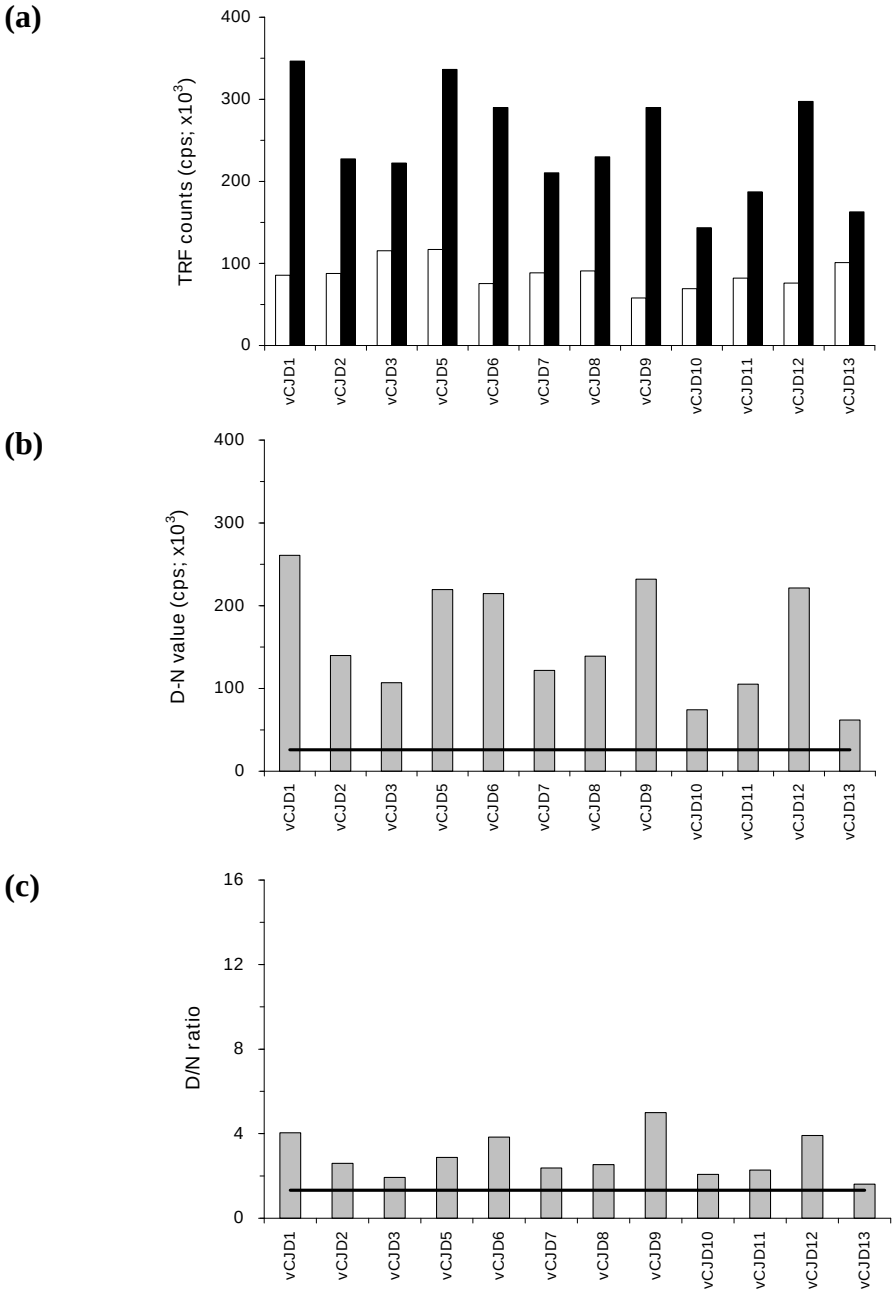

Figure 2.3 Comparison of CDI results between native and denatured states in vCJD brains. Twelve vCJD cases were analysed by CDI using brain homogenates from tissues of frontal cortex. (a) Comparison of TRF counts measured in the native (white bars) and the denatured states (black bars). (b) [D-N] values in vCJD brains, which were generated by subtracting TRF counts of native aliquots from those of corresponding denatured aliquots. (c) D/N ratios in vCJD brains, which were generated by dividing TRF counts of denatured aliquots by those of corresponding native aliquots. Solid lines in (b) and (c) represent the average [D-N] values and D/N ratios of non-CJD brains, respectively. Data shown represent the average for duplicate wells.

2.3.1.3 sCJD cases

For further analysis, tissues of frontal cortex from 13 MM1 sCJD cases were assayed by CDI. When the MM1 sCJD samples were analysed by CDI in the native state, the fluorescence signals were readily detectable in all cases despite significant variation between cases (white bars in Figure 2.4a). The levels of CDI signal in some cases (for example, MM1-4) were more than five times higher than those in others (for example, MM1-10). Since CDI fluorescence counts obtained from native samples represent PrP^C, this kind of variation was thought to reflect variable amounts of PrP^C between MM1 sCJD cases. While the level of PrP^C in four MM1 sCJD cases (MM1-2, 3, 6, 10) was recognizably lower than that of control even with lowest level, that of other MM1 cases was overall within the range of controls. The relatively low level of PrP^C in some MM1 cases did not appear to be directly associated with factors such as post mortem interval. For example, MM1-10 case with longest post mortem interval (10 days) among cases examined in this study showed PrP^C amount similar to MM1-2 or MM1-3 cases with one to two day post mortem interval. Moreover, MM1-6 was greatly shorter in disease duration than MM1-3 (3 months *versus* 24 months), but PrP^C level was not greatly different between the two cases. In comparison, PrP^C level in frontal cortex of one MM2 case (MM2-2) was approximately five times higher than MM1-3, despite their similarity in disease duration (23 months *versus* 24 months) (Figure 2.5c).

In denatured aliquots of those samples, significant increase of CDI signals was observed in most cases except for MM1-7 (black bars in Figure 2.4a). The [D-N] values were quite variable between cases and were in the range of 52,000 ~ 272,000, except for one case whose value was 34,000 (MM1-7) (Figure 2.4b). In case of MM1-7, the [D-N] value was higher than the average of non-CJD controls, but lower than that of non-CJD2 (average: 25,900, non-CJD2: 46,000). Similar to the vCJD-affected samples, the variation in the [D-N] values was thought to reflect difference in the level of PrP^{Sc}.

The D/N ratios of MM1 sCJD cases were in the range of 2.0 ~ 14.0, except for two cases whose ratios were 1.4 (MM1-7) and 1.9 (MM1-12) (Figure 2.4c). In case of MM1-7, the ratio was higher than the average of the non-CJD cases, but lower than that of non-CJD1(1) (average: 1.3, non-CJD1(1):1.5). In four MM1 cases, the D/N ratios were remarkably higher than those of other remaining MM1 cases or those of vCJD cases with the ratios around or over than 10 (MM1-2, 3, 6, 10 in Figure 2.4c). When compared to other MM1 cases, the CDI signals obtained in the native state from these four cases were quite low and their [D-N] values were relatively high (Figures 2.4a and 2.4b). In a similar context, the CDI signals of native aliquots from these four MM1 cases were much lower than vCJD cases showing similar levels of [D-N] values (for example, vCJD1 or vCJD5 in Figure 2.3b), resulting in significantly higher D/N rations than those vCJD cases. The samples with higher [D-N] values overall displayed higher D/N ratios, but the difference in the D/N ratios between MM1 sCJD and controls was not as distinct as that observed in [D-N] values.

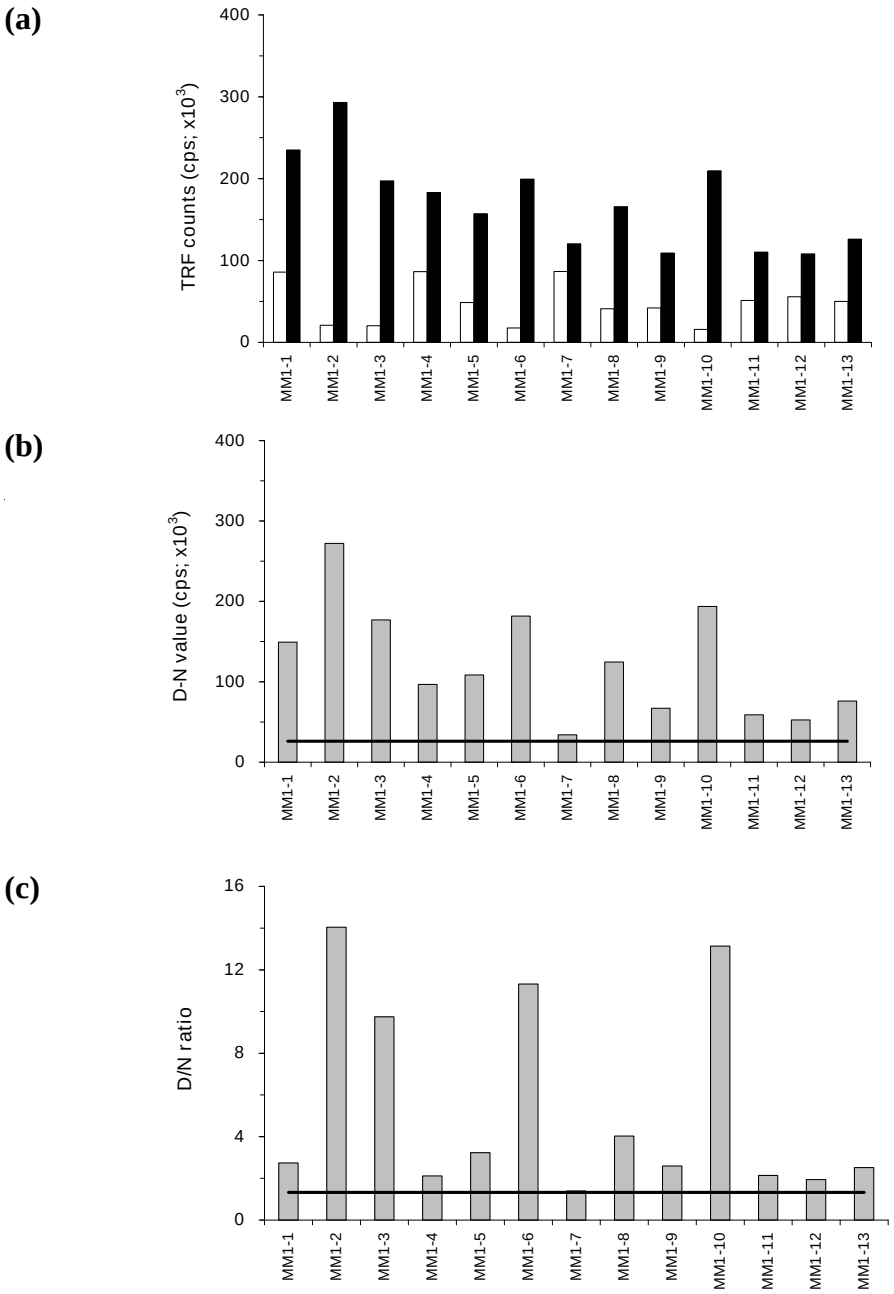

Figure 2.4 Comparison of CDI results between native and denatured states in MM1 sCJD brains. Thirteen MM1 sCJD cases were analysed by CDI using brain homogenates from tissues of frontal cortex. (a) Comparison of TRF counts measured in the native (white bars) and the denatured states (black bars). (b) [D-N] values in MM1 sCJD brains, which were generated by subtracting TRF counts of native aliquots from those of corresponding denatured aliquots. (c) D/N ratios in MM1 sCJD brains, which were generated by dividing TRF counts of denatured aliquots by those of corresponding native aliquots. Solid lines in (b) and (c) represent the average [D-N] values and D/N ratios of non-CJD brains, respectively. Data shown represent the average for duplicate wells.

2.3.2 PrP^{C} and PrP^{Sc} in CJD brains with different disease phenotypes

For further investigation of PrP^{C} and PrP^{Sc} in CJD brains, multiple samples from vCJD and sCJD (MM1, MM2, MV1 and MV2 subtypes) were investigated by CDI without any pre-treatment such as NaPTA precipitation or PK digestion. In each CJD phenotype, three cases were analysed using tissues of frontal cortex (FC), cerebellum (Cb) and thalamus (Th). Three samples (~ 100mg in each sample) were taken each from the three brain regions in individual cases (i.e. nine brain specimens per case), except for MM2 cases where six samples were taken in each region (i.e. 18 brain specimens per case). Thus, 27 samples (nine samples per case multiplied by three cases) were examined in each phenotype, except for MM2 sCJD in which 54 samples were assayed. In total, 162 brain samples from different CJD phenotypes were assayed by CDI, without pre-treatment such as NaPTA precipitation.

CDI fluorescent counts obtained from native samples were considered to represent PrP^{C}. In this section, CDI [D-N] value was used as a main indicator to estimate the amount of PrP^{Sc} in a sample, given that the level of PrP^{C} was variable between regions within individual brains or between cases and that CDI D/N ratios were significantly influenced by the amounts of PrP^{C} (see sections 2.3.1.3 and 2.3.2.1). CDI D/N ratios were mentioned occasionally where necessary. In order to compare the amount of PrP^{Sc} inferred from CDI [D-N] value with PrP^{res}, the same brain homogenates used for CDI analysis were examined by Western blot after limited proteolysis (For clarity, the abnormal form of PrP with buried 3F4 epitope is designated as "PrP^{Sc}" and abnormal PrP leaving PK-resistant core fragments after limited proteolysis is referred to as "PrP^{res}").

It is well known that direct comparison of PrP^{res} amounts between samples run on different gels is not valid due to the variations in the Western blotting process, antibody binding efficiencies, and/or differences in visualization reactions (Schoch *et al.* 2006; Yuan *et al.* 2006). In this study, nine samples from each case (three samples per region multiplied by three regions) were run on same gels and the comparison of

PrP^{res} amounts was considered only between the nine samples. Additionally, the quantitative analysis of PrP^{res} signals obtained in Western blot is further limited by narrow linear range in densitometry (for more details, see section 2.3.5.2).

2.3.2.1 PrP^C in CJD brains with different disease phenotypes

In sections 2.3.1.2 and 2.3.1.3, it was shown that PrP^C was readily detectable in FC tissues from vCJD and MM1 sCJD brains. For further analysis of PrP^C in CJD brains, multiple samples from vCJD and sCJD (MM1, MM2, MV1 and MV2 subtypes) were investigated by CDI. CDI fluorescent counts obtained from native aliquots were considered to represent PrP^C. Consistent with the results in sections 2.3.1.2 and 2.3.1.3, PrP^C was readily detectable in all examined CJD samples, but its amounts were variable between cases and regions (Figures 2.5 and 2.6). In vCJD, the levels of PrP^C in the frontal cortex were similar between the three cases (white bars in Figure 2.5a) and those in Cb or Th tissues were similar to or two-fold larger than FC (grey and black bars in Figure 2.5a). In sCJD brains, the levels of PrP^C were more variable between regions and/or cases (Figures 2.5b, 2.5c and 2.6) and it appeared to be difficult to find any consistent pattern reflecting distinct sCJD subtypes. While the levels of PrP^C in vCJD samples were overall within the range of PrP^C amounts identified in control samples, those from some sCJD samples were significantly lower than controls (see section 2.3.1.1).

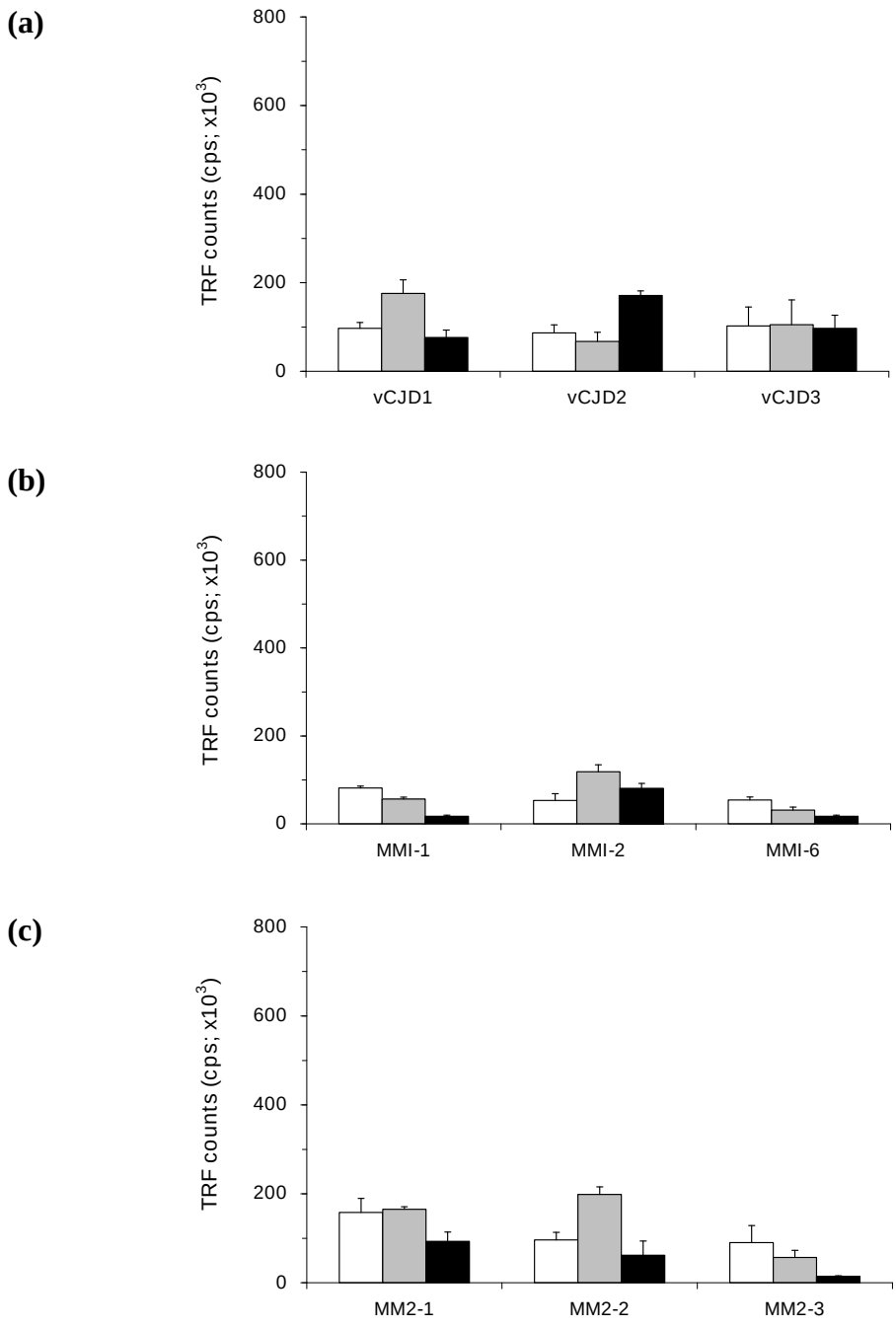

Figure 2.5 PrP^C in CJD brains with MM genotype at codon 129. Three cases each from vCJD (a), MM1 sCJD (b) and MM2 sCJD (c) were analysed using multiple tissues of frontal cortex (white bars), cerebellum (grey bars) and thalamus (black bars). The amount of PrP^C in each sample was investigated by CDI in the native state. In vCJD and MM1 sCJD, data shown represent the average ± S.D. of three samples. Data for MM2 cases were based on six samples in each region. The result in each sample was an average for duplicate wells.

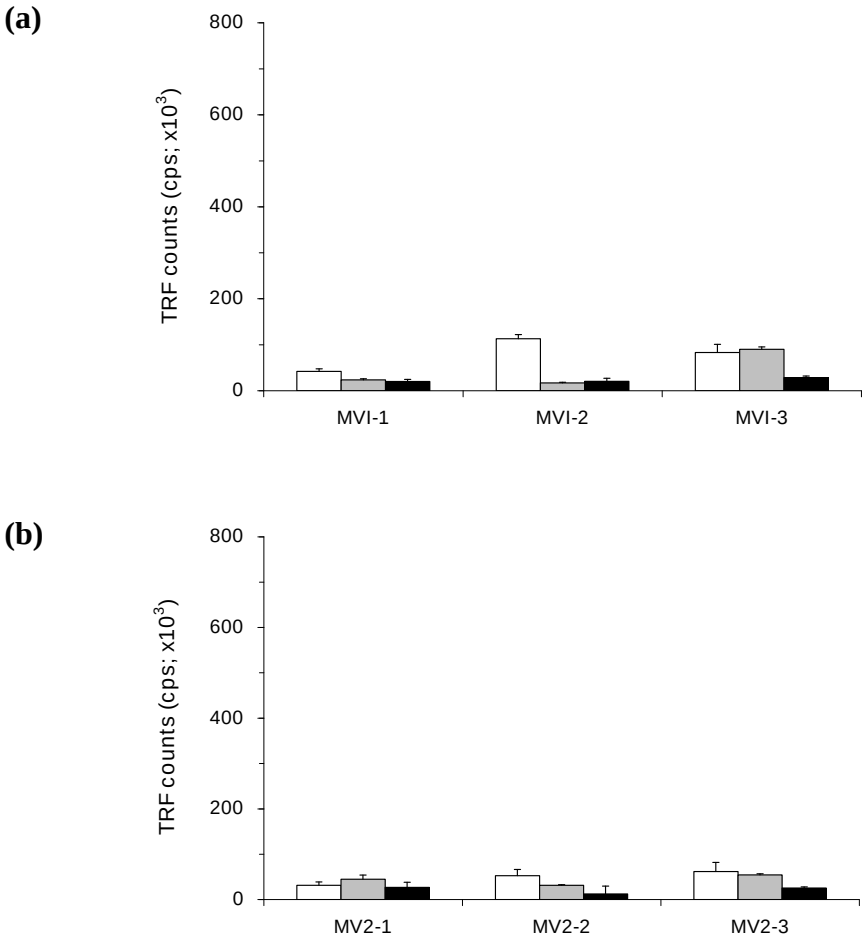

Figure 2.6 PrP^C in CJD brains with MV genotype at codon 129. Three cases each from MV1 sCJD (a) and MV2 sCJD (b) were analysed using triplicate tissues of frontal cortex (white bars), cerebellum (grey bars) and thalamus (black bars). The amount of PrP^C in each sample was investigated by CDI in the native state. Data shown represent the average ± S.D. of three samples. The result in each sample was an average for duplicate wells.

2.3.2.2 PrP^{Sc} in CJD brains: comparison of conformational change (CDI) with resistance to limited proteolysis (WB)

2.3.2.2.1 vCJD

In each region, [D-N] values were presented as an average of three samples. CDI [D-N] values in vCJD samples were usually significantly higher than the average of five controls shown as solid line (Figure 2.7a). In each case, the [D-N] value in cerebellum (Cb) was higher than those in frontal cortex (FC) or thalamus (Th), despite overlaps of standard deviations between cerebellum and thalamus (Figure 2.7a). In the cerebellum and thalamus, the levels of [D-N] value were roughly similar between the three vCJD cases (grey and black bars in Figure 2.7a). In comparison, the level of [D-N] value in the frontal cortex was highly variable between the cases (white bars in Figure 2.7a); the value of vCJD1 FC was almost as high as that of vCJD1 Th, whereas the value of vCJD3 FC was about 20% of that of vCJD3 Th. A direct comparison of TRF counts between the two different folding states from nine individual samples of vCJD3 was shown in Figure 2.7b.

In order to compare the amount of PrP^{Sc} inferred from CDI [D-N] value with PrP^{res}, the same brain homogenates used for CDI analysis were digested with PK at 50μg/ml for 1 hour at 37°C and assayed by Western blot. The results from individual samples (nine samples per case [three samples per region multiplied by three regions]) were shown in Figure 2.8. In most vCJD samples, PrP^{res} was readily detectable in a short exposure (30 seconds); PrP^{res} signals in the two FC samples (FC2 and FC3) from vCJD3 were detected after extended exposures. In each case, PrP^{res} signals from Th samples were stronger than those of frontal cortex or cerebellum; exceptionally, in vCJD1, the level of PrP^{res} in Th3 sample was similar to those of FC (1 and 2) or Cb samples. This pattern of PrP^{res} distribution was in contrast to that of PrP^{Sc} inferred from CDI [D-N] value, because the levels of PrP^{Sc} from Cb samples were overall higher than or similar to those from Th samples of the corresponding cases. Similarly, PrP^{res} signals in Cb2 and Cb3 samples of vCJD3

were much weaker than those in the Th samples of the same brain, although [D-N] values in the two Cb samples were similar to or slightly higher than those in the Th samples (compare bottom row in Figure 2.8 with Figure 2.7b); densitometric analysis revealed that PrP^{res} amounts in the two Cb samples were only 10 ~ 15% of those in the Th samples. Additionally, high variation in the intensity of PrP^{res} signals was occasionally observed between samples of same regional origin (FC region of vCJD1 or Cb region of vCJD3). For example, PrP^{res} signal in FC3 sample of vCJD1 was less than 30% of FC1 or FC2 samples in densitometry, although [D-N] value in FC3 was more than 80% of the two other FC samples.

Collectively, abnormal forms of PrP which were determined by its conformation or partial resistance to limited proteolysis were readily detectable in most of the vCJD samples, but their abundance was variable between regions and/or cases; while the amounts of PrP^{Sc} inferred from CDI [D-N] value were most abundant in cerebellum, the immunoreactivity of proteolytic fragments of PrP^{Sc} was strongest in thalamus.

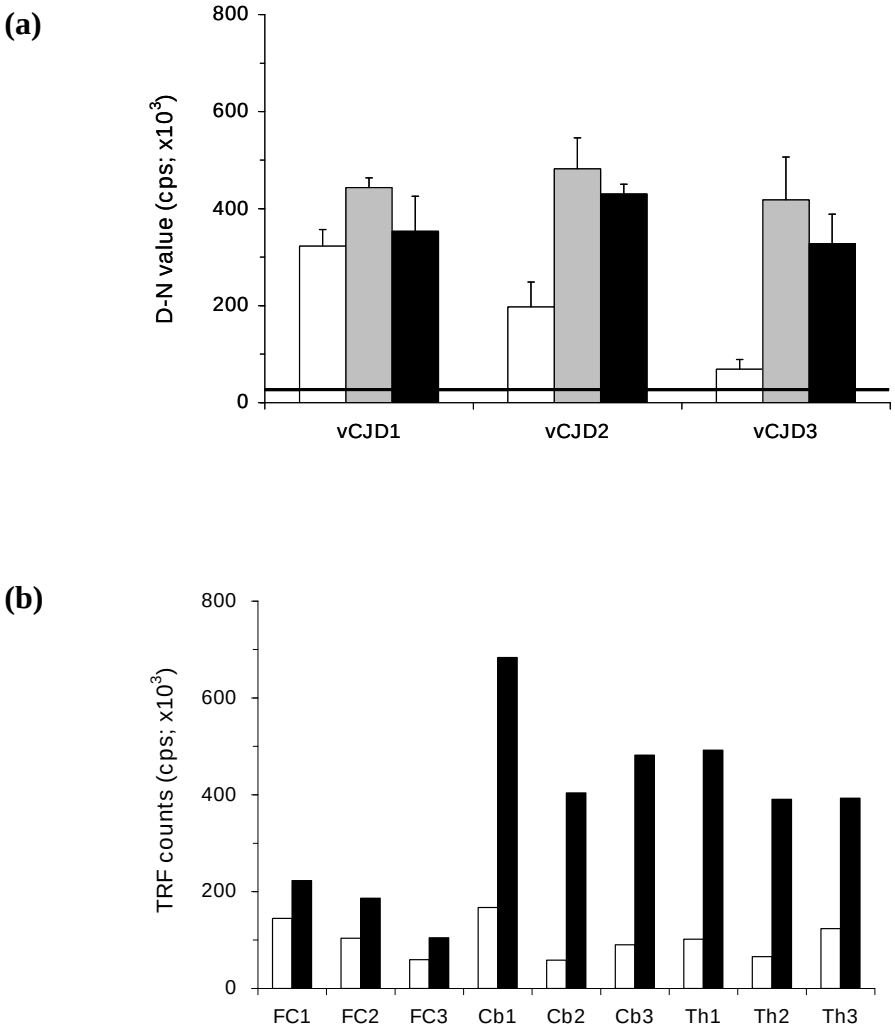

Figure 2.7 CDI [D-N] values for tissues of FC, Cb and Th from vCJD brains. (a) Samples of FC (white bars), Cb (grey bars) and Th (black bars) from three vCJD brains were analysed by CDI in the native and denatured states. CDI [D-N] values were generated by subtracting TRF counts measured in the native state from those measured in the denatured state. The solid line shows the average of [D-N] values of five controls. Data shown represent the average ± S.D. of three samples and the result in each sample was an average for duplicate wells. (b) The TRF counts from nine individual samples of vCJD3 were directly compared between the native (white bars) and denatured (black bars) states. Data shown represent the average for duplicate wells.

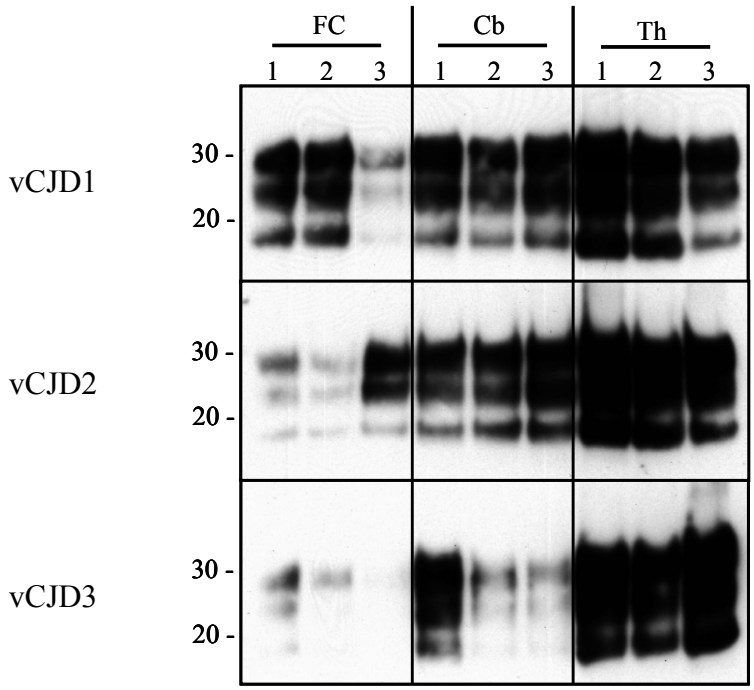

Figure 2.8 Distribution of PrP^{res} in three regions of vCJD brains. The brain homogenates used for CDI analysis were digested with PK at 50µg/ml for 1 hour at 37°C and then analysed by Western blot using mAb 3F4. In each row, the results from nine samples of each case (three samples per region multiplied by three regions) were shown. Molecular weight expressed in KDa is shown to the left.

2.3.2.2.2 MM1 sCJD

In each region, [D-N] values were presented as an average of three samples. In the three cases of MM1 sCJD, [D-N] values in frontal cortex were higher than or similar to those in the two other regions (Figure 2.9a). In MM1-1, the [D-N] values in FC samples was significantly higher than those of cerebellum or thalamus; additionally, the [D-N] values in the Th samples were not greatly different from that of non-CJD controls expressed as solid line (Figure 2.9a). However, the levels of PrP^{C} in the Th samples of MM1-1 were very low, which resulted in the generation of D/N ratios higher than 1.8 (range: 2.9 ~ 3.3). Therefore, a low level of abnormal PrP appeared to be present in this region. In MM1-2, overall distribution pattern of [D-N] values between regions was similar to that of MM1-1, although [D-N] values from three Th samples were highly variable ([D-N] value in Th1: 259,198; Th2: 31,168; and Th3: 23,454). In MM1-6, the levels of [D-N] value were relatively similar between the three regions; as in MM1-2, the values between the three Th samples were significantly variable (Figure 2.9b). A direct comparison of TRF counts between the two different folding states from individual nine samples of MM1-6 was shown in Figure 2.9b.

In order to compare the amount of PrP^{Sc} inferred from CDI [D-N] value with PrP^{res}, the same brain homogenates used for CDI analysis were digested with PK and immunoblotted with mAb 3F4. The results from individual samples (nine samples per case [three samples per region multiplied by three regions]) were shown in Figure 2.10. In MM1-1, PrP^{res} was detectable only in three FC samples although trace of PrP^{res}-like signals was seen in samples of the two other regions (upper row in Figure 2.10). In MM1-2, PrP^{res} immunoreactivity was detected in all three regions with FC samples having highest levels of signals (middle row in Figure 2.10); in thalamus, PrP^{res} was detectable only in one of the three samples which showed the highest [D-N] value. In MM1-6, PrP^{res} signals were detected in all three regions showing roughly similar intensity between them (except for Th3 sample with little PrP^{res}) (bottom row in Figure 2.10).

Collectively, in MM1 sCJD brains, PrP^{Sc} was more consistently detectable in samples of frontal cortex and cerebellum when compared to those of thalamus. When the distribution patterns of PrP^{Sc} determined by CDI [D-N] value were compared with those of PK-resistant fragments of PrP^{Sc}, there was an overall correlation between the two (compare Figures 2.9a and 2.9b with Figure 2.10); exceptionally, PrP^{Sc} was detectable at low levels by CDI in the cerebellum and thalamus of MM1-1, in which PrP^{res} was not reliably detectable by WB.

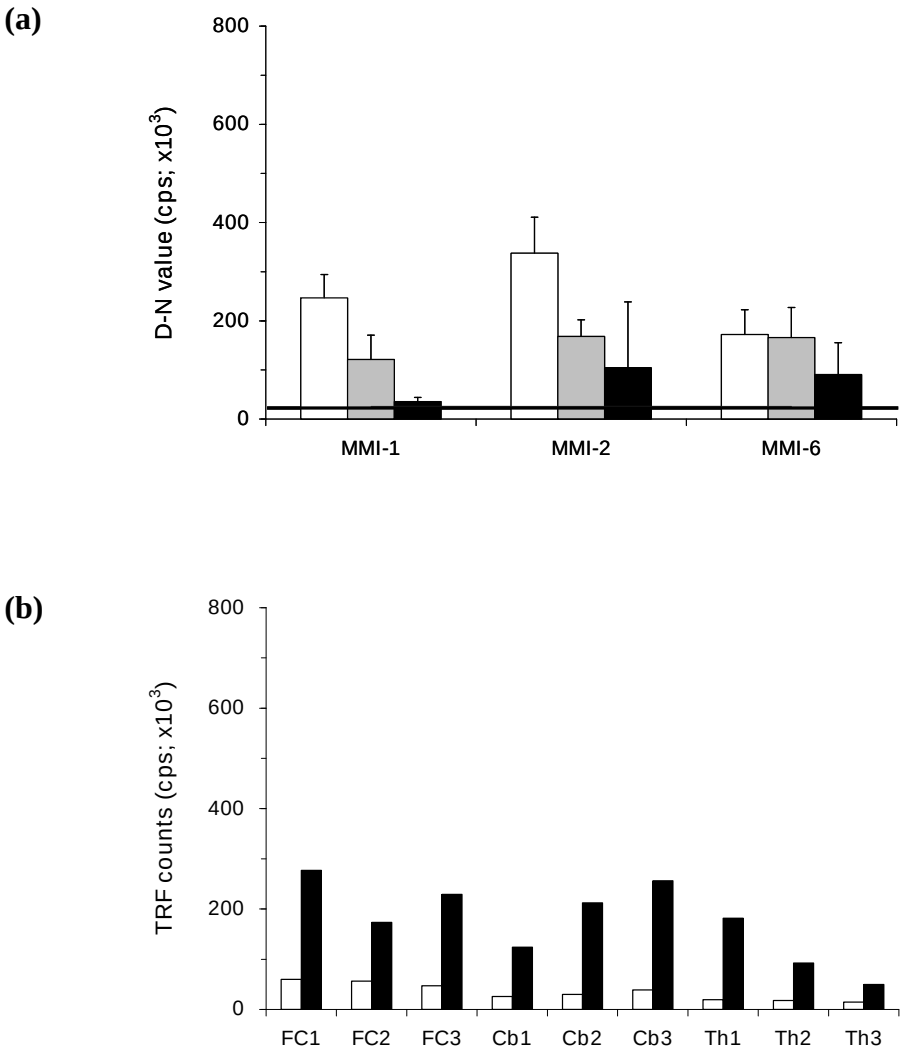

Figure 2.9 CDI [D-N] values for tissues of FC, Cb and Th from MM1 sCJD brains. (a) Samples of FC (white bars), Cb (grey bars) and Th (black bars) from three MM1 sCJD brains were analysed by CDI in the native and denatured states. CDI [D-N] values were generated by subtracting TRF counts measured in the native state from those measured in the denatured state. The solid line shows the average of [D-N] values of five controls. Data shown represent the average ± S.D. of three samples and the result in each sample was an average for duplicate wells. (b) The TRF counts from nine individual samples of MM1-6 were directly compared between the native (white bars) and denatured (black bars) states. Data shown represent the average for duplicate wells.

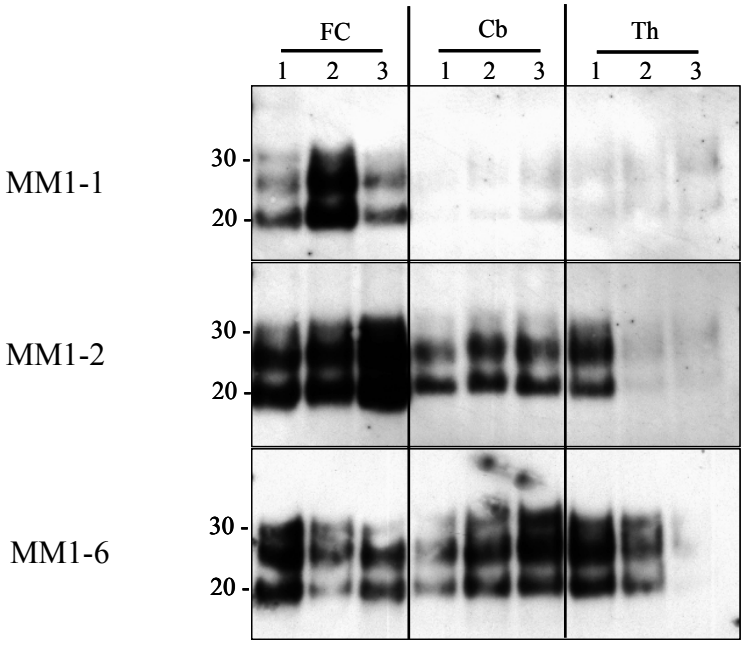

Figure 2.10 Distribution of PrP^{res} in three regions of MM1 sCJD brains. The brain homogenates used for CDI analysis were digested with PK at 50µg/ml for 1 hour at 37°C and then analysed by Western blot using mAb 3F4. In each row, the results from nine samples of each case (three samples per region multiplied by three regions) were shown. Molecular weight expressed in KDa is shown to the left.

2.3.2.2.3 MM2 sCJD

Initially, as in vCJD or MM1 sCJD, nine samples from each case (i.e. three samples in each region multiplied by three regions) were examined. [D-N] values were presented as an average of three samples in each region (Figure 2.11a). In all three cases, [D-N] values were quite low when compared to the results from vCJD or MM1 sCJD and only those from FC tissues were barely distinguishable from the solid line representing the average of [D-N] values of five controls (Figure 2.11a). When additional nine samples in each case were examined for a more thorough analysis, the results were overall similar to those from initial group of samples except for the slight increase of the [D-N] values in the cerebellum (Figure 2.11b). A direct comparison of TRF counts between the two different folding states from individual samples of MM2-1 (additional group) was shown in Figure 2.11c.

In the MM2-3 case, D/N ratios in some of Th samples were slightly higher than 1.8 despite their very low [D-N] values; one of the three Th samples of the initial group and all three samples of the additional group had D/N ratios slightly higher than 1.8 (range: 1.9 ~ 2.1). In the thalamus of MM2-3, the levels of PrP^{C} in all examined samples were very low (see Figure 2.5c) and thus the [D-N] values in these samples with D/N ratios slightly higher than 1.8 were also clearly lower than controls.

The proteolytic fragments of PrP^{Sc} obtained after limited proteolysis were analysed by Western blot and the results from individual samples were shown in Figures 2.12a (initial group) and 2.12b (additional group). In consistent with the results based on CDI [D-N] value, PrP^{res} was reliably detectable from FC samples despite occasional sample-to-sample variation. Intriguingly, weak but reliable three-band PrP immunoreactivity was detected in several Th samples from the additional group despite their negligible [D-N] values (for example, Th3 sample of MM2-1 in the additional group). Among Th samples showing faint PrP^{res} signals, only one sample had a D/N ratio higher than 1.8 (Th3 sample of MM2-3; D/N ratio: 2.0). The gel migration of nonglycosylated fragment of PrP^{res} from Th samples appeared to be

slightly slower than that of FC samples. It should be noted that, in the analysis of samples from the additional group, two times more brain lysates were loaded onto the wells of the gels when compared to those from the initial group.

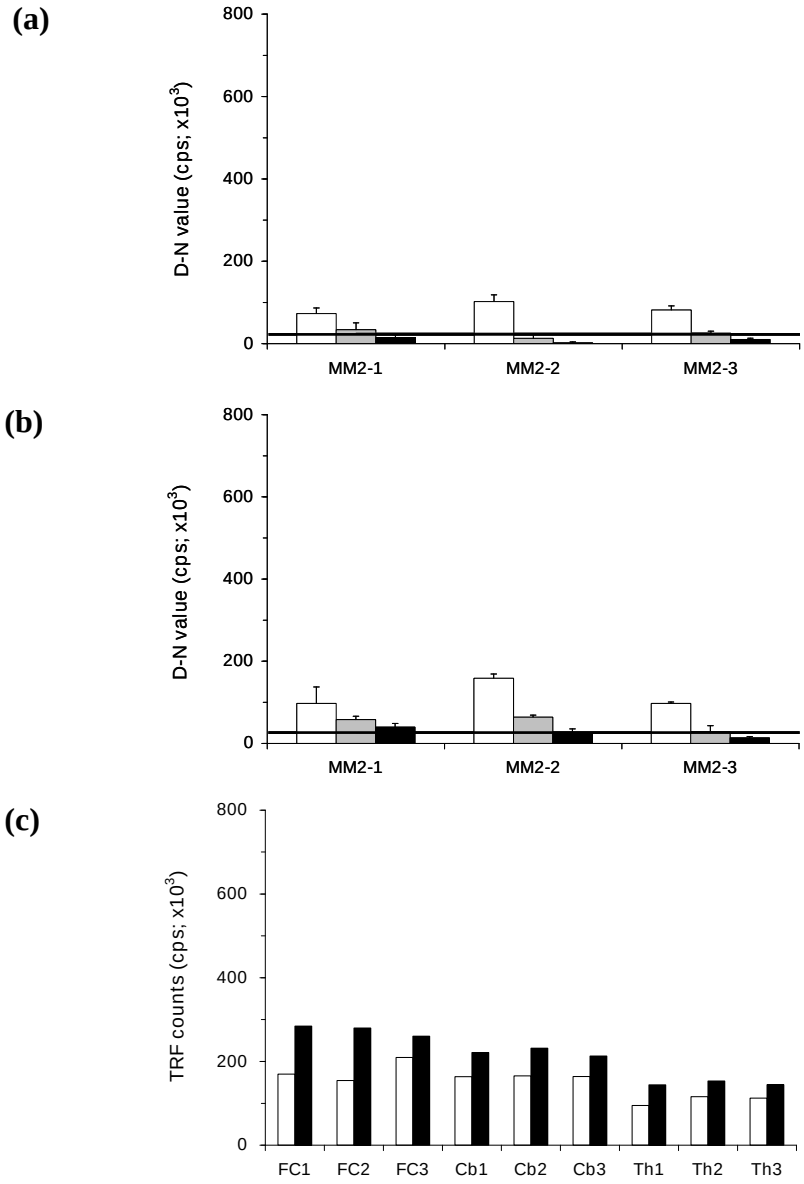

Figure 2.11 CDI [D-N] values for tissues of FC, Cb and Th from MM2 sCJD brains. (a) Samples of FC (white bars), Cb (grey bars) and Th (black bars) from three MM2 sCJD brains were analysed by CDI in the native and denatured states. CDI [D-N] values were generated by subtracting TRF counts measured in the native state from those measured in the denatured state. (b) Additional group of samples were taken from the regions of FC (white bars), Cb (grey bars) and Th (black bars) and were analysed in the same way. Solid lines in (a) and (b) show the average of [D-N] values of five controls. In both (a) and (b), data shown represent the average ± S.D. of three samples and the result in each sample was an average for duplicate wells. (c) The TRF counts from nine individual samples of MM2-1 (additional group) were directly compared between the native (white bars) and denatured (black bars) states. Data shown represent the average for duplicate wells.

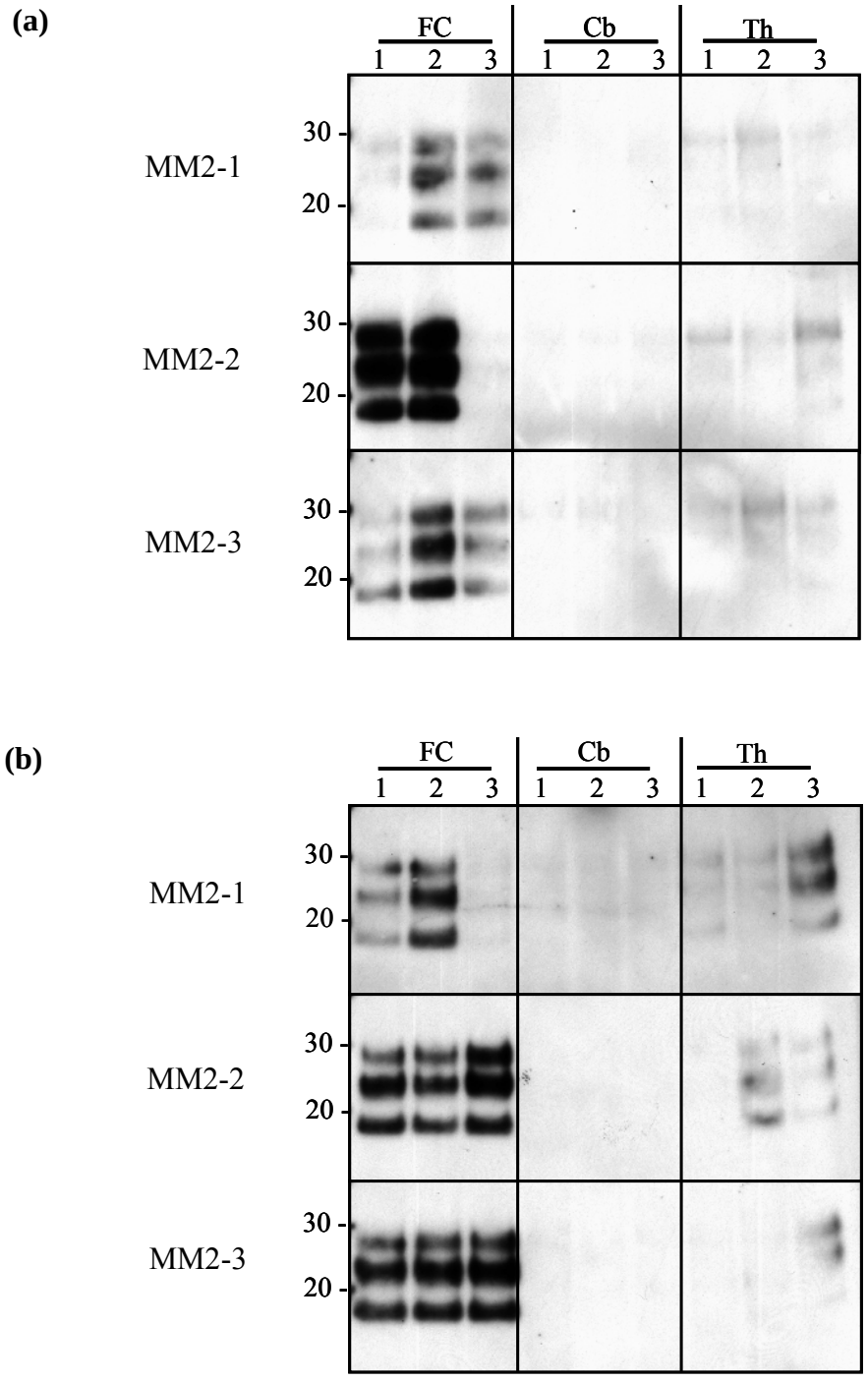

Figure 2.12 Distribution of PrP^{res} in three regions of MM2 sCJD brains. The brain homogenates from initial group of samples (a) or from additional group of samples (b) digested with PK at 50µg/ml for 1 hour at 37°C and then analysed by Western blot using mAb 3F4. In each row, the results from nine samples of each case (three samples per region multiplied by three regions) were shown. All blots shown here were given a maximal exposure (30 minutes). Molecular weight expressed in KDa is shown to the left.

2.3.2.2.4 MV1 sCJD

As in CJD with the MM genotype at codon 129, nine samples (i.e. three samples in each region multiplied by three regions per case) each from three cases were examined by CDI. The [D-N] values were presented as an average of three samples in each region. In cases of MV1-1 and MV1-3, [D-N] values in the three regions were readily distinguishable from the solid line showing the average of [D-N] values of five control cases. In both cases, the [D-N] values in the cerebellum and thalamus were similar to each other, but higher than that in the frontal cortex (Figure 2.13a). In MV1-2, [D-N] values were noticeably lower than the two other cases and its level in the cerebellum was lower than the average of controls (Figure 2.13a). A direct comparison of TRF counts between the two different folding states from individual nine samples of MV1-2 was shown in Figure 2.13b.

For further analysis of abnormal PrP present in MV1 sCJD brains, the same brain homogenates used for CDI analysis were digested with PK and immunoblotted with mAb 3F4. The results from individual samples (nine samples per case) were shown in Figure 2.14. In MV1-1, PrP^{res} signals were detected in all three regions with the frontal cortex having relatively lower PrP immunoreactivity (upper row in Figure 2.14). In MV1-2, PrP^{res} was detected in the frontal cortex and thalamus with the cerebellum being spared from PrP^{res} accumulation; PrP^{res} signals in FC samples were quite weak and barely detectable in two of three FC samples after a maximal exposure (30 minutes) (middle row in Figure 2.14). In MV1-3, PrP^{res} signals were detected in all three regions showing roughly similar intensity between samples of different regional origins (bottom row in Figure 2.14).

When the distribution patterns of PrP^{res} were compared with those of PrP^{Sc} inferred from CDI [D-N] values, a good correlation was observed between the two; exceptionally, PrP^{res} signals from FC samples of MV1-3 was overall similar to those from Cb or Th samples, although PrP^{Sc} levels inferred from CDI [D-N] values were a bit lower in FC samples than Cb or Th samples. Given that MV1 subtype of sCJD is

considered one uniform disease phenotype (Parchi 1999), distinct PrP^{Sc} distribution profile seen in case MV1-2 was a somewhat unexpected. Mechanism underlying this kind of heterogeneity between MV1 cases remains to be determined, but this distinct topology of PrP^{Sc} accumulation does not appear to be explicable in terms of clinical factors such as sex and disease duration or post mortem interval considering the similarity between these factors in cases MV1-1 and MV1-2 sCJD (Table 2.2).

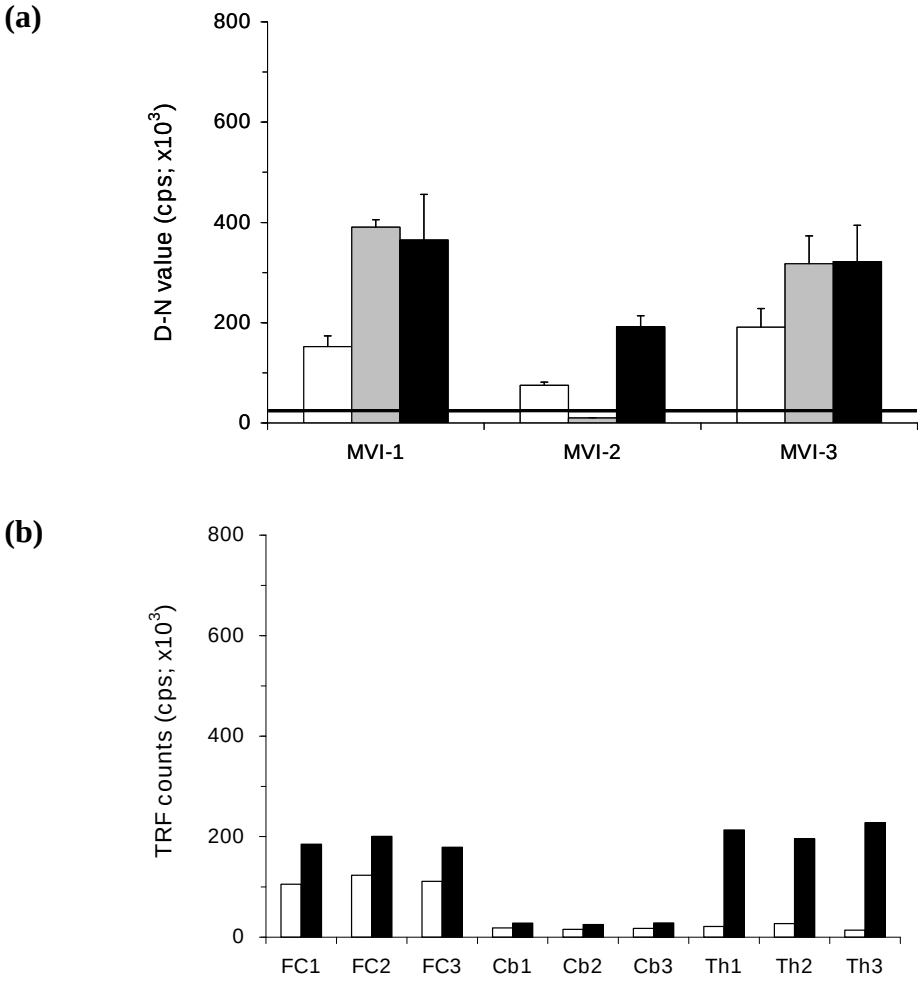

Figure 2.13 CDI [D-N] values for tissues of FC, Cb and Th from MV1 sCJD brains. (a) Samples of FC (white bars), Cb (grey bars) and Th (black bars) from three MV1 sCJD brains were analysed by CDI in the native and denatured states. CDI [D-N] values were generated by subtracting TRF counts measured in the native state from those measured in the denatured state. The solid line shows the average of [D-N] values of five controls. Data shown represent the average ± S.D. of three samples and the result in each sample was an average for duplicate wells. (b) The TRF counts from nine individual samples of MV1-2 were directly compared between the native (white bars) and denatured (black bars) states. Data shown represent the average for duplicate wells.

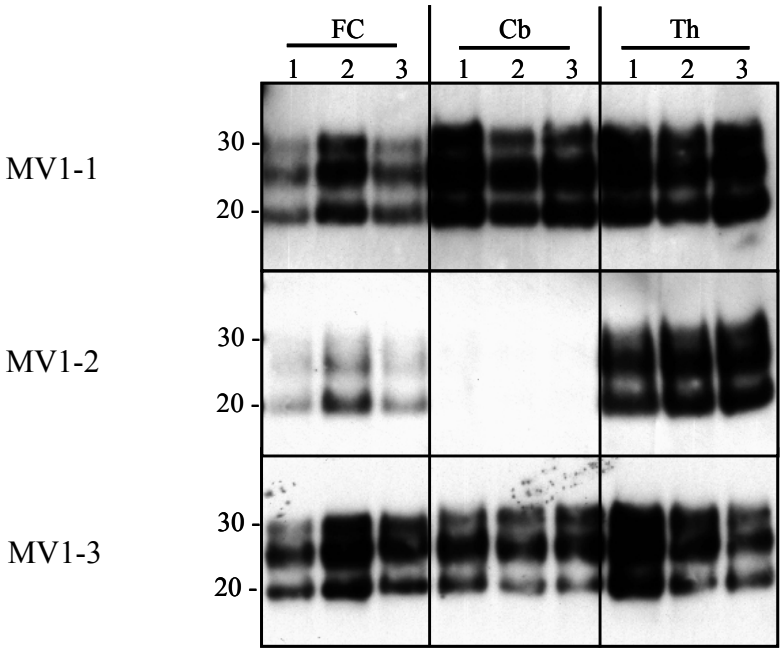

Figure 2.14 Distribution of PrP^{res} in three regions of MV1 sCJD brains. The brain homogenates used for CDI analysis were digested with PK at 50μg/ml for 1 hour at 37°C and then analysed by Western blot using mAb 3F4. In each row, the results from nine samples of each case (three samples per region multiplied by three regions) were shown. Molecular weight expressed in KDa is shown to the left.

2.3.2.2.5 MV2 sCJD

As in other CJD phenotypes, nine brain samples from individual brains were analysed by CDI. When the [D-N] values were presented as an average of three samples in each region, their profiles were distinct between the three cases as shown in Figure 2.15a. In MV2-1, [D-N] values in every three region were greatly higher than the solid line representing the average of five control cases. In MV2-2, [D-N] values were recognizably lower than the two other MV2 cases and its level in the cerebellum region was lower than the average of controls. In MV2-3, although the levels of [D-N] value in the cerebellum and thalamus were similar to those of corresponding regions of MV2-1, its level in the frontal cortex region did not seem significantly distinguishable from that of non-CJD controls. A direct comparison of TRF counts between the two different folding states from individual nine samples of MV2-3 was shown in Figure 2.15b.

For further analysis of abnormal PrP present in MV2 sCJD brains, the same brain homogenates used for CDI analysis were analysed by Western blot following proteolysis at 50μg/ml PK for 1 hour at 37°C. The results from individual samples (nine samples per case) were shown in Figure 2.15a. In MV2-1, PrP^{res} was readily detectable in a short exposure (30s) from all samples; PrP immunoreactivity was strongest in the cerebellum, followed by the thalamus and frontal cortex (upper row in Figure 2.16a). In MV2-2, PrP^{res} was detected in the frontal cortex and thalamus with much stronger immunoreactivity in the former region; the cerebellar region in this case was spared from PrP^{res} accumulation (middle row in Figure 2.16a). Intriguingly, while PrP^{res} detected in the frontal cortex showed typical type 2 migration pattern with a nonglycosylated fragment migrating at ~19 KDa, PrP^{res} detected in the thalamus appeared to have type 1 pattern with a nonglycosylated fragment migrating at ~21 KDa (Th1 or Th2 samples) or to have a mixture of both types (Th3 sample). Similar results were obtained in the repeated examination of MV2-2 samples (Figure 2.16b). In MV2-3, PrP^{res} was readily detectable in the cerebellum and thalamus with the frontal cortex being spared from PrP^{res}

accumulation (bottom row in Figure 2.16a). In this case, although PrP^{Sc} level in Cb3 sample (inferred from [D-N] value) was higher than those of Th2 and Th3 samples, PrP^{res} signal in the Cb sample was much weaker than the two Th samples (compare bottom row in Figure 2.16a with Figure 2.15b); densitometric analysis showed that PrP^{res} amount in the Cb3 sample was about 15 ~ 20% of those of the two Th samples. Additionally, in this MV2-3 case, the intensity of PrP^{res} signals was significantly variable between samples of same regional origins when compared to the CDI [D-N] values. In the Cb3 sample, PrP^{res} amount was 10 ~ 15% of those of Cb1 or Cb2 samples in densitometry, whereas [D-N] value in the Cb3 was around 90% of the two other Cb samples (compare bottom row in Figure 2.16a with Figure 2.15b). Similarly, PrP^{res} signal in Th1 sample was less than 30% of Th1 or Th2 samples in densitometry, whereas [D-N] value in Th3 sample was around 70 ~ 80% of those of two other Th samples.

Overall, on a region-to-region comparison basis, the distribution patterns of PrP^{Sc} inferred from CDI [D-N] value were overall correlated with those of PrP^{res}; however, disagreement between the results of the two biochemical methods was also present in some samples of MV2-3. Interestingly, the distribution patterns of PrP^{Sc}/PrP^{res} were recognizably variable between cases.

The topography of PrP^{res} accumulation in the MV2 subtype of sCJD is known to be influenced by disease duration (Parchi *et al.* 1996; Parchi *et al.* 2000a). While the patients with a short clinical duration of illness accumulate large amounts of PrP^{res} in the subcortical regions, but less in the neocortex, those with a longer duration accumulate relatively larger amounts of PrP^{res} in the neocortex (Parchi *et al.* 1996). Therefore, in comparison with MV2-1 (duration: 14 months), the scant accumulation of abnormal PrP in the frontal cortex of MV2-3 (duration: 9 months) may be explained from this viewpoint. In comparison, despite its short disease duration of 7 months, case MV2-2 harboured much more amount of PrP^{Sc}/PrP^{res} in the frontal cortex than the thalamus with the cerebellum being spared from the accumulation of

abnormal PrP; this PrP^{res} distribution pattern was rather similar to that of MM2 cases (Figure 2.12). Post mortem interval in MV2-2 was rather longer than other two MV2 cases (7 days *versus* 4 days), but this "moderate" difference in post mortem interval did not appear to be associated with the distinct topology of PrP^{Sc}/PrP^{res} accumulation between cases.

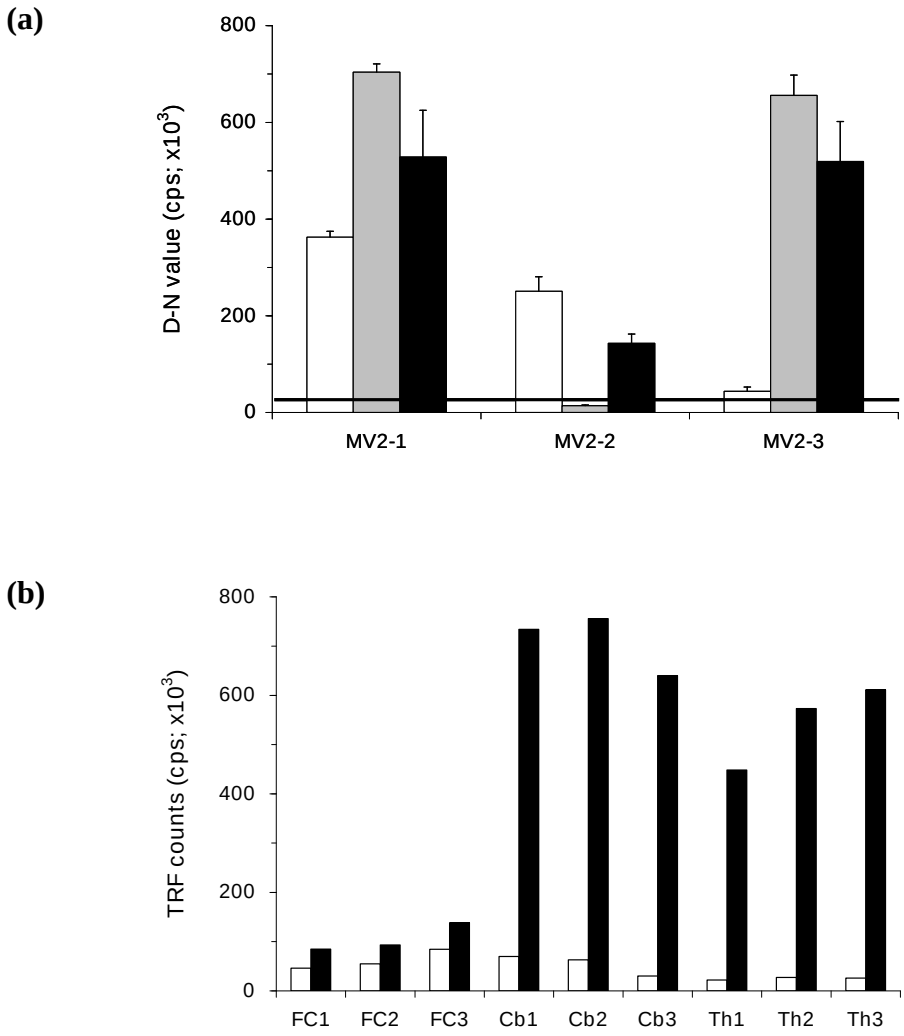

Figure 2.15 CDI [D-N] values for tissues of FC, Cb and Th from MV2 sCJD brains. (a) Samples of FC (white bars), Cb (grey bars) and Th (black bars) from three MV1 sCJD brains were analysed by CDI in the native and denatured states. CDI [D-N] values were generated by subtracting TRF counts measured in the native state from those measured in the denatured state. The solid line shows the average of [D-N] values of five controls. Data shown represent the average ± S.D. of three samples and the result in each sample was an average for duplicate wells. (b) The TRF counts from nine individual samples of MV2-3 were directly compared between the native (white bars) and denatured (black bars) states. Data shown represent the average for duplicate wells.

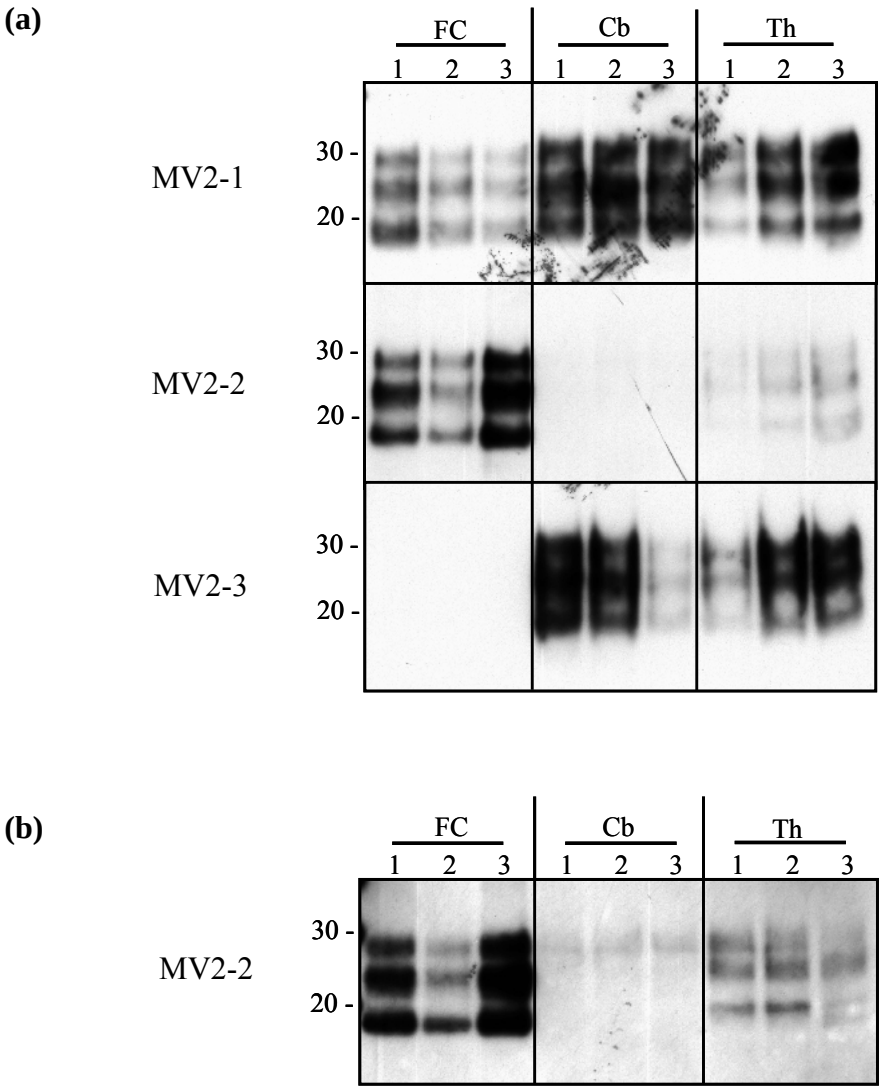

Figure 2.16 Distribution of PrP^{res} in three regions of MV2 sCJD brains. (a) The brain homogenates used for CDI analysis were digested with PK at 50μg/ml for 1 hour at 37°C and then analysed by Western blot using mAb 3F4. In each row, the results from nine samples of each case (three samples per region multiplied by three regions) were shown. (b) The nine samples of MV2-2 were repeatedly examined by Western blotting using mAb 3F4 after the limited proteolysis. In both (a) and (b), molecular weight expressed in KDa is shown to the left.

2.3.3 Further analysis of CJD brains by CDI: comparison before and after proteolysis

In the initial study describing CDI, it was reported that a substantial proportion of PrP^{Sc} was PK-sensitive and different hamster prion strains were distinguishable based on the ratio of PK-resistant PrP^{Sc} to PK-sensitive PrP^{Sc} (Safar *et al.* 1998). A recent study based on CDI argued that as much as 90% of PrP^{Sc} in sCJD brains was PK-sensitive (Safar *et al.* 2005a). In this context, in order to examine the degree of loss of CDI signals after proteolysis, three CJD cases (one case each from vCJD, MM1 sCJD and MM2 sCJD) were analysed by CDI before and after proteolysis. In each case, three samples from FC region were examined. As control, FC samples from two non-CJD brains were also contained in this study.

2.3.3.1 Non-CJD brains

The 5% homogenates were prepared from frontal cortex of two non-CJD cases in PBS containing 2% Sarcosyl and then digested by various concentrations of PK starting at the concentration of 2.5μg/ml for 1 hour at 37°C. After PK digestion, proteins were precipitated by overnight incubation with methanol and then assayed by CDI in the denatured state or by Western blot. Unexpectedly, PrP was undetectable in the non-CJD brains by either detection method after proteolysis with as little as 2.5μg/ml PK (Figure 2.17); as shown in Figure 2.17a, the fluorescence counts obtained after proteolysis with 2.5μg/ml PK was similar to those obtained after proteolysis with 50μg/ml PK. Therefore, it appeared that PrP^{C} in non-CJD brains was highly susceptible to the proteolytic treatment even at the concentration of 2.5μg/ml PK under the experimental condition in this study.

(a)

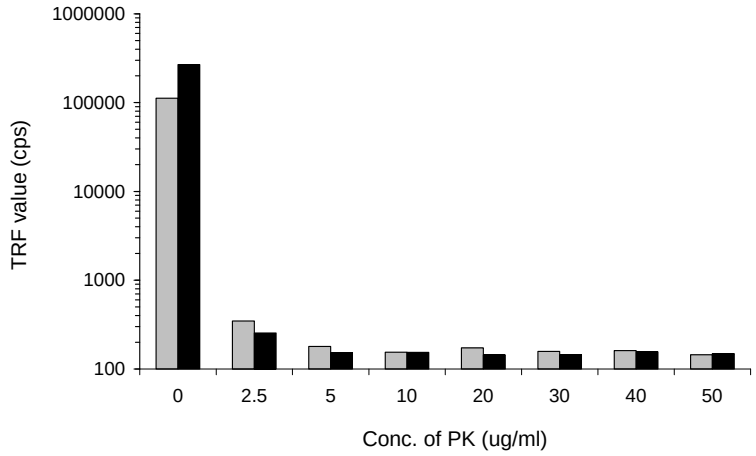

(b)

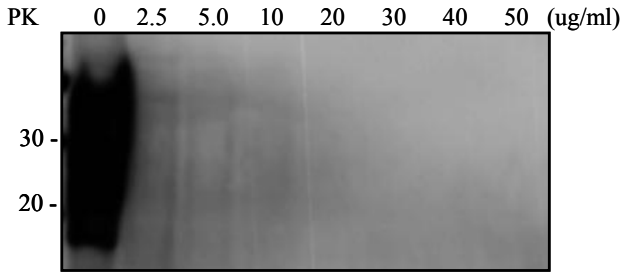

Figure 2.17 High susceptibility of PrP^C to proteolytic treatment in non-CJD brains. Brain homogenates prepared from frontal cortex of non-CJD brains remained undigested or digested with varying concentrations of PK (range: 2.5μg/ml ~ 50μg/ml) followed by methanol precipitation of proteins. (a) Samples were analysed by CDI in the denatured state. Data shown represent the average for duplicate wells and error bars showing S.D. were omitted (Grey bars: non-CJD1; black bars: non-CJD2). (b) Samples from the non-CJD2 case were assayed by Western blot using mAb 3F4.

2.3.3.2 CJD brains

In order to compare the CDI signals before and after proteolysis, triplicate samples were taken from FC region of CJD brains (one vCJD, one MM1 sCJD and one MM2 cases). The 5% brain homogenates were prepared in PBS containing 2% Sarcosyl and then digested with 2.5μg/ml PK or 50μg/ml PK for 1 hour at 37°C.

Figure 2.18 shows a direct comparison of fluorescence counts between the two different folding states in a representative sample of each case. When the samples were assayed by CDI in the native state, the fluorescence signals obtained from undigested samples were no longer present following proteolysis with 2.5μg/ml PK (grey bars in Figure 2.18); however, the CDI signals were readily detectable following denaturation of samples digested with 2.5μg/ml PK (black bars in Figure 2.18). Thus, similar to the results from non-CJD brains, the application of mild proteolysis at 2.5μg/ml PK appears to be quite efficient in digesting PrP^C present in the frontal cortex of CJD brains. After digestion with 50μg/ml PK, more than a half of total PrP signal was lost when compared to the results of corresponding samples digested with 2.5μg/ml PK (black bars in Figure 2.18).

When the ratios of the TRF counts between native and denatured aliquots were generated (D/N ratios), they were in the range of 2 ~ 5 in undigested samples (white bars in Figure 2.19). After proteolysis with 2.5μg/ml, a dramatic increase in the D/N ratios was observed in all the samples (grey bars in Figure 2.19); the ratios increased from 50 times up to 200 times, reaching the range of 100 ~ 400. After proteolysis in the diagnostic standard condition (50μg/ml PK, 1 hour, 37°C), the D/N ratios in every sample dropped “moderately” to the range of 70 ~ 200 showing some variation between the three samples of each case (black bars in Figure 2.19). The three CJD phenotypes were broadly similar in their patterns of changes of CDI D/N ratio following the proteolysis at the two different conditions.

When the [D-N] values found in undigested samples were compared with those of corresponding samples digested with 50µg/ml PK, only 30 ~ 60% of [D-N] values were detectable after the standard proteolysis (Figure 2.20a). When compared to those digested with 2.5µg/ml PK, there remained about 30 ~ 50% of [D-N] values in samples digested with 50µg/ml PK (Figure 2.20b). In both comparisons, some variation between the three samples of each case was observed. The distinction between the three CJD phenotypes did not seem possible based on the change of [D-N] values following proteolysis.

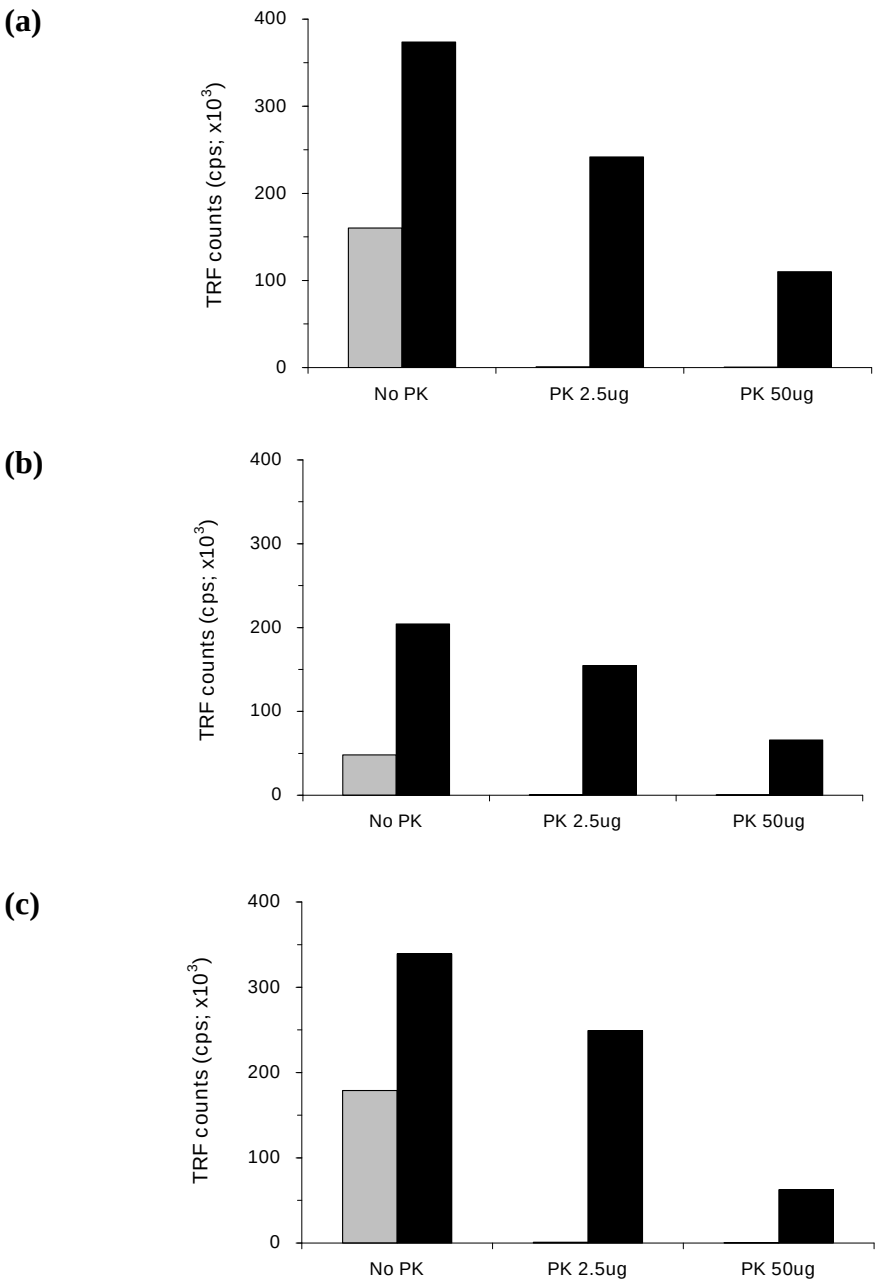

Figure 2.18 Comparison of CDI results before and after proteolysis. Brain homogenates were prepared from frontal cortex of vCJD3 (a), MM1-6 (b) and MM2-2 (c). The homogenates left undigested or digested with two different concentrations of PK (2.5µg/ml PK or 50µg/ml PK) and were then analysed by CDI. Grey bars: TRF counts obtained in the native state; Black bars: TRF counts obtained in the denatured state. Data shown represent the average for duplicate wells.

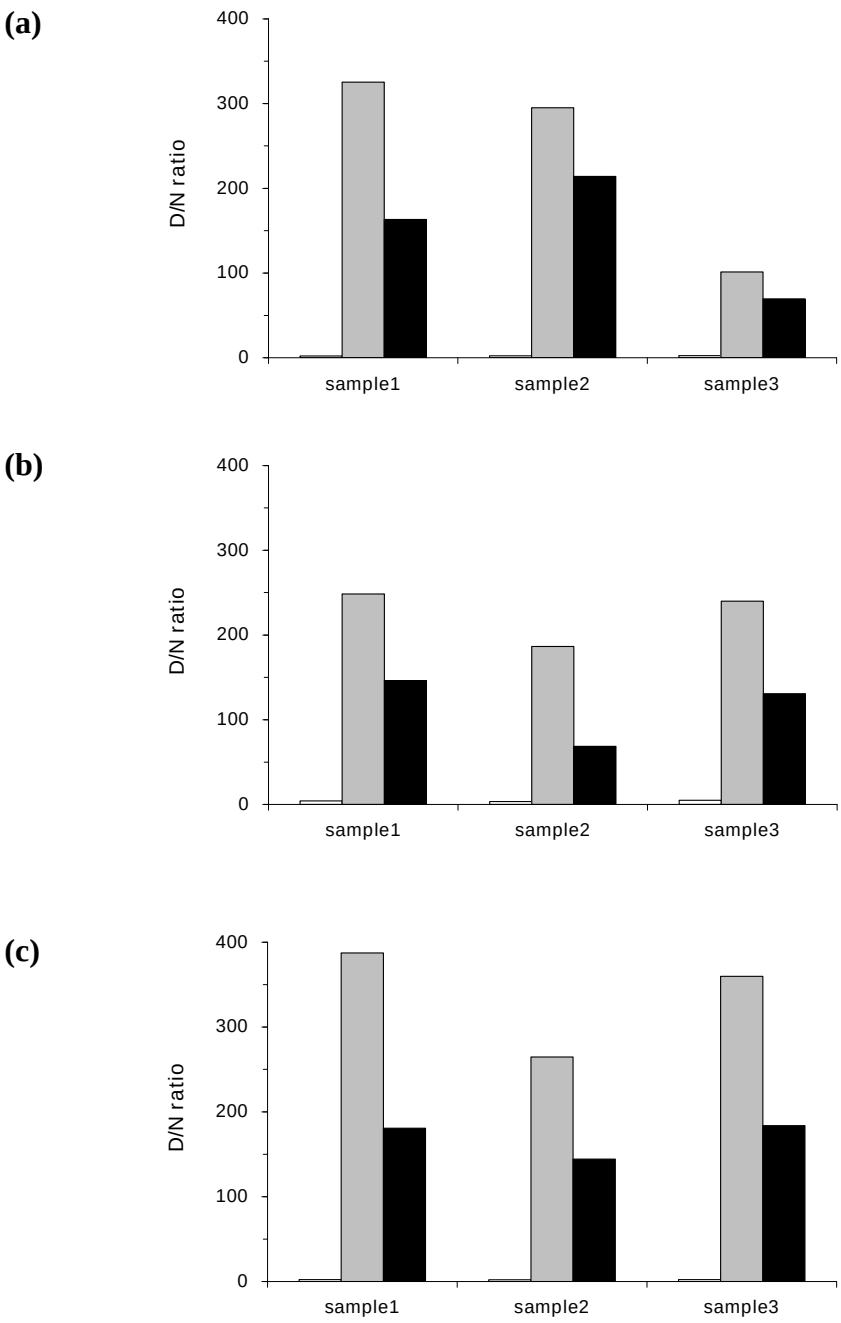

Figure 2.19 Comparison of CDI D/N ratios before and after proteolysis. Brain homogenates were prepared from triplicate FC samples of vCJD3 (a), MM1-6 (b) and MM2-2 (c). The brain homogenates left undigested (white bars) or digested with 2.5µg/ml PK (grey bars) or 50µg/ml PK (black bars) and were then analysed by CDI. D/N ratios were generated by dividing TRF counts of denatured aliquots by those of corresponding native aliquots.

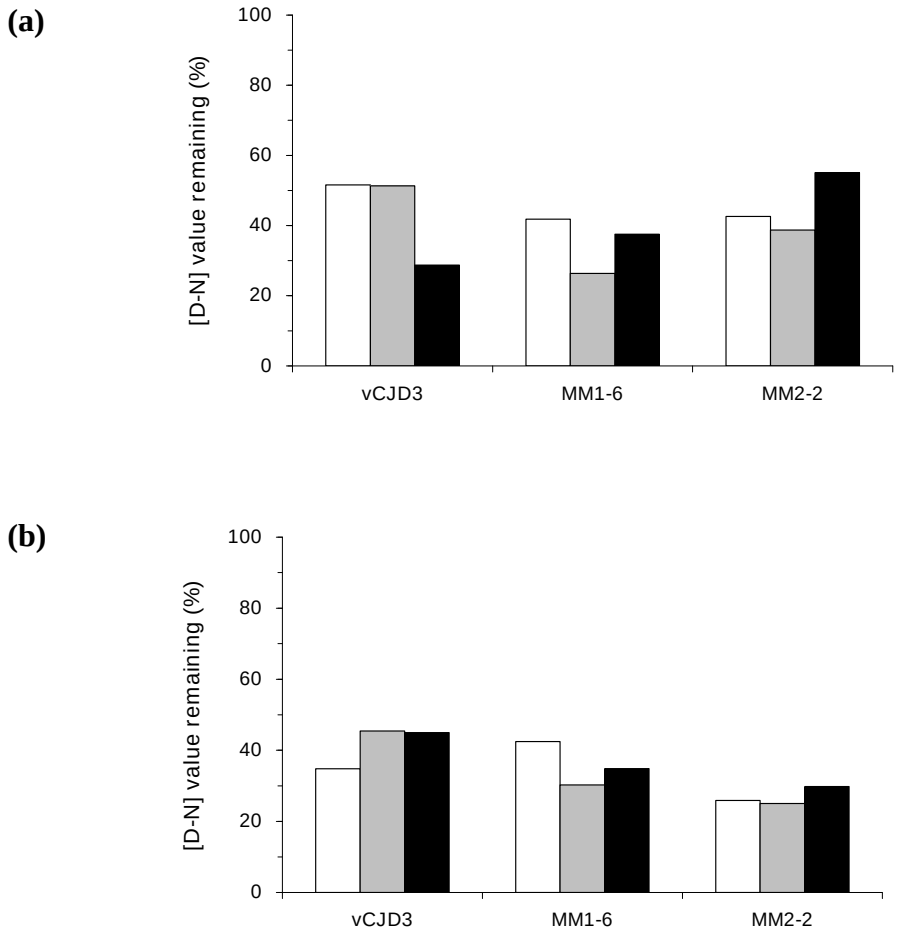

Figure 2.20 Comparison of CDI [D-N] values before and after proteolysis. Brain homogenates were prepared from triplicate FC samples of vCJD3, MM1-6 and MM2-2. The brain homogenates left undigested or digested with 2.5µg/ml PK or 50µg/ml PK and were then analysed by CDI. [D-N] values were generated by subtracting TRF counts measured in the native state from those measured in the denatured state. (a) [D-N] values obtained from samples digested with 50µg/ml PK were expressed as relative values (%) to those obtained from corresponding undigested samples. (b) [D-N] values obtained from samples digested with 50µg/ml PK were expressed as relative values (%) to those obtained from corresponding samples digested with 2.5µg/ml PK. Each bar represents individual samples (white bars: sample 1; grey bars: sample 2; black bars: sample 3).

2.3.4 Further characterization of proteolytic fragments of PrP^{Sc} in Western blot

2.3.4.1 PrP^{res} type analysis

In some of the CJD cases analysed in section 2.3.2.2, PrP^{res} appeared to be slightly different in its gel migration between regions. For further analysis, samples from these cases were digested with PK and run on the gel between PrP^{res} type 1 and type 2B standards (which are used as PrP^{res} type standards for routine diagnostic Western blot analysis in NCJDSU). The standard sample with type 1 PrP^{res} was from cerebral cortex of a case of MM1 sCJD and the standard sample with type 2B PrP^{res} was from cerebral cortex of a case of vCJD; both samples were used after enzymatic hydrolysis with 50µg/ml PK.

In the three cases of MM2 sCJD, the gel mobility of PrP^{res} from Th samples appeared to be slightly slower than that of FC samples (see Figure 2.12b). In order to examine PrP^{res} type more precisely, one FC sample and one Th sample in each case were run on the gel between PrP^{res} type standards following limited proteolysis. While equal amount of brain lysate was analysed in all FC samples and a Th sample from MM2-2, Th samples from MM2-1 and MM2-3 were analysed using pellet fraction obtained after centrifuging brain homogenate (250µl) at 20,800 × g for 1 hour. As shown in Figure 2.21, in all three cases, gel mobility of PrP^{res} was similar between FC and Th samples; the migration of an unglycosylated PrP^{res} band was clearly faster than type 1 standard, showing type 2 electrophoretic mobility.

In MV2-2, while FC samples had type 2 PrP^{res}, Th samples appeared to have type 1 PrP^{res} (Th1 and Th2 samples) or both types (Th3 sample) (see Figure 2.16). To examine PrP^{res} type more precisely in this MV2 case, one sample each from frontal cortex and thalamus were run on the gel between PrP^{res} type standards following limited proteolysis. In order to obtain PrP^{res} signals similar to the type controls, two times more brain lysate in the Th sample was loaded onto the well of the gel when compared to FC sample. For comparison, samples from MV2-1 (one sample each

from the three regions) were also analysed in the same way. In MV2-1, PrP^{res} in the FC and Cb samples had a type 2 migration pattern; interestingly, a nonglycosylated fragment of PrP^{res} in the Th sample migrated faster than that of type 1 standard but slower than that of type 2 standard (Figure 2.22a). In MV2-2, PrP^{res} in the FC sample had a type 2 migration pattern, whereas PrP^{res} in the Th sample had a type 1 migration pattern (Figure 2.22b).

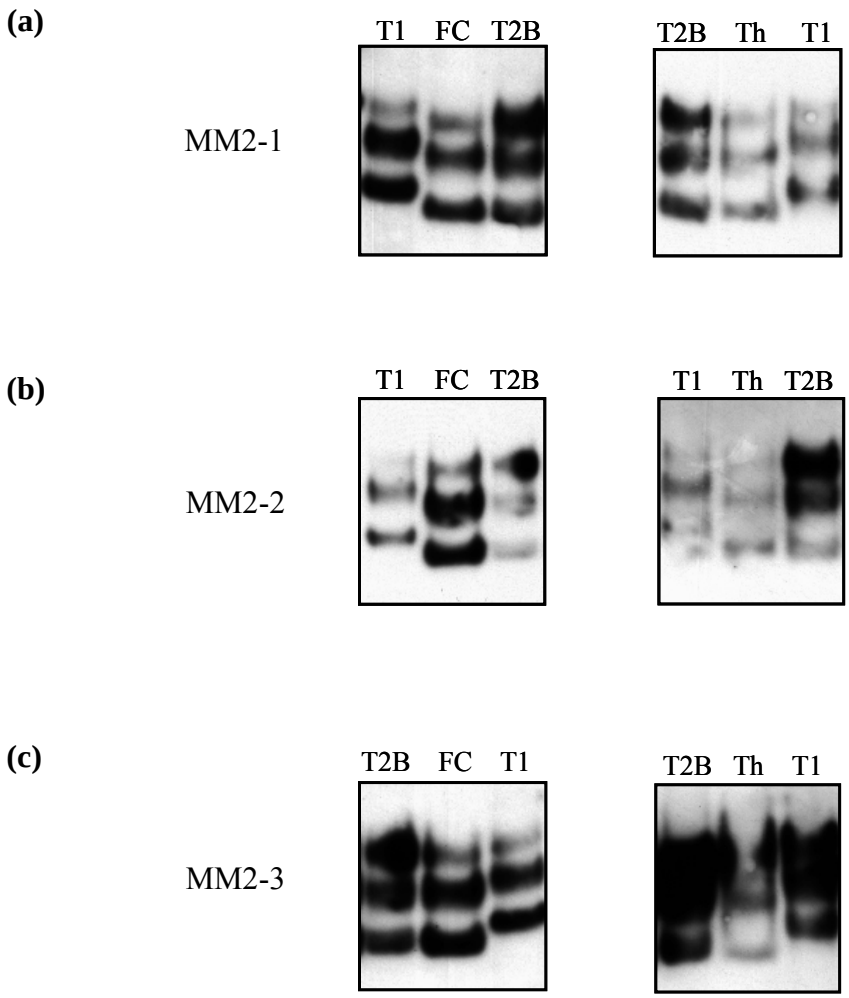

Figure 2.21 Analysis of PrP^{res} type in MM2 sCJD brains. Brain homogenates were prepared from frontal cortex (FC) and thalamus (Th) of the MM2 cases as described in section 2.2.3. The homogenates were digested with 50µg/ml PK for 1 hour at 37°C and then analysed by Western blot using mAb 3F4. For precise determination of PrP^{res} type, these samples were run between in-house standard samples with type 1 (T1) PrP^{res} or type 2B (T2B) PrP^{res}. While Th samples from MM2-1 and MM2-3 were analysed using pellet fraction obtained after centrifuging 250µl of sample at 20,800 × g for 1 hour, the other MM2 samples were analysed using equal volume of brain lysates (24µl).

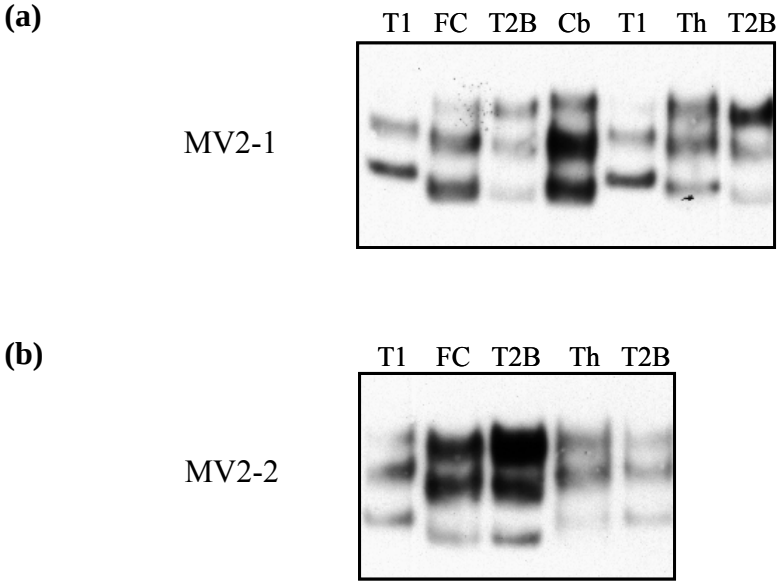

Figure 2.22 Analysis of PrP^{res} type in MV2 sCJD brains. Brain homogenates were prepared from frontal cortex (FC), cerebellum (Cb; [a] only) and thalamus (Th) of the MV2 cases as described in section 2.2.3. The homogenates were digested with 100µg/ml (a) or 50µg/ml PK (b) for 1 hour at 37°C and then analysed by Western blot using mAb 3F4. For precise determination of PrP^{res} type, these samples were run between in-house standard samples with type 1 (T1) PrP^{res} or type 2B (T2B) PrP^{res}. In MV2-1(a), the amount of brain lysate loaded onto the well was equal between the three regions. In MV2-2 (b), the amount of brain lysate examined was two times more in the Th sample than that in the FC sample.

2.3.4.2 A small proteolytic fragment of PrP^{Sc} in MV2-2

When the blot in Figure 2.22b was given a maximal exposure (30 minutes), a PK-resistant fragment with lower molecular weight was detected (Figure 2.23a). For further analysis of this small-size proteolytic fragment of PrP^{Sc}, brain homogenates prepared from frontal cortex and thalamus of the MV2 case (MV2-2) were digested with PK at 50μg/ml PK for 1 hour at 37°C; brain homogenate from a GSS case with small-size proteolytic fragments of PrP^{Sc} was also digested at the same time under the same condition. For Western blot analysis, equal amount of sample was loaded onto each lane, except for G2 lane in which pellet fraction obtained after centrifuging brain homogenate (100μl) at 20,800 × g for 1 hour was analysed. As shown in Figure 2.23b, a proteolytic fragment with low molecular weight was clearly detectable in the duplicate lanes of the Th sample and its molecular weight was similar to that from the GSS case. It did not seem clear whether a proteolytic fragment with low molecular weight was present in the FC sample.

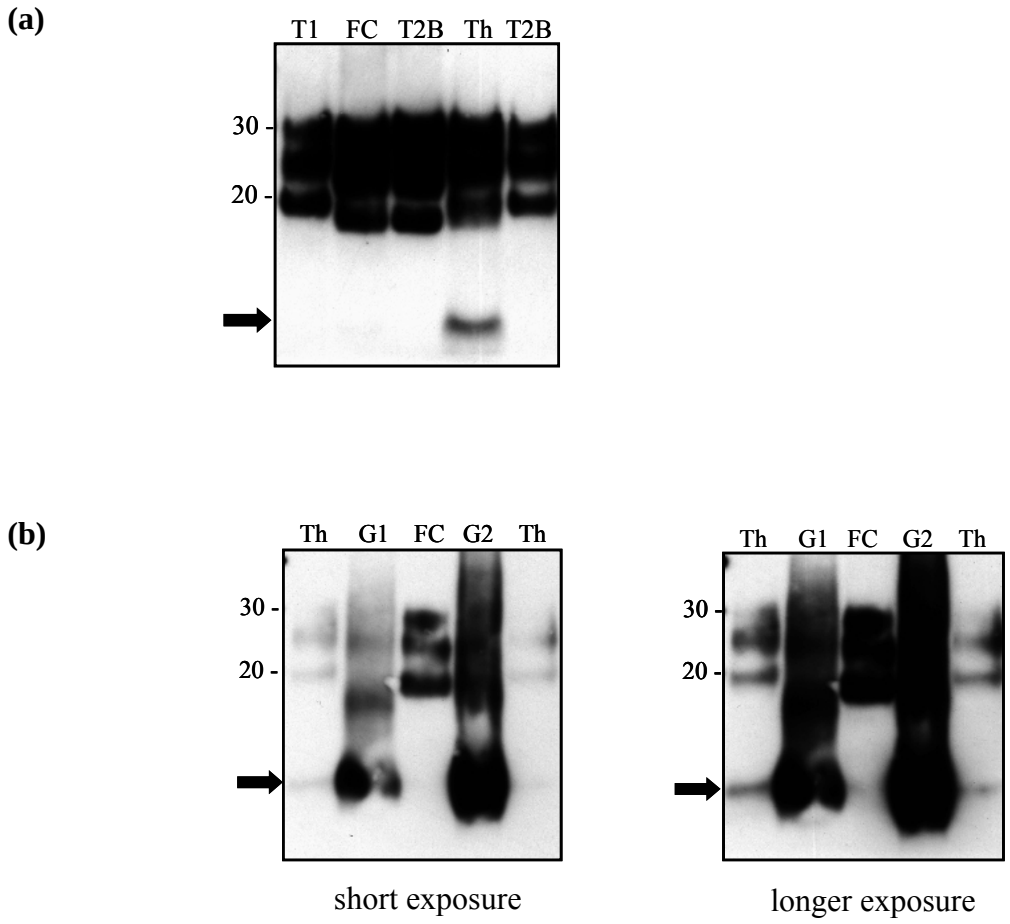

Figure 2.23 A proteolytic fragment of PrP^{Sc} with low molecular weight in a case of MV2 sCJD. (a) A maximal exposure (30 minutes) of the blot shown in Figure 2.21b. A lower-molecular-weight band (a small fragment marked as arrow) was seen in the tissue of thalamus (Th lane). For more details, refer to Figure 2.21b. (b) Brain homogenates were prepared from frontal cortex (FC) and thalamus (Th) of MV2-2 case or from frontal cortex of a GSS case (G1 and G2). The homogenates were digested with 50µg/ml PK at the same time and analysed by Western blot using mAb 3F4. A lower-molecular-weight band (marked as arrow) was seen in the duplicate lanes of the Th sample as well as in both GSS lanes. In each lane, equal amount of sample was loaded, except for G2 lane in which pellet fraction obtained after centrifuging 100µl of sample at 20,800 × g for 1 hour was examined.

2.3.5 Supplementary data

2.3.5.1 Linear range investigation in CDI

To examine the linear range of the conformation-dependent immunoassay (CDI) under the experimental condition adopted in this study, the 5% brain homogenates were prepared in PBS containing 2% Sarcosyl from tissues of CJD brains. The brain homogenates were serially diluted by a factor of two using the homogenization buffer and assayed by CDI in the native and denatured states without any additional treatment like NaPTA precipitation or PK digestion. The homogenization buffer was contained in each CDI plate to show background levels.

The TRF counts obtained from the native 5% samples were lower than 200,000 in all the three CJD brain samples (Figure 2.24). When the CDI results obtained in the native state from serially diluted samples were plotted against the concentration of brain homogenate, they decreased in a linear form until they reached a solid line represent background level (open symbols in Figure 2.24). Given that the recognition site of the mAb 3F4 is hidden in PrP^{Sc} (Kascsak *et al.* 1987; Safar *et al.* 1998), the fluorescence signals observed from the native CJD samples are believed to represent PrP^{C} present in those CJD brain samples.

After denaturation, the TRF counts increased significantly when compared to their native corresponding samples; the increase of CDI signals was more outstanding in FC tissue of a vCJD brain or in Th tissue of another vCJD brain in comparison with FC tissue of a sCJD MM1 brain (Figure 2.24). These newly detected PrP signals after unfolding are thought be mainly derived from PrP^{Sc} (Safar *et al.* 1998). In the sCJD brain sample, the TRF counts of 5% brain homogenate were around 300,000; the CDI signals decreased in a liner form despite few minor fluctuations as the 5% sample was serially diluted (filled symbols in Figure 2.24a). In cases of the two vCJD brain samples, the TRF counts were around 700,000 (FC of vCJD4) and 600,000 (Th of vCJD2) in the concentration of 5%. When serially diluted samples

were assayed by CDI, the TRF counts began to decrease in a linear way from the points of few steps serial dilution (filled symbols in Figures 2.24b and 2.24c).

Collectively, these results have shown that the CDI assay in this study has a 10^3-fold linear range (roughly from the value of 500 to 500,000) under the experimental condition in this study. It is of note that the same format of CDI as one in this study was reported to be linear over a 10^4-fold range when NaPTA precipitation step was incorporated into the sample treatment procedures (Safar *et al.* 2005a).

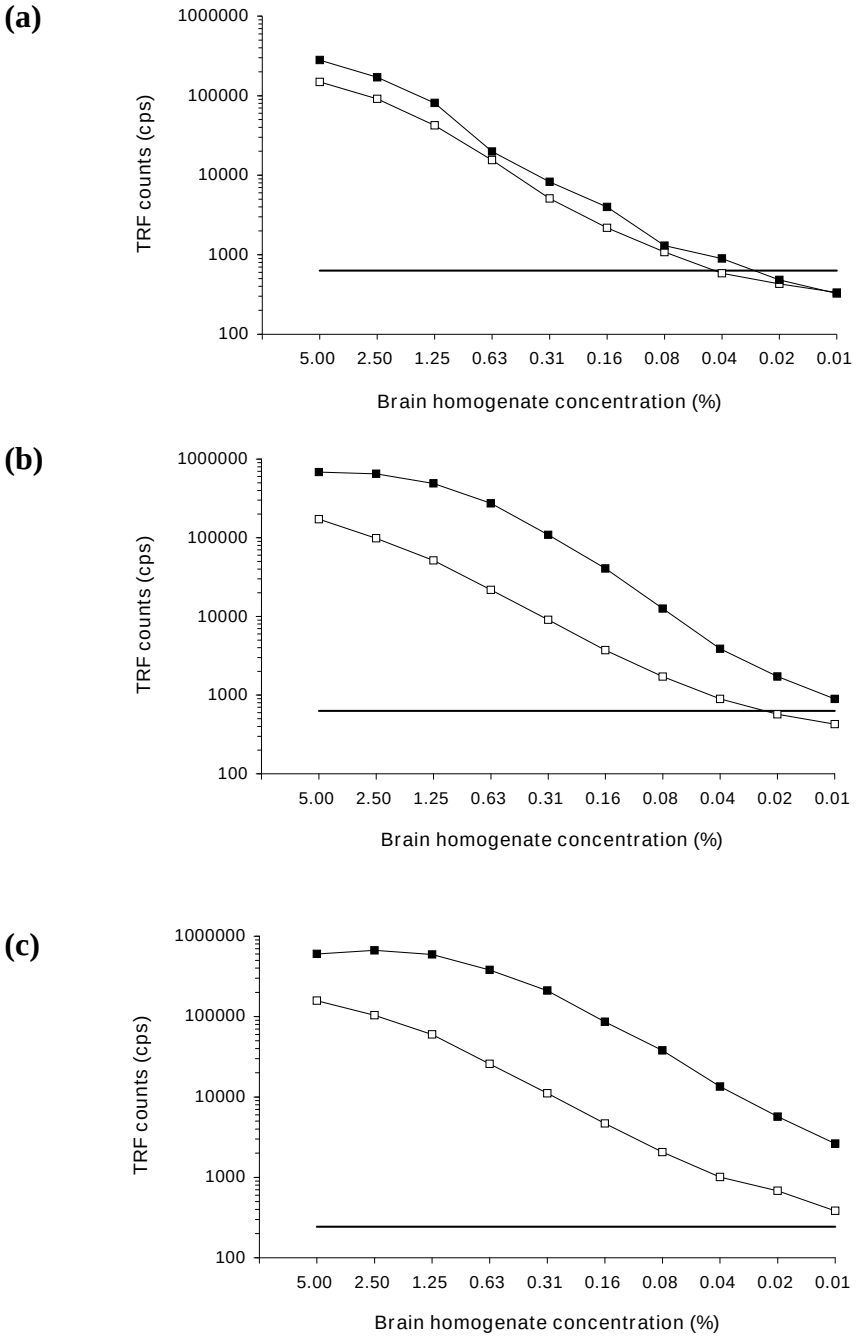

Figure 2.24 Investigation of linear range in CDI. Brain homogenates were prepared from frontal cortex of a case of MM1 sCJD (a) or a case of vCJD (b) or from thalamus of another case of vCJD (c) as described in section 2.2.3. The 5% brain homogenates were serially diluted by a factor of two using homogenization buffer and then assayed by CDI. Empty symbols represent the results obtained from native samples and filled symbols represent the results from corresponding denatured samples. Background level obtained from homogenization buffer was shown as a solid line in each figure. Data shown represent the average for duplicate wells.

2.3.5.2 Linear range investigation in Western blot analysis of PrP^{res}

To examine the linear range of Western blot analysis of PrP^{res} combined with densitometry, the 5% brain homogenates were prepared from thalamus of two vCJD cases and they were digested with PK at 50μg/ml PK for 1 hour at 37°C. Subsequently, the PK-digested samples were serially diluted by a factor of two using the homogenization buffer (PBS containing 2% Sarcosyl) and analysed by Western blotting.

As shown in Figure 2.25a, PrP^{res} signals gradually declined according as the PK-treated brain samples were serially diluted. Densitometry was performed using Quantity One Software (Bio-Rad Laboratories) and values of optical density (OD) were determined by measuring the three PrP^{res} bands as a whole (i.e. not adding up the OD values of individual PrP^{res} bands). In case of the Th sample of vCJD2, the PrP^{res} signals declined in a linear range from the concentration of 1.25% (OD value: 50) to the concentration of 0.08% (OD value: 2.4) (left blot in Figure 2.25a and Figure 2.25b). In another vCJD Th sample, a linear range was observed from the concentration of 1.25% (OD value: 38.6) to the concentration of 0.16% (OD value: 3.2); in this sample, the linear range may extend further at the higher end (toward the concentration of 2.5%) (right blot in Figure 2.25a and Figure 2.25c). In summary, the liner range under the experimental condition in this study seems to extend at least from the OD value of 2.5 to 40. The linear range for WB analysis was found to lie between OD values of 0.8 and 8.0 when the three PrP^{res} bands were measured separately for the glycoform ratio analysis of PrP^{res} (personal communication with Dr. Mark Head).

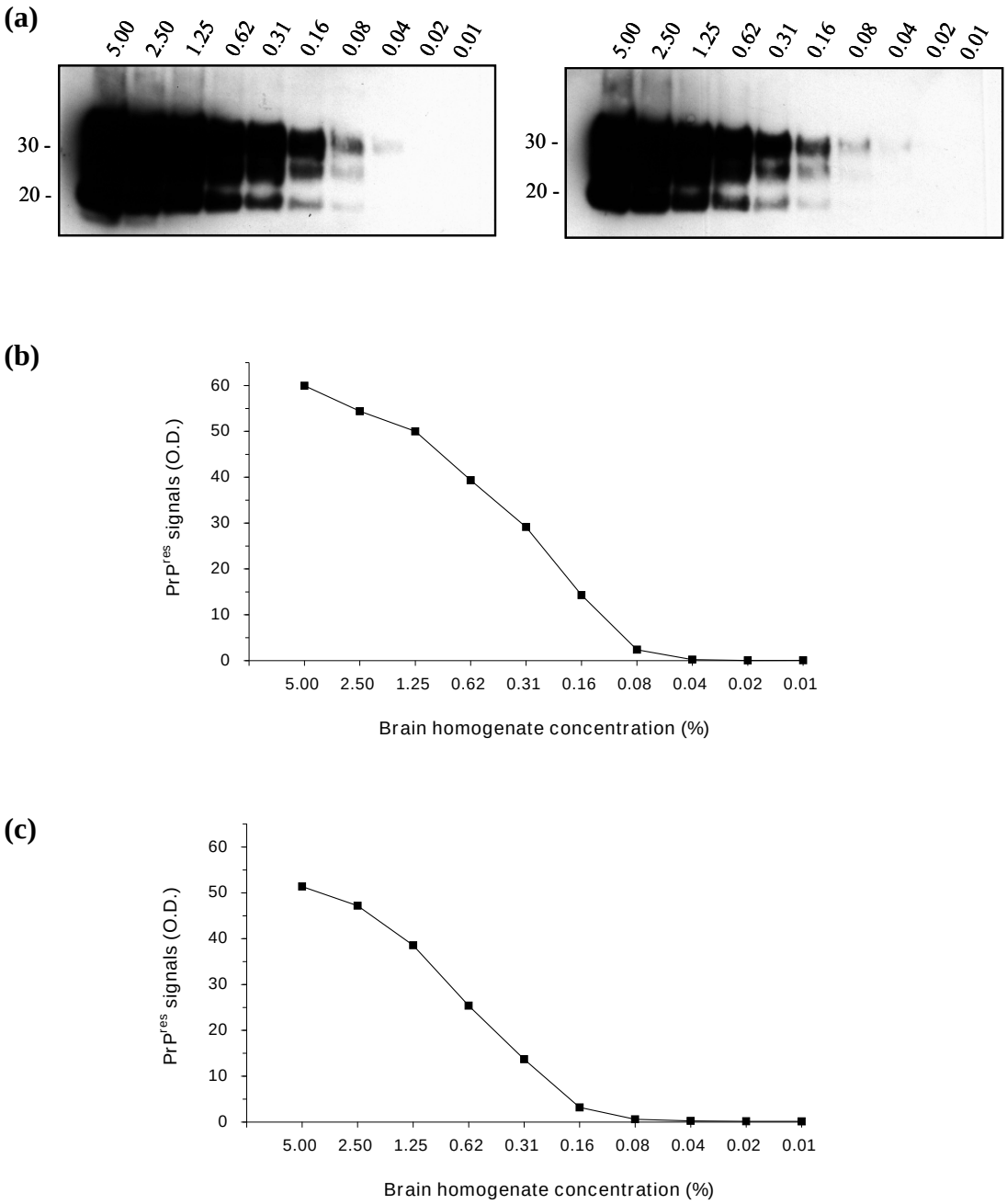

Figure 2.25 Investigation of linear range in Western blot analysis of PrP^{res}. (a) Brain homogenates were prepared from thalamus of two cases of vCJD as described in section 2.2.3. The 5% brain homogenates were digested with 50µg/ml PK for one hour at 37°C and then serially diluted by a factor of two using homogenization buffer. PrP^{res} in the serially diluted samples was investigated by Western blot using mAb 3F4. The concentration of brain lysate in each lane was shown on the top of the blots. (b) and (c) The two blots in (a) were quantified by densitometry; (b) represents the left blot and (c) represents the right one.

2.3.5.3 Analytical precision

To examine the analytical precision of CDI, a 5% brain homogenate was prepared from frontal cortex of a case of vCJD and was denatured as described in section 2.2.3. After diluting and adjusting the concentration of GdnHCl to 0.35M, two hundred microliters of the vCJD sample was loaded into each of the 96 wells of two plates and then assayed by CDI. In plate 1, the mean TRF counts of 96 wells were 400,000 with standard deviation of 20,000; in plate 2, the mean was 420,000 with standard deviation of 15,000 (Figure 2.26). The coefficient of variation (CV; %) was obtained by dividing the standard deviation by the mean and then multiplying the value by 100. The intra-assay CV was 5.1% (plate 1) and 3.5% (plate 2), respectively.

The analytical precision of CDI was further assessed by analysing CDI results obtained from eight CJD samples tested repeatedly on three to four separate occasions. These samples were examined by CDI for the conformation stability analysis (Chapter 4). The analytical precision between assays (inter-assay variation) expressed as the (CV; %) for these samples ranged from 6.6% to 16.1%, except for one sample with the value of 20.4%.

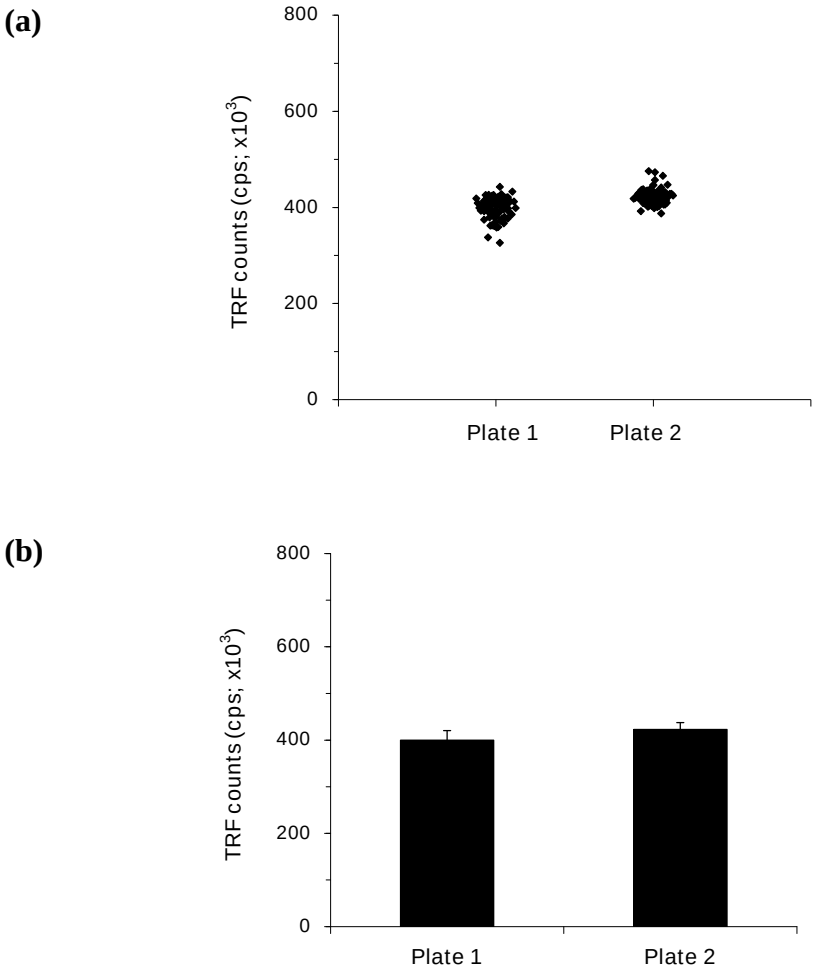

Figure 2.26 Intra-assay variation in CDI. The 5% brain homogenates prepared from frontal cortex of a case of vCJD were applied to two CDI plates after denaturation. (a) Scatter diagram of TRF counts of individual wells in the two plates. (b) The average of TRF counts of the 96 wells in each plate is shown and error bars represent S.D.

2.4 Discussion

2.4.1 PrP^C in CJD brains

Since the epitope of mAb 3F4 employed as a detector in CDI is not accessible in PrP^{Sc} and becomes exposed only after denaturation, the CDI fluorescence signals obtained from native samples represent PrP^C. When brain samples from different forms of CJD were analysed by CDI in the native state, PrP^C was readily detectable in all examined CJD samples. The level of PrP^C was variable between regions and/or cases (particularly in sCJD brains). This PrP^C variation may be partly associated with variations in sampling and difference in age, post-mortem intervals, etc. between individual cases. While the levels of PrP^C in vCJD samples were overall within the range of PrP^C amounts identified in the controls, those in some sCJD samples were significantly lower than the controls. However, since only tissues of frontal cortex from non-CJD controls were analysed by CDI in this study, the direct comparison of PrP^C levels between non-CJD and CJD samples (from Cb and Th regions) may not be accurate. Moreover, given that the non-CJD controls were initially referred to the Unit for a consideration of CJD but received an alternative diagnosis (see Table 2.4) and that the upregulation of PrP^C was observed in various neurodegenerative diseases (Kovacs *et al.* 2002b; Voigtlander *et al.* 2001), the levels of PrP^C in these neurological controls do not necessarily represent those in "normal" brains.

To the best of my knowledge, this is the first description of PrP^C present in human brains infected with prions. The presence of PrP^C in diseased brains, however, was previously described in the brains of scrapie-infected hamsters (Meyer *et al.* 1986; Safar *et al.* 1998). Meyer and colleagues reported that the level of PrP^C was similar between the brains of scrapie-infected and control hamsters when the two isoforms of PrP were separated based on their difference in detergent solubility (Meyer *et al.* 1986). In another study based on CDI employing the mAb 3F4 as a detector, Safar and colleagues have shown that PrP^C is present in the hamster brains infected with

various prion strains with some variation in its level between strains (Safar *et al.* 1998).

The presence of PrP^{C} in CJD brains appears to be natural because PrP^{C} serves as a precursor protein of PrP^{Sc} and thus its presence is a prerequisite for the replication of PrP^{Sc} (Bueler *et al.* 1993; Caughey and Raymond 1991). More interestingly, a growing body of evidence suggests that PrP^{C} is quite possibly linked to neurotoxicity in prion-infected brains. The first experimental evidence supporting this concept was provided by grafting brain tissue overexpressing PrP^{C} into the brain of PrP knockout mice, in which PrP^{Sc} is not toxic to PrP-deficient neurons (Brandner *et al.* 1996). This finding was further supported by Mallucci and colleagues, who has shown that the depletion of neuronal PrP^{C} expression in mice infected with scrapie reversed the early spongiform degeneration and prevented the development of neurological symptoms despite further accumulation of PrP^{Sc} in astrocytes (Mallucci *et al.* 2003). It was then reported that the accumulation of PrP^{Sc} amyloids did not accompany clinical disease in GPI-negative transgenic mice (Chesebro *et al.* 2005). A more recent observation from Rambold and colleagues that PrP^{C} was required for the pathologic effects of PrP^{Sc} also supports this notion (Rambold *et al.* 2008). In different studies, minor populations of PrP^{C} molecules with topological variants have been reported to be toxic species of PrP. A small population of newly synthesized PrP molecules can be localized in the cytosol (cyPrP) as a result of inefficient translocation into the endoplasmic reticulum (ER)(Rane *et al.* 2004). The stress in the ER which can be triggered by the accumulation of PrP^{Sc} was reported to lead to the increase of cyPrP (Rane *et al.* 2008), which could possibly contribute to the neurotoxicity during prion infection (Hetz *et al.* 2005; Kang *et al.* 2006; Orsi *et al.* 2006). Expression of cyPrP in transgenic mice with a deleted N-terminal ER targeting signal sequence caused severe cerebellar degeneration (Ma and Lindquist 2002). Another minor isoform of PrP that is claimed to be linked to neurotoxicity is a transmembrane form of PrP in which central hydrophobic domain spans the membrane with its N-terminus exposed to the cytosol (Hegde *et al.* 1998).

Transgenic mice expressing this variant of PrP (termed ^{ctm}PrP) developed a fatal neurodegenerative disease (Hegde *et al.* 1998; Stewart *et al.* 2005). Interestingly, a very recent study has shown that both cyPrP and ^{ctm}PrP can interact with and disrupt the function of Mahogunin, a cytosolic ubiquitin ligase whose loss causes spongiform degeneration in mice (Chakrabarti and Hegde 2009). Taken together, PrP^{C} molecules detected by CDI in this study may contribute to the disease pathogenesis in CJD.

It has been known that several genetic forms of human prion diseases, especially FFI, do not accumulate substantial amounts of PrP^{Sc} in the brain, despite fatal clinical diseases (Almer *et al.* 1999; Brown *et al.* 1995; Tateishi *et al.* 1990; Tateishi *et al.* 1995). Moreover, the distribution and severity of pathological changes do not always correlate with the amounts and distribution of PrP^{Sc} deposition (Almer *et al.* 1999; Budka 2003; Schoch *et al.* 2006). In particular, neuronal loss and gliosis in prion-infected human brains were reported not to be directly related to the amount of PrP^{Sc} deposition (Parchi *et al.* 2000a). In this context, the region of thalamus in MM2-2 is of interest because abnormal PrP was not demonstrable by PrP immunostaining and barely detectable by the biochemical methods despite the presence of severe neuronal loss and marked gliosis along with mild vacuolation; interestingly, PrP^{C} molecules were easily identifiable by CDI in this region. Since CDI-based detection of PrP^{C} cannot distinguish secreted form of PrP^{C} from cyPrP and ^{ctm}PrP, it would be interesting to investigate the level of those topological variants in these regions using an antibody that selectively recognizes them by virtue of their uncleaved ER-targeting signal peptide (Stewart and Harris 2003; Stewart and Harris 2005). Additionally, it would be also interesting to analyse PrP^{C} molecules (both secreted and topologically variant forms) present in cases of FFI or other inherited diseases in which little PrP^{Sc} is detectable despite fatal clinical disease.

2.4.2 CDI-based distinction between non-CJD and CJD brains: FC tissue analysis

In contrast to PrP^{C}, the binding site of the mAb 3F4 is hidden in the native form of PrP^{Sc} but become exposed after denaturation (Peretz *et al.* 1997). Thus, in the CDI employing the mAb 3F4 as a detector, newly detected fluorescence signals after denaturation in PrP^{Sc}-containing samples are considered to be mainly derived from PrP^{Sc} (Safar *et al.* 1998). In the CDI analysis frequently combined with NaPTA precipitation, the difference of fluorescence signals between native and denatured aliquots (D-N) and/or the ratio of CDI signals between the two folding states (D/N) have been used as indicators for PrP^{Sc} (Bellon *et al.* 2003; Jones *et al.* 2009a; Jones *et al.* 2008; Safar *et al.* 2002; Safar *et al.* 2005a; Thackray *et al.* 2007a).

In the analysis of non-CJD brains containing only PrP^{C}, CDI fluorescence signals increased slightly after denaturation when compared those measured from native aliquots and the D/N ratios were in the range of 1.2 ~ 1.5. Similar to the observation in this study, the D/N ratios observed in normal hamster brains were reported to be less than or equal to 1.8 (Safar *et al.* 1998). The [D-N] values were in the range of 13,000 ~ 46,000 with the average of 25,900. However, the increases of CDI signals after denaturation were much more significant in the CJD brains and most of them were easily distinguishable from the non-CJD controls on the basis of [D-N] values and/or D/N ratios. Among the 25 CJD cases (12 vCJD and 13 MM1 sCJD cases), only one MM1 case was not distinguishable from the non-CJD controls by both indicators. The D/N ratios in vCJD brains were in the range of 1.8 ~ 5.0 except for one case. In comparison, the ratios in MM1 sCJD brains were more widely spread with values in the range of 1.8 ~ 14.0 except for one case. While the vCJD case with the D/N ratio lower than 1.8 were easily distinguishable from controls by its [D-N] value, the MM1 case showing low D/N ratio was also indistinguishable from controls by its [D-N] value. When compared to the D/N ratios obtained from various laboratory prion strains propagated in hamsters (Safar *et al.* 1998), the ratios obtained from vCJD cases are in a similar range to those of DY or 139H strains; in contrast, no hamster prion strains have shown such a wide variability of D/N ratios as those seen between cases of MM1 sCJD.

Among the two CDI indicators, [D-N] values are thought to more properly reflect the amounts of PrP^{Sc} in CJD samples, although fluorescence counts of PrP^{C} molecules were shown to increase up to 50% after denaturation in this study (non-CJD control brains) or reported to increase up to 80% in a previous study (normal hamster brains)(Safar *et al.* 1998). In comparison, low D/N ratios do not necessarily mean low levels of PrP^{Sc} and high ratios do not necessarily mean high levels of PrP^{Sc}, because the ratios are influenced by amounts of PrP^{C} as well as those of PrP^{Sc}. For example, when some of the vCJD and MM1 cases which were similar in their [D-N] values were compared, the ratios in the former were significantly lower than the latter due to their difference in the amounts of PrP^{C}. Nonetheless, when compared within each phenotype, the CJD samples with higher D/N ratios showed overall higher [D-N] values.

2.4.3 PrP^{Sc} in CJD brains determined by CDI or resistance to limited proteolysis (WB)

2.4.3.1 Analysis of multiple samples from different brain regions

In each CJD case, three brain regions (frontal cortex, cerebellum and thalamus) were examined by the two biochemical methods. The frontal cortex was selected because this area has been most commonly used for diagnostic purpose, i.e. for the detection of PrP^{res} and biochemical PrP typing (Parchi *et al.* 2009b). The cerebellum was selected because clinical and neuropathological features in this region are important in classifying some forms of sCJD (Parchi *et al.* 1999b; Parchi *et al.* 1996; Schulz-Schaeffer *et al.* 1996). The thalamus was selected as a representative region of subcortical structure mainly because its pathological features in vCJD patients were strikingly different from those of cerebral and cerebellar cortex (Ironside *et al.* 2000; Ironside *et al.* 2002). Interestingly, the regions of cerebellum and thalamus were recently reported to be important for a reliable classification of sCJD (Cali *et al.* 2009; Parchi *et al.* 2009b). Considering the complexity of PrP^{res} types between the samples from the same anatomical area of a patient (Cali *et al.* 2009; Head *et al.*

2004a; Parchi *et al.* 2009b), triplicate samples (six samples in MM2 cases) were examined in each brain region.

2.4.3.2 A conformational change (CDI) versus resistance to limited proteolysis (WB)

In this study, multiple brain specimens with different regional origins from various CJD phenotypes were analysed by CDI without NaPTA precipitation and Western blot after limited proteolysis. PrP^{Sc} present in the CJD brain samples were determined by the two biochemical criteria: a conformational change in N-terminal region (CDI) or resistance to limited proteolysis (WB).

When the distribution patterns of PrP^{Sc} inferred from CDI [D-N] value were compared with those of PK-resistant fragments of PrP^{Sc} (PrP^{res}), there was an overall correlation between the two biochemical criteria to define disease-associated isoform of PrP, despite their differences in the principle and platform. The samples and/or regions in which CDI [D-N] values were negligible or not significantly distinguishable from those of controls were usually spared from PrP^{res} accumulation. The distribution patterns of abnormal PrP in individual brains were generally similar between the two biochemical measurements; in each case, generally speaking, a brain region with highest level of PrP^{Sc} showed strongest PrP^{res} immunoreactivity and another region with lowest level of PrP^{Sc} had least abundant PrP^{res}.

However, occasional disagreement was also evident between the two biochemical measurements of PrP^{Sc}. For example, in all three vCJD cases, PrP^{res} was more abundant in the thalamus despite similar or higher levels of PrP^{Sc} in the cerebellum. In the Cb samples from the MM1-1 case, little PrP^{res} was detectable despite significant levels of PrP^{Sc} inferred from [D-N] values. In MM2 cases, faint but reliable three-band PrP^{res} signals were detectable in few Th samples despite their negligible [D-N] values. In the MV2-3 case, PrP^{res} signal in a Cb sample was greatly weaker than two Th samples, although PrP^{Sc} level in the Cb sample was slightly

higher than the two Th samples. In addition, significant variation in PrP^{res} immunoreactivity was occasionally seen between samples from the same region despite relative similarity in the level of PrP^{Sc}. This discordance between PrP^{Sc} and PrP^{res} may be related to non-uniform distribution of PK-sensitive PrP^{Sc} to total PrP^{Sc} between samples from the same region or between regions within the same brain. In a previous study, PK-sensitive fraction of PrP^{Sc} was reported to comprise as much as 90% of PrP^{Sc} in the frontal cortex and white matter of sCJD-infected brains (Safar *et al.* 2005a). However, it has been unclear whether the PK-sensitive isoform PrP^{Sc} is uniformly distributed within the same brain. The results in this study suggest that the ratio of PK-sensitive PrP^{Sc} to total PrP^{Sc} is not always uniform in individual CJD brains.

2.4.3.3 CDI analysis following limited proteolysis

PrP^{C} molecules present in non-CJD brains as well as CJD brains were shown to be highly susceptible to the digestion with 2.5μg/ml PK. This condition of mild proteolysis resulted in the great increase in CDI D/N ratios in all CJD samples examined. The proteolytic treatment of CJD samples under diagnostic standard condition (50μg/ml PK, 1 hour, 37°C) led to “moderate” decrease both in [D-N] values and in the D/N ratios (when compared to those measured following digestion with 2.5μg/ml PK).

The high susceptibility of PrP^{C} molecules present in non-CJD brains to PK was also observed in a recent study reporting "protease-sensitive prionpathy" cases (Gambetti *et al.* 2008), in which PrP^{C} molecules became undetectable following treatment even with 1μg/ml PK for 1 hour at 37°C. In a similar context, PrP^{C} molecules became fully digested with 50μg/ml PK even after 5 minute incubation (Yull *et al.* 2009). In this study and other studies described above, the immunodetection of PrP^{C} following proteolysis was performed by the mAbs recognizing the N-terminus of PrP. Since PrP^{C} is first degraded by PK to an intermediate fragment of 25 - 28 KDa prior to the complete degradation and its initial cleavage site is known to lie between residues

113 and 144 (Buschmann *et al.* 1998), it appears quite possible that a partially degraded form of PrP^{C} which is not detectable by 3F4 is present following the proteolysis with 2.5μg/ml PK in this study or in those above-described studies.

The significant loss of CDI signals observed in the CJD samples following limited proteolysis with 50μg/ml PK is consistent with the previous studies (Safar *et al.* 1998; Safar *et al.* 2005a). The three CJD phenotypes (vCJD, MM1 and MM2 sCJD) are broadly similar in the degree of loss of fluorescence signals following the proteolysis, which makes it difficult to distinguish the three CJD phenotypes with MM genotype at codon 129, unlike the hamster prion strains (Safar *et al.* 1998). In this study, it is difficult to determine exactly what the proportion of PK-sensitive fraction of PrP^{Sc} is for the following reasons: first, CDI [D-N] values obtained from in undigested CJD samples would not to be fully attributed to PrP^{Sc} molecules because fluorescence signals of PrP^{C} molecules also increase slightly after denaturation (see section 2.3.1.1); second, it remains unknown whether a subset of PK-sensitive isoform of PrP^{Sc} is susceptible to the enzymatic hydrolysis even with 2.5μg/ml PK. Although it seems unlikely, this kind of possibility cannot be fully excluded because a fraction of PK-sensitive PrP^{Sc} with converting activity in PMCA was shown to be highly sensitive to the proteolysis even with 5μg/ml PK (Pastrana *et al.* 2006). Even when taking these limitations into account, the estimated proportion of PK-susceptible PrP^{Sc} in this study does not appear as high as the level (~90% of total PrP^{Sc}) reported by Safar et al. (Safar *et al.* 2005a). For example, the level of CDI [D-N] values in the CJD samples treated with 50μg/ml PK lies in the range of 30 ~ 60% of those of undigested corresponding samples; moreover, given the above-mentioned limitation on CDI [D-N] values obtained from undigested CJD samples, a minor portion of loss of CDI signals following the standard proteolysis is thought to be related with the enzymatic hydrolysis of PrP^{C} molecules. Despite the close similarity in the CDI format and procedures, the main difference between the two studies is whether NaPTA precipitation is incorporated in sample processing procedures. While pellet fraction recovered by NaPTA precipitation is used for CDI

analysis in Safar's study (Safar *et al.* 2005a), cleared brain homogenate is directly applied to CDI in this study. It remains to be determined whether NaPTA precipitation is related with the discrepancy between the two studies, however it should be noted that a significant portion of PrP molecules recovered by NaPTA precipitation was shown to be PK-resistant in WB analysis (Gambetti *et al.* 2008; Wadsworth *et al.* 2001)

2.4.3.4 Speculation on the distribution profiles of PrP^{Sc}/PrP^{res} in CJD brains

The distribution patterns of abnormal PrP in the three brain regions appeared to be different between vCJD and two MM sCJD subtypes. In the vCJD brains, abnormal PrP was more abundant in the cerebellum (based on CDI) or in the thalamus (based on PK-resistance). In contrast, both types of MM sCJD harboured more abundant amounts of abnormal PrP in the frontal cortex, except for one MM1 case showing similar levels of abnormal PrP between the three regions. In both MV subtypes of sCJD, regional distribution patterns of abnormal PrP were more variable between cases. While abnormal PrP was detectable in all the three regions in two MV1 cases, abnormal PrP was not detectable in the cerebellum in the remaining case. In two MV2 cases, abnormal PrP was more abundant in the cerebellum and thalamus than the frontal cortex, whereas the distribution profile of abnormal PrP in the remaining case was rather similar to the MM2 case with cerebellum being spared from accumulation of abnormal PrP.

The distribution profiles of abnormal PrP obtained from sCJD cases appears to be in agreement with previous studies in which distribution profiles of PrP^{res} were investigated in wider brain areas from more sCJD cases. Previous studies have shown that both MM1 and MM2 subtypes of sCJD harbour more amounts of PrP^{res} in the cerebral cortex than the thalamus or cerebellum (Parchi *et al.* 1996; Schoch *et al.* 2006). In both MV subtypes of sCJD, regional profiles of PrP^{res} were reported to be more variable between cases (Schoch *et al.* 2006); in this study, MV cases containing very low or undetectable levels of PrP^{res} in various regions including FC,

Cb and Th were readily identifiable when only limited numbers of cases were investigated.

The distribution pattern of abnormal PrP in the MV2-2 case deserves further comment. In contrast to these two MV2 cases, the MV2-2 case (disease duration: 7 months) harboured much more amount of PrP^{Sc}/PrP^{res} in the frontal cortex than the thalamus, with the cerebellum being spared from the accumulation of abnormal PrP. This topography of abnormal PrP obtained from MV2-2 looks overall more similar to those described from MM2 cases. Consistent with this biochemical observation, the MV2-2 case has features of MM2 pathology without showing any detectable kuru plaques in the cerebellum. The atypical biochemical and neuropathological features of the MV2-2 which look close to those of MM2 subtype may be associated with the propagation of different prion strains, given that MV2 and MM2 subtypes of sCJD showed different biological properties on transmission into the bank voles (Nonno *et al.* 2006). Alternatively, the phenotypic variation between the MV2-2 case and other MV2 cases may be related with where prion replication initiates (peripheral *versus* central initiation) rather than the propagation of different prion strain (Wadsworth *et al.* 2008a; Will 2003). It would be interesting to compare clinical symptoms of the MV2-2 case with other MV2 or MM2 cases.

In vCJD, to the best of my knowledge, there is no published paper with which to compare the distribution profiles of abnormal PrP identified in this study; additionally, it does not appear to be possible to generalize this study's results due to the small number of cases. Nonetheless, the regional distribution of PrP^{Sc}/PrP^{res} obtained from the three vCJD cases suggests that the accumulation of abnormal PrP in vCJD brains may start earlier in the cerebellum and subcortical area than in the neocortex. It is of note that a recent vCJD transmission study has shown that incubation periods with inocula prepared from cerebellum were consistently shorter than inocula from frontal cortex, suggesting higher titres of infectivity in the former tissue (Ritchie *et al.* 2009). The accumulation of abnormal PrP in MV2 and VV2

subtypes of sCJD appears to happen in a similar way as discussed above or as shown in the previous studies (Parchi *et al.* 1996; Schoch *et al.* 2006).

2.4.4 PK-resistant fragments of PrP^{Sc} (PrP^{res})

2.4.4.1 Mixed PrP^{res} types

Although this study was designed to investigate abnormal PrP defined by the two biochemical criteria (a conformational change [CDI] and limited proteolysis [WB]), it is also necessary to discuss the coexistence of PrP^{res} types in sCJD cases considering the current significance of this issue in sCJD classification (Cali *et al.* 2009; Parchi *et al.* 2009b).

The original PrP^{res} type determined previously from routine examination of frontal cortex was confirmed in most of the sCJD cases examined in this study, although multiple samples which originated from three different brain regions were analysed. Exceptionally, the existence of both PrP^{res} types was seen in the MV2-2 case. In this case, the frontal cortex had only type 2 PrP^{res}, whereas the thalamus showed both types of PrP^{res}. Among the three samples of the thalamus from this case, two samples had only type 1 PrP^{res} and the remaining one sample had both types of PrP^{res}.

The occurrence of both types of PrP^{res} in the brains of individual patients has been addressed extensively in previous studies (Collins *et al.* 2006; Haik *et al.* 2004; Head *et al.* 2004a; Head *et al.* 2001; Lewis *et al.* 2005; Puoti *et al.* 1999; Schoch *et al.* 2006; Uro-Coste *et al.* 2008). Since the initial report that about 5% of sCJD cases had both types of PrP^{res} (Parchi *et al.* 1999b), the concurrence of both PrP^{res} types in the brains of individual patients has been detected in a substantial proportion of sCJD cases (Head *et al.* 2004a; Puoti *et al.* 1999; Schoch *et al.* 2006; Uro-Coste *et al.* 2008). The use of mAbs that specifically recognize type 1 PrP^{res} led to the suggestion that all CJD cases associated with type 2 PrP^{res} could contain type 1 PrP^{res} (Polymenidou *et al.* 2005; Yull *et al.* 2006), which was questioned in a later study in relation to partially cleaved PrP^{Sc} fragments (Notari *et al.* 2007). Two recent studies

that examined extensive samples of different brain areas from larger scale of cases have shown that there are sCJD cases associated with only type 1 PrP^{res} or type 2 PrP^{res}; the sCJD cases with mixed PrP^{res} types account for 30 ~ 40% in both studies (Cali *et al.* 2009; Parchi *et al.* 2009b), which is broadly consistent with the prevalence reported from some of previous studies (Head *et al.* 2004a; Puoti *et al.* 1999; Uro-Coste *et al.* 2008).

Although only one of the 12 sCJD cases examined in this study was shown to contain both types of PrP^{res}, the coexistence of PrP^{res} types may be found in more cases. When the mAb 3F4 that binds to both types of PrP^{res} is used, the conventional western blot system has been shown to have limited analytical sensitivity in detecting the concurrence of PrP^{res} types in individual samples (Polymenidou *et al.* 2005; Yull *et al.* 2006); the two studies performed independently failed to distinguish type 1 PrP^{res} representing up to 20~40% of total PrP^{res} in artificial mixtures of both PrP^{res} types. A more refined method employing a high resolution gel electrophoresis system or the use of more discriminatory antibodies may help detect the coexistence of PrP^{res} types more accurately (Notari *et al.* 2007; Yuan *et al.* 2008). Furthermore, in many of the sCJD cases showing type coexistence, one minor PrP^{res} type was found focally in very limited brain areas in contrast to the other predominant PrP^{res} type found in most affected areas (Cali *et al.* 2009; Head *et al.* 2004a; Parchi *et al.* 2009b). Although the brain region of thalamus contained in this study is one of the areas showing type co-occurrence most frequently (Cali *et al.* 2009; Parchi *et al.* 2009b), the analysis of more brain areas may reveal the presence of type concurrence in additional cases.

2.4.4.2 PrP^{res} migrating between type 1 and type 2 standards

The Western blot analysis of PK-treated brain homogenate from the thalamus of MV2-1 (a typical MV2 case with kuru plaques) revealed the presence of PK-resistant fragments migrating faster than type 1, but slower than type 2 standards. The band representing the unglycosylated fragment of this PrP^{res} species appears to migrate at

~20 KDa. In MV2 subtype of sCJD, the existence of a PK-resistant core fragment migrating at 20 KDa in addition to typical type 2 PrP^{res} was described previously (Notari *et al.* 2007). While the 20 KDa fragment has been always found as a doublet in association with type 2 PrP^{res} in the previous studies (Notari *et al.* 2007; Parchi *et al.* 2009b), the 20 KDa fragment found in this study is present independently from type 2 PrP^{res}.

2.4.4.3 PK-resistant fragment of PrP^{Sc} with low molecular mass comparable to that of GSS

In the thalamus from the MV2-2 case, a low molecular weight PK-resistant fragment is observed in addition to the typical three PrP^{res} bands. The gel mobility of this small proteolytic fragment is similar to that seen in a P102L GSS case, indicating that the molecular weight of this small PrP fragment is presumably of ~8 KDa (Parchi *et al.* 1998; Piccardo *et al.* 1998). The PrP^{res} profile seen in the MV2-2 case is closely similar to those seen in P102L GSS cases which have typical three PrP^{res} bands in addition to a small fragment of ~8 KDa (Parchi *et al.* 1998; Piccardo *et al.* 1998). Although the proteolytic fragment of PrP^{Sc} of 7 - 8 KDa is well known to be characteristic of GSS, PrP^{res} species of similar molecular weight has been occasionally detected in other phenotypes of human prion disease (Piccardo 1998, Kascsak 1993, Krebs 2007). Interestingly, previous studies which extensively examined PK-resistant fragments of PrP^{Sc} in sCJD brains have not detected this PrP^{res} species (Cali *et al.* 2009; Notari *et al.* 2008; Parchi *et al.* 1999b; Parchi *et al.* 2009b); C-terminal fragments of PrP^{Sc} migrating to 12 - 13 KDa which are not detectable by mAb 3F4 due to the cleavage of its epitope were the smallest form of PrP^{res} identified in these studies. The prevalence of the PrP^{Sc} fragment of ~8 KDa in sCJD brains remains to be determined. Since the full genotyping of PrP could not be performed due to the absence of consent in this MV patient with low molecular weigh fragment of PrP, the possibility of a pathogenic mutation in the *PRNP* gene can not be fully excluded.

2.4.5 Speculation on potential limitation associated case selection

CJD cases examined in this study were mainly selected based on the availability of half-frozen brain, consent for research use of brain material, typical cases of a particular disease phenotype of interest. Since clinical details such as age at onset and disease duration are important parameters distinguishing vCJD from sCJD or between various subtypes of sCJD (Brandel *et al.* 2009; Parchi *et al.* 1999b; Will *et al.* 1996) and clinically typical cases in each phenotype were selected, difference in age at clinical onset and/or disease duration between vCJD and sCJD is inevitable. Additionally, the proportion of male and female cases was not equivalent with male patients occupying ~ 70% of cases in both vCJD and sCJD. Age at clinical onset may influence disease duration in both vCJD and sCJD (Pocchiari *et al.* 2004); patients who developed clinical signs at a younger age resulted in longer survival time in both CJD phenotypes. Similarly, gender can also have influence on disease progress and female patients were found to survive longer than male patients (Pocchiari *et al.* 2004). Although there are no studies showing that these clinical parameters influence PrP^{Sc} biochemistry (conventionally represented by PrP^{res} type), their possible influence on topography of PrP^{Sc} accumulation in the brain or on the amount of PK-sensitive PrP^{Sc} cannot be fully excluded given their influence on disease progression.

Another parameter which was difficult to control during case selection is post mortem interval (PMI). PMI was in the range of 1 - 5 days except for three sCJD cases and one GSS cases whose PMI was 6 days or longer. PMI in one sCJD was 10 days. Considering that PrP^{Sc} is a highly robust molecule showing strong resistance to conventional chemical and physical treatments, the results on PrP^{Sc} biochemistry are not thought to be substantially influenced by variation in PMI. This view is supported by studies showing that the intensity of PrP^{res} signals from BSE-affected cattle brains remained unchanged after controlled autolysis at 37°C up to 7 days (Chaplin *et al.* 2002; Hayashi *et al.* 2004). In comparison, PrP^{C} is a labile molecule and thus it appears possible long delay in post mortem may influence the abundance of PrP^{C}. However, any direct correlation between PMI and PrP^{C} abundance was not

observed in this study. For example, the level of PrP^C was similar between MM1 cases that greatly differ in PMI (1 - 2 days *versus* 10 days). Accordingly, it remains to be determined how exactly PrP^C level in brain samples might be influenced by different PMI.

2.4.6 Analytical sensitivity of CDI

In this study, 34 CJD cases (12 vCJD and 22 sCJD cases) were examined by CDI without using NaPTA precipitation. Although this study was not designed for diagnostic applications, all CJD cases except for one MM1 case were found to be distinguishable from control cases even without the use of a NaPTA precipitation step. The analytical sensitivity was 97% (33/34 cases). Western blot analysis for the detection of PrP^{res} for this MM1 case (or sample) was not performed, but its PrP^{res} level is believed to be quite low given the overall correlation between the two biochemical criteria that define disease-associated PrP.

CDI assay variability that is expressed as the coefficient of variation (CV) was less than 5.2% (intra-assay) or ranged from 6.6% to 20.4% (inter-assay), which is largely within the acceptable range of less than 20% (Maple *et al.* 2004; Pombo *et al.* 2004). Additionally, the nature of this chapter is to compare the two biochemical criteria as discussed before. Nine brain samples from each CJD case were examined by CDI in the same plate or were run on the same gel, and then the results of the two methods were directly compared on a case-to-case basis. Therefore, inter-plate variation of CDI is thought to be less important when compared to intra-plate variation. Similarly, CDI results in other chapters were also presented in normalized forms (D/N ratio in Chapter 3 or fractional denaturation in Chapter 4), which would serve to minimize the effect of inter-plate variation.

2.4.7 Mixed phenotypes in neuropathology: implication for sCJD classification

Among the 6 sCJD cases (3 MM and 3 MV) in which only type 1 PrP^{res} was detectable, three cases (1 MM and 2 MV) have shown focally confluent type of vacuoles along with perivacuolar PrP deposition, in addition to the predominant phenotype composed of fine spongiform degeneration and synaptic immunostaining. Although only type 2 PrP^{res} was detectable in the three MM2 cases, the mixture of both phenotypes of neuropathology is easily identifiable in all three cases. While two of the three MV2 cases have typical pathological features of this subtype characterized by the presence of kuru plaques in the cerebellum, the remaining MV2 case (MV2-2) with mixed PrP^{res} types and a small proteolytic fragment of ~ 8 KDa does not have any detectable kuru plaques and has neuropathological features more similar to the MM2 subtype of sCJD (Parchi *et al.* 1999b; Parchi *et al.* 1996).

Although the coexistence of PrP^{res} types was not detected in any of the sCJD cases showing a mixture of synaptic and perivacuolar pattern of staining, the lack of detection of mixed PrP^{res} types can be associated with analytical sensitivity or sampling issue as discussed in this study (see section 2.4.4.1) or in previous studies (Cali *et al.* 2009; Head *et al.* 2004a; Parchi *et al.* 2009b; Yull *et al.* 2006). In a recent study, Parchi et al. proposed that sCJD cases showing a mixed synaptic and perivacuolar pattern of immunostaining could be classified into "mixed subtypes" even without the detection of co-occurrence of PrP^{res} types in Western blot (Parchi *et al.* 2009b). Therefore, some of cases examined in this study (one of the three MM1, two of three MV1 and all MM2 cases) could be classified into "mixed" subtypes, as described in the recent studies (Cali *et al.* 2009; Parchi *et al.* 2009b).

The MV2-2 case showing pathological features resembling the MM2 subtype of sCJD deserves further comment. Although the large, confluent vacuoles and perivacuolar immunostaining are observable in a subgroup of MV2 cases with kuru plaques (Parchi *et al.* 1999b; Parchi *et al.* 2009b), to the best of my knowledge, a MV2 case that shows typical MM2 pathology without any kuru plaque has not yet been reported. Given the biochemical and neuropathological profiles identified in

this case, it is questionable whether this case can fit in with even an updated version of the molecular classification system of sCJD (Parchi *et al.* 2009b).

2.4.8 Summary

In summary, this chapter has addressed the relation of the two biochemical criteria (CDI *versus* WB following limited proteolysis) using multiple brain samples from various forms of CJD brains. Despite overall agreement between the two biochemical measurements, occasional disagreement between PrP^{Sc} (inferred from CDI [D-N] value) and PrP^{res} (WB following limited proteolysis) was also evident. The analysis of CJD brain samples by CDI following proteolysis has shown that a significant proportion of PrP^{Sc} is susceptible to this treatment. Therefore, the occasional discordance between PrP^{Sc} and PrP^{res} could be explained by non-uniform distribution of PK-sensitive PrP^{Sc} to total PrP^{Sc} in individual brains. Additionally, one MV2 sCJD case which showed the topography of abnormal PrP similar to those seen MM2 cases displayed pathological features resembling MM2 subtype of sCJD. These results indicate that Western blot analysis of PK-resistant fragments of PrP^{Sc} is an incomplete description of PrP^{Sc} present in CJD brains and that further complexity of PrP^{Sc} is present.

CHAPTER 3

Distribution profiles of different PrP conformers after fractionation in sucrose step gradient

3.1 Introduction

The hallmark of prion disease is the accumulation of pathogenic disease-associated isoform of PrP (PrP^{Sc}), which is thought to be the main component of prions (Prusiner 1998). PrP^{Sc} can be distinguished from cellular isoform of PrP (PrP^{C}) by its biochemical properties. While α-helix-rich PrP^{C} is detergent-soluble and sensitive to PK, ß-sheet-rich PrP^{Sc} is detergent-insoluble and partially resistant to PK (Caughey *et al.* 1991; Meyer *et al.* 1986; Pan *et al.* 1993).

In contrast to monomeric or dimeric PrP^{C} (Meyer *et al.* 2000; Pergami *et al.* 1996), PrP^{Sc} is an assembled multimer that often forms amyloid plaques in the brain. The size of PrP^{Sc} can range from small oligomers to large aggregates (Tzaban *et al.* 2002; Yuan *et al.* 2006) and may vary between different disease phenotypes (Gambetti *et al.* 2008). When separated in 10 - 60% sucrose step gradients, PrP molecules from prion-infected brains were dispersed throughout the gradients; in contrast, PrP^{C} molecules from normal brains were observed only in the top few fractions of the gradients (Pan *et al.* 2004; Pan *et al.* 2005a; Pan *et al.* 2005c; Tzaban *et al.* 2002). In diseased brains, PrP species which migrated to heavy bottom fractions of the 10 - 60% gradient were partially resistant to proteolysis, whereas those recovered in the other fractions were susceptible to PK (Tzaban *et al.* 2002). Although the separation of protein in the velocity sedimentation in sucrose gradients is known to be a function of distinct molecular densities, sizes and shapes, the sedimentation property of PrP molecules in the 10 - 60% sucrose gradient was shown to reflect their sizes, as determined by size exclusion chromatography (Tzaban *et al.* 2002; Yuan *et al.* 2006). In another study performed by Pastrana et al., a PK-sensitive fraction of PrP^{Sc} was first obtained based on its detergent-insolubility and then subject to the 10 - 60% sucrose gradient (Pastrana *et al.* 2006). This PK-sensitive fraction of PrP^{Sc} was mainly present in the light upper fractions of the gradient, whereas PK-resistant PrP^{Sc} mostly migrated to the denser bottom fractions (Pastrana *et al.* 2006); moreover, the

PK-sensitive fraction of PrP^{Sc} was shown to have the ability to convert PrP^{C} into PrP^{Sc} in PMCA.

In this study, the homogenates from neurological control brains and CJD brains were subject to 10 - 60% sucrose step gradients in order to examine the distribution profiles of different PrP conformers in the gradients. For the analysis of CJD brains, tissues of frontal cortex from vCJD and MM1 sCJD were compared. Additionally, in vCJD, tissues from two other brain regions (cerebellum and thalamus) were also examined. Following fractionation in the sucrose gradients, the distribution profiles of PrP^{C} in control and CJD brains were determined by CDI using native aliquots of individual fractions. The distribution of PrP^{Sc} in the sucrose gradients was inferred from CDI D/N ratios. In some cases, the fractionated samples from CJD samples were examined by CDI following mild proteolysis with 2.5µg/ml PK. The existence of PrP^{res} in individual fractions was displayed by Western blotting following treatment with 50µg/ml PK.

3.2 Materials and methods

3.2.1 Human brain materials

Seven variant CJD (vCJD) cases, six cases of MM1 subtype of sporadic cases (MM1 sCJD) and five control (non-CJD) cases with neurological symptoms were examined. All of these CJD and control cases were also analysed in Chapter 2. Their clinical, genetic and biochemical details were shown in Tables 2.1, 2.2 and 2.4 in Chapter 2. In all instances the tissues used were grey matter-enriched frontal cortex (FC) and, additionally, cerebellar cortex (Cb) and thalamus (Th) in vCJD, dissected from frozen half-brain specimens.

3.2.2 Methods

Preparation of brain tissue

Brain homogenates were prepared in nine volumes (w/v) of phosphate-buffered saline (PBS), pH 7.4 by two cycles of homogenization in the FastPrep instrument (Qbiogene). Each cycle was run for 45 seconds at the speed of $6.5ms^{-1}$ with the interval of 10 minutes between the runs. The samples were aliquoted and stored at -80°C until use.

Velocity sedimentation in sucrose step gradient

Fractionation in sucrose step gradient was performed as described previously (Tzaban *et al.* 2002) with minor modifications. The 10% brain homogenate in PBS was mixed with equal volume of lysis buffer (4% n-octyl-β-D-glucopyranoside [NOG] in PBS) and then incubated for 30 minutes in ice. After clarifying the sample for 1 minute at 3,800 × g to remove insoluble material, the supernatant was incubated for 30 minutes on ice in the presence of 1% Sarcosyl, followed by carefully loading on top of a 10 - 60% sucrose step gradient. Gradient was prepared in a 5ml ultracentrifuge tube (Beckman Coulter) from 745µl of each of the following sucrose concentration: 10, 15, 20, 25, 30, 60% in TNS buffer (20mM Tris-HCl, pH 7.5,

150mM NaCl, 1% Sarcosyl). The samples were centrifuged for 1 hour at 4°C at 50,000 rpm ($g_{average}$ = 200,000 × g) in a MLS-50 rotor in the Optima MAX ultracentrifuge (Beckman Coulter). Eleven fractions of 450µl were then collected from the top of the tube and were stored at -80°C. In some cases, aliquots of collected fractions were stored at -80°C

Conformation-dependent immunoassay (CDI)

Each fraction from the sucrose gradient was prepared in two parts for CDI application. On some occasions, samples were assayed by CDI after digestion with 2.5µg/ml or 50µg/ml PK for 1 hour at 37°C. One part was mixed with same volume of PBS containing Complete EDTA-free® protease inhibitors (native sample, N) and the other part was mixed with the same volume of 4M GdnHCl and incubated for 6 minutes at 81°C (denatured sample, D). Both D and N samples were adjusted using distilled water containing EDTA-free protease inhibitors to a final concentration of GdnHCl of 0.35M in 435µl final volume. Subsequently, CDI was performed as described in section 2.2.3 without any modification.

CDI D/N ratio

TRF counts obtained from CDI were used to generate D/N ratios (Safar *et al.* 1998; Safar *et al.* 2005a). The D/N ratios were obtained by dividing time-resolved fluorescence counts (TRF) counts of denatured samples (D) by the TRF counts of the corresponding native samples (N).

Western blot (WB) analysis

Polyacrylamide gel electrophoresis was carried out using NuPAGE Novex gel system (Invitrogen) as described in section 2.2.3. Each fraction from the sucrose gradient was analysed before or after digestion with 2.5µg/ml or 50µg/ml PK for 1 hour at 37°C. Undigested or digested samples were mixed with NuPAGE LDS 4X sample buffer to a final concentration of 1X. The samples were incubated for 10 minutes at 100°C and then separated on a 10% Bis-Tris NuPAGE gel. The separated

proteins were transferred to polyvinylidene difluoride (PVDF) membrane. Subsequent immunodetection of PrP and quantitative analysis of the blots were performed as described in section 2.2.3 without any modification.

Coomassie blue staining

Samples from each fraction were incubated for 10 minutes at 100°C in the presence of 1X sample buffer and electrophoresed on a 10% Bis-Tris NuPAGE gel (Invitrogen). After electrophoresis, separated proteins in the gel were stained with 0.1% Coomassie blue in 10% acetic acid and 45% methanol for 2 hours and then background of the gel were removed by destaining with 10% acetic acid and 45% methanol.

Protein quantification

Total protein concentration in the fractionated samples was determined by using the Bio-Rad DC Protein Assay according to the manufacturer's instruction. Aliquots from individual fractions were analysed by the protein assay and then read at 750nm on a spectrometer. Total protein concentration in individual fractions was calculated using a standard curve which was generated using Bovine Serum Albumin (BSA) prepared in TNS buffer with 10% sucrose (0 - 2 mg/ml in the increment of 0.25mg/ml).

Statistics

Statistical analysis was performed with the student's *t*-test or one-way ANOVA in Microsoft® Office Excel.

3.3 Results

3.3.1 Distribution profiles of PrP^C, total PrP and PrP^{Sc} in sucrose gradient

The distribution profiles of different PrP conformers in sucrose step gradients were investigated using frontal cortex (FC) tissue from CJD brains and neurological controls. In vCJD, additional cerebellum (Cb) and thalamus (Th) tissues were also analysed in order to compare the sedimentation profiles of PrP from different regions of vCJD-affected brains. Brain lysates prepared from non-CJD, vCJD and MM1 sCJD brains were loaded on a 10 – 60% sucrose gradient and separated by ultracentrifugation at 200,000 × g for 60 minutes. Eleven fractions of 450µl were collected from top to bottom after velocity sedimentation and analysed by conformation-dependent immunoassay (CDI). CDI fluorescence counts obtained from an aliquot in the native state represent cellular isoform of PrP (PrP^C), whereas CDI results obtained from denatured aliquots represent total PrP present in a sample irrespective of their conformations (Safar *et al.* 1998). The distribution of disease-associated PrP conformer (PrP^{Sc}) in the sucrose gradient was inferred from the ratio of the time-resolved fluorescence (TRF) counts between native and denatured aliquots (D/N ratio) (Bellon *et al.* 2003; Safar *et al.* 1998).

3.3.1.1 Distribution profiles of PrP^C in sucrose gradient

FC samples from five non-CJD brains were analysed to investigate the distribution of PrP^C after fractionation in the sucrose gradients. The distribution of PrP^C in each fraction was measured by CDI in the native state. Although considerable variations in the level of PrP^C were present between cases, PrP^C was mostly detected in top few fractions (Figure 3.1a). When the relative distribution of PrP^C between fractions was expressed as a percentage of the total in all fractions, it became clearer that PrP^C was mostly present in the light fractions (fraction 1 ~ fraction 3) in each case (Figure 3.1b). The amount of PrP recovered in the top three fractions was around 90% of total PrP, irrespective of case when determined by CDI using native aliquots. In the intermediate and bottom fractions of the gradient, however, trace of CDI signals was

also detectable. These results indicate that cellular isoform of PrP present in non-CJD brains mostly failed to sediment and stayed in the light top fractions after ultracentrifugation in the sucrose gradient.

In order to examine the sedimentation profiles of PrP^C present in CJD brains, FC tissues from seven vCJD cases and six MM1 sCJD cases were fractionated by centrifugation in the 10 – 60% sucrose step gradient. For the three of the seven vCJD cases, Cb and Th were also analysed for comparison with FC. When fractions from vCJD FC samples were assayed by CDI in the native state, most fluorescence counts were detected in the top few fractions indicating that PrP^C from vCJD FC also failed to sediment after centrifugation in the sucrose gradients (Figure 3.2a). Despite the variation in the level of PrP^C, the normalized distribution profiles of PrP^C were similar between vCJD cases and were not distinguishable from those of non-CJD controls (Figure 3.2b; compare it with Figure 3.1b). When samples from Cb and Th of vCJD brains were separated in the gradients and analysed in the same way, the distribution profiles of PrP^C were similar to those of vCJD FC, although a minor fraction of PrP^C from Th samples was recovered in the intermediate and bottom fractions (black and striped bars in Figure 3.4a). PrP^C from FC of MM1 sCJD brains was also predominantly recovered in the light, top fractions of the gradients, although normalization also revealed the presence of a small proportion of PrP^C in the intermediate and bottom fractions (Figure 3.3). It is of note that, except for one case, the levels of PrP^C from MM1 sCJD brains were lower than those of non-CJD brains and vCJD brains (compare Figure 3.3a with Figures 3.1a and 3.2a).

For further analysis, the eleven fractions from the gradient were categorized into three groups. The fractions 1 to 3 (in which most of PrP^C was found) was grouped as "top fractions" and fractions 9 to 11 were grouped into "bottom fractions." The remaining fractions (fractions 4 - 8) were grouped as "intermediate fractions." As described above, the distribution profiles of vCJD FC or Cb were similar to that of

non-CJD FC, with ~90% of PrP^C being recovered in the top fractions (P in the top fraction = 0.135) (white, grey and black bars in Figure 3.4b).

In contrast, in vCJD Th, only 60% of PrP^C molecules were present in the top fractions, with ~20% of PrP^C being recovered in the intermediate and bottom fractions (striped bars in Figure 3.4b). The distribution profile of vCJD Th was significantly different when compared to those of the two other vCJD regions ($P <$ 0.0001 in top and intermediate fractions; $P = 0.001$ in bottom fractions). The results from FC of MM1 sCJD were similar to that of vCJD Th ($P > 0.05$ in all three grouped fractions) (dotted bars in Figure 3.4b).

Collectively, the analysis of fractionated samples by CDI in the native state showed that cellular isoform of PrP from both non-CJD and CJD brains remains mainly in the top fractions of the sucrose gradients, although small amounts of PrP^C were also identifiable in the intermediate or bottom fractions from Th samples of vCJD and FC sample of MM1 sCJD.

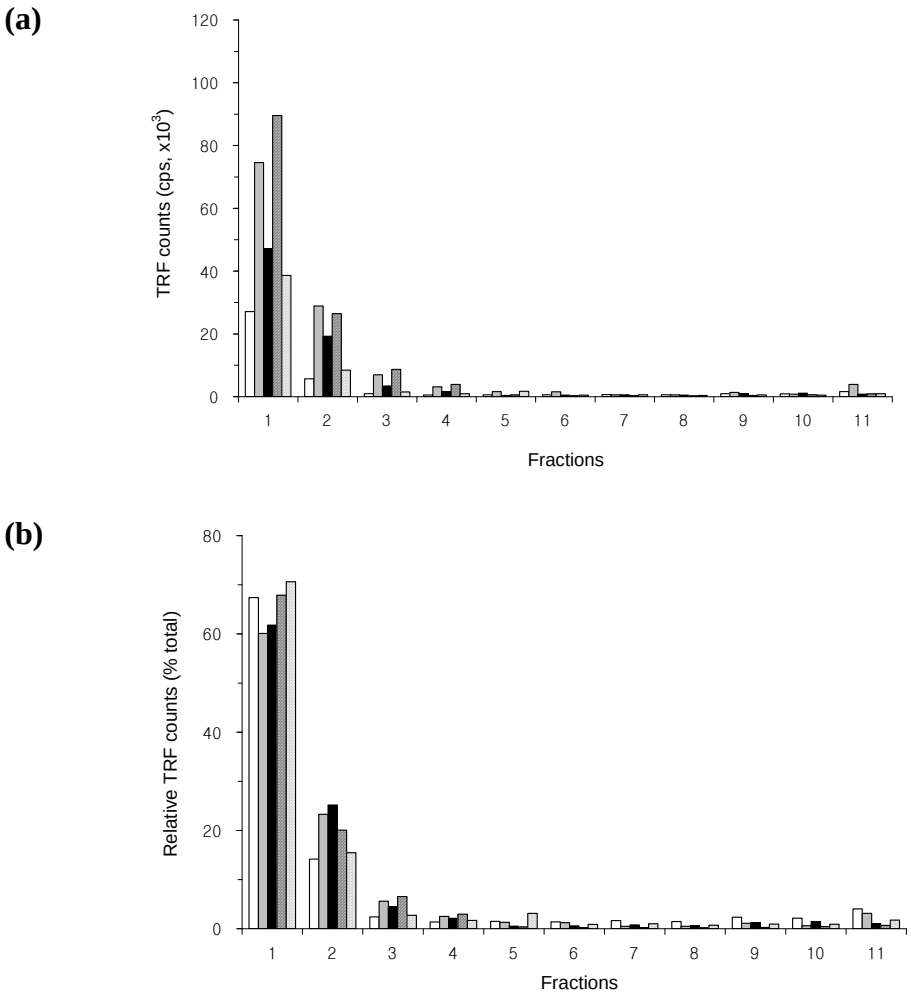

Figure 3.1 Distribution profiles of PrP^C from FC of non-CJD brains after fractionation in sucrose step gradient. Brain lysates from the frontal cortex of neurological control (non-CJD) brains were fractionated in 10 – 60% sucrose step gradients and eleven fractions were collected from top to bottom. Each fraction was analysed by CDI in the native state to measure the amount of PrP^C (a) and the relative distribution of PrP^C between fractions was expressed as a percentage (%) of the total in all fractions (b). Each bar represents individual cases (white bars: non-CJD1; grey bars: non-CJD2; black bars: non-CJD3; striped bars: non-CJD4; dotted bars: non-CJD5). Data shown represent the average for duplicate wells.

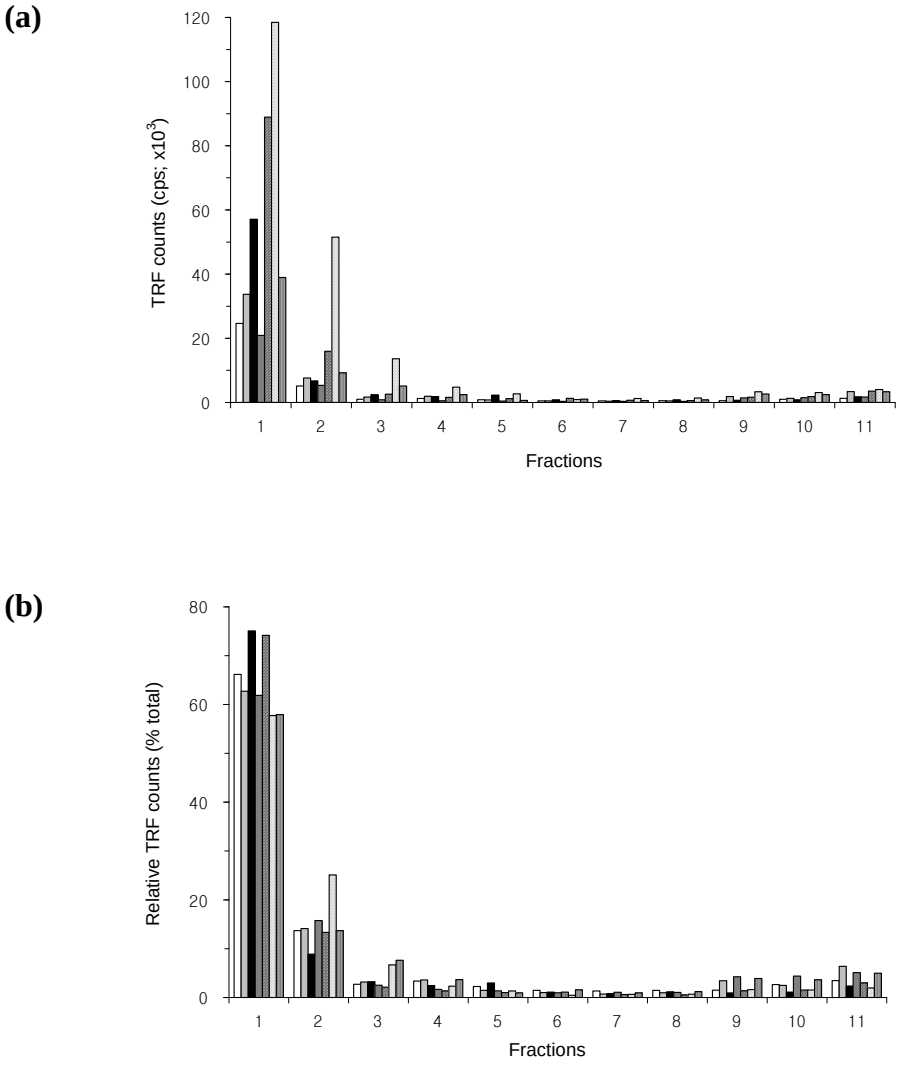

Figure 3.2 Distribution profiles of PrP^C from FC of vCJD brains after fractionation in sucrose step gradient. Brain lysates from the frontal cortex of vCJD-affected brains were fractionated in 10 – 60% sucrose step gradients and eleven fractions were collected from top to bottom. Each fraction was analysed by CDI in the native state to measure the amount of PrP^C (a) and the relative distribution of PrP^C between fractions was expressed as a percentage (%) of the total in all fractions (b). Each bar represents individual cases (white bars: vCJD1; light grey bars: vCJD2; black bars: vCJD3; dark grey bars: vCJD4; striped bars: vCJD5, dotted bars: vCJD8; vertical line bars: vCJD9). Data shown represent the average for duplicate wells.

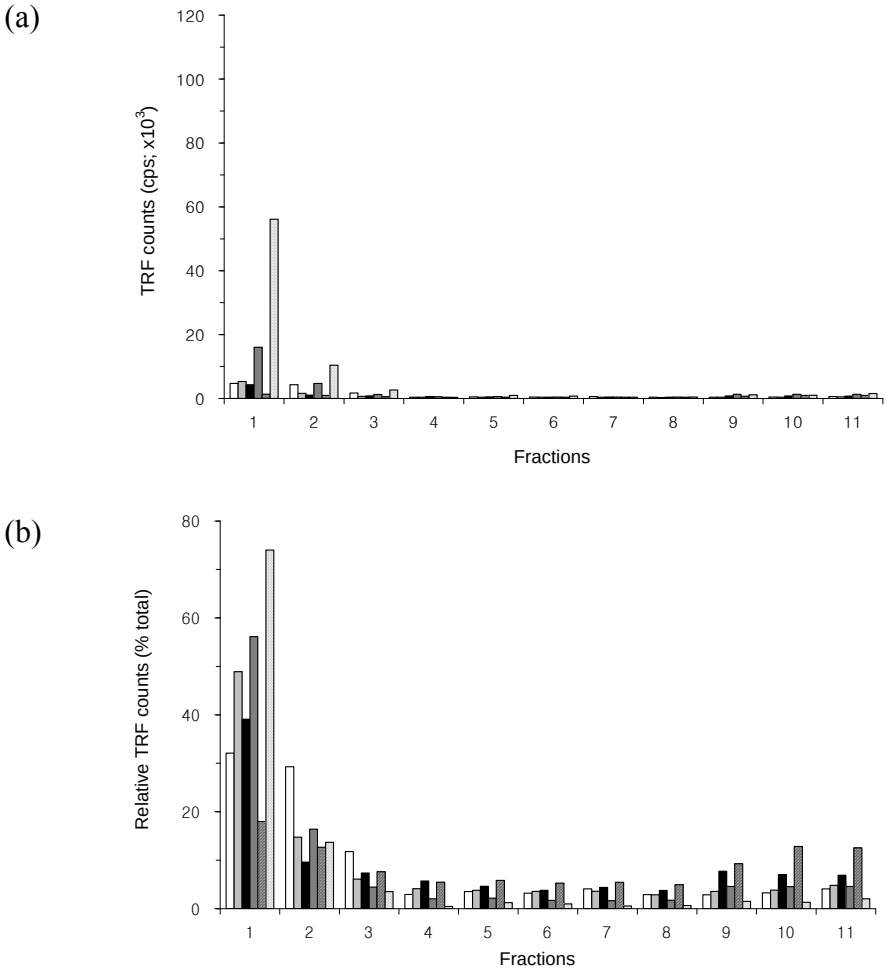

Figure 3.3 Distribution profiles of PrP^C from FC of MM1 sCJD brains after fractionation in sucrose step gradient. Brain lysates from the frontal cortex of MM1 sCJD brains were fractionated in 10 – 60% sucrose step gradients and eleven fractions were collected from top to bottom. Each fraction was analysed by CDI in the native state to measure the amount of PrP^C (a) and the relative distribution of PrP^C between fractions was expressed as a percentage (%) of the total in all fractions. Each bar represents individual cases (white bar: MM1-1; light grey bar: MM1-2; black bar: MM1-6; dark grey bark: MM1-8; striped bar: MM1-10; dotted bar: MM1-13). Data shown represent the average for duplicate wells.

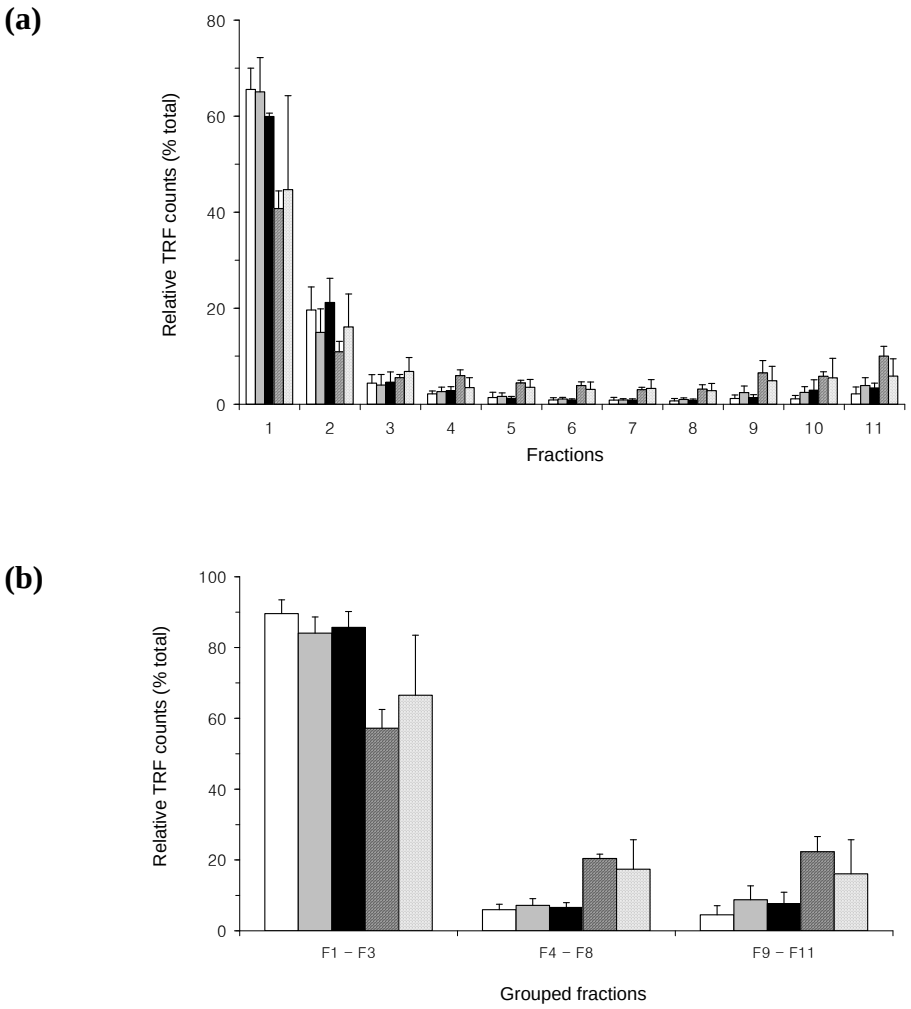

Figure 3.4 Comparison of PrP^C distribution in sucrose step gradient between non-CJD and CJD brains. Eleven fractions were obtained after ultracentrifugation of brain lysates in the sucrose step gradients. (a) The amount of PrP^C in each fraction investigated by CDI in the native state was expressed as a percentage (%) to the sum of eleven fractions. (b) Eleven fractions were categorized into three groups (top fractions: fractions 1 ~ 3; intermediate fractions: fractions 4 ~ 8; bottom fractions: fractions 9 ~ 11) and the distribution of PrP between groups was expressed as a percentage (%) to the sum of the three groups. Data shown represent the average ± S.D. obtained from five cases of FC of control (white bars), from seven cases of vCJD FC (grey bars) or from six cases of FC of MM1 sCJD (dotted bars). In vCJD Cb (black bars) and vCJD Th (striped bars), data shown represent the average ± S.D. obtained from three cases. The result in every individual was an average for duplicate wells.

3.3.1.2 Distribution profiles of total PrP in sucrose gradient

In order to examine the distribution of total PrP in the sucrose gradient after velocity sedimentation, aliquots of fractionated samples were assayed by CDI after denaturation by incubation at 81° for 6 minutes in the presence of 4M GdnHCl. In non-CJD brains, similar to the results obtained from native aliquots, more than 90% of total PrP was recovered in light factions of the gradients (fractions 1 ~ 3) and trace of CDI signals was also dispersed in the intermediate and bottom fractions (Figure 3.5a). Thus, in case of the neurological control brains without prion involvement in their pathogenesis, the distribution profiles of PrP obtained in the two different folding states were very similar to each other (compare Figure 3.5a with Figure 3.1b).

In contrast, samples from FC of vCJD brains showed clearly distinct results in CDI measurement between native and denatured states. While fluorescence counts obtained from native samples were mostly present in the top three fractions (Figure 3.2b), CDI signals detected in those top fractions after denaturation were reduced to less than 50% of the total recovered in all fractions; the remainder was mostly recovered in the bottom fractions (fractions 9 ~ 11) in which only a trace CDI signal was detected in the native state (Figure 3.5b). Thus, the distribution of total PrP in the sucrose gradient emerged in a bipolar pattern when fractionated samples from vCJD FC were investigated by CDI in the denatured state. An exception to this "bipolar pattern" was observed in a sample from vCJD3 FC; more than 80% of total PrP signals were recovered in the top few fractions when measured by CDI in the denatured state, which was similar to the results obtained from native aliquots (black bars of figure 3.5b; compare them with black bars of Figure 3.2b).

In order to further examine the distribution of total PrP in the gradients, fractionated samples from additional regions of vCJD brains and FC of MM1 sCJD brains were assayed by CDI in the denatured state. In vCJD Cb, the distribution profiles of total PrP emerged in a "bipolar" pattern in the gradients (black bars in Figure 3.6a), which was similar to that found in FC of vCJD brains. In comparison, relatively higher

proportion of PrP signal was detected in the intermediate fractions of the gradients when samples from vCJD Th or from FC of MM1 sCJD were analysed in the same way (striped and dotted bars in Figure 3.6a). To compare the level of PrP sedimentation to intermediate fractions more generally, the eleven fractions from the gradients were categorized into three groups. The fractions 1 to 3 in which most of PrP^C remained were grouped as "top fractions" and the fractions 9 to 11 in which PrP molecules were mostly detected by CDI only after denaturation were grouped as "bottom fractions." The remaining fractions (fractions 4 ~ 8) were grouped as "intermediate fractions." The comparison of levels of PrP in these three groups showed more clearly the relative abundance of PrP molecules in the intermediate fractions of vCJD Th and of FC of MM1 sCJD (Figure 3.6b). While the levels of PrP molecules detected in the intermediate fractions from FC and Cb of vCJD brains were less than 10%, they were higher than 20% in the intermediate fractions from Th of vCJD brains and FC of MM1 sCJD brains. Statistical analysis confirmed that this difference in the intermediate fractions was significant with *P* values of <0.001 (vCJD Th *versus* vCJD FC/Cb) and of <0.01 (FC of MM1 sCJD *versus* vCJD FC/Cb), respectively.

In summary, in the non-CJD control brains containing only PrP^C, distribution profiles of PrP were similar when measured in the native or denatured states. When fractionated samples from CJD brains were assayed by CDI, significant differences were observed between the two different folding states; newly detected PrP species after denaturation was mainly present in the bottom fractions of the gradient. Given that the recognition site of mAb 3F4 employed as a detector in the CDI is hidden in native PrP^{Sc} but becomes accessible after denaturation, newly detected CDI signals after denaturation (mainly in bottom fractions) were thought to be mostly attributed to PrP^{Sc} present in those bottom fractions. In this context, the similarity of sedimentation profiles between PrP^C and total PrP observed in the vCJD3 FC sample could be explained by low level of PrP^{Sc} present in that sample.

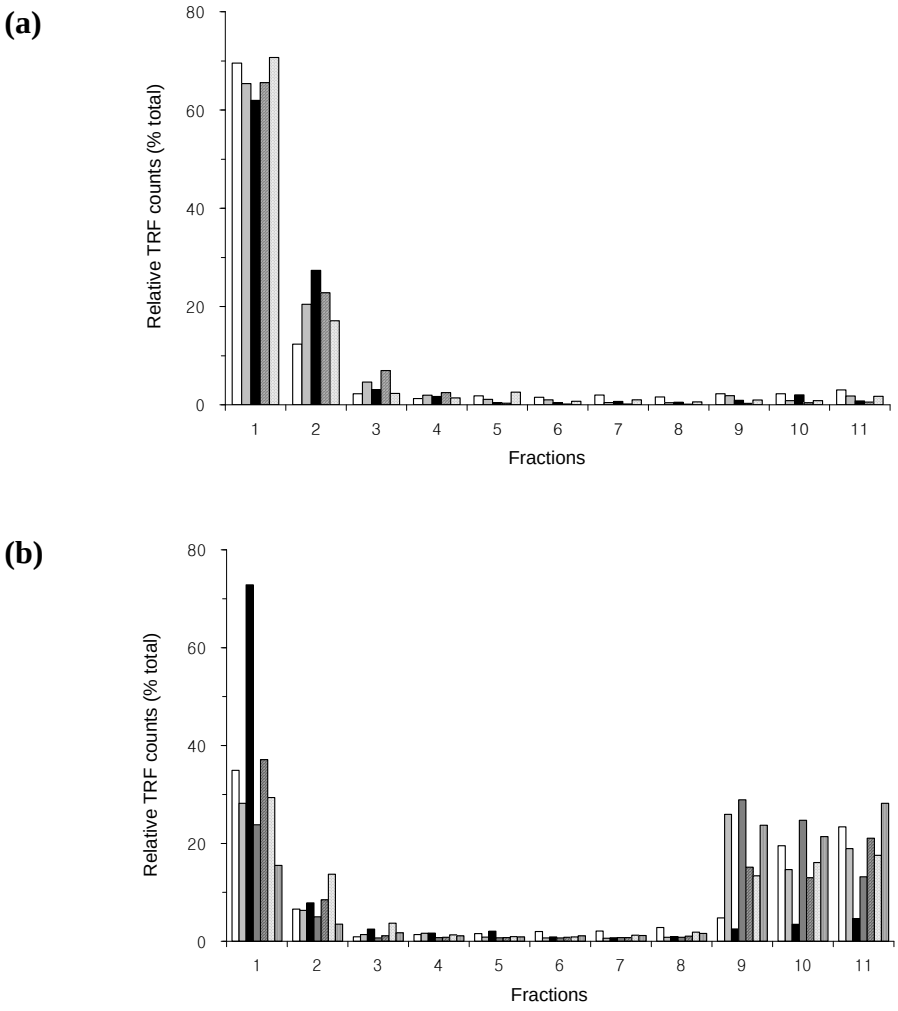

Figure 3.5 Distribution of total PrP in sucrose step gradient. Brain lysates from frontal cortex of non-CJD brains (a) or vCJD brains (b) were fractionated in 10 – 60% sucrose step gradients and eleven fractions were collected from top to bottom. The amounts of total PrP present in individual fractions were determined by CDI in the denatured state and their relative distribution between fractions was expressed as a percentage (%) to the total recovered in all fractions. Each bar represents individual cases and their details are described in Figure 3.1 (for [a]) or Figure 3.2 (for [b]). Data shown represent the average for duplicate wells and error bars showing S.D. were omitted.

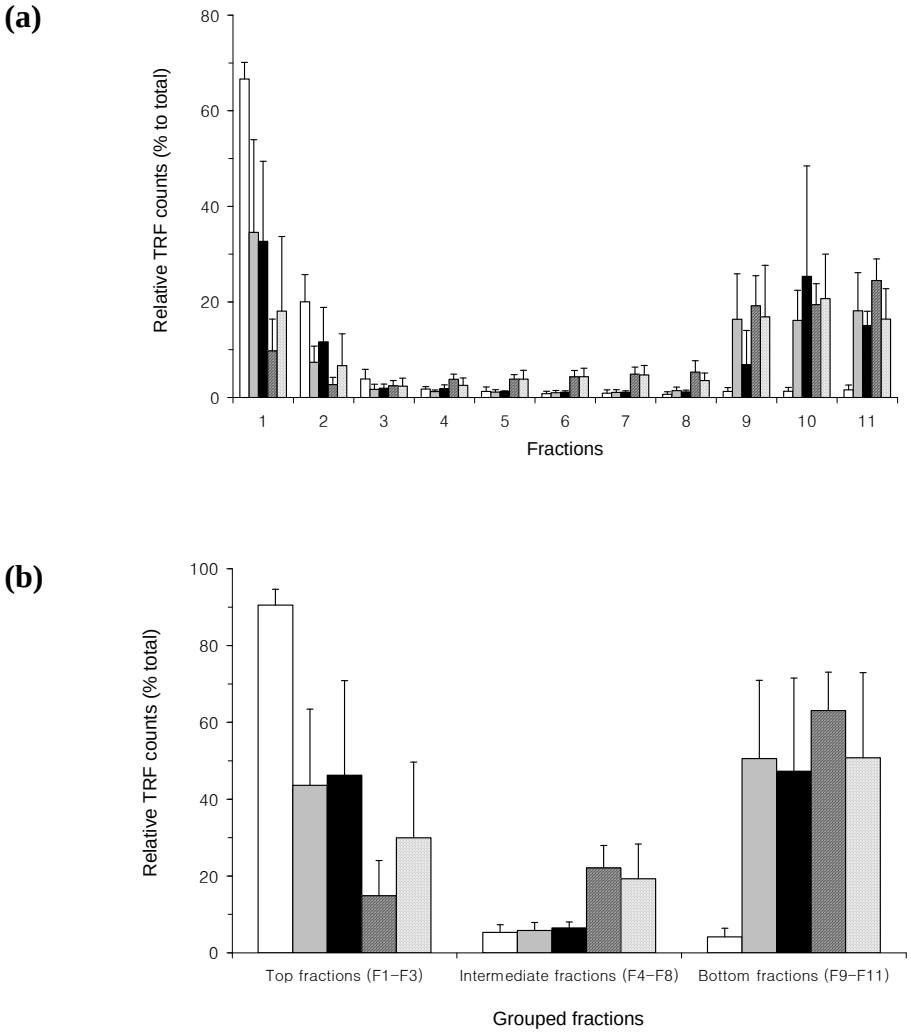

Figure 3.6 Comparison of the distribution profiles of total PrP in sucrose step gradient. Eleven fractions were obtained after ultracentrifugation of brain lysates in the sucrose step gradients. The amount of total PrP present in each fraction was determined by CDI in the denatured state. (a) The amount of total PrP present in each fraction was expressed as a percentage (%) to the sum of eleven fractions. (b) Eleven fractions were categorized into three groups (top fractions: fractions 1 ~ 3; intermediate fractions: fractions 4 ~ 8; bottom fractions: fractions 9 ~ 11) and the distribution of PrP between groups was expressed as a percentage (%) to the sum of the three groups. Data shown represent the average ± S.D. obtained from five cases of FC of control (white bars), from seven cases of vCJD FC (grey bars) or from six cases of FC of MM1 sCJD (dotted bars). In vCJD Cb (black bars) and vCJD Th (striped bars), data shown represent the average ± S.D. obtained from three cases. The result in every individual was an average for duplicate wells.

3.3.1.3 Distribution profiles of PrP^{Sc} in sucrose gradient

The ratio of mAb 3F4 binding to denatured/native PrP was used as an indicator in a direct ELISA-formatted CDI for the presence of PrP^{Sc} in hamster brains (Safar *et al.* 1998). This D/N ratio was also successfully used to detect PrP^{Sc} when serially diluted human CJD brain samples were semi-purified by NaPTA precipitation and assayed by the sandwich format CDI with the mAb Mar-1 as a capture antibody and the 3F4 as a detector (Bellon *et al.* 2003). Based on these previous studies, the distribution of PrP^{Sc} in the sucrose gradient was inferred from CDI D/N ratios which were generated by dividing the TRF counts of the denatured aliquots by those of corresponding native aliquots.

As shown in figure 3.7a, D/N ratios from FC of the non-CJD brains were similar in all fractions of the gradients. The D/N ratios in the top three fractions in which PrP^{C} was mostly present were indistinguishable from those in the intermediate or the bottom fractions. The ratios were usually lower than 1.5 except for three fractions each from three different cases (fraction 10 of non-CJD2, fraction 10 of non-CJD3 and fraction 2 of non-CJD4). D/N ratios in those three fractions were in the range of 1.5 ~ 1.8. It is of note that the D/N ratios in normal hamster brains were lower or equal to 1.8 and the D/N ratios higher than 1.8 were considered to indicate the presence of PrP^{Sc} in hamster brains (Safar *et al.* 1998). A direct comparison of TRF counts between the two different folding states from fractions of a non-CJD control sample was shown in Figure 3.7b.

To examine the distribution of PrP^{Sc} in the sucrose step gradient, D/N ratios of fractionated samples from vCJD FC were generated and compared with those of non-CJD brains. The D/N ratios of top three fractions in all investigated vCJD FC samples were in the range of 1.0 to 1.7, which were indistinguishable from the non-CJD counterparts (Figures 3.8a). The D/N ratios in the intermediate fractions (fractions 4 ~ 8) increased slowly as the fractions became heavier and increased dramatically in the bottom fractions (fractions 9 ~ 11). Although the D/N ratios in the

intermediate fractions were slightly higher than the non-CJD counterparts, the high D/N ratios in the bottom fractions compared to the non-CJD counterparts or other fractions of vCJD FC were much more obvious (Figures 3.8a). A direct comparison of CDI results in the two different folding states from fractions of a vCJD FC sample was shown in Figure 3.8b. In case of the vCJD3 sample which showed similarity between PrP^{C} distribution and total PrP distribution in the sucrose gradient, the D/N ratios in the intermediate fractions were indistinguishable from those of controls; the ratios in the bottom fractions were higher than those of non-CJD brains but greatly lower than those of the other vCJD cases (black bars in Figure 3.8a). Overall, the analysis of fractionated samples by CDI D/N ratio showed that a majority of PrP^{Sc} from FC of vCJD brains migrated to the bottom fractions of the sucrose gradients after ultracentrifugation.

In order to compare the distribution profiles of PrP^{Sc} in the gradient between different regions of vCJD brains, the CDI D/N ratios were generated from fractionated samples of vCJD Cb and vCJD Th. In the fractions from vCJD Cb, the pattern of D/N ratios was overall similar to vCJD FC; while the ratios in the top fractions were indistinguishable from those of non-CJD counterparts, the ratios in the bottom fractions were noticeably higher than those in intermediate fractions (black bars in Figures 3.9a and 3.11). In comparison, the pattern of D/N ratios from fractions of vCJD Th appeared distinct from those of vCJD FC or Cb. Although the D/N ratios in bottom fractions were higher than intermediate fractions, the difference between intermediate and bottom fractions appeared less distinct in vCJD Th when compared to vCJD FC or Cb (striped bars in Figures 3.9a and 3.11). In addition, the D/N ratios from the top fractions of vCJD Th were slightly but measurably higher than those of the corresponding fractions from the control brains or from the two other regions of vCJD brains (striped bars in Figures 3.9a and 3.11). In two of the three vCJD cases in which Th samples were analysed, the D/N ratios were higher than 2 in fraction 1 (vCJD1 and vCJD3) and reached to 4.6 and 6.1 in fraction 3, respectively. In the remaining case (vCJD2), the ratio was 1.8 in fractions 1 and 2 but

increases to 3.1 in fraction 3. Therefore, at least a small portion of PrP^{Sc} molecules from vCJD Th samples was found to remain in the light fractions after ultracentrifugation in the sucrose gradient. A direct comparison of CDI results in the two different folding states from fractions of a vCJD Th sample was shown in Figure 3.9b. Overall, the analysis based on CDI D/N ratios suggests that PrP^{Sc} molecules from vCJD Th distributed more evenly throughout the sucrose gradient compared to those from vCJD FC or Cb.

In order to address the phenotypic influence on the sedimentation profiles of PrP^{Sc}, the CDI D/N ratios were generated from fractions of FC of MM1 sCJD and compared with those of vCJD FC. In the top fractions, the D/N ratios were undistinguishable from those of non-CJD FC without showing any indication of the presence of PrP^{Sc} (Figures 3.10a). The ratios began to increase gradually from fraction 4 and then increased dramatically in the bottom fractions, which were similar to the pattern of D/N ratios of vCJD FC (dotted bars in Figure 3.11). A direct comparison of CDI results in the two different folding states from fractions of a FC sample of MM1 sCJD was shown in Figure 3.10b. However, despite this overall pattern of the D/N ratios, variations were also easily recognizable between cases of MM1 sCJD. For example, the D/N ratios were relatively similar between intermediate and bottom fractions in MM1-1 in which the D/N ratios were low in the bottom fractions compared to others (white bars of Figure 3.10a). Therefore, it appears that the relative distribution of PrP^{Sc} between fractions varied between cases and the predominant abundance of PrP^{Sc} in the heavy bottom fractions may not be the rule in FC of MM1 sCJD.

In summary, when brain lysates from CJD brains were subjected to sedimentation in the 10 – 60% sucrose gradients, a majority of PrP^{Sc} migrated to the bottom heavy fractions (fractions 9 ~11) judging from CDI D/N ratios. A minor fraction of PrP^{Sc} was also present in the intermediate fractions (fractions 4 ~ 8). In the top fractions, the presence of PrP^{Sc} was also identified only in vCJD Th; it is not clear, however,

whether or not PrP^{Sc} is present in a low level in the top fractions from other regions of vCJD or from FC of MM1 sCJD because the presence of high levels of PrP^{C} in those fractions has the effect of lowering the D/N ratios.

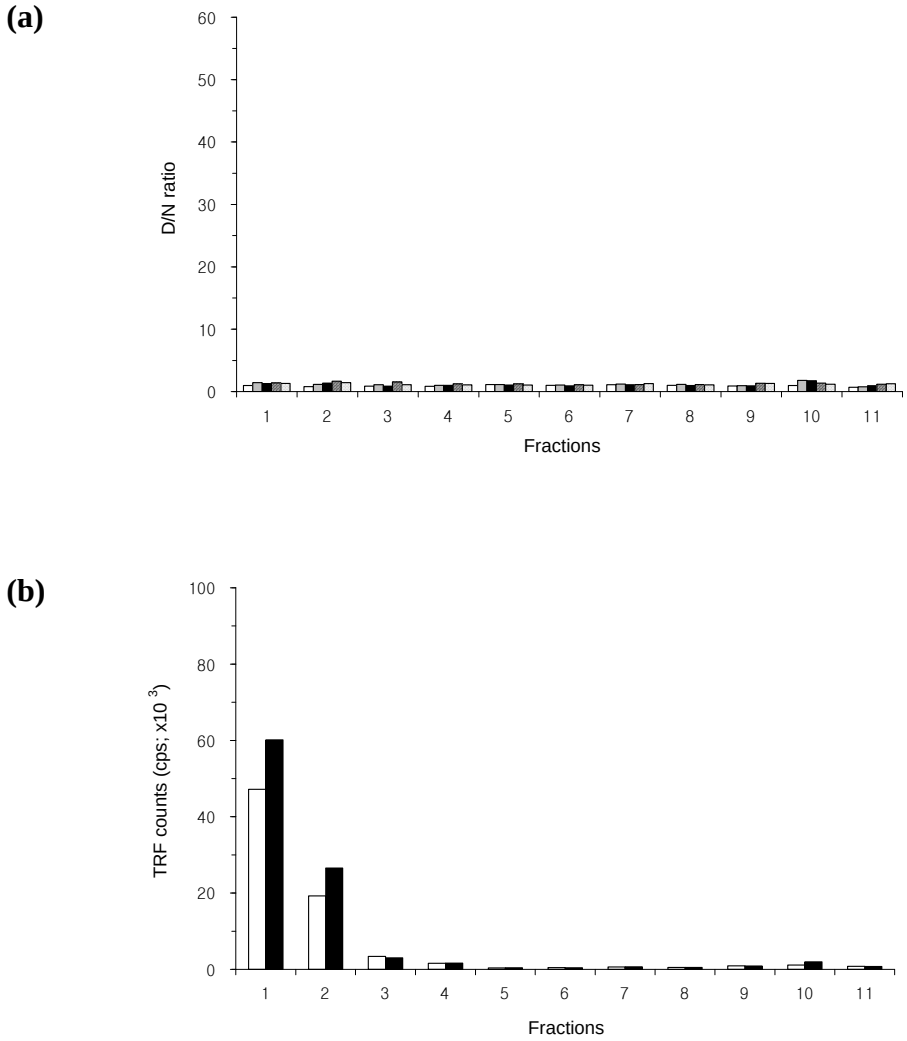

Figure 3.7 CDI D/N ratios for fractions from FC of non-CJD brains. (a) The CDI results on fractionated samples from FC of non-CJD brains were described in 3.3.1.1 (for native samples) and in 3.3.1.2 (for denatured samples). The CDI D/N ratios were calculated by dividing TRF counts of denatured samples by the counts of the corresponding native samples. Each bar represents individual cases and their details were described in Figure 3.1. (b) The CDI TRF counts from fractions of a control brain (non-CJD3) were directly compared between the native (white bars) and denatured (black bars) states. Data shown represent the average for duplicate wells.

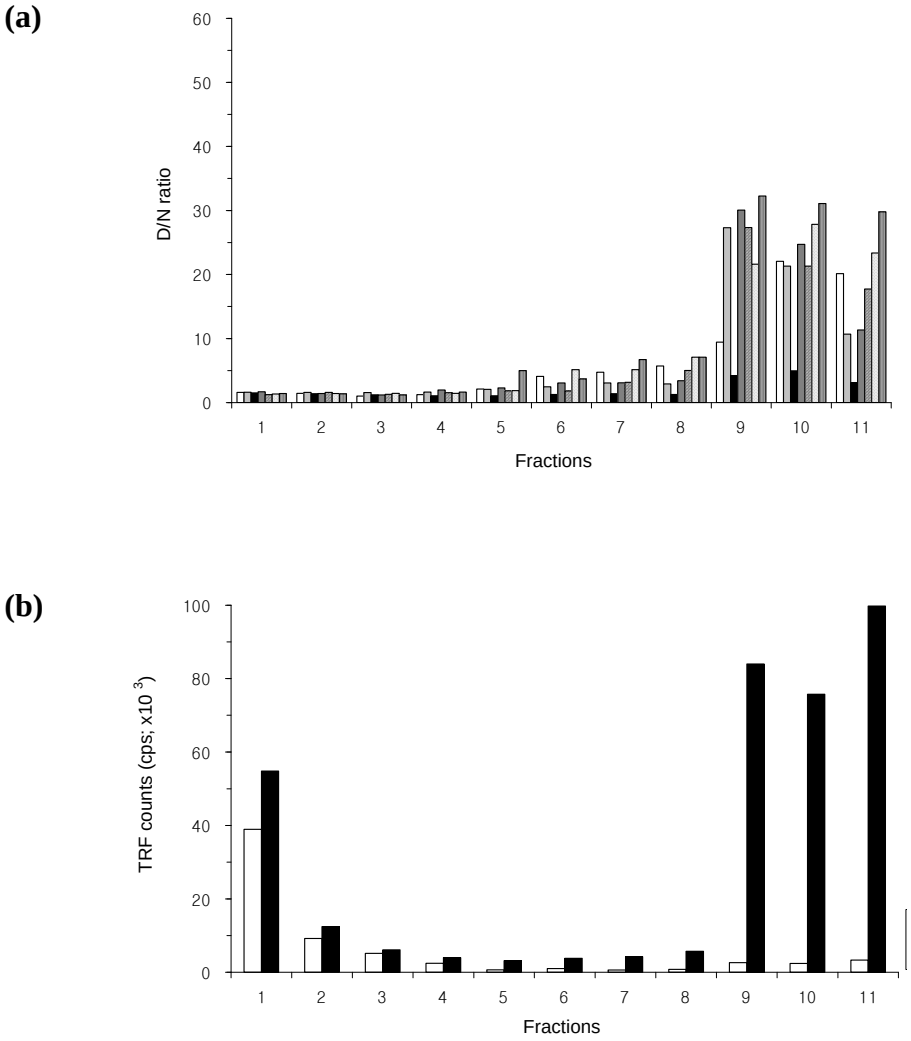

Figure 3.8 CDI D/N ratios for fractions from FC of vCJD brains. (a) The CDI results on fractionated samples from FC of vCJD brains were described in 3.3.1.1 (for native samples) and in 3.3.1.2 (for denatured samples). The CDI D/N ratios were calculated by dividing TRF counts of denatured samples by the counts of the corresponding native samples. Each bar represents individual cases and their details were described in Figures 3.2. (b) The CDI TRF counts from fractions of FC tissue of a vCJD brain (vCJD9) were directly compared between the native (white bars) and denatured (black bars) states. Data shown represent the average for duplicate wells. .

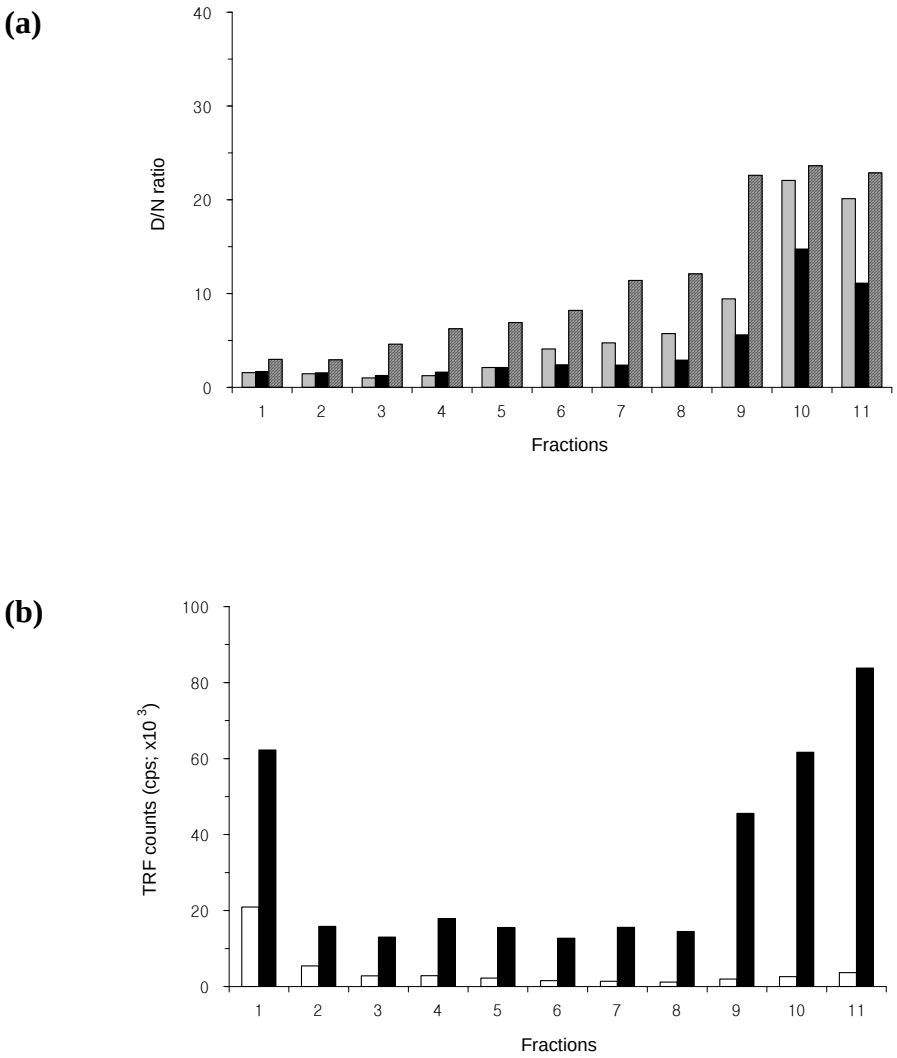

Figure 3.9 Comparison CDI D/N ratios between fractions derived from different regions of a vCJD brain. (a) The D/N ratios for eleven fractions from different regions of a vCJD brain (vCJD1) were generated by dividing TRF counts of denatured samples by the counts of the corresponding native samples. Grey bars: vCJD FC; Black bars: vCJD Cb; Striped bars: vCJD Th. (b) The CDI TRF counts from fractions of Th tissue of vCJD1 were directly compared between the native (white bars) and denatured (black bars) states. Data shown represent the average for duplicate wells.

(a)

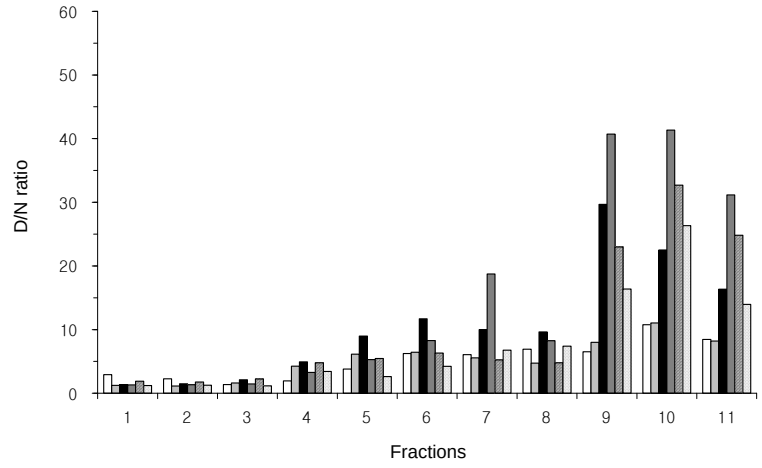

(b)

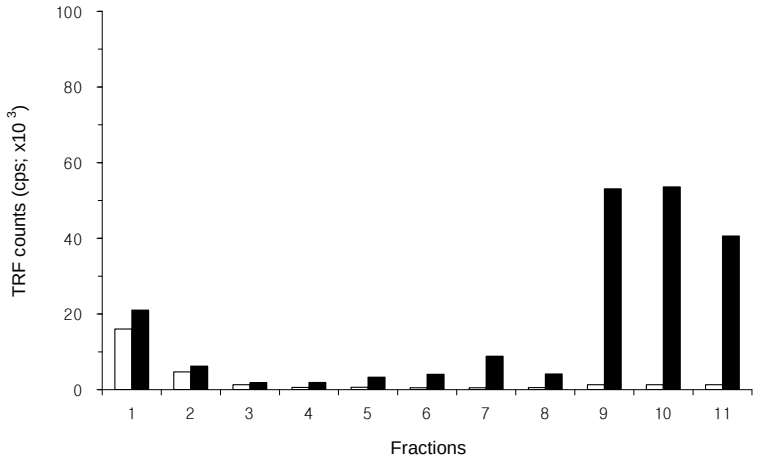

Figure 3.10 CDI D/N ratios for fractions from FC of MM1 sCJD brains. (a) The D/N ratios for eleven fractions from FC of MM1 sCJD brains were generated by dividing TRF counts of denatured samples by the counts of the corresponding native samples. Each bar represents individual cases and their details were described in Figure 3.3. (b) The CDI TRF counts from fractions of FC tissue of a MM1 sCJD case (MM1-8) were directly compared between the native (white bars) and denatured (black bars) states. Data shown represent the average for duplicate wells.

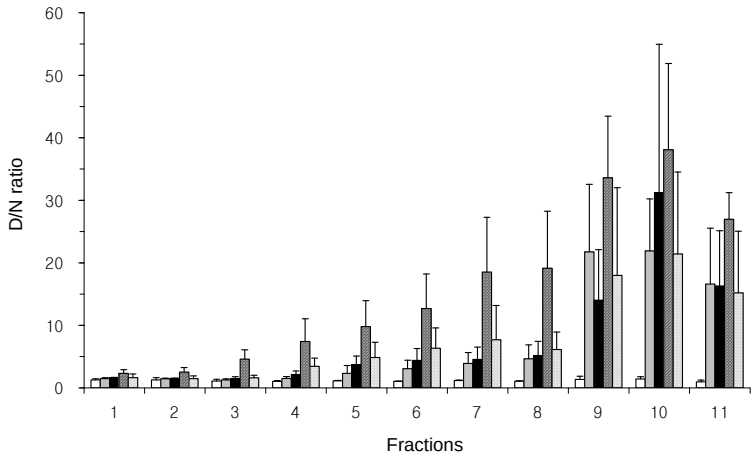

Figure 3.11 Comparison of CDI D/N ratios for fractions derived from different regions of vCJD brains and FC of MM1 sCJD brains. The CDI D/N ratios were calculated by dividing TRF counts of denatured samples by the counts of the corresponding native samples. Data shown represent the average ± S.D. obtained from five cases of FC of control (white bars), from seven cases of vCJD FC (grey bars) or from six cases of FC of MM1 sCJD (dotted bars). In vCJD Cb (black bars) and vCJD Th (striped bars), data shown represent the average ± S.D. obtained from three cases. The result in every individual was an average for duplicate wells.

3.3.2 Distribution profiles of PrP^{Sc} in sucrose gradient after mild proteolysis

As shown in 3.3.1.1, PrP^{C} in both non-CJD and CJD brains stays mostly in light top fractions of the sucrose gradient. If low levels of PrP^{Sc} are present in the top fractions, the increase of CDI TRF counts after denaturation may not be sufficient for the D/N ratio to be distinguishable from those of non-CJD brains. In this context, the presence of PrP^{Sc} in the top fractions of the gradient was further investigated after digesting PrP^{C} in the fractionated samples with mild proteolysis.

3.3.2.1 Effect of PK treatment to PrP conformers in fractionated samples

For the analysis of the effect of PK treatment, first, the fractionated samples from two neurological control brains were digested with 2.5µg/ml PK for 1 hour at 37°C and then assayed by CDI. When the CDI signals in the denatured state were compared before and after the proteolysis, only background levels of signals were detected after proteolysis indicating that the PrP^{C} present in the non-CJD fractions was fully susceptible to this proteolysis under these conditions (Figure 3.12).

Next, the fractionated samples from different areas of a vCJD brain were digested with 2.5µg/ml PK or 50µg/ml PK for 1 hour at 37°C and then assayed by CDI. The fluorescence signals from native samples which were mainly present in the top few fractions largely disappeared after PK digestion at 2.5µg/ml, reflecting the high susceptibility of PrP^{C} to this condition of proteolysis (upper row in Figure 3.13). When the samples digested with 2.5µg/ml PK were analysed after denaturation, PrP immunoreactivity was not detectable in the top three fractions from vCJD FC or vCJD Cb; in comparison, PrP signals were readily detectable in those top fractions from vCJD Th at a third to a quarter of the level detected prior to digestion (grey bars in bottom row of Figure 3.13). In the intermediate and bottom fractions digested with 2.5µg/ml PK, about a third to a half of PrP signals remained, irrespective of brain regions (grey bars in bottom row of Figure 3.13). Following the treatment with 50µg/ml PK, PrP signals were further reduced to a great extent. In vCJD FC and Cb, PrP signals were barely detectable only in bottom few fractions; in vCJD Th, PrP

signals were present in all fractions but their levels were only 10 ~ 30% of those treated with 2.5 µg/ml PK except for fraction 10 (black bars in bottom row of Figure 3.13).

Collectively, the results in this section showed that PrP^{C} is highly susceptible to the digestion with 2.5µg/ml PK and that the presence of PrP^{Sc} in the top fractions can be revealed by this mild condition of proteolysis. However, the treatment of sucrose fractions with 2.5µg/ml PK also appears to digest a subset of PrP^{Sc}, given that PrP signals in the intermediate or bottom fractions were mostly derived from abnormal form of PrP and that they were reduced to levels lower than a half of the undigested corresponding fractions.

(a)

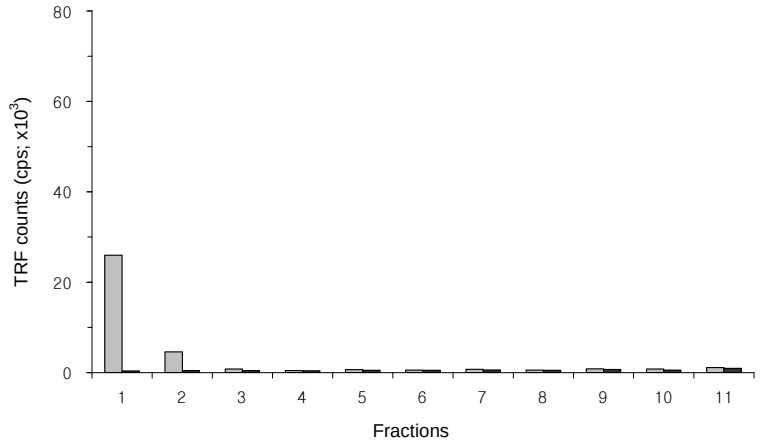

(b)

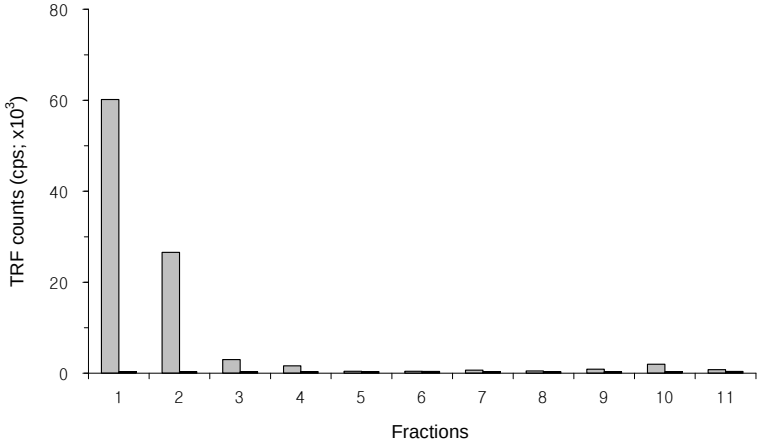

Figure 3.12 Absence of detectable PrP in the fractionated samples from FC of non-CJD1 (a) or non-CJD3 (b) after digestion with 2.5µg/ml PK. Brain lysates from FC of non-CJD brains were centrifuged in 10 – 60% sucrose step gradient and eleven fractions were collected from top of the gradients. Samples from individual fractions left undigested or were digested with 2.5µg/ml PK and then assayed by CDI in the denatured state for the measurement of total PrP. Grey bars represent fluorescence signals obtained from undigested samples and black bars represent those obtained from samples digested with 2.5µg/ml PK. Data shown represent the average for duplicate wells.

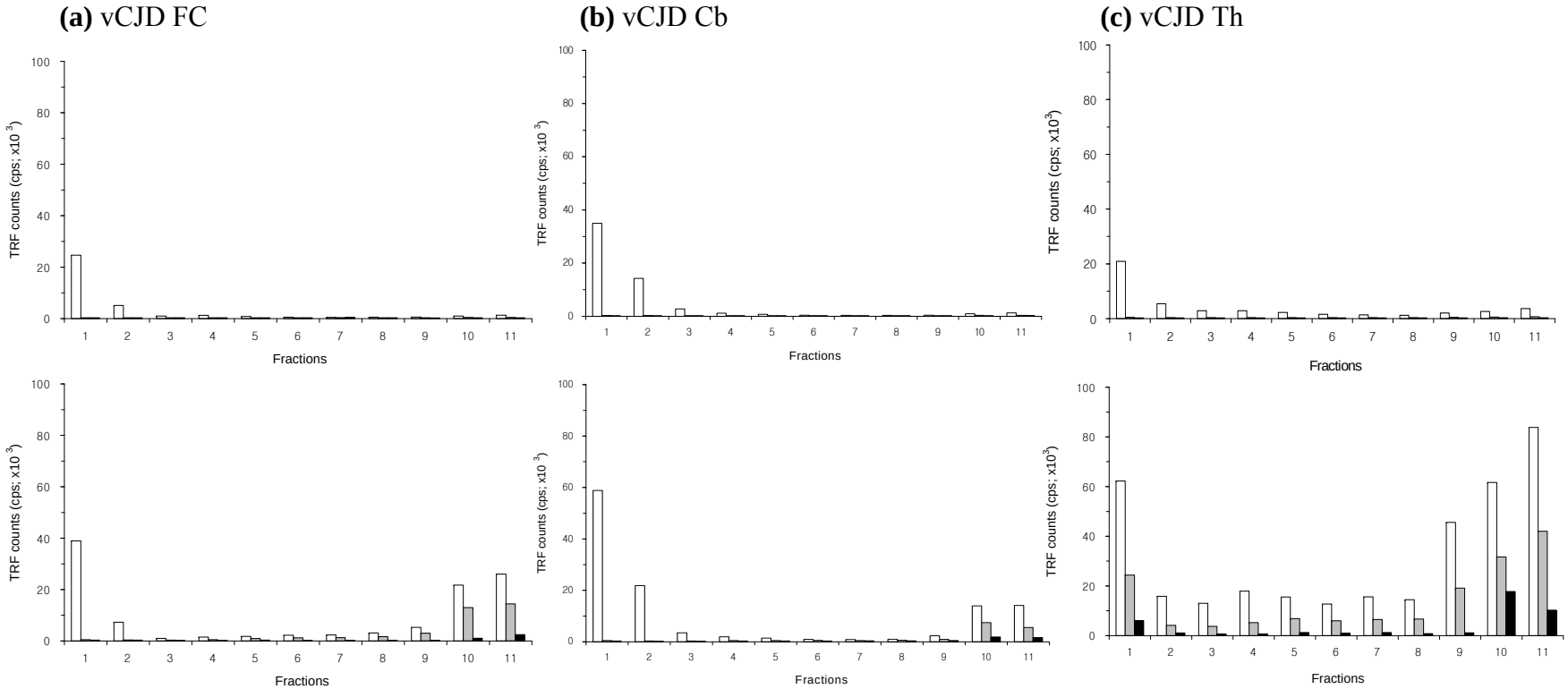

Figure 3.13 Effects of PK treatment to different PrP conformers in fractionated samples from different regions of a vCJD brain. Brain lysates prepared from FC (a), Cb (b) or Th (c) of a vCJD brain were fractionated in 10 – 60% sucrose step gradients and eleven fractions were collected from top of the gradients. Three aliquots from individual fractions left undigested (white bars) or were digested with two different concentrations of PK (2.5µg/ml [grey bars] or 50µg/ml [black bars]). Then, the fractionated samples undigested or digested with PK were analysed by CDI. The fluorescence signals obtained from native aliquots are shown in the upper row and those from denatured aliquots are shown in the bottom row. Data shown represent the average for duplicate wells.

3.3.2.2 Distribution of PrP^{Sc} after digestion with 2.5µg/ml PK

Based on the results in section 3.3.2.1, the fractionated samples from more CJD brains were first treated with 2.5µg/ml PK for 1 hour at 37°C and then assayed by CDI. In vCJD FC, the high D/N ratios in the bottom fractions were quite outstanding when compared to the intermediate fractions with the ratios usually lower than 5 or to the top fractions with the ratios lower than 1.5 (white bars in Figure 3.14; also refer to Figure 3.13a). Therefore, in vCJD FC, the application of the mild proteolysis prior to the CDI measurement did not cause any meaningful change in the overall pattern of D/N ratios, showing once more the absence of detectable PrP^{Sc} in the top fractions and the migration of a major fraction of PrP^{Sc} to the bottom fractions. When eleven fractions from Cb of a vCJD case were analysed by CDI after the mild proteolysis, as in vCJD FC, there was no detectable PrP^{Sc} in the top fractions and a major fraction of PrP^{Sc} was present in the bottom fractions (refer to Figure 3.13b). Also in FC of MM1 sCJD, the prior treatment of fractions with low level of PK did neither cause any change in the profile of D/N ratios nor reveal any sign of PrP^{Sc} in the top fractions; the D/N ratios were noticeably high in the bottom fractions (fractions 9 ~ 11), indicating the predominant abundance of PrP^{Sc} in those fractions (black bars in Figure 3.14).

In contrast to the two other regions of vCJD brains or FC of MM1 sCJD, the application of mild proteolysis to the fractions of vCJD Th caused a great change in the CDI results in the top fractions. While the overall profiles of the D/N ratios in the intermediate and bottom fractions were similar before and after the proteolysis, the D/N ratios in the top fractions were greatly increased (grey bars in Figures 3.14; also refer to Figure 3.13c). The increase of the D/N ratios was particularly remarkable in fraction 1 from all three vCJD cases investigated (including the case described in 3.3.2.1); the ratios of fraction 1 were in range of 1.8 to 3 before the proteolysis, but they reached the range of 20 to 57 after the PK treatment. Thus, the introduction of the mild proteolysis to the fractions of vCJD Th prior to the CDI measurement has revealed the presence of readily detectable amounts of PrP^{Sc} in the light fractions of

the sucrose gradient. Overall, PrP^{Sc} from vCJD Th was relatively evenly distributed throughout the gradient, when compared to vCJD FC or Cb in which a major fraction of PrP^{Sc} was detected in the bottom fractions.

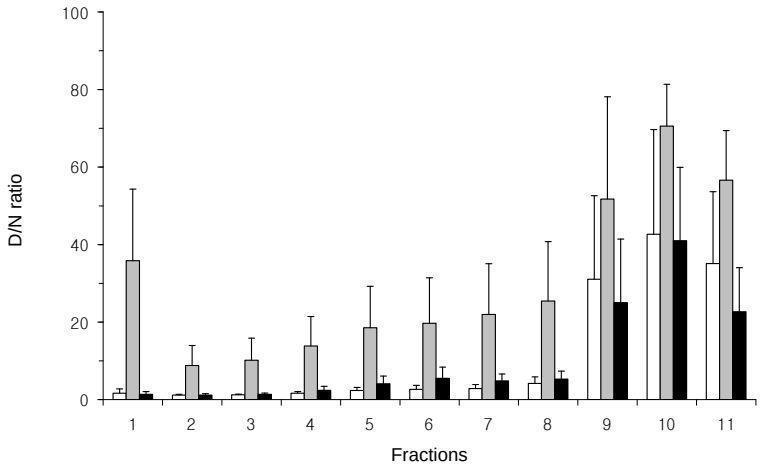

Figure 3.14 Comparison of CDI D/N ratios for PK-treated fractions between vCJD FC, vCJD Th and MM1 sCJD FC. Eleven fractions each from vCJD FC, vCJD Th or FC of MM1sCJD were digested with 2.5µg/ml PK for 1 hour at 37°C and then analysed by CDI. The D/N ratios for individual fractions were calculated by dividing TRF counts of denatured samples by the counts of the corresponding native samples. Data shown represent the average ± S.D. obtained from six cases of vCJD FC (white bars), three cases of vCJD Th (grey bars) and five cases of MM1 sCJD FC (black bars). The result in every individual was an average for duplicate wells.

3.3.3 Distribution of PrP^{res} in sucrose gradient

Partial resistance to protease digestion is commonly used as an operational definition of PrP^{Sc}. In addition to digestion of PrP^{C}, proteolytic treatment results in N-terminal truncation of PrP^{Sc}, leaving PK-resistant core fragments of PrP^{Sc} (termed PrP^{res}). In order to compare the distribution profiles of PrP^{res} in the sucrose gradient with those of CDI-based PrP^{Sc}, the eleven fractions each from one case of vCJD (FC and Th samples) or from one case of MM1 sCJD (FC sample) were analysed by Western blot before and after proteolysis.

Firstly, the eleven fractions from a non-CJD brain left undigested or were digested with 2.5µg/ml PK, and were analysed by Western blot. In undigested samples, PrP^{C} immunoreactivity was mostly found in top two fractions as in the CDI analysis (upper row in Figure 3.15). Additionally, very faint, ambiguous signals which were similar to the molecular mass of PrP were just detectable in the bottom three fractions. PrP signals were no longer detectable after digesting each fraction with 2.5µg/ml PK (bottom row in Figure 3.15).

Next, the eleven fractions from CJD brain samples were analysed similarly. When each fraction from tissue of vCJD1 FC was immunoblotted with mAb 3F4, PrP signals were mainly detected in top two fractions and in bottom three fractions with weak immunoreactivity being present in some of the intermediate fractions (upper row in Figure 3.16a). In densitometric analysis, the amount of PrP in the top three fractions was 33% of the total and that in the bottom three fractions was 57% of the total. After digestion of individual fractions with 2.5µg/ml PK, PrP molecules found in the top fractions were no longer detectable and the amount of PrP detected in the bottom fractions accounted for 84% of the total PrP remaining (middle row in Figure 3.16a). Following PK digestion at 50µg/ml, PrP species were mostly detectable in the bottom three fractions (bottom row in Figure 3.16a), accounting for ~98% of the total PrP remaining. Thus, similar to the results shown by CDI, total PrP in vCJD FC

was detected in a "bipolar" pattern in the gradient and PrP^{res} was mostly detected in the bottom fractions of the gradient.

In contrast to vCJD FC, PrP immunoreactivity from fractions of vCJD1 Th was dispersed throughout the gradient (upper row in Figure 3.16b). After proteolysis of individual fractions with 2.5µg/ml PK, PrP immunoreactivity was still present in all fractions including the top three fractions (middle row in Figure 3.16b). In the densitometric analysis, the amount of PrP was 16% of the total in the top three fractions, 47% in the intermediate five fractions and 37% in the bottom three fractions. Following PK digestion at 50µg/ml, PrP signals were still detectable in all fractions, although PrP species present in fractions 2 ~ 3 were severely reduced (bottom row in Figure 3.16b). In the densitometric analysis, the amount of PrP was 6% of the total in the top three fractions, 29% in the intermediate five fractions and 65% in the bottom three fractions.

In FC of MM1 sCJD, PrP was detected throughout the gradients (upper row in Figure 3.16c). After PK treatment at 2.5µg/ml, PrP in the top three fractions was completely digested and PrP immunoreactivity was detected in the intermediate and bottom fractions (middle row in Figure 3.16c). The amount of PrP signals detected in the bottom three fractions was about 65% of the total and the remaining 35% was present in the intermediate fractions. Following PK digestion at 50µg/ml, PrP^{res} was mainly detectable in the bottom few fractions leaving faint three-band signals in some of the intermediate fractions (bottom row in Figure 3.16c). The amount of PrP^{res} detected in the bottom three fractions was about 90% of the total PrP^{res} signal and the remaining 10% was present in the intermediate fractions.

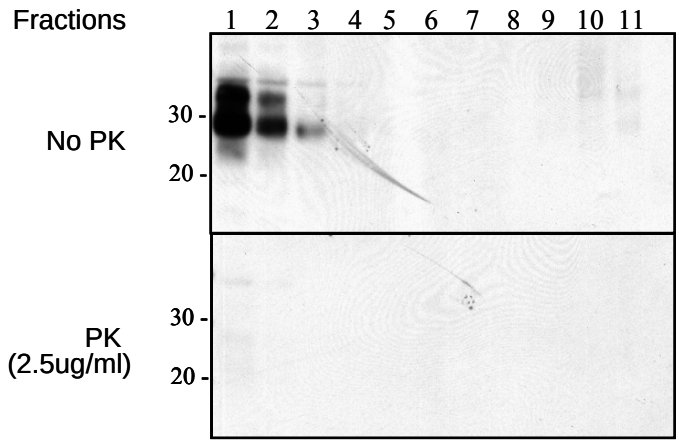

Figure 3.15 PrP distribution after fractionation in sucrose step gradient. Brain lysates from FC of a neurological control brain (non-CJD3) were centrifuged in 10 – 60% sucrose step gradient and eleven fractions were collected from top of the gradient. Samples from each fraction left untreated (upper row) or treated with 2.5µg/ml PK (bottom row) for 1 hour at 37°C. The distribution of PrP before and after the proteolysis was investigated by Western blot using mAb 3F4.

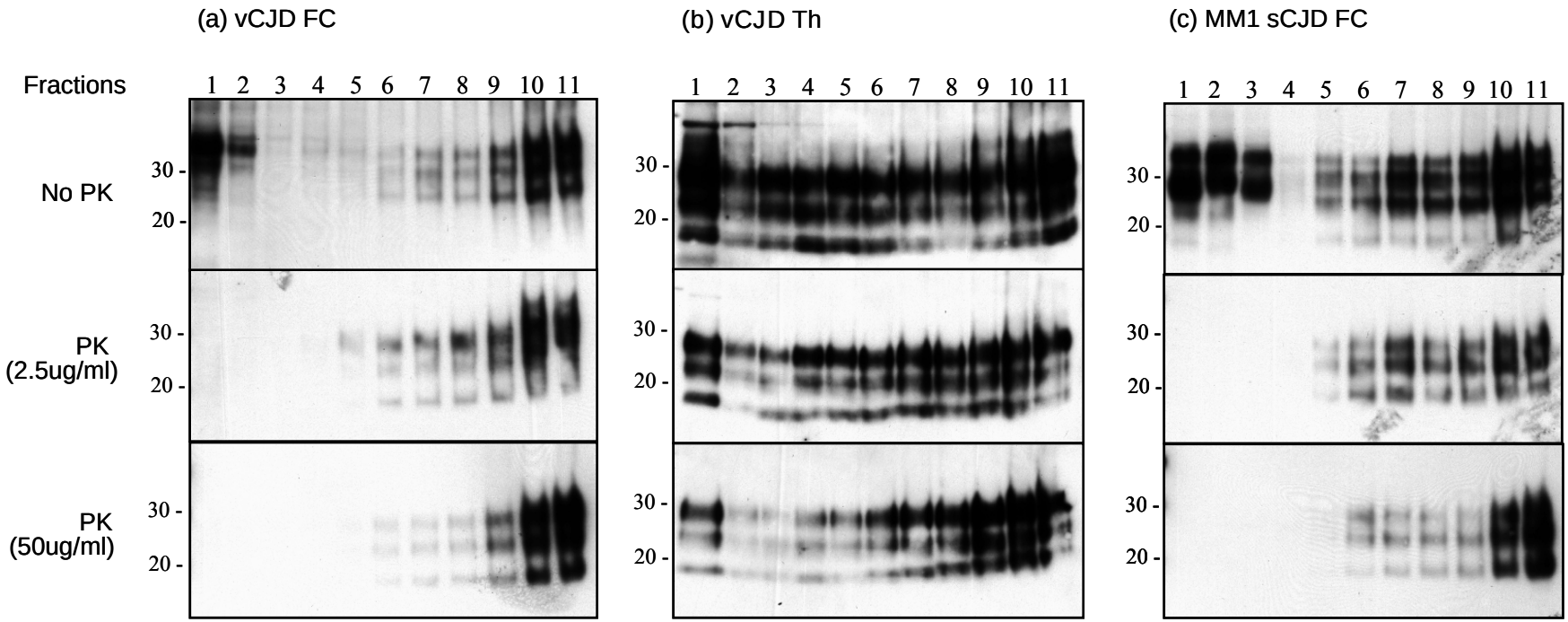

Figure 3.16 PrP distribution after fractionation in sucrose step gradient. Brain lysates from vCJD1 FC (a), vCJD1 Th (b) and MM1-1 FC (c) were fractionated in 10 – 60% sucrose step gradients and eleven fractions from top to bottom were collected. Three aliquots from individual fractions remained untreated (upper row) or were digested with PK at 2.5µg/ml (middle row) or at 50µg/ml (bottom row) for 1 hour at 37°C. The distribution of PrP before and after the proteolysis was investigated by Western blot using mAb 3F4. MM1 denotes MM1 sCJD.

3.3.4 Supplementary data: total protein distribution in sucrose gradient

To investigate the distribution of total protein in the sucrose gradient, first, the fractionated samples from non-CJD control brains or vCJD brains were run on a gel and then separated proteins on the gel were stained with Coomassie blue. As shown in Figure 3.17, a majority of total protein stayed in the light top fractions of the gradient and low levels of protein were recovered in the bottom fractions.

In order to measure the levels of total protein in each fraction more precisely, the Bio-Rad DC protein assay was performed as described in section 3.2.2. A standard curve generated using BSA (range: 0mg ~ 2mg in the increment of 0.25mg) was shown in Figure 3.18 and a trend line for this standard curve was determined using Excel as follows: $y = 6.9358x - 0.1113$ (y = protein amount; x = absorbance at 750 nm). When the amount of total protein in each fraction was determined by this equation after the Bio-Rad DC protein assay, in both non-CJD control and vCJD brains, protein was predominantly present in the top two fractions with a minority of protein in the bottom few fractions (Figure 3.19).

Collectively, these results have shown that the distribution of total protein in the sucrose gradient after ultracentrifugation was highly variable between fractions with its predominant amount stationary in the top few fractions.

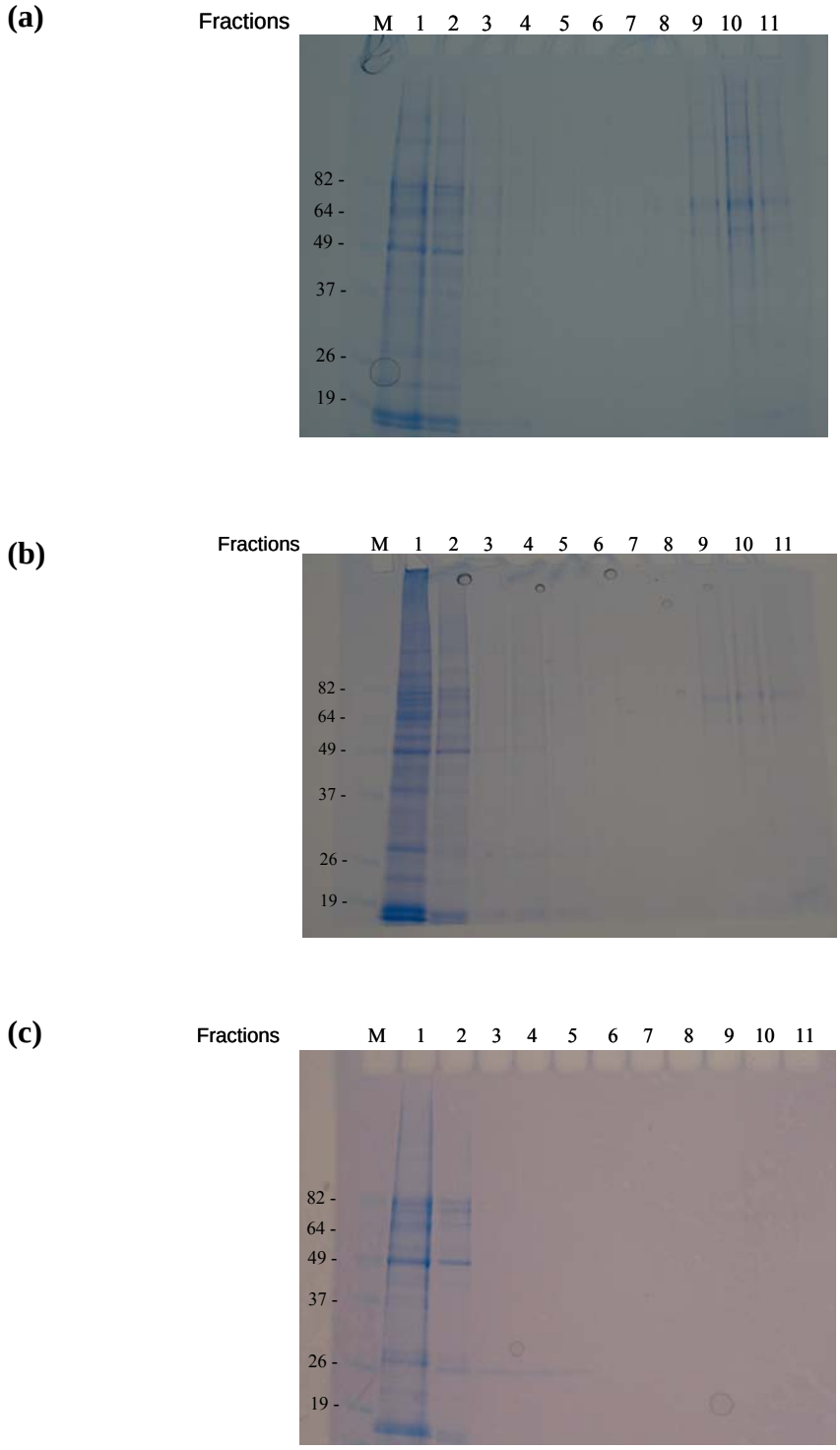

Figure 3.17 Total protein distribution after fractionation in sucrose step gradient. Brain lysates from FC of non-CJD3 (a), vCJD1 FC (b) and vCJD1 Th (c) were fractionated in 10 – 60% sucrose step gradients. Eleven fractions collected from top to bottom were separated by electrophoresis and the gels were stained with Coomassie blue.

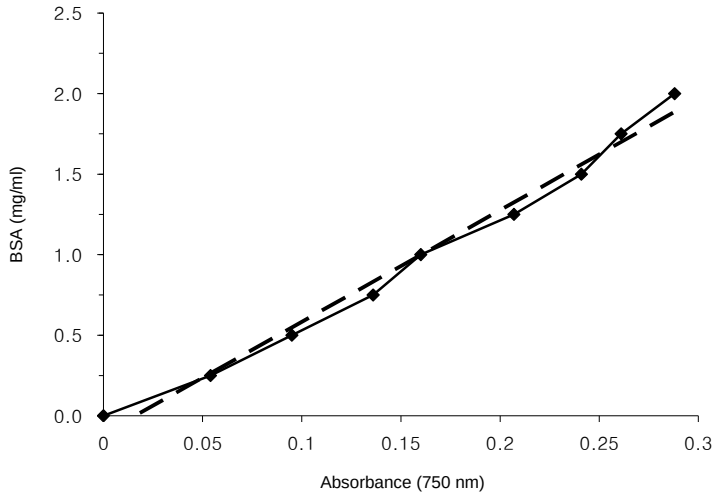

Figure 3.18 A standard curve generated using BSA. Bovine Serum Albumin (BSA) prepared in various concentrations was assayed as described in section 3.2.2 and read at 750nm on a spectrometer (solid line). A trend line for this standard curve was generated using Excel (dashed line). The equation for this trend line was described in the text.

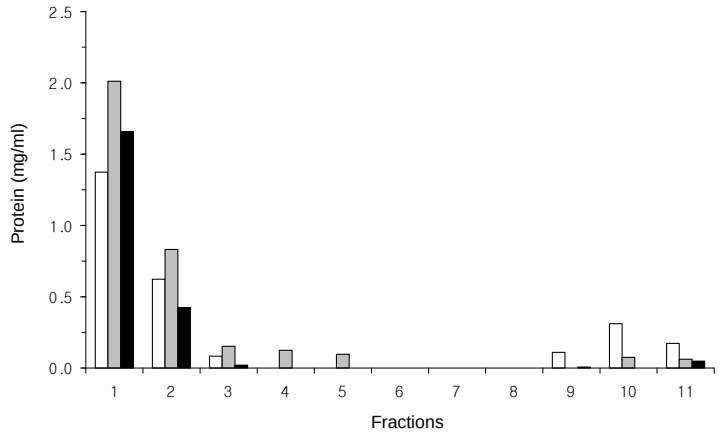

Figure 3.19 Total protein distribution after fractionation in sucrose step gradient. Brain lysates from FC of non-CJD3 (white bars), vCJD1 FC (grey bars) and vCJD1 Th (black bars) were fractionated in 10 – 60% sucrose step gradients and eleven fractions were collected from top to bottom. The amounts of total protein in individual fractions were determined by the standard reference curve described in Figure 3.18.

3.4 Discussion

3.4.1 PrP^C: sedimentation profiles in sucrose gradient

3.4.1.1. Non-CJD control brains

When brain lysates from frontal cortex of the neurological controls containing only PrP^C were fractionated by ultracentrifugation in the sucrose gradient, PrP molecules mostly stayed in the light, top few fractions despite the presence of trace of signals in the intermediate and bottom fractions. The PrP distribution profiles obtained from native and denatured aliquots were indistinguishable and the D/N ratios were similar between the eleven fractions. In WB analysis, PrP signals were present mostly in top few fractions, although faint immunoreactivity migrating to similar position of PrP in the gel was barely seen in the bottom fractions.

The PrP^C distribution profiles observed in this study were in good agreement with those reported from previous studies employing the 10 - 60% sucrose step gradient. PrP^C molecules from normal mice brains were recovered mostly in the top three fractions after fractionation in the same sucrose gradient (Pan *et al.* 2004; Pan *et al.* 2005a; Pan *et al.* 2005c). Identical results were also seen in the normal hamster brains (Tzaban *et al.* 2002). The results from normal human brains were in line with the observation in this study in that the major proportion of PrP was distributed throughout the upper fractions and that low levels of PrP were also detectable in the remaining fractions (Gambetti *et al.* 2008; Yuan *et al.* 2006). Based on additional biochemical analysis, small amounts of PrP aggregates found in the heavier fractions were interpreted to suggest that abnormal, PrP^{Sc}-like species was present in normal human brains (Yuan *et al.* 2006). The presence of detergent-insoluble aggregates of PrP^C was also described in uninfected cells under some metabolic insults (Lehmann and Harris 1997; Yedidia *et al.* 2001). However, CDI analysis in this study did not display any indication of abnormal PrP in the intermediate or bottom fractions of the gradient. Thus, it remains unclear whether PrP species recovered in the heavier

fractions have really "PrP^{Sc}-like" properties and more studies will be required to clarify this issue.

3.4.1.2 CJD brains

The conformation-dependent immunoassay (CDI) makes it possible to separately measure the cellular isoform of PrP (PrP^{C}) from disease-associated PrP (PrP^{Sc}) in CJD brains. In this study, the distribution of PrP^{C} in the sucrose gradient after ultracentrifugation was determined by analysing aliquots of native fractions in CDI. The distribution profiles of PrP^{C} from various CJD samples were basically similar to that of non-CJD brains in that PrP^{C} was predominantly present in the top few fractions. However, recognizable difference was also evident between regions of vCJD brains or between FC regions of the two CJD phenotypes. PrP^{C} distribution profiles obtained from vCJD FC and Cb tissues were almost identical to that of FC of non-CJD. In contrast, when tissues of vCJD Th or FC of MM1 sCJD were fractionated in the gradient, relatively higher levels of PrP^{C} molecules migrated to the intermediate and bottom fractions.

The relative abundance of PrP^{C} in the intermediate and bottom fractions of the gradient may indicate that PrP^{C} forms aggregates in some of prion-infected tissues. The accumulation of PrP^{Sc} during prion infection was reported to cause ER stress (Hetz *et al.* 2005; Hetz and Soto 2006; Rane *et al.* 2008), which would favour the accumulation of newly synthesized PrP in the cytosol (Kang *et al.* 2006; Orsi *et al.* 2006). Cytosolic PrP is known to form aggregates (Ma and Lindquist 2001). Furthermore, the accumulation of oligomeric forms of PrP^{Sc} could inhibit proteasome activity (Kristiansen *et al.* 2007), which would accelerate cytosolic accumulation of nascent PrP (Ma and Lindquist 2002; Yedidia *et al.* 2001). Of note, the relative levels of PrP^{Sc} in the intermediate fractions were higher in vCJD Th than in vCJD FC. Taken together, PrP^{C} species observed in the heavier fractions of the gradient appear to be aggregates of PrP^{C} present in CJD brains. Alternatively, PrP^{C} molecules observed in heavier fractions may represent partly those recruited by PrP^{Sc}

aggregates but not yet converted into pathogenic isoform, given that the formation PrP^{C}/PrP^{Sc} complex occurs in the propagation of PrP^{Sc} (Meier *et al.* 2003; Prusiner *et al.* 1990) and the formation of PrP^{Sc} in cultured cells happens slowly (Borchelt *et al.* 1990).

3.4.2 Total PrP in CJD brains: sedimentation profiles in sucrose gradient

In non-CJD brains containing only PrP^{C}, the distribution profiles of PrP measured using native aliquots were similar to those measured using denatured aliquots. In contrast, when fractions obtained from CJD brains were assayed by CDI in the native and denatured states, significant levels of fluorescence signals were newly detectable after denaturation. In tissues of vCJD FC and Cb, the distribution profiles of total PrP appeared as a bipolar pattern in the gradient; i.e., PrP signals were mostly detected in the top three fractions and bottom three fractions. In vCJD Th or FC of MM1 sCJD, PrP molecules distributed throughout the gradient more evenly with significant PrP immunoreactivity detected in the intermediate fractions. The Western blot analysis also showed similar results.

In previous studies describing the fractionation of brain samples in sucrose step gradients, the distribution of PrP species in the gradient has usually been shown by Western blot. Therefore, their results have shown the sedimentation profiles of total PrP (containing both PrP^{C} and PrP^{Sc}) in the gradients, as in the results from CDI in the denatured state. In a study comparatively analysing two groups of MM1 sCJD in which differ in their disease durations (Cali *et al.* 2006), prominent PrP was observed in the bottom fractions of the gradient with relatively weak PrP immunoreactivity present in the intermediate fractions. Interestingly, in Cali's study, the levels of PrP staying in the top fractions were overall lower than those of MM1 sCJD cases in this study. In another study describing a novel human prion disease designated "protease-sensitive prionpathy" (or PSPr), the sedimentation profile of PrP from this novel prion disease was different from any of this study's in that quite low levels of PrP were distributed in the intermediate and bottom fractions (Gambetti *et al.* 2008);

interestingly, the result from GSS with A117V mutation was similar to that of PSPr. In laboratory prion strains such as ME7, 22L in mice or Sc237 in hamsters, PrP dispersed throughout the 10 - 60% gradient after ultracentrifugation (Pan *et al.* 2004; Pan *et al.* 2005a; Pan *et al.* 2005c; Tzaban *et al.* 2002). The results from these laboratory prion stains were quite similar to those from vCJD Th or FC of MM1 sCJD.

3.4.3 PrP^{Sc}/PrP^{res} in CJD brains: sedimentation profiles in sucrose gradient

3.4.3.1 Two possible indicators for PrP^{Sc} in CDI: D/N ratio and [D-N] value

In abnormal prion protein (PrP^{Sc}), the binding site for the mAb 3F4 is hidden and becomes accessible after denaturation (Safar *et al.* 1998). Therefore, CDI fluorescence signals obtained from native samples represent PrP^{C} and those obtained from denatured samples represent total PrP irrespective of its conformation. For the analysis of fractionated samples without any proteolytic treatment, the distribution profiles of PrP^{Sc} in the gradient were inferred from the ratios of TRF counts between native and denatured aliquots (D/N ratios). Although the difference of TRF counts between the two folding states (D-N value) is a highly useful indicator for the presence of PrP^{Sc}, [D-N] value does not seem to be appropriate for the analysis of fractions for the following reasons: 1) PrP^{C} is not distributed uniformly and mainly observed in top few fractions, particularly in fraction 1; 2) CDI signals of neurological control brains containing only PrP^{C} increase slightly after denaturation; 3) the combination of (1) and (2) make it difficult to estimate the distribution of PrP^{Sc} in the gradient based on the distribution of [D-N] value in the gradient, particularly in the samples with low levels of PrP^{Sc}.

3.4.3.2 PK digestion of sucrose fractions

In this study, in addition to the CDI analysis of undigested sucrose fractions, proteolytic treatments for the sucrose fractions were performed with 2.5μg/ml PK or 50μg/ml PK. While the former condition of proteolysis was introduced mainly to investigate further the distribution of PrP^{Sc} (particularly in the top fractions) by CDI,

the latter condition of proteolysis was performed to investigate the distribution of PrP^{res} in the gradient.

One significant limitation of applying PK digestion to the sucrose fractions is the varying concentration of protein between them, as shown in section 3.3.4. In the 10 - 60% sucrose gradient employed in this study, a major proportion of protein was recovered in the early few fractions. The amount of protein can have substantial effect on the efficiency of proteolytic digestion of protein (Notari *et al.* 2007). The highly varying concentration of sucrose between the eleven fractions of the gradient (from 0% to 60%) may additionally affect PK activity. Therefore, the relative efficiency of PK activity does not appear to be identical between the eleven fractions. The efficiency of PK activity is thought to be higher in the intermediate or bottom fractions with significantly lower levels of protein, which is further strengthened by the emergence of three-band proteolytic fragments migrating ~ 20 - 30KDa even after digesting fractions with 2.5µg/ml PK. It has to be mentioned here that amino-terminal region of PrP^{Sc} was shown to be highly susceptible to proteolysis with relatively low concentrations of PK (10 - 20µg/ml PK), despite progressive further truncation in higher concentrations of PK (Notari *et al.* 2007; Yull *et al.* 2009).

Accordingly, substantial loss of PrP^{Sc} signals in CDI after treatment with 2.5µg/ml PK can to be partly explained by the viewpoint described above. Since a fraction of PK-sensitive PrP^{Sc} was found to be highly susceptible to the digestion even with 5µg/ml PK (Pastrana *et al.* 2006), the loss of PrP^{Sc} signals in the intermediate and bottom fractions following 2.5µg/ml PK can also be a reflection of loss of a subset of PK-sensitive PrP^{Sc}. Collectively, the results obtained following digestion with 2.5µg/ml PK are not thought to be a full reflection of PrP^{Sc} distribution in the gradients. Nonetheless, this mild condition of proteolysis is still useful in examining the presence of PrP^{Sc} in the top fractions of the gradient by digesting PrP^{C} found mostly in those fractions.

When compared to those obtained following hydrolysis with 2.5µg/ml PK, further great loss of PrP^{Sc} signals following standard condition of proteolysis (50µg/ml PK, 1 hour and 37°C) is thought to be the result of hydrolysis of PK-sensitive fraction of PrP^{Sc}. Additionally, the great loss of PrP^{Sc} signals after treating fractions with 50µg/ml PK can be associated with digestion of some of PrP^{res} considering the followings: 1) the immunoreactivity of PrP^{res} obtained following standard proteolysis becomes gradually reduced over a wide range of higher concentrations of PK (Notari *et al.* 2007; Yull *et al.* 2009); 2) the relative efficiency of PK digestion is thought to be higher in fractionated samples than that in brain homogenates due to difference in the level of protein (Notari *et al.* 2007)

3.4.3.3 PrP^{Sc}/PrP^{res} sedimentation profiles in sucrose gradient: between size and density

When tissues of vCJD FC or Cb were fractionated in the sucrose gradient and the sedimentation profiles of PrP^{Sc} were examined by CDI, PrP^{Sc} was mainly recovered in the bottom three fractions leaving very low levels of PrP^{Sc} in the intermediate fractions; the sedimentation profiles of PrP^{Sc} from these two regions of vCJD brains were not influenced by the mild proteolytic treatment of individual fractions. The distribution of PrP^{res} in the gradient was similar to that of PrP^{Sc} determined by CDI. When fractions from vCJD Th were examined by CDI, PrP^{Sc} was present throughout the gradient although PrP^{Sc} signals were still strongest in the bottom three fractions; the presence of PrP^{Sc} in the top fractions became clear after treating them with 2.5µg/ml PK. The results from Western blot analysis of undigested or PK-digested fractions were also identical to those of CDI. Similar to observation obtained from vCJD FC, PrP^{Sc}/PrP^{res} molecules from FC of MM1 sCJD were also predominantly recovered in the bottom three fractions of the gradient and not detectable in the top three fractions; a minor difference in FC between the two phenotypes was seen in the intermediate fractions, in which PrP^{Sc} species were a bit more abundant in MM1 sCJD than vCJD.

The separation of prion protein in the 10 - 60% sucrose gradient employed in this study can be a function of distinct molecular densities, sizes and shapes. In previous studies, the separation of PrP molecules achieved in the 10 - 60% sucrose gradient was shown to correlate with their sizes determined by gel filtration (Tzaban *et al.* 2002; Yuan *et al.* 2006). Thus, the distribution of PrP molecules in the gradient can reflect their sizes, although additional experiment like size exclusion chromatography was not conducted in this study. Considering the results from Tzaban et al. and other relevant studies, the sizes of aggregates of abnormal PrP observed in the intermediate and bottom fractions can range from less than 600 KDa to more than 20,000 KDa or to that of prion rods composed of as many as 1,000 PrP molecules (Prusiner *et al.* 1983; Silveira *et al.* 2005; Tzaban *et al.* 2002). Similarly, in an electrophoresis study on agarose gels (conducted before the discovery of PrP), scrapie infectious agents were reported to form a continuum of aggregate sizes ranging from 1,000 KDa to more than 20,000 KDa (Prusiner *et al.* 1980b), which was considered to be consistent with previous findings showing that sedimentation coefficients of scrapie agents ranged from 30S to more than 300S (Prusiner *et al.* 1978; Prusiner *et al.* 1980a). By contrast, recent studies have proposed ß-helical PrP trimers as minimal structures of PrP^{Sc} (DeMarco and Daggett 2004; Govaerts *et al.* 2004). Similarly, inactivation curves of scrapie infectivity by ionizing radiation implied that the infectious particle might consist of PrP dimers (Bellinger-Kawahara *et al.* 1988). Therefore, the PrP^{Sc} species present in the top fractions of the gradient, which were identified only in Th samples of vCJD, may correspond to the fraction of PrP^{Sc} with the sizes of PrP dimmers or trimers.

However, it remains unclear whether aggregates containing PrP molecules consist exclusively of PrP. If PrP aggregates contain chemical species like lipids, the separation of PrP molecules in sucrose gradients may be influenced by their buoyant densities in addition to their sizes. Both PrP^{C} and PrP^{Sc} were found to have strong affinity for lipids like cholesterol- and sphingolipid-enriched membrane domains (named "rafts") (Safar *et al.* 2006; Taraboulos *et al.* 1995; Vey *et al.* 1996). Although

both Sarcosyl and NOG are known to solubilize lipid rafts, PrP^{Sc} may be bound to abnormal membrane structures that behave differently from physiological membranes (Brown and Rose 1992; Tzaban *et al.* 2002). In agreement with this possibility, Klein et al. showed that sphingolipids were still easily detectable even in highly purified prion rods obtained after harsh extraction using detergents and chloroform-methanol (Klein *et al.* 1998). Moreover, recent studies have shown that lipid can be involved in the formation of PrP^{Sc} as a cofactor facilitating the conversion of PrP^{C} into PrP^{Sc} (Wang *et al.* 2007; Wang *et al.* 2010). This kind of possibility can be more significant in the analysis of fractionated samples from vCJD Th, in which PrP^{Sc} (both PK-sensitive and PK-resistant) was observed throughout the gradient including the top first fraction. Although PrP^{Sc} molecules in hamster scrapie were reported to stay in the light fractions (including the earliest fraction) of the 10 - 60% gradient, they were found to be sensitive to proteolysis (Pastrana *et al.* 2006). Therefore, a level of aggregation size may be needed for PrP^{Sc} to acquire PK-resistance (Pastrana *et al.* 2006; Tzaban *et al.* 2002). In this context, if the separation of PrP molecules in the gradient was influenced by their buoyant densities, PK-resistant fraction of PrP^{Sc} observed in the top fractions of vCJD Th would be most probable candidate PrP species.

3.4.3.4 Further speculations on regional difference of vCJD brains

In vCJD, the sedimentation profiles of PrP^{Sc} in the sucrose step gradient were significantly different between FC/Cb and Th. Although it remains to be determined whether the distinct sedimentation properties of PrP^{Sc} between regions of vCJD have any biological significance, several things are worth being discussed.

First, the PrP^{Sc} species emerging in the intermediate fractions of the gradient after ultracentrifugation was significantly more abundant in vCJD Th than the two other regions. This significant abundance of PrP^{Sc} in the intermediate fractions from vCJD Th can be easily identified in the CDI analysis of undigested fractions or of fractions digested with 2.5μg/ml PK, and in the WB analysis of fractions digested with two

different concentrations of PK. The PrP^{Sc} species recovered in the intermediate fractions is thought to quite possibly represent oligomeric forms of PrP^{Sc} (Tzaban *et al.* 2002). There is growing evidence showing the importance of oligomeric forms of PrP^{Sc} in prion pathogenesis. In prion disease, small aggregates of PrP^{Sc} may be more relevant to neurotoxicity than large aggregates species (Caughey and Lansbury 2003), as observed in other neurodegenerative diseases (Kaylor *et al.* 2005; McLean *et al.* 1999; Okamoto *et al.* 2003; Walsh *et al.* 2002). In a study comparing the particle size of PrP^{res} and their prion infectivity, relatively small oligomeric species of PrP^{res} particles were found to be most efficient in disease initiation (Silveira *et al.* 2005). Lastly, the accumulation of oligomeric forms of PrP^{Sc} was shown to impair proteasome activity, which was suggested to lead to neuronal loss (Kristiansen *et al.* 2007). It is of note that the posterior thalamus of vCJD brains is pathologically featured by severe neuronal loss accompanied by marked astrocytosis (Ironside *et al.* 2000; Ironside *et al.* 2002); moreover, hyperintensity on MRI scanning in this brain region is one of important diagnostic criteria of vCJD (Zeidler *et al.* 2000).

Second, the deposition patterns of abnormal PrP in vCJD brains are significantly different between regions (Ironside *et al.* 2000; Ironside *et al.* 2002). In cerebral and cerebellar cortex, PrP immunostaining was detected in the form of multiple florid plaques, multiple smaller plaques and amorphous deposits. In thalamus, there is a liner and perineuronal pattern of PrP deposits with occasional plaques. Therefore, the results of PrP immunostaining suggest that the size of PrP deposits in vCJD brains could be bigger in cerebral or cerebellar cortex than thalamus. Alternatively, PrP^{Sc} in the thalamus of vCJD might be in a tighter relation with cell membrane, which can lead to the presence of membrane products bound to PrP^{Sc} even after detergent extraction. In this context, it will be interesting to investigate sedimentation profiles of PrP^{Sc} from CJD brains showing Kuru plaques (MV2 sCJD) or prominent perineuronal PrP accumulation (VV2 sCJD) (Ironside *et al.* 2005; Parchi *et al.* 1999b).

The third thing is the biological strain typing of vCJD agent. Transmission studies using a panel of wild-type mice demonstrated that BSE in cattle and vCJD in humans were caused by the same prion strain (Bruce *et al.* 1997). Subsequent studies using various transgenic mice models have strongly supported that vCJD is caused by the BSE agent (Hill *et al.* 1997; Scott *et al.* 1999). A recent large-scale transmission study using a standard panel of wild-type mice confirmed that vCJD is associated with one strain of BSE agent (Ritchie *et al.* 2009). Although a possibility was raised that the vCJD agent could propagate in two distinct prion strains following transmission into transgenic mice (Beringue *et al.* 2008), the biological properties of the vCJD agent were not largely altered in transfusion-related secondary transmission (Bishop *et al.* 2008) and histopathological characteristics and PrP biochemistry were similar between primary and secondary vCJD cases (Head *et al.* 2009b; Peden *et al.* 2004; Wroe *et al.* 2006). However, one limitation of these transmission studies which examined biological properties of vCJD agents lies in that they were mostly based on the analysis of frontal cortex and/or cerebellum. In this context, a study performed by Korth et al. was an exception because the thalamus of vCJD brains as well as frontal lobe was used for the transmission study into transgenic mice (Korth *et al.* 2003). Interestingly, inocula prepared from the thalamus of vCJD brains resulted in two distinct prion strains in subsequent passages, one of which was similar to the strain derived from the frontal cortex of vCJD brains (Korth *et al.* 2003). It remains unclear whether the distinct sedimentation properties of PrP^{Sc} between regions of vCJD brains are associated with the emergence of distinct prion strains reported by Korth and colleagues.

3.4.4 Considerable additional experiments using fractionated samples

In this study, the distribution profiles of PrP^{Sc} in the 10 - 60% sucrose gradients were investigated by CDI using undigested fractions or those digested with 2.5μg/ml PK and they showed overall correlation with PrP^{res} distribution. Although CDI has its advantage in that it can measure both PrP^{C} and PrP^{Sc} in prion-infected samples, the detection of PrP^{Sc} in CDI has been frequently performed by the combination with

NaPTA precipitation in order to minimize the intervention of PrP^{C} (Bellon *et al.* 2003; Jones *et al.* 2007; Safar *et al.* 2005a). Although NaPTA is widely used to enrich disease-associated PrP, a minor fraction of PrP^{C} in normal human brains has been shown to be precipitated by NaPTA (Wadsworth *et al.* 2001; Yuan *et al.* 2006). Thus, it would be of interest to see whether a minor fraction of PrP^{C} molecules identified in the intermediate and bottom fractions can be more efficiently precipitated by NaPTA. Additionally, it would be also interesting to compare the distribution profiles of PrP^{Sc} determined by the combination of CDI and NaPTA with those in this study, given a recent report that oligomeric form of PrP^{Sc} was not effectively retrieved by NaPTA precipitation (Sasaki *et al.* 2009). One technical point that needs to be mentioned is the variable concentration of sucrose between the eleven fractions (0% to 60%); thus it would be necessary to remove sucrose in each fraction by filtration or to lower its concentration into a level which is not influential in NaPTA precipitation.

In the last decade, more than ten antibodies have been reported to be specific for PrP^{Sc} (Jones *et al.* 2009c; Korth *et al.* 1997; Lau *et al.* 2007; Moroncini *et al.* 2004; Paramithiotis *et al.* 2003; Servac *et al.* 2004; Solforosi *et al.* 2007; Zou *et al.* 2004). Recently, some of them were shown to recognize structural features shared by infectious and non-infectious aggregates of PrP (Biasini *et al.* 2008). It would be of interest to investigate the reactivity of these so-called "PrP^{Sc}-specific" antibodies with PrP^{Sc} molecules that are different in their sizes and/or their densities (particularly fractions from vCJD Th).

A recent study by Silveira et al. showed that prion infectivity was influenced by their aggregate sizes (Silveira *et al.* 2005). While prion infectivity was peaked in small oligomers of PrP^{Sc} with 300 - 600 KDa, these activities became significantly lower in smaller and larger aggregates. The results from *in vitro* converting activity were also similar to those of *in vivo* assays. One limitation in this study is that they used purified PrP^{res} particles, which is different in its structure from undigested PrP^{Sc}

molecules (McKinley *et al.* 1991; Pan *et al.* 1993). Additionally, various sizes of PrP^{res} particles were generated by sonication but the relevance of these artificially disaggregated PrP^{res} particles to the *in vivo* sizes of PrP^{Sc} aggregates remains unclear. In this context, it would be of interest to compare prion infectivity between the fractions which can be different in their sizes and/or densities.

CHAPTER 4

Conformational stability states of PrP^{Sc} measured by CDI in different forms of human prion disease

4.1 Introduction

It is known that protein structure can be probed by exposure to a chaotrope salt over an appropriate range of concentrations (Shirley 1995). On the basis of this concept, Peretz et al. developed an assay termed conformation stability assay (CSA), in which the stability of PK-resistant PrP^{Sc} is measured as a loss of resistance to protease digestion following exposure to increasing concentrations of GdnHCl (Peretz *et al.* 2001). The increase of GdnHCl concentration lead to the dissociation of PrP^{Sc} aggregates and denaturation of its ß-sheet-rich structure, which renders PK-resistant fragment of PrP^{Sc} susceptible to proteolytic treatment (Peretz *et al.* 2001; Safar *et al.* 1993). The concentration of GdnHCl required to make half of PrP^{Sc} susceptible to proteolytic treatment ($GdnHCl_{1/2}$) was used as a measure to compare the stability of PK-resistant PrP^{Sc} between prion strains. Prion strains which were indistinguishable by electrophoretical mobility of PrP^{res} could be separated by the $GdnHCl_{1/2}$ values in the CSA (Peretz *et al.* 2001; Peretz *et al.* 2002). In the following studies from this group, it was shown that PrP^{Sc} from transgenic mice inoculated with synthetic prions was very highly resistant to GdnHCl-induced denaturation (Legname *et al.* 2005), and that $GdnHCl_{1/2}$ values obtained from synthetic and naturally occurring prion strains propagated in mice correlated with their incubation periods (Legname *et al.* 2006). Although this finding is important in that biochemical properties of PrP^{Sc} were addressed in relation with biological properties, a limitation of this methodology is the preclusion of protease-sensitive fraction of PrP^{Sc} due to the reliance on proteolysis (Legname *et al.* 2006).

In this study, in order to overcome the limitation that CSA has, the stability of both PK-sensitive and PK-resistant fractions of PrP^{Sc} was measured by the conformation-sensitive mAb 3F4 in CDI, instead of limited proteolysis. Aliquots of a PrP^{Sc}-containing sample were firstly incubated with increasing concentrations of GdnHCl and then assayed by CDI. The recognition site of the mAb 3F4 is located in N-terminus of PrP (residues 109-112 of human PrP), which is masked in the native

form of PrP^{Sc} but becomes accessible after denaturation (Bolton *et al.* 1991; Kanyo *et al.* 1999; Kascsak *et al.* 1987; Rogers *et al.* 1991; Safar *et al.* 1998). Thus, the conformational stability of PrP^{Sc} was measured as a loss of disease-associated structure in its 3F4 binding site following exposure to GdnHCl at various concentrations. Given the location of the mAb 3F4 epitope within PrP, the conformational stability measured by this methodology is thought to represent that of N-terminus of PrP^{Sc}.

In order to investigate the conformational stability of PrP^{Sc} in CJD brains, tissues of frontal cortex from vCJD and MM1 sCJD case were compared. In some of vCJD cases, tissues of cerebellum and thalamus were also examined. Additionally, one case of VV2 sCJD and two GSS cases with P102L mutation were analysed using tissues of frontal cortex.

4.2 Materials and methods

4.2.1 Human brain materials

Thirteen variant CJD (vCJD) cases, fourteen sporadic CJD (sCJD) cases, two GSS cases with P102L mutation and five control (non-CJD) cases with other neurological disorders were analyzed in this chapter. Among the fourteen sporadic CJD cases, thirteen cases were MM1 subtype and the remaining one case was VV2. One GSS case showed typical three PrP^{res} bands in addition to a PrP fragment of ~8 KDa, whereas the other GSS case produced a predominantly ~8 kDa proteolytic fragment. The details of these cases were described in Tables 2.1 to 2.4 in Chapter 2. In all instances the tissues used were grey matter-enriched frontal cortex (FC) and, additionally cerebellar cortex (Cb) and thalamus (Th) in vCJD, dissected from frozen half-brain specimens.

4.2.2 Methods

Preparation of brain tissue

Brain tissue homogenates were prepared in nine volumes (w/v) of phosphate-buffered saline (PBS), pH 7.4, containing 2% Sarcosyl by two cycles of homogenization in the FastPrep instrument (Qbiogene). The homogenized brain samples were stored at -80°C until use.

Enrichment of disease-associated PrP

The 10% homogenates were diluted to 5% w/v using PBS containing 2% Sarcosyl (w/v) and were incubated for 10 minutes at room temperature on a shaking platform. The samples were then centrifuged at 500 × g for 5 minutes at 20°C and the supernatants were collected. For the enrichment of disease-associated isoform of PrP, one hundred microlitre aliquots of cleared brain homogenates in PBS containing 2% Sarcosyl were centrifuged at 20,800 × g for 1 hour at 4°C as described previously (Thackray *et al.* 2007a; Wadsworth *et al.* 2006). After careful aspiration of the

supernatants, pellets containing detergent-insoluble fraction of PrP were used for the analysis of denaturation transition induced by GdnHCl. On some occasions, pellets were resuspended in the starting volume (100 µl) of homogenization buffer to investigate the effect of this method in enriching PrP^{Sc}.

Conformation-dependent immunoassay (CDI)

Samples prepared in 2% Sarcosyl in PBS were divided into two parts; one part was mixed with same volume of PBS containing Complete EDTA-free® protease inhibitors (native sample, N) and the other part was mixed with the same volume of 8M GdnHCl and incubated for 6 minutes at 81°C (denatured sample, D). Both N and D samples were adjusted using distilled water containing EDTA-free® protease inhibitors to a final concentration of GdnHCl of 0.35M in 435µl final volume. Subsequently, CDI was performed as described in section 2.2.3 without any modification.

Denaturation transition of PrP^{C} and PrP^{Sc} in CDI

PrP^{Sc} in brain homogenates or in the pellets containing detergent-insoluble fraction of PrP was treated with GdnHCl at various concentrations as described previously (Peretz *et al.* 2001; Safar *et al.* 1998). The 10% brain homogenates were mixed with an equal volume of 2% Sarcosyl in PBS and incubated for 10 minutes at room temperature. After clarification at 500 × g for 5 minutes, aliquots of samples were mixed with GdnHCL at final concentrations ranging from 0 to 7M. Alternatively, the pellets containing detergent-insoluble fraction of PrP were resuspended in a solution containing GdnHCl at various concentrations (range: 0 - 7M). Samples containing different amounts of GdnHCl were incubated overnight at room temperature on a shaking platform and were adjusted using distilled water containing EDTA-free® protease inhibitors, to a final concentration of GdnHCl of 0.35M in 720µl of final volume. The extents of unfolding of PrP^{Sc} exposed to different concentrations of GdnHCl were measured by the CDI in triplicate.

CDI D/N ratio and [D-N] value

Time-resolved fluorescence (TRF) counts obtained from CDI were used to generate D/N ratios and [D-N] values (Safar *et al.* 1998; Safar *et al.* 2005a). The folding state of PrP^{Sc} induced by overnight incubation at 7M GdnHCl or by incubation at 81°C in the presence of 4M GdnHCl was taken to be full denaturation (Safar *et al.* 1993; Safar *et al.* 1998). The D/N ratios were obtained by dividing TRF counts of denatured samples (D) by the counts of the corresponding native samples (N; 0M GdnHCl). For the generation of [D-N] values, TRF counts measured in the native state were subtracted from those measured in the denatured state.

Determination of denatured fraction of PrP^{Sc}

CDI results obtained from PrP^{Sc}-enriched pellets were used to determine denatured fractions of PrP^{Sc} after overnight incubation with particular concentrations of GdnHCl. For this, TRF counts obtained from an aliquot incubated in the absence of GdnHCl (0M GdnHCl) were firstly subtracted from those obtained from aliquots treated with GdnHCl at various concentrations. Then, denatured fraction of PrP^{Sc} at a particular concentration of GdnHCl was expressed as a relative value (%) of TRF counts at the concentration against the counts at 7M GdnHCl and was plotted against the corresponding concentrations of GdnHCl.

$$\text{Denatured fraction of } PrP^{Sc}\ (\%) = \frac{\text{TRF Counts}_{\text{XM GdnHCL}} - \text{TRF Counts}_{\text{0M GdnHCL}}}{\text{TRF Counts}_{\text{7M GdnHCL}} - \text{TRF Counts}_{\text{0M GdnHCL}}} \times 100$$

Western blot (WB) analysis

Polyacrylamide gel electrophoresis was performed using NuPAGE Novex gel system (Invitrogen) as described in section 2.2.3. Samples left undigested or digested with proteinase K (PK) at 50µg/ml for 1 hour at 37°C were mixed with NuPAGE LDS sample buffer to a final concentration of 1X. Subsequently, the samples were

incubated for 10 minutes at 100°C and then separated on a 10% Bis-Tris NuPAGE gel. The separated proteins were transferred to polyvinylidene difluoride (PVDF) membrane and subsequent immunodetection of PrP was performed as described in section 2.2.3 without any modification.

Conventional conformation stability assay (CSA)

For the study of stability of PrP^{res} against GdnHCl-induced denaturation, aliquots of the 10% brain homogenates prepared in PBS were mixed with equal volume of GdnHCl giving a range of concentrations of GdnHCl (Peretz *et al.* 2001). After 2 hour incubation of the mixtures at 37°C, samples were adjusted to a final concentration of 0.4M GdnHCl in Tris buffer (10mM Tris-HCl [pH 7.4], 0.5% NP-40 and 0.5% sodium deoxycholate) and then digested with PK at 20µg/ml for 1 hour at 37°C. PK activity was terminated by adding Pefabloc at a final concentration of 1mM. Proteins were then precipitated, by mixing the samples with five volumes of pre-chilled methanol and incubated at -80°C overnight. Samples were then centrifuged at 16,000 × g for 30 minutes at 4°C and the supernatants were carefully aspirated. The remaining pellets were resuspended with 25µl of 2X LDS buffer and boiled for 10 minutes. Proteins were analysed by Western blot as described above.

Statistics

Statistical analysis was performed with the student's *t*-test using TTest worksheet function in Microsoft® Office Excel.

4.3 Results

4.3.1 GdnHCl-induced denaturation of PrP^{Sc} in brain homogenates

When the extents of unfolding of PrP^{Sc} induced by GdnHCl at different concentrations were measured by the conformation-sensitive mAb 3F4 in CDI, the resistance of PrP^{Sc} to GdnHCl-induced denaturation was reported to differ between prion strains propagated in hamsters (Safar *et al.* 1998). In order to investigate whether the stability of PrP^{Sc} against GdnHCl-induced denaturation also differs between distinct human CJD phenotypes, the brain homogenates from vCJD and MM1 sCJD cases were exposed to increasing concentrations of GdnHCl (range: 0 - 7M GdnHCl) overnight before being assayed by CDI. TRF counts obtained from an aliquot incubated in the absence of GdnHCl were considered to represent PrP^{C}, and those obtained from an aliquot incubated with 7M GdnHCl were thought to represent all PrP molecules present in a sample irrespective of their conformation.

When the CDI results from neurological control (non-CJD) brains were compared between native (N; 0M GdnHCl) and denatured (D; 7M GdnHCl) states, fluorescence signals were similar between the two folding states or increased slightly after denaturation (Figure 4.1a). CDI D/N ratios in the three controls were in the range of 0.8 - 1.8 (Figure 4.1b). In contrast, when samples of vCJD and MM1 sCJD brains were analysed by CDI, there were significant increases in fluorescence counts after denaturation (Figure 4.1a). D/N ratios were usually higher in CJD samples than control samples (Figure 4.1b). The increase of fluorescence counts in CJD samples after denaturation is thought to result from the exposure of 3F4 binding site of PrP^{Sc}, which is hidden in native PrP^{Sc}. However, the degree of increase of CDI signals after denaturation was variable between individual CJD samples, implying variable amounts of PrP^{Sc} (Figure 4.1a). In one MM1sCJD case (MM1-1 in Figure 4.1), the change of CDI signal after denaturation did not seem distinguishable from neurological controls probably due to a low level of PrP^{Sc} in the sample. It is noteworthy that PrP^{C} was readily detectable in CJD brains despite variation in its

amount and that CDI D/N ratios were greatly influenced by the amounts PrP^C in these samples (for example, compare vCJD1 with MM1-3 in Figure 4.1). The amounts of PrP^C in the vCJD brains appeared larger than those in the brains of MM1 sCJD or neurological controls, but direct comparison of PrP^C amounts between groups (and individuals) requires caution when considering variations in sampling and the difference in age, post-mortem intervals, gender, etc. between individual cases.

To look at unfolding of PrP molecules more precisely, samples from non-CJD, vCJD and MM1 sCJD brains were incubated with a range of GdnHCl concentrations (range: 0 - 7M) and the extents of unfolding of PrP molecules were measured by mAb 3F4 binding in CDI. TRF counts at each concentration of GdnHCl were expressed as a relative value (%) to those at 7M GdnHCl. In the non-CJD brains containing only PrP^C, no significant changes in fluorescence counts were observed although minor irregular fluctuating variation was noticeable irrespective of the concentrations of GdnHCl (Figure 4.2a). In the same context, D/N ratios of non-CJD brains were overall unchanged by increasing concentrations of GdnHCl (Figure 4.3a). In contrast, CJD brains showed clearly different denaturation patterns compared to control brains. In both vCJD and MM1 sCJD brains, the CDI signals gradually increased with increasing concentrations of GdnHCl and reached their plateaus at the concentration of 3 M GdnHCl (Figures 4.2b and 4.2c). This result implies that the exposure to 3M GdnHCl allowed mAb 3F4 access to its epitope in most of PrP^{Sc} molecules present in the CJD samples, and that most of them lost their disease-related structure to this condition of treatment at least in their N-terminus. The MM1 sCJD case (MM1-1 in Figure 4.1), which was indistinguishable from non-CJD brains in fluorescence counts in both N and D states and thus in D/N ratio, was different in its denaturation profile from neurological control brains (compare squares of Figure 4.2c with Figure 4.2a). Similar to the denaturation profiles, D/N ratios gradually increased with increasing concentrations of GdnHCl and reached their plateaus at the concentration of 3M (Figures 4.3b and 4.3c). Interestingly, while GdnHCl-induced

denaturation of vCJD brain samples appeared to result in an increase of TRF counts from 1M GdnHCl treatment, the increase of fluorescence counts in MM1 sCJD was not seen until the concentration of GdnHCl reached 1.5M. Although greatly different amounts of PrP^{C} between cases made more precise comparison difficult, this observation suggests that there is difference between the two phenotypes of CJD in the stability of PrP^{Sc} to GdnHCl-induced denaturation.

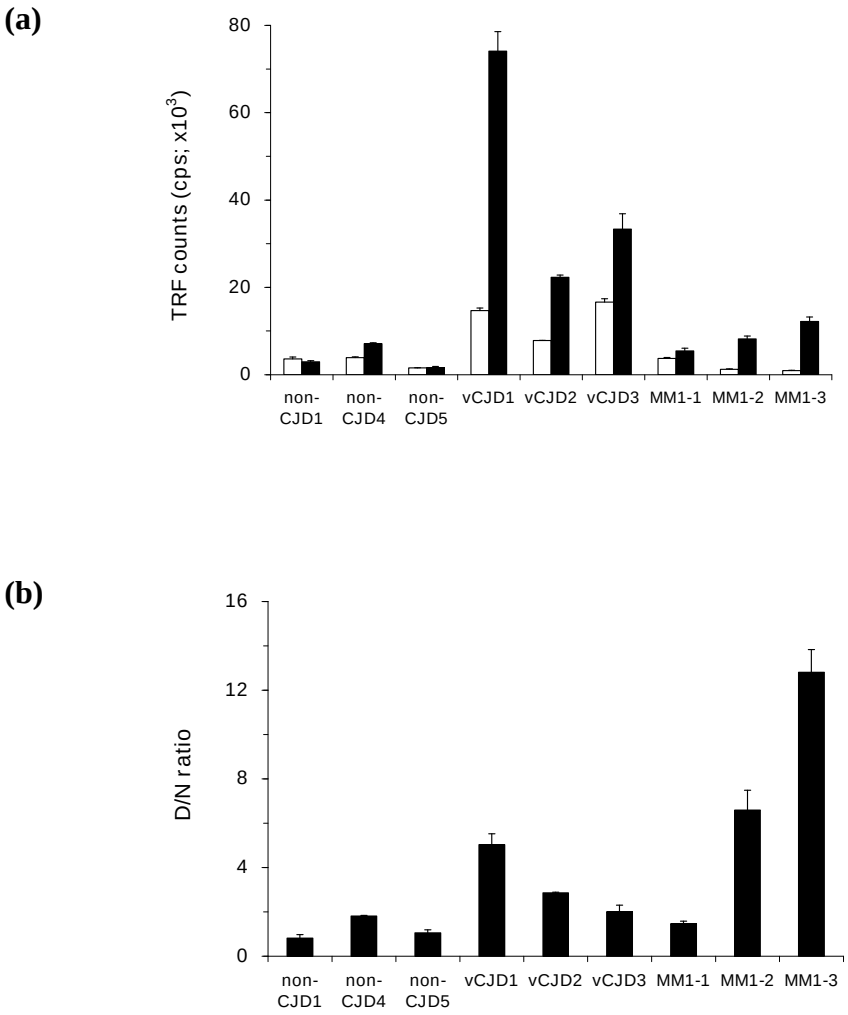

Figure 4.1 Comparison of CDI results between native (N) and denatured (D) states. Three cases each from neurological control, vCJD and MM1 sCJD were analysed using brain homogenates prepared from frontal cortex. (a) Comparison of TRF counts measured in N state (0M GdnHCl treatment, white bars) and D state (7M GdnHCl, black bars). (b) Comparison of D/N ratio between non-CJD and CJD brains. TRF counts of D samples were divided by the counts of N samples to give D/N ratios. Data shown represent the average ± S.D. for triplicate wells

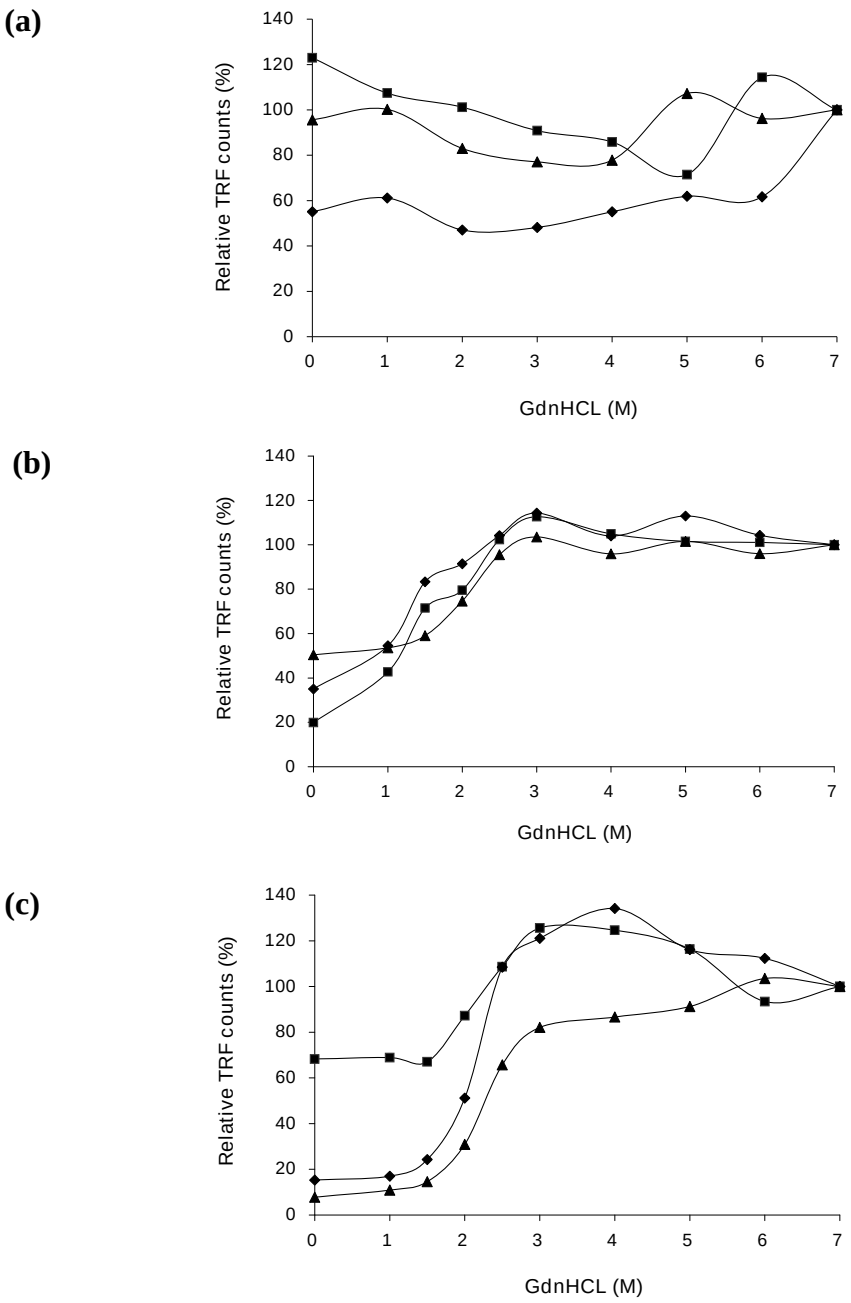

Figure 4.2 Change of CDI TRF counts with exposure to increasing concentrations of GdnHCl. Brain homogenates prepared from frontal cortex were treated with increasing concentrations of GdnHCl (range: 0 - 7M) and measured by CDI. Three cases each from neurological control (a), vCJD (b) and MM1 sCJD (c) were analysed. Each symbol (squares, diamonds, triangles) represent individual cases of each phenotype. TRF counts at particular concentrations of GdnHCl were expressed as relative values (%) to those at 7M GdnHCl. Data shown represent the average for triplicate wells except for non-CJD 4 (diamonds in [a], duplicate wells).

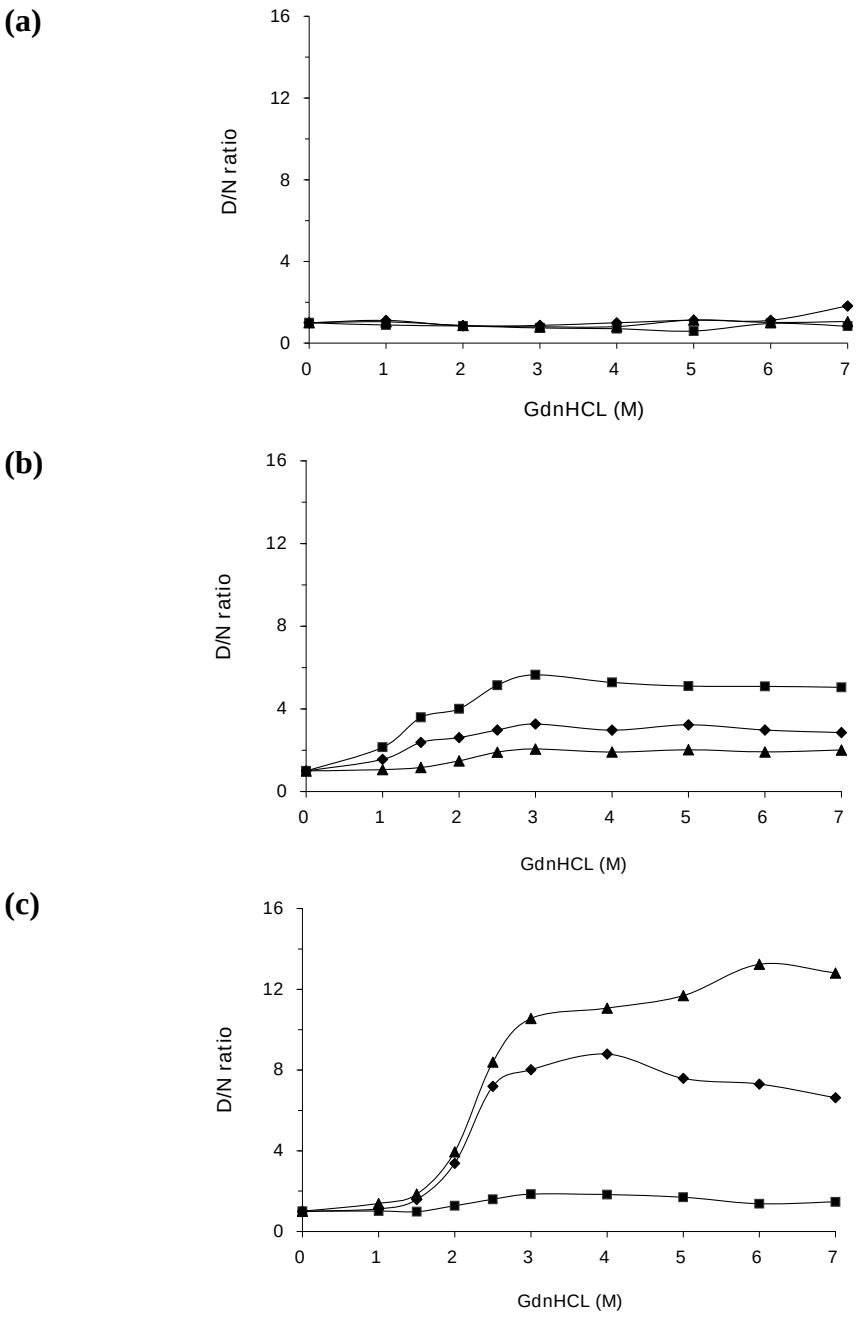

Figure 4.3 Change of CDI D/N ratio with exposure to increasing concentrations of GdnHCl. Brain homogenates prepared from frontal cortex were treated with increasing concentrations of GdnHCl (range: 0 - 7M) and measured by CDI. Three cases each from neurological control (a), vCJD (b) and MM1 sCJD (c) were analysed. Each symbol (squares, diamonds, triangles) represent individual cases of each phenotype. CDI D/N ratios were obtained by dividing TRF counts in the native state (0M GdnHCl) into those at particular concentrations of GdnHCl. Data shown represent the average for triplicate wells except for non-CJD 4 (diamonds in [a], duplicate wells).

4.3.2 Enrichment of PrP^{Sc} by Sarcosyl extraction and centrifugation

CDI revealed that readily detectable amounts of PrP^{C} are present in CJD brains. However, the amounts of PrP^{C} were variable between individual cases, which caused difficulty in comparing fractional transition of PrP^{Sc} according to the increase of concentration of GdnHCl not only between different forms of CJD but also between individual CJD cases. In order to measure the degree of GdnHCl-induced denaturation of PrP^{Sc} more preciously by minimizing the effect of PrP^{C}, this study made use of the difference in detergent solubility of the two isoforms of PrP: PrP^{C} is soluble in non-denaturing detergent, whereas PrP^{Sc} is insoluble (Meyer *et al.* 1986). In order to harvest detergent-insoluble fraction of PrP species, brain homogenates prepared in PBS containing 2% Sarcosyl were centrifuged at 20,800 × g for 1 hour as described previously (Thackray *et al.* 2007a; Wadsworth *et al.* 2006). After careful isolation of the supernatants, pellets were resuspended as described in section 4.2.2. The detergent-soluble (supernatants) and insoluble (pellets) fractions were assayed by CDI. The investigation of PrP^{res} distribution in these fractions was performed after PK digestion.

When brain materials from neurological controls were centrifuged following Sarcosyl extraction and were subjected to measurement in CDI in native state, most of fluorescent counts detected in brain homogenates were recovered in the supernatants leaving only trace of CDI signals in the pellets (Figure 4.4a). In both types of CJD brains, similar results were obtained although minor variations between cases were observed (Figure 4.4a). Since TRF counts obtained in the native state represent PrP^{C}, most of the cellular isoform of PrP present in both CJD and non-CJD brain samples were thought to remain in the detergent-soluble (supernatant) fraction after Sarcosyl extraction followed by centrifugation. In order to determine the distribution of disease-associated conformer of PrP in the supernatants and pellets, fluorescence counts in the denatured state were divided by those in the native state (D/N ratios). In neurological controls, the D/N ratios were in the range of 0.8 - 1.6 and were similar between brain homogenates, supernatants and pellets (Figure 4.4b).

In both vCJD and MM1 sCJD brains, the D/N ratios for the pellets were greatly increased compared to those for brain homogenates, but the D/N ratios for the supernatants were clearly lower than those for brain homogenates (Figure 4.4b). This result indicates that the majority of PrP^{Sc} precipitated in the pellet fraction, although the great increase of D/N ratios was thought to be attributed in part to the loss of PrP^{C} in the pellets.

Together with the fact that the epitope of mAb 3F4 is hidden only in PrP^{Sc}, another representative feature of PrP^{Sc} is its partial resistance to protease digestion. Proteinase K (PK) treatment of PrP^{Sc} leaves N-terminally truncated, PK-resistant form of PrP^{Sc} (PrP^{res}). To investigate the distribution of PrP^{res} in the supernatant and pellet fractions, these two fractions were analysed separately with and without PK treatment (Figure 4.5). Western blot analysis of supernatants and pellets before proteolysis shows the presence of PrP in both fractions. After digestion with PK, PrP^{res} was mainly detected in the detergent-insoluble pellet fraction of both vCJD and MM1 sCJD brain samples, although weak 3 bands representing PrP^{res} was recognizable in the supernatant fraction of vCJD sample (Figure 4.5).

Collectively, the observation regarding the distribution of PrP^{C}, PrP^{Sc} and PrP^{res} after Sarcosyl extraction followed by centrifugation shows that this method is efficient in enriching PrP^{Sc} in the pellet, leaving PrP^{C} in the supernatant.

(a)

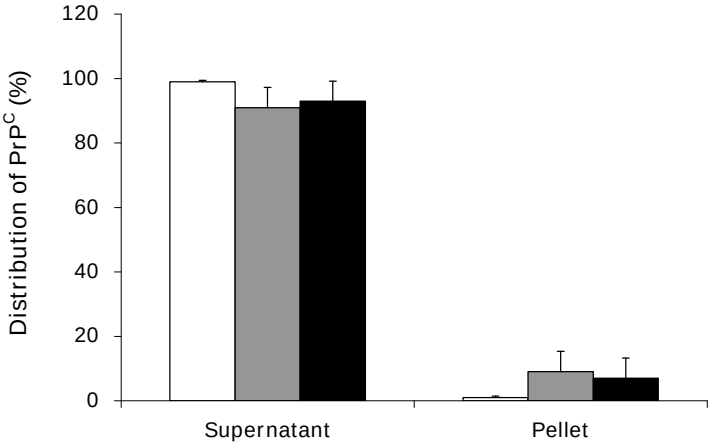

(b)

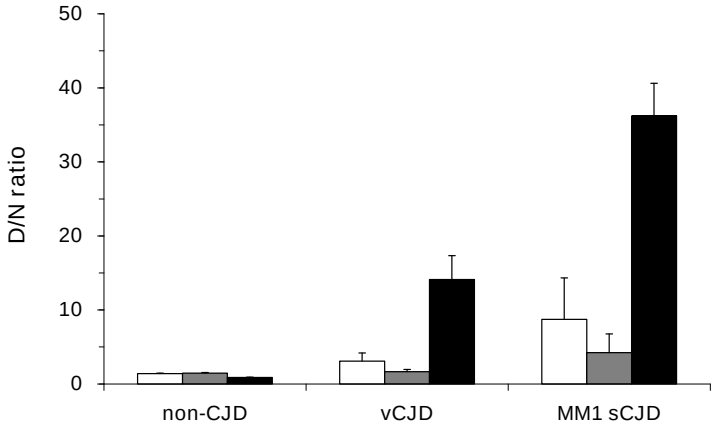

Figure 4.4 Distribution of PrP^C and PrP^{Sc} after Sarcosyl extraction and centrifugation. Brain homogenates were prepared from frontal cortex as described in section 4.2.2 and the supernatants and resuspended pellets were analysed by CDI. (a) Distribution of PrP^C in supernatants and pellets. The amount of PrP^C was investigated by CDI in the native state and relative distribution of PrP^C between supernatants and pellets was expressed as percent (%). White bars: control; Grey bars: vCJD; Black bars: MM1 sCJD. (b) Comparison of D/N ratios between initial brain homogenates, supernatants and pellets. TRF counts of denatured samples were divided by the counts in the corresponding native samples to give D/N ratios. White bars: brain homogenates; Grey bars: supernatants; Black bars: pellets. Data shown represent the average ± S.D. obtained from three different cases.

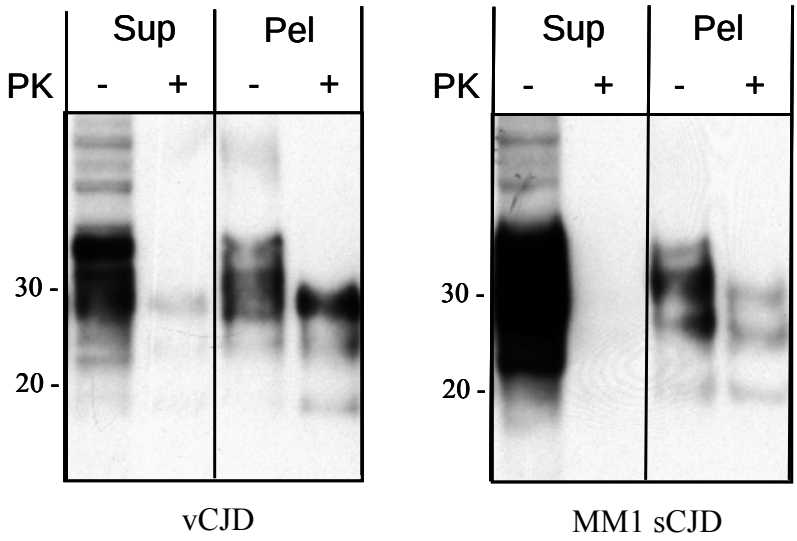

Figure 4.5 Enrichment of PrP^{res} in pellets after Sarcosyl extraction and centrifugation. The supernatant (Sup) and pellet (Pel) fractions obtained after Sarcosyl extraction and centrifugation were digested with 50µg/ml PK for 1 hour at 37°C. The distribution of PrP^{res} in both fractions was investigated by Western blot using mAb 3F4.

4.3.3 Conformational stability of PrP^{Sc}: comparison between vCJD and sCJD

Relative resistance of PrP^{Sc} or PrP^{res} to GdnHCl-induced denaturation has been reported to characterize prion strains in hamster and mouse models (Legname *et al.* 2006; Peretz *et al.* 2001; Safar *et al.* 1998). To investigate whether there are any differences in resistance to GdnHCl-induced denaturation between vCJD and sCJD PrP^{Sc}, the homogenates of frontal cortex prepared in 2% Sarcosyl in PBS were centrifuged and then pellets containing detergent-insoluble fraction of PrP were assayed by CDI following incubation with GdnHCl at different concentrations (range: 0 - 7M).

As shown in Figure 4.6a, the levels of PrP^{Sc} were variable between samples when they were measured by the difference of TRF counts between native and denatured states in CDI ([D-N] value). In order to compare samples with different levels of PrP^{Sc}, denatured fractions of PrP^{Sc} at particular concentrations were expressed as relative values (%) against that at 7M GdnHCl (100%), which was taken to be fully denatured. When the normalized results of both vCJD and sCJD (MM1 and VV2 subtypes) were plotted against the concentration of GdnHCl, the gradual unfolding of PrP^{Sc} formed a single sigmoidal curve with one major transition and the denaturation curves plateaued at around 3M GdnHCl (Figure 4.6b). However, the degrees of denaturation of PrP^{Sc} appeared distinct between vCJD and sCJD cases at lower GdnHCl concentrations. In vCJD cases, the major fractional transition was observed in the range of 1 - 2.5M GdnHCl (Figure 4.6b). Approximately 10% of the PrP^{Sc} was denatured by treatment with 1M GdnHCl and almost 90% of PrP^{Sc} was denatured in the concentration of 2.5M GdnHCl (Figure 4.6b). The concentration of GdnHCl required to denature half of the PrP^{Sc} molecules present, named $GdnHCl_{1/2}$ value (Lau *et al.* 2007), was 1.809M GdnHCl (row of sample 1 in Table 4.1). In contrast, the major transition from native to denatured state in both types of sCJD was observed in the range 1.5 - 3M GdnHCl (Figure 4.6b). The denatured fraction of sCJD PrP^{Sc} seen after treatment with 1.5M GdnHCl was similar to that of vCJD

PrP^{Sc} after incubation with 1M GdnHCl. Fractional transition of PrP^{Sc} from native to denatured state in both sCJD types was overall 0.5M higher than that of vCJD. The discrimination between vCJD cases and sCJD cases was more prominent in the range of 1.5 - 2M GdnHCl. Statistical analysis confirmed that fractional transition was significantly different between vCJD and MM1 sCJD in the two concentrations of GdnHCl ($P < 0.01$ at 1.5M and $P < 0.05$ at 2M GdnHCl). The $GdnHCl_{1/2}$ values for MM1 sCJD and VV2 sCJD were 2.342M and 2.308M, respectively (for MM1, see row of sample 1 in Table 4.2). These results overall show that PrP^{Sc} from frontal cortex of sCJD brains was more resistant to GdnHCl-induced denaturation than that of vCJD, implying that N-terminus of PrP^{Sc} is structurally more stable in sCJD than that of vCJD.

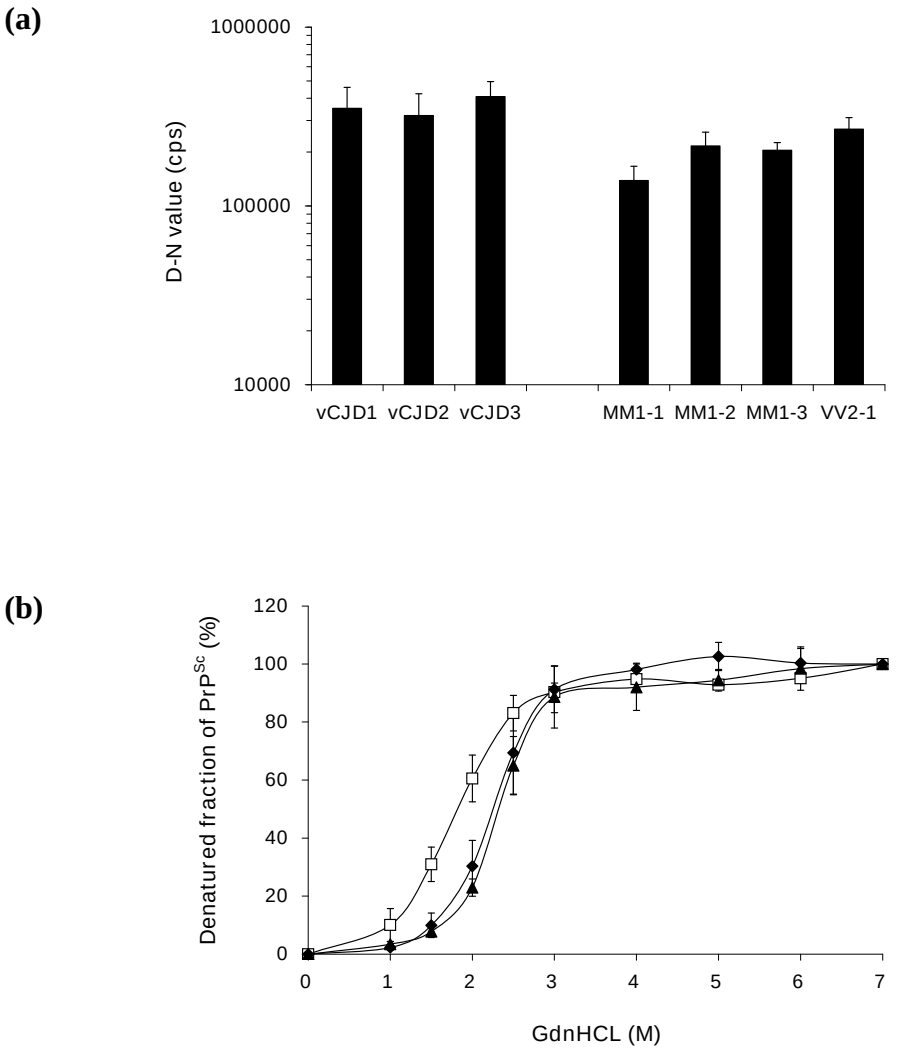

Figure 4.6 GdnHCl-induced denaturation of PrP^{Sc}. (A) PrP^{Sc}-enriched pellets of frontal cortex tissue from vCJD, MM1 sCJD and VV2 sCJD cases were assayed by CDI. TRF counts obtained in the native state (0M GdnHCl) were subtracted from the counts in the denatured state (7M GdnHCl) to measure the amounts of PrP^{Sc}. In *x*-axis, MM1 denotes MM1 sCJD and VV2 denotes VV2 sCJD. (B) The extent of unfolding of PrP^{Sc} between native (0M) to denatured (7M) state was investigated by CDI. Denatured fraction of PrP^{Sc} in each concentration of GdnHCl was calculated as described in section 4.2.2. In vCJD (white squares) and MM1 sCJD (black diamonds), data represent the average ± S.D. of three individuals. Data for VV2 sCJD (black triangles) was based on one case. The result in every individual was an average of three to four independent experiments in triplicate.

4.3.4 Conformational stability of PrP^{Sc}: variation between samples

In order to compare the stability of PrP^{Sc} in the frontal cortex more precisely between vCJD and MM1 sCJD, additional samples from the same cases were analysed by CDI following treatment with increasing concentrations of GdnHCl. Two additional samples for each vCJD case and one additional sample for each MM1 sCJD case were investigated. Among the three cases of vCJD, different samples of vCJD3 were similar in their unfolding kinetics induced by increasing concentrations of GdnHCl and the $GdnHCl_{1/2}$ values for this case were in the range of 1.785M ~ 1.933M (Figure 4.7b, Table 4.1). In contrast, the denaturation profiles of PrP^{Sc} induced by increasing concentrations of GdnHCl were significantly variable between samples of vCJD1 (Figure 4.7a). In the initial sample of vCJD1 less than 5% of PrP^{Sc} molecules were unfolded to the exposure to 1M GdnHCl, whereas more than 20% of PrP^{Sc} molecules from the 2nd sample of this case were denatured by the exposure to 1M GdnHCl. The difference between sample 1 and sample 2 was more prominent in the concentration of 1.5M GdnHCl; about 25% of PrP^{Sc} molecules were denatured in the sample 1, whereas more than 60% of PrP^{Sc} molecules were denatured in the sample 2. The $GdnHCl_{1/2}$ value for the sample 1 was 1.993M, which is significantly higher than the sample 2 with the value of 1.297M (Table 4.1). The $GdnHCl_{1/2}$ value for the sample 3 was 1.202M, which was the lowest among all the $GdnHCl_{1/2}$ values obtained in this study from various tissues. vCJD2 case also showed some variability between samples in its extent to the denaturation of PrP^{Sc}, but was not as severe as the variability in vCJD1 (range of $GdnHCl_{1/2}$ value: 1.511M ~ 1.911M) (Table 4.1). Contrary to sample-to-sample and case-to-case variations in vCJD, the unfolding kinetics of PrP^{Sc} in the frontal cortex of MM1 sCJD was relatively similar between the initial and additional samples (Figures 4.7c and 4.7d). The $GdnHCl_{1/2}$ values were also relatively similar between the two samples each of three MM1 sCJD cases (Table 4.2). The investigation of additional samples showed that significant variations of PrP^{Sc} in the degrees of resistance to GdnHCl-induced denaturation are present in the frontal cortex of vCJD, but not in MM1 sCJD. However, the initial observation that PrP^{Sc} from MM1 sCJD brains was more resistant to GdnHCl

treatment than that of vCJD remains true even when variations in vCJD readings are taken into account. The additional groups of samples from the vCJD cases generally had higher or similar susceptibility to GdnHCl-induced denaturation than initial group of samples. When all tested vCJD and MM1 sCJD samples were considered, difference between the two disease phenotypes was highly significant for the 1.5M and 2.0M readings with P values of < 0.001. Overall, these results strengthen the suggestion that PrP^{Sc} in the frontal cortex of MM1 sCJD is more stable to a chaotrope-induced denaturation than that of vCJD.

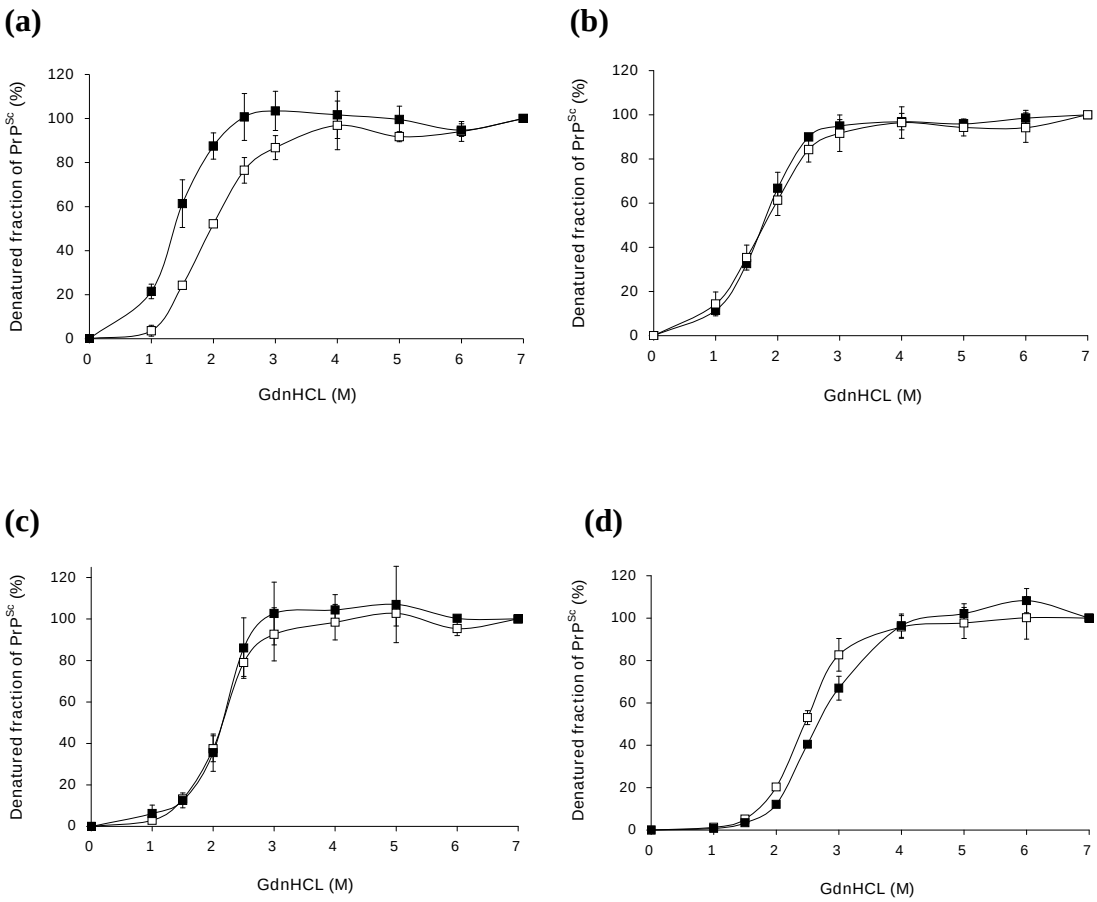

Figure 4.7 Comparison of GdnHCl-induced denaturation of PrP^{Sc} between samples. Frontal cortex samples from individual brains (vCJD1[a], vCJD3[b], MM1-1[c], and MM1-3[d]) were treated with increasing concentrations of GdnHCl and assayed by CDI. Denatured fraction of PrP^{Sc} in each concentration of GdnHCl was calculated as described in section 4.2.2. The initial results (empty symbols, sample 1 in Tables 4 and 5) were compared with the results of additional samples (filled symbols, sample 2 in Tables 4 and 5). Data represent average ± S.D. of three to four independent experiments in triplicate except for the 2nd samples of vCJD3 and MM1-3 (one-time experiment in triplicate).

Table 4.1 $GdnHCl_{1/2}$ values for PrP^{Sc} from frontal cortex of vCJD[a]

ID	vCJD1	vCJD2	vCJD3	Average
Sample 1	1.993±0.018[b]	1.650±0.060[b]	1.785±0.129[b]	1.809±0.173
Sample 2	1.297±0.162[b]	1.911±0.099[b]	1.821±0.020[c]	1.676±0.331
Sample 3	1.202±0.066[c]	1.511±0.118[c]	1.933±0.031[c]	1.549±0.367
Average	1.497±0.432	1.690±0.203	1.846±0.077	1.678±0.175[d]

Note a. The $GdnHCl_{1/2}$ values were interpolated using a best-fit of a second order polynomial curve in Excel.
b. Data represent average ± S.D. of three to four independent experiments in triplicate.
c. Data represent average ± S.D. for triplicate wells of one-time experiment except for 3rd sample of vCJD3 (duplicate wells).
d. This average represents average ± S.D. for horizontal axis.

Table 4.2 $GdnHCl_{1/2}$ values for PrP^{Sc} from frontal cortex of MM1 sCJD[a]

ID	MM1-1	MM1-2	MM1-3	Average
Sample 1	2.266±0.074[b, c]	2.350±0.043[c, d]	2.411±0.085[d]	2.342±0.073
Sample 2	2.281±0.138[d]	2.115±0.026[e]	2.642±0.072[e]	2.346±0.269
Average	2.274±0.011	2.232±0.166	2.527±0.163	2.344±0.159[f]

Note a. The $GdnHCl_{1/2}$ values were interpolated using a best-fit of a second order polynomial curve in Excel.
b. Data represent average ± S.D. of two independent experiments in triplicate.
c. Results from two different samples are combined.
d. Data represent average ± S.D. of three independent experiments in triplicate.
e. Data represent average ± S.D. for triplicate wells of one-time experiment.
f. This average represents average ± S.D. for horizontal axis.

4.3.5 Analysis of additional cases at concentrations of 1.5M and 2M GdnHCl

The analysis of multiple samples from three cases each of vCJD and MM1 sCJD revealed difference in the stability of N-terminal region of PrP^{Sc}. The discrimination between the two phenotypes was clear in the range of 1.5M ~ 2M of GdnHCl. In order to investigate further the discrimination based on the stability of PrP^{Sc}, 10 cases each from these two CJD phenotypes were analysed to determine their denatured fraction of PrP^{Sc} at these two concentrations of GdnHCl. After aliquots of samples were centrifuged and supernatants were carefully removed, pellets were resuspended to a final volume of 36µl with GdnHCl at different concentrations (0M, 1.5M, 2M, and 7M) and assayed by CDI. The denatured fractions of PrP^{Sc} at the concentrations of 1.5M and 2M GdnHCl were expressed as the relative values (%) of the TRF counts at these concentrations of GdnHCl against the counts at 7M GdnHCl (100%). As shown in Figure 4.8, the denatured fractions of PrP^{Sc} from the two phenotypes were clearly separated in both concentrations of GdnHCl. While the denatured fraction of PrP^{Sc} after incubation with 1.5M GdnHCl was lower than 20% in all MM1 cases, there was no case of vCJD with denatured fraction of PrP^{Sc} being lower than 20%. At the concentration of 2M GdnHCl, the two phenotypes were also separated around the point of 40% of denatured fraction. Statistical analysis confirmed that the degree of fractional denaturation was significantly different between vCJD and MM1 sCJD at both concentrations with *P* values of < 0.001 (1.5M) and < 0.0001 (2.0M) respectively.

The degree of denaturation of PrP^{Sc} in MM1 sCJD was similar between cases in both concentrations of GdnHCl, except for one case. In comparison, the extent of unfolding of PrP^{Sc} in vCJD was found to vary between cases, as shown by widely scattered data points in Figure 4.8a. This variable stability of vCJD PrP^{Sc} against GdnHCl-induced denaturation was in accordance with the results obtained from triplicate samples of the 3 vCJD cases in section 4.3.4.

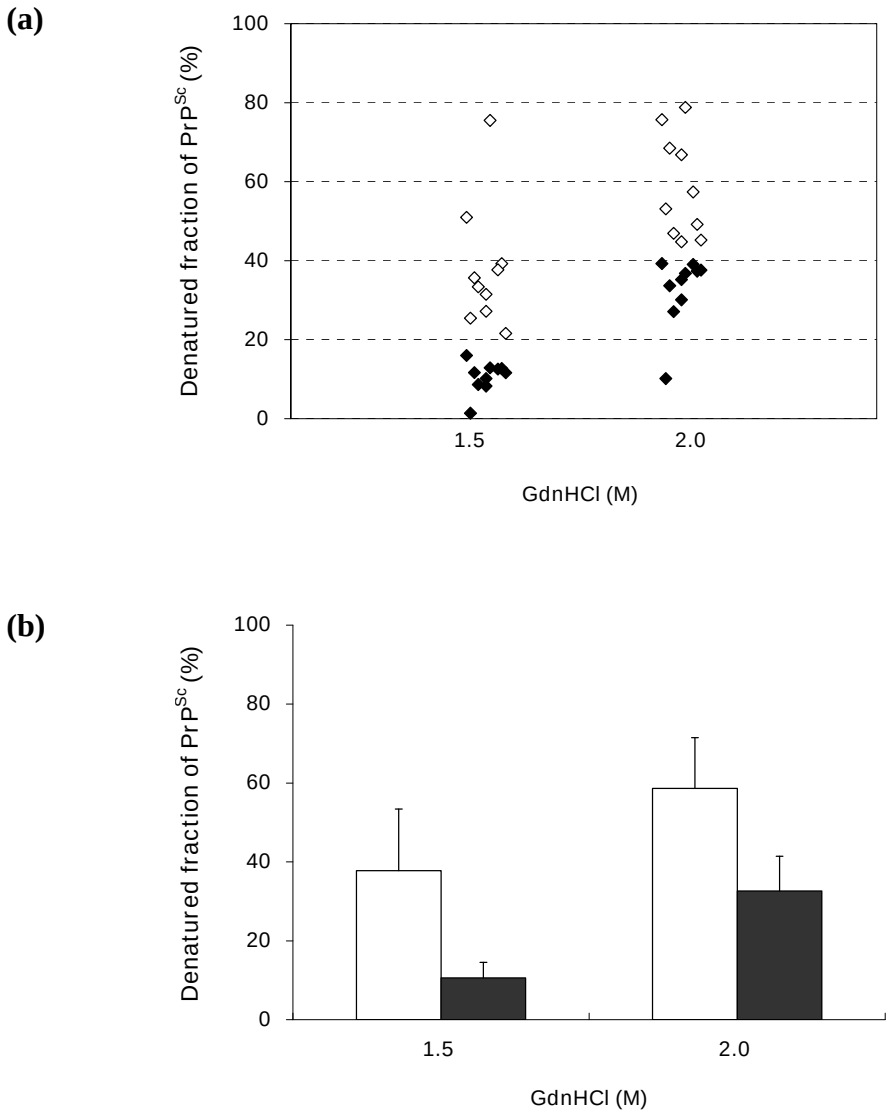

Figure 4.8 Denatured fraction of PrP^{Sc} after treatment with 1.5M or 2M GdnHCl. Frontal cortex samples from vCJD or MM1 sCJD were treated with different concentrations of GdnHCl (0M, 1.5M, 2M, and 7M) and assayed by CDI. Denatured fraction of PrP^{Sc} in each concentration of GdnHCl was calculated as described in section 4.2.2. (A) Scatter diagram of denatured fraction of PrP^{Sc} from 10 vCJD cases (white diamonds) and 10 MM1 sCJD cases (black diamonds). The results from individual cases were plotted against the concentration of GdnHCl. (B) The averages of the 10 vCJD cases (white bars) and of the 10 MM1 sCJD (black bars) are shown and error bars represent S.D.

4.3.6 Conformational stability of vCJD PrP^{Sc}: comparison between brain regions

To examine the conformational stability of PrP^{Sc} in additional regions of vCJD brains, extracts of cerebellum and thalamus from three vCJD cases were analysed by CDI following GdnHCl-induced denaturation as described for frontal cortex. Similar to the results from vCJD FC, the denaturation profiles of PrP^{Sc} from both brain regions formed a single sigmoidal curve with one major transition around 1M ~ 2.5M (Figure 4.9). In both regions, around 15 ~ 20% of PrP^{Sc} molecules were denatured at 1M GdnHCl and most of PrP^{Sc} molecules were denatured by the treatment with 2.5M GdnHCl. When the results from vCJD cerebellum and thalamus in Figure 4.9 were compared with those of frontal cortex in Figures 4.6 and 4.7, the denaturation profiles from the two regions did not seem to significantly differ from that of frontal cortex. Statistical analysis of the values obtained at 1.5M and 2.0M confirmed that none of these pair-wise comparisons achieved significance ($P > 0.05$). The $GdnHCl_{1/2}$ values for vCJD cerebellum and thalamus were 1.643M and 1.445M, respectively (Table 4.3), which were within the range of the $GdnHCl_{1/2}$ values for frontal cortex samples (Table 4.1).

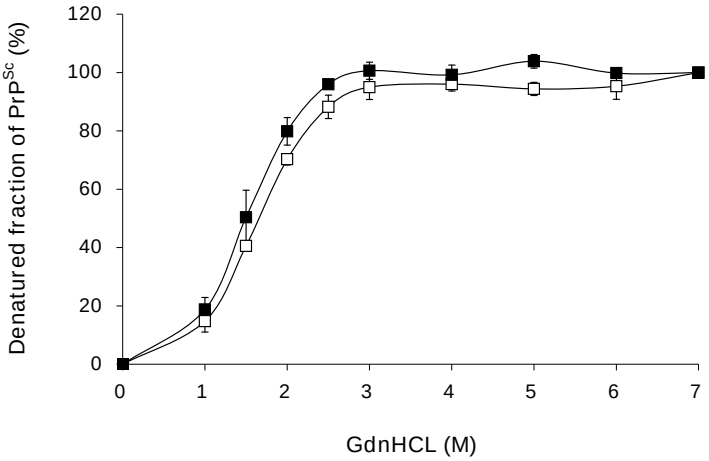

Figure 4.9 GdnHCl-induced denaturation of PrP^{Sc} from cerebellum or thalamus of vCJD brains. Extracts of cerebellum or thalamus from vCJD brains were centrifuged and the resultant pellets were exposed to increasing concentrations of GdnHCl. The degree of unfolding of PrP^{Sc} was measured by CDI and denatured fraction of PrP^{Sc} was calculated as described in section 4.2.2. Data represent the average ± S.D. of three individuals. The result from cerebellum was an average of three independent experiments in triplicate and the result from thalamus was an average of one-time experiment in triplicate.

Table 4.3 $GdnHCl_{1/2}$ values for PrP^{Sc} from cerebellum and thalamus of vCJD[a,b]

Region	vCJD1	vCJD2	vCJD3	average
Cerebellum[c]	1.626±0.022	1.658±0.087	1.646±0.211	1.643±0.016
Thalamus[d]	1.440±0.044	1.289±0.030	1.607±0.118	1.445±0.159

Note a. The $GdnHCl_{1/2}$ values were interpolated using a best-fit of a second order polynomial curve in Excel.

b. Data from both regions are based on the examination of one sample in all three cases.

c. Data represent average ± S.D. of three independent experiments in triplicate.

d. Data represent average ± S.D. for triplicate wells of one-time experiment.

4.3.7 Conformational stability of PrP^{res}

PrP^{Sc} molecules in vCJD and sCJD (MM1, VV2) were distinguishable by their difference in the conformational stability as measured by access to the 3F4 epitope in CDI following incubation with GdnHCl at various concentrations. In order to investigate whether the stability of PK-resistant core fragment of PrP^{Sc} (PrP^{res}) can also distinguish distinct human CJD phenotypes, the homogenates prepared from vCJD and MM1 sCJD brains were exposed to increasing concentrations of GdnHCl and then digested with PK as described previously (Legname *et al.* 2006; Peretz *et al.* 2001). In CDI the extent of unfolding of PrP^{Sc} after treatment with GdnHCl was measured by access to the 3F4 epitope, whereas in this assay (named conformational stability assay; CSA) the degree of unfolding of PrP^{res} was measured as a loss of resistance to PK-induced degradation, as measured by 3F4 binding in Western blot.

When blots were detected by mAb 3F4, the amounts of PrP^{res} from frontal cortex of both vCJD and MM1 sCJD cases were largely unchanged at concentrations up to 1.5M GdnHCl. In vCJD, the major transition of denaturation of PrP^{res} was observed between 2.0M and 3.0M GdnHCl and most of PrP^{res} became susceptible to PK digestion after incubation with 3M GdnHCl (Figure 4.10a). In comparison, PrP^{res} in MM1 sCJD was not greatly influenced by treatment with 2M or 2.5M GdnHCl. Exposure to 3M GdnHCl rendered a significant proportion of PrP^{res} sensitive to proteolysis and PrP^{res} was not detectable after treatment with 3.5M GdnHCl (Figure 4.10a). These findings suggest overall that PrP^{res} in MM1 sCJD is more stable to GdnHCl-induced denaturation than that of vCJD, in agreement with the relative stability of PrP^{Sc} between vCJD and MM1 sCJD shown by CDI. To investigate whether the mAb used for the detection of PrP has any influence on the result of CSA, another vCJD case was analysed in duplicate, using both the 3F4 and 6H4 mAbs to detect the protease resistant prion protein. In both immuoblots, the decrease of PrP^{res} became clear after treatment with 2.5M GdnHCl and exposure to 3M GdnHCl made most of PrP^{res} susceptible to PK digestion, leaving only trace of PrP^{res} (Figure 4.10b)

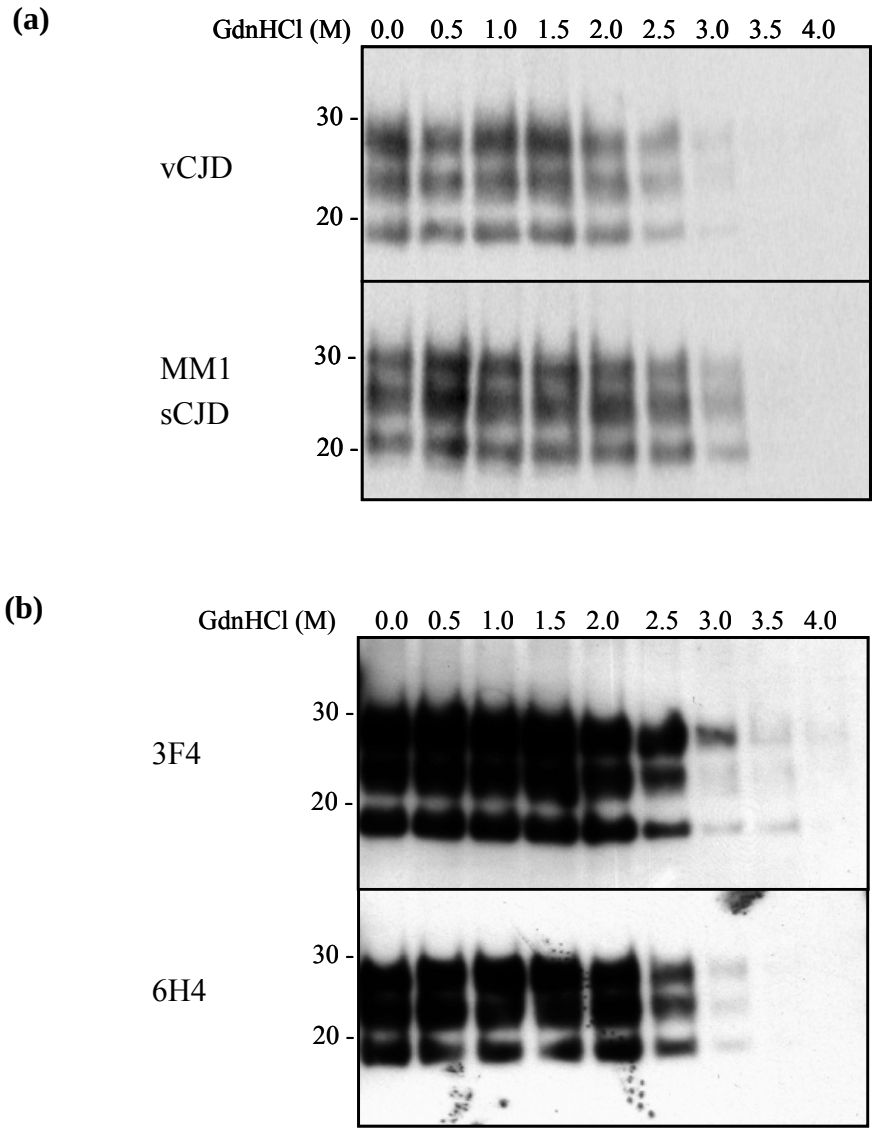

Figure 4.10 Conformational stability of PrP^{res} from frontal cortex of vCJD and MM1 sCJD brains. Brain samples were treated with increasing concentrations of GdnHCl (0 - 4M, as indicated) and then subjected to PK digestion at the concentration of 20μg/ml for 1 hour at 37°C. After methanol precipitation of protein, samples were analysed by Western blotting. (A) PrP^{res} from vCJD and MM1 sCJD were probed with anti-PrP mAb 3F4. This image was obtained by scanning on a storm 860. (B) Duplicate blots from another vCJD case were probed with the mAb 3F4 recognizing N-terminal region of PrP or with the mAb 6H4 recognizing PrP core region.

4.3.8 Conformational stability of PrP^{Sc} in GSS cases with P102L mutation

To examine the conformational stability of PrP^{Sc} in an additional phenotype of human prion disease, two GSS cases that carried the P102L mutation linked to methionine at codon 129 but differed radically in their PrP^{res} Western blot profiles were examined by CDI following incubation with GdnHCl at various concentrations. For analysis, detergent-insoluble pellet fraction of PrP was prepared using frontal cortex tissue. In both GSS cases, the denaturation curves of PrP^{Sc} formed a single sigmoidal curve with one major transition and reached their plateaus at the concentration of 3M GdnHCl (Figure 4.11). However, the degrees of unfolding of PrP^{Sc} appeared distinct between the two GSS cases at lower concentrations of GdnHCl. In the case showing typical three bands of PrP^{res} in addition to a small fragment of ~8 KDa, the major fractional transition of PrP^{Sc} from native to denatured state was observed in the range of 1.5 - 3M GdnHCl ($GdnHCl_{1/2}$: 2.399M). In comparison, the major fractional transition was seen in the range of 1 - 2.5M GdnHCl in the other case with proteolytic fragments of predominantly ~8 KDa ($GdnHCl_{1/2}$: 1.877M). Therefore, the two P102L GSS cases that differed radically in their PrP^{res} profiles were also distinct in the stability of PrP^{Sc} against GdnHCl-induced denaturation when measured by access to the 3F4 epitope in CDI.

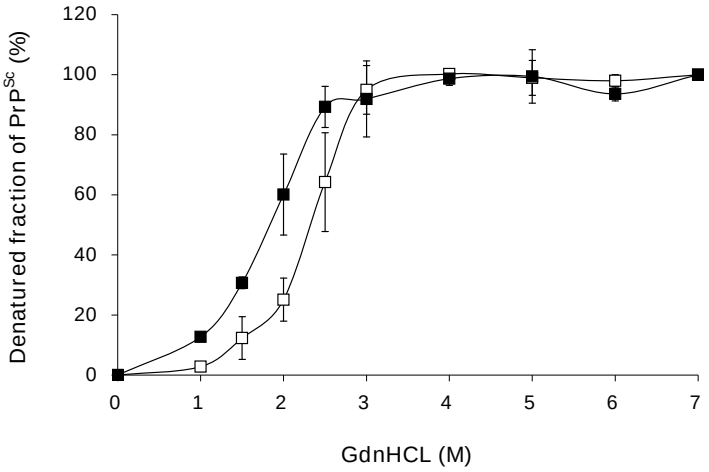

Figure 4.11 Comparison of denaturation profiles of PrP^{Sc} between two GSS cases with different PrP^{res} patterns. PrP^{Sc} denaturation profile from a GSS case with typical three-band PrP^{res} (empty squares) was compared with that from another GSS case with proteolytic fragments of predominantly ~8 KDa (filled squares). Extracts of frontal cortex from the two cases were centrifuged and the resultant pellets were incubated with increasing concentrations of GdnHCl. The extent of unfolding of PrP^{Sc} between native (0M) to denatured (7M) state was investigated by CDI. Data shown represent average ± S.D. of three independent experiments in triplicate.

4.4 Discussion

4.4.1 GdnHCl-induced denaturation of brain homogenate containing mixed PrP conformers

Initially, in this study, crude brain homogenates were assayed by CDI following incubation with various concentrations of GdnHCl. In contrast to the samples from control brains, CJD samples containing both PrP^{C} and PrP^{Sc} showed gradual increase of CDI signals according to the increase of GdnHCl, implying fractional transition of PrP^{Sc} from native to denatured state. Similar to the observation in hamster prion strains (Safar *et al.* 1998), most of PrP^{Sc} molecules in both vCJD and MM1 sCJD lost their disease-associated structure in the 3F4 epitope with the exposure to the 3M GdnHCl. Although it appears that the 3F4 binding site of PrP^{Sc} in vCJD started being exposed in lower concentration of GdnHCl than that of MM1 sCJD, variations in the level of PrP^{C} between samples/cases make more precise comparison difficult.

4.4.2 Conformational stability of PrP^{Sc}: analysis of detergent-insoluble fraction of PrP

In order to measure the extent of unfolding of PrP^{Sc} more precisely by avoiding the interference of PrP^{C}, this study utilized detergent-insoluble fraction of PrP. As described previously (Meyer *et al.* 1986; Thackray *et al.* 2007a; Wadsworth *et al.* 2006), PrP^{C} molecules in both control and CJD brains were mostly present in the detergent-soluble supernatant fraction and a major proportion of PrP^{Sc} in CJD brains was recovered in the detergent-insoluble pellet fraction.

The analysis of PrP^{Sc} (or detergent-insoluble fraction of PrP) from frontal cortex tissues has shown that gradual unfolding of PrP^{Sc} by increasing concentrations of GdnHCl produced a single sigmoidal curve with the major transition occurring between GdnHCl concentrations of 1M and 3M. The denaturation curve for vCJD was displaced to the left when compared to sCJD (MM1 and VV2) and the $GdnHCl_{1/2}$ value in vCJD was ~ 0.65M lower than those of both subtypes of sCJD.

Further comparative analysis of multiples cases at the concentrations of 1.5M and 2.0M GdnHCl also displayed clear separation between vCJD and MM1 sCJD. Therefore, it appears evident that PrP^{Sc} in MM1 and VV2 subtypes of sCJD is structurally more stable against GdnHCl-mediated denaturation than that of vCJD when measured by access to the 3F4 epitope in CDI. Although the difference between vCJD and MM1 sCJD is clear and reproducible, a degree of inter-sample and/or inter-case variability was also observed in the frontal cortex of vCJD. This variability may reflect genuine micro-heterogeneity in PrP^{Sc} stability, or it may reflect confounding factors associated with cellular and molecular properties of the tissue sampled. Intriguingly, the stability of PrP^{Sc} in the GSS case characterized by PrP^{res} of 20 - 30KDa is closely similar to that of sCJD, whereas the stability of PrP^{Sc} in the other GSS case with proteolytic fragment of predominantly ~8KDa is similar to that of vCJD.

Although this study examined the stability of the "detergent-insoluble" fraction of PrP and was conducted in a limited number of disease phenotypes and/or cases, taken together, the results suggest that the structural stability of PrP^{Sc} as determined by CDI is not uniform among human prion diseases and is at least partly independent of the conventional Western blot PrP^{res} type (fragment size) and the *PRNP* genotype (pathogenic mutations and codon 129). This notion is further supported by a recent study that investigated the stability of PrP^{res} in sCJD with MM genotype at codon 129 (Cali *et al.* 2009). It would be of interest to investigate whether further meaningful distinctions can be made between examples of the full range of human prion diseases, including other subtypes of sCJD, fatal familial insomnia and the more recently described protease sensitive prionopathy.

Similar to the findings in this study, a recent study characterizing PrP^{Sc}-specific peptides also reported that PrP^{Sc} in vCJD was more sensitive to GdnHCl-mediated denaturation than PrP^{Sc} in MM1 sCJD (Lau *et al.* 2007). In the study by Lau and colleagues, CJD brain samples were treated with increasing concentrations of

GdnHCl and subsequently incubated with beads coated with a PrP^{Sc}-specific peptide. When the peptide-bound PrP molecules were examined by sandwich ELSIA employing a capture antibody recognizing C-terminal region of PrP, the difference in $GdnHCl_{1/2}$ values was ~ 0.6M between the two forms of CJD (Table 4.4) (Lau *et al.* 2007). Thus, the result based on PrP^{Sc}-specific peptide is very closely similar to that of this study, despite the difference in methodology between the two studies. Moreover, the unfolding pattern of PrP^{Sc} shown by the two studies is practically identical to each other in that they formed a single sigmoidal curve with one major transition, although Lau's denaturation curves were turned upside down compared to this study's due to the difference in methodology (Lau *et al.* 2007).

4.4.3 Conformational stability of PrP^{res}

The conformational stability assay based on the CDI has shown that the 3F4 epitope of PrP^{Sc} is more stable in sCJD (MM1 and VV2 subtypes) than that of vCJD, but this result may not necessarily mean that C-terminus of PrP^{Sc} is also more stable in sCJD than vCJD. To explore this possibility, one vCJD and one MM1 sCJD cases were examined by CSA, in which the degree of susceptibility to GdnHCl-induced denaturation is measured as a loss of resistance to PK-induced degradation. Consistent with the results based on the CDI, CSA has also shown that PrP^{res} in MM1 sCJD is more resistant to GdnHCl-induced denaturation than that of vCJD.

However, unlike PrP^{res} in vCJD and MM1 sCJD, the region-dependent conformational stability of PrP^{res} was reported in the Chandler strain in a recent study (Shindoh *et al.* 2009); the region comprising residues 81 and 137 of PrP^{res} in this laboratory strain was found to be denatured by GdnHCl at relatively lower concentration and thus more easily became PK-susceptible, whereas the remaining C-terminal region was highly resistant to GdnHCl-induced denaturation. Thus, the $GdnHCl_{1/2}$ values determined by mAbs recognizing amino acids 81 and 137 were significantly lower than those determined by mAbs recognizing C-terminal region (~ 1.8M *versus* ~ 3.5M). Interestingly, the loss of the region encompassing amino acids

81 and 137 led to the almost complete loss of prion infectivity, although the intensity of PrP^{res} bands composed of the remaining C-terminal region was compatible to that of PrP^{res} starting at residue 81 (Shindoh *et al.* 2009). It is of note that the low infectivity in the synthetic prions, the amyloid form of mouse recombinant PrP spanning residues 89-230, was also explained by the proteolytic liability of the region spanning residues 90-138, which is almost identical to the region described by Shindoh et al. (Bocharova *et al.* 2005; Legname *et al.* 2004)

Cali et al. examined the stability of PrP^{res} using CSA in sCJD with MM genotype at codon 129 (Cali *et al.* 2009). In this study, PrP^{res} in MM1 sCJD was found to be significantly more stable than that of MM2 with the difference in $GdnHCl_{1/2}$ values of ~1.3M (Table 4.4). Therefore, the results from Cali's study is consistent with this study in that type 1 PrP^{res} is more stable than type 2 PrP^{res} in CJD with MM genotype at codon 129. Another group of investigators examined the stability of PrP^{Sc} from bank voles which were inoculated with various kinds of natural TSE sources (Pirisinu *et al.* 2009). The methodology used to measure the stability of PrP^{Sc} by Pirisinu et al. was different from this study as well as CSA; while the conventional CSA measures the extent of unfolding of PrP^{Sc} as a loss of resistance to PK-induced degradation, the conformational stability assay employed by Pirisinu et al. assesses the degree of unfolding of PrP^{Sc} as a loss of detergent insolubility (Pirisinu *et al.* 2009). Interestingly, the higher structural stability of PrP^{res} in MM1 sCJD (as compared to MM2 sCJD) was found to be conserved when these diseases were transmitted to bank voles (Table 4.4). This positive correlation in the conformation stability of PrP^{Sc} between sCJD and bank voles propagating sCJD prions strongly supports the notion that this biochemical parameter plays an important role in determining biological properties of prion strains (Colby *et al.* 2009; Legname *et al.* 2006).

4.4.4 Conformational stability of PrP^{res}: importance in determining disease incubation periods

The conformational stability of PrP^{res} was found to correlate with incubation periods of synthetic and laboratory prion strains that have been propagated in mice (Legname *et al.* 2006); generally, the prion strains with higher stability of PrP^{res} exhibited longer incubation periods. The hypothesis that incubation time is a function of PrP^{Sc} stability (in addition to the known factors such as titre, route and PrP expression level and sequence) was further tested by artificially producing an array of synthetic PrP amyloids differing in their conformational stability and then testing their biological properties (Colby *et al.* 2009). The results showed that a more labile PrP^{Sc} conformation correlated with faster replication and shorter incubation periods. How such considerations might relate to human prion diseases is unclear at this point in time, however the finding that vCJD PrP^{Sc} is less stable than that of sCJD may be interpreted as a further reason for concern regarding the potential for secondary transmission of the promiscuous BSE/vCJD prion strain.

4.4.5 Conformational stability of PrP^{Sc}/PrP^{res}: limitation in inferring the conformational state

Despite the emerging importance of conformational stability as a biochemical parameter that is associated with disease incubation periods, its limitation is also evident in inferring conformational state of PrP^{Sc}. For example, the conformational stability of PrP^{Sc} expressed as the $GdnHCl_{1/2}$ value was indistinguishable between MM1 and VV2 subtypes of sCJD, despite their phenotypic difference (Parchi *et al.* 1999b; Parchi *et al.* 1996); a GSS case with P102L mutation characterized by the presence of PrP^{res} of 20 - 30KDa was also indistinguishable from the two subtypes of sCJD. Similarly, the stability of PrP^{res} measured by CSA was shown to be similar between laboratory prion strains that differ in disease phenotype and/or in the fragment size of PrP^{res} (Makarava *et al.* 2010; Peretz *et al.* 2001; Peretz *et al.* 2002). Thus, the similarity in the stability of PrP^{Sc} does not necessarily mean the propagation of a same prion strain. Although the stability of PrP^{Sc}/PrP^{res} alone is of limited use in discriminating prion strains, however, this methodology may be useful in distinguishing prion strains that are phenotypically distinct but not distinguishable

by one-dimensional gel electrophoresis as shown in previous studies (Peretz *et al.* 2001; Peretz *et al.* 2002).

4.4.6 Speculation on the effects of detergent in protein conformation

In this study, the detergent of N-laurylsarcosinate sodium salt (Sarcosyl) was used at the concentration of 2% for the preparation of brain homogenates, which may interfere with the tertiary and quaternary structures of PrP^{Sc} aggregates by disrupting hydrophobic interactions (Tanford 1968). This possibility is supported by a recent study that showed the differential susceptibility of PrP^{Sc} to Sarcosyl-induced denaturation between mouse-adapted scrapie strains (Thackray *et al.* 2007b). This detergent is also known to induce the aggregation and fibril formation of PrP^{C} molecules at low concentrations (0.001 - 0.1%), enhancing ß-sheet secondary structure (Xiong *et al.* 2001).

4.4.7 Speculation on the mechanism of PrP^{Sc} denaturation by GdnHCl

Chaotropic agents like GdnHCl disrupt hydrogen bonds that are responsible for the secondary structure (α-helices and ß-sheets) of proteins (Tanford 1968). Since hydrogen bonding also helps maintain tertiary and quaternary structures of proteins, chaotropic agents can also affect these structural aspects. Thus, the GdnHCl-induced denaturation of PrP^{Sc} molecules can occur at least in two different levels: loss of secondary structure (i.e. uncoiled into an irregularly coiled polypeptide) and loss of tertiary/quaternary structure (i.e. dissociation of PrP^{Sc} aggregates).

In a previous study that examined dissociation/unfolding pathways of PrP^{Sc} in hamster prion strains during exposures to ascending concentrations of GdnHCl (Safar *et al.* 1993), the GdnHCl-induced denaturation of PrP^{Sc} molecules was reported to consist of a four-step pathway: (a) aggregates → (b) dissociated folded monomer → (c) partially unfolded intermediate → (d) unfolded monomer. The dissociation of PrP^{Sc} aggregates into folded monomers occurred with the midpoint of transition at 1.5 - 2.0M GdnHCl, followed by the state of stable intermediate

(midpoint of transition: ~ 3.5M GdnHCl). Given that the hidden recognition site of mAb 3F4 becomes accessible in most of the PrP^{Sc} molecules following incubation with 3M GdnHCl, the degree of unfolding of PrP^{Sc} molecules measured by CDI probably reflects the degree of dissociation of aggregated PrP^{Sc}. However, the loss of ß-sheet structure following incubation with GdnHCl may also contribute to the CDI-based denaturation profiles, since the region with the 3F4 epitope acquires high ß-sheet content during the conversion of PrP^{C} into PrP^{Sc} (Huang *et al.* 1995; Langedijk *et al.* 2006) and the acquisition of ß-sheet structure makes the 3F4 epitope inaccessible (Safar *et al.* 1998). Despite these speculations, the exact mechanism by which GdnHCl denatures PrP^{Sc} remains elusive (Legname *et al.* 2006).

4.4.8 Summary

In summary, this study has addressed the conformational stability of PrP^{Sc} in different phenotypes of human prion disease using the conformation-sensitive mAb 3F4 in CDI, which reveals that this biochemical parameter may represent another marker of PrP^{Sc} structure that is not directly associated with the PrP^{res} type and/or the *PRNP* genotype. Given the relevance of conformational stability to disease incubation periods (Colby *et al.* 2009; Legname *et al.* 2006), the analysis of conformational stability of PrP^{Sc} in human prion diseases is believed to help understand molecular aspects relevant to determining disease phenotypes.

Table 4.4 Comparison of $GdnHCl_{1/2}$ values between relevant studies

Assay principle	vCJD	MM1 sCJD	MM2 sCJD	VV2 sCJD	Material analysed	Reference
CDI (3F4)	1.678	2.344	N.D[a]	2.308	human brain	(this study)
PrP^{Sc}-specific peptide	1.850	2.450	N.D[a]	N.D[a]	human brain	(Lau *et al.* 2007)[b]
CSA (PK-resistance)	N.D.	2.760	1.420	N.D[a]	human brain	(Cali *et al.* 2009)
Detergent insolubility	N.D.	2.950	1.460	2.690	bank vole brain	(Pirisinu *et al.* 2009)

Note a. N.D = not determined

b. Lau et al. used sandwich ELISA to detect PrP^{Sc} following capture with a PrP^{Sc}-specific peptide. Two different capture antibodies were used in the sandwich ELISA. The results shown in this table are based on the capture antibody recognizing C-terminus of PrP. When the antibody recognizing N-terminus was used in sandwich ELISA, the difference in the $GdnHC_{l/2}$ value between vCJD and MM1 sCJD was ~0.85M (vCJD: 1.6M, MM1: 2.44M). It is worth noting that the recognition site of Mar-1 used as a capture antibody in CDI recognizes C-terminus of PrP associated with a disulphide bridge (Bellon *et al.* 2003)

CHAPTER 5

Discussion

5.1 Summary of findings

The main goal of this study was to investigate disease-associated prion protein (PrP^{Sc}) accumulated in CJD brains through biochemical approaches that differ in principle from conventional Western blot analysis of PK-resistant fragments of PrP^{Sc} (PrP^{res}). For this, pathological human brain materials were examined by assays including conformation-dependent immunoassay (CDI), sucrose gradient centrifugation and stability assay combined with CDI. These novel biochemical approaches have allowed for the analysis of conformational and size classes of PrP^{Sc}, thus providing a more complete description of PrP^{Sc} species occurring in human brains affected with prion disease.

5.1.1 PrP^{C} in CJD brains

Since the binding site of the mAb 3F4 employed as a detector in CDI is not accessible in native PrP^{Sc} in contrast to PrP^{C}, CDI fluorescence signals obtained from native samples represent PrP^{C}. Therefore, CDI can distinguish PrP^{C} from PrP^{Sc} in CJD brains. When multiple samples from different forms of CJD brains were analysed by CDI, PrP^{C} was readily detectable in all examined CJD samples irrespective of disease phenotypes or brain regions. To the best of my knowledge, this study is the first direct approach to a description of PrP^{C} present in human brains infected with prions. The presence of PrP^{C} in CJD brains is perhaps to be expected because PrP^{C} serves as a precursor protein of PrP^{Sc} and thus its presence is a prerequisite for the replication of PrP^{Sc} (Bueler *et al.* 1993; Caughey and Raymond 1991). Moreover, the ubiquitous presence of PrP^{C} in CJD brains appears to provide additional support for the notion that PrP^{C} is closely linked to the neurotoxicity observed in prion-infected brains (Brandner *et al.* 1996; Mallucci *et al.* 2003).

In this study, PrP^{C} is defined as PrP molecules with the 3F4 epitope accessible in CDI. If topological variants of PrP such as cytosolic PrP (cyPrP) and a transmembrane form of PrP with its N-terminus exposed to the cytosol (^{ctm}PrP) are accessible by the mAb 3F4 (which looks quite possible), they will be classified as

"PrP^{C}" in CDI. Accordingly, PrP molecules defined as "PrP^{C}" in this study are thought to contain not only secreted form of cell-surface PrP but also those aberrant PrP species. A proportion of PrP^{C} from the thalamus of vCJD or frontal cortex of MM1 sCJD was found to migrate to the heavier fractions of the sucrose gradient, which may be associated with the aggregates formed from those topological variants (Ma and Lindquist 2001). Given that transgenic mice expressing cyPrP and/or ^{ctm}PrP were found to develop fatal neurodegeneration (Chakrabarti and Hegde 2009; Hegde *et al.* 1998; Ma and Lindquist 2002; Stewart *et al.* 2005), they may contribute to the disease pathogenesis. These aberrant PrP species can be more important in several genetic forms of human prion disease such as FFI, which do not accumulate substantial amount of PrP^{Sc} in the brain despite fatal clinical disease (Almer *et al.* 1999; Brown *et al.* 1995; Parchi *et al.* 2000a). Moreover, neuronal loss and gliosis in diseased human brains do not appear to be directly associated with the local burden of PrP^{Sc} (Parchi *et al.* 1995; Parchi *et al.* 2000a). Therefore, it would be interesting to investigate the level of these topological variants of PrP in prion-affected human brains and to determine their sedimentation profiles in the sucrose gradient. For this, an antibody that selectively recognizes them by virtue of their uncleaved ER-targeting signal peptide may be methodologically helpful (Stewart and Harris 2003).

5.1.2 PrP^{Sc} in CJD brains: comparison between 3F4-based CDI and resistance to limited proteolysis

When PrP^{Sc} as defined by the accessibility of 3F4 binding site (in CDI) was compared with that defined by resistance to limited proteolysis (in WB) using multiple samples with different regional origins from various CJD phenotypes, there was a good overall correlation between the two possible biochemical criteria that define PrP^{Sc}. However, the occasional discordance between the two measurements of PrP^{Sc} was also evident between samples from the same brain. Interestingly, in all three vCJD cases, PrP^{res} (based on PK-resistance) was more abundant in the thalamus despite similar or higher levels of PrP^{Sc} (based on CDI) in the cerebellum. The CDI analysis following limited proteolysis has shown that PK-sensitive form of PrP^{Sc} is

present to a significant level in CJD brains, although the estimated proportion of PK-susceptible PrP^{Sc} to total PrP^{Sc} does not appear as high as the level reported by Safar and colleagues (Safar *et al.* 2005a). Taken together, the occasional disagreement between the two biochemical measurements of PrP^{Sc} can be most likely explained by non-uniform distribution of PK-sensitive isoform of PrP^{Sc} in individual prion-infected brains. Currently, it remains to be determined whether PK-sensitive PrP^{Sc} is a metabolic intermediate in the formation of PK-resistant PrP^{Sc} or whether it represents another pathogenic isoform of PrP, which is specific to CJD brain, but is not associated with metabolic pathway leading to the formation of PK-resistant PrP^{Sc} (Tremblay *et al.* 2004; Tzaban *et al.* 2002). Serial transmission of PK-sensitive synthetic prions, which were generated by polymerizing recombinant mouse PrP into amyloid fibers did not lead to the formation of PK-resistant PrP (Colby *et al.* 2010). In naturally occurring prion diseases, it remains largely obscure how significantly PK-sensitive fraction of PrP^{Sc} contributes to the biological properties of prions such as disease infectivity and strain property (Cronier *et al.* 2008; Deleault *et al.* 2008).

5.1.3 Distribution profiles of PrP^{Sc} between the three regions in CJD brains

In this study, multiple brain samples with three different regional origins (frontal cortex, cerebellum and thalamus) from different CJD phenotypes were examined by CDI and WB (following limited proteolysis), which made it possible to compare the distribution profiles of PrP^{Sc} in the three brain regions between cases and phenotypes. When the three forms of CJD with MM genotype at codon 129 were compared, the topography of abnormal PrP appears to be different between vCJD and two MM sCJD subtypes. In the vCJD brains, abnormal PrP was more abundant in the cerebellum (based on CDI) or in the thalamus (based on PK-resistance). In contrast, both types of MM sCJD harboured more abundant amounts of abnormal PrP in the frontal cortex, except for one MM1 case showing similar levels of abnormal PrP between the three regions. Although it is not legitimate to generalize this observation due to the very small number of cases (three cases per phenotype), it should be stressed that the results obtained from both MM subtypes of sCJD are consistent with

previous studies in which distribution profiles of PrP^{res} were examined in wider brain areas from more sCJD cases (Parchi *et al.* 1996; Schoch *et al.* 2006).

Interestingly, one MV2 case (MV2-2) has shown the distribution profile of abnormal PrP which is distinct from the two other MV2 cases but is similar to those of MM2 cases. Furthermore, this MV2 case has pathological features resembling MM2 subtype of sCJD without showing any detectable kuru plaques in the cerebellum. This atypical MV2 case whose biochemical and neuropathological profiles are similar to MM2 subtype of sCJD does not appear to fit in with even an updated version of the classification system of sCJD (Parchi *et al.* 2009b). The identification of MM2-like MV2 case raises a question on whether sCJD can be fully classified into distinct subtypes based on the *PRNP* codon 129 genotype and PrP^{res} type. This question has a common thread with whether sCJD comprises discrete clinico-pathological entities or is a wide phenotypic spectrum of disease (Head and Ironside 2009). It remains uncertain whether biochemical and neuropathological similarities between the MV2-2 and MM2 cases are associated with the propagation of the same prion strain.

5.1.4 PrP^{Sc} in CJD brains: sedimentation profiles in the sucrose step gradient

When fractionated in the 10 - 60% sucrose step gradient, PrP molecules from the non-CJD brains were mostly recovered in top few fractions, whereas those from CJD brains spread throughout the gradient, reaching the heaviest bottom fraction. When fractionated samples from different regions of vCJD brains were assayed by CDI, the distribution profiles of PrP^{Sc} in the sucrose gradient were significantly different between regions. While PrP^{Sc} from the frontal cortex and cerebellum of vCJD was mainly recovered in the bottom three fractions leaving very low levels of PrP^{Sc} in the intermediate fractions, PrP^{Sc} from the thalamus was present throughout the gradient although PrP^{Sc} signals were still strongest in the bottom three fractions. The sedimentation profile of PrP^{Sc} from the frontal cortex of MM1 sCJD was similar to

that of frontal cortex of vCJD, except that PrP^{Sc} species recovered in the intermediate fractions were a bit more abundant in MM1 sCJD than vCJD.

It remains to be determined whether the separation of PrP molecules achieved in the 10 - 60% sucrose gradient fully reflects their size or is influenced by their buoyant density. If PrP^{Sc} consists exclusively of PrP, its sedimentation property in the sucrose gradient will be a direct reflection of size. In this case, PrP species recovered in the intermediate fractions are believed to represent oligomeric forms of PrP^{Sc} with sizes as small as 600 KDa (Tzaban *et al.* 2002). The significant abundance of PrP^{Sc} in the intermediate fractions from the thalamus of vCJD is of particular interest because the oligomeric forms of PrP^{Sc} may be more relevant to neurotoxicity than large aggregates (Caughey and Lansbury 2003; Kristiansen *et al.* 2007; Simoneau *et al.* 2007). The pathological feature seen in the posterior thalamus of vCJD (severe neuronal loss and marked astrocytosis) may be associated with the abundance of the oligomeric species of PrP^{Sc} in this region. It also appears possible that certain population of neurons may be more vulnerable to certain species of PrP^{Sc} such as oligomeric forms of PrP^{Sc}, which is conceptually similar to the selective neuronal vulnerability described in previous studies (Bouzamondo *et al.* 2000; Guentchev *et al.* 1997; Guentchev *et al.* 1998; Guentchev *et al.* 1999). The PrP^{Sc} molecules identified in the top first fraction of the gradient (again in the thalamus of vCJD) may be as small as the size of PrP dimers or trimers, judging from the ionizing radiation study (Bellinger-Kawahara *et al.* 1988) or recently proposed trimeric PrP^{Sc} models (DeMarco and Daggett 2004; Govaerts *et al.* 2004).

However, PrP^{Sc} is known to have strong affinity for lipids (Safar *et al.* 2006) and sphingolipids are still detectable in highly purified prion rods (Klein *et al.* 1998). In contrast to PrP^{C}, PrP^{Sc} is not cleaved from plasma membrane by the enzymatic treatment with phosphatidylinositol-specific phospholipase C (PIPLC)(Safar *et al.* 1991; Stahl *et al.* 1990). Moreover, lipids may facilitate the conversion of PrP^{C} into a PrP^{Sc}-like conformation (Kazlauskaite *et al.* 2003; Wang *et al.* 2007) and act as a

cofactor facilitating the formation of prions (Wang *et al.* 2010). Taken together, PrP^{Sc} may contain lipids after the detergent extraction of the condition used. In this case, the sedimentation property of PrP^{Sc}-containing complex can be influenced by its buoyant density in addition to its size. This possibility appears to be more relevant to the thalamus of vCJD in which a significant proportion of PrP^{Sc} was identified in the top and intermediate fractions of the sucrose gradient.

5.1.5 Conformational stability of PrP^{Sc} in CJD brains

When PrP^{Sc}-enriched, detergent-insoluble fraction was first incubated with a wide range of concentrations of GdnHCl and then assayed by the 3F4-based CDI, the incubation with 3M GdnHCl was found to be enough to disrupt disease-associated structure in most of the PrP^{Sc} molecules, irrespective of disease phenotypes. However, the degrees of stability of PrP^{Sc} to GdnHCl-induced denaturation were distinct between vCJD and sCJD (MM1 and VV2 subtypes) at lower concentrations of GdnHCl. In vCJD, the major fractional transition of PrP^{Sc} from native to denatured state was observed in the range of 1.0 - 2.5M GdnHCl. In both types of sCJD, the major fractional transition was observed in the range of 1.5 - 3.0M GdnHCl. The average $GdnHCl_{1/2}$ value in the frontal cortex of vCJD was 1.678M, which was ~0.65M lower than those of both sCJD phenotypes.

Although this study examined the stability of the "detergent-insoluble" fraction of PrP and was conducted in a limited number of cases, the results strongly suggest that PrP^{Sc} in MM1 sCJD is more resistant to GdnHCl-induced denaturation than that of vCJD. A recent study performed by Cali and colleagues has shown that PrP^{res} in MM1 sCJD is more stable than that of MM2 sCJD (Cali *et al.* 2009). If the three CJD phenotypes with MM genotype at codon 129 are considered, such a conformational difference may be attributable to the same molecular property that is responsible for the Western blot type 1 / type 2 PrP^{res} difference. However, the VV2 sCJD case examined here shared the conformational stability of MM1 sCJD (but not that of vCJD), suggesting that the conformational stability measured by CDI is based on a

property of PrP^{Sc} that is different from the property of PrP^{res} that determines the Western blot type. Consistent with this suggestion, the behaviour of stability of PrP^{res} in natural and artificial mixtures of both PrP^{res} types could not be simply explained in association with their types (Cali *et al.* 2009). Moreover, two GSS cases which share P102L mutation and MM genotype at codon 129 could be distinguished by the stability of PrP^{Sc}. While the stability of PrP^{Sc} in the GSS case characterized by type 1 PrP^{res} was similar to that of sCJD, the other GSS case with proteolytic fragments of predominantly ~8 KDa was found to be similar in stability to vCJD. Taken together, the stability of PrP^{Sc} as determined by CDI does not correlate fully with PrP^{res} type or the *PRNP* genotype (codon 129 and the presence/absence of pathogenic mutation), suggesting that this biochemical parameter may represent a further dimension to a complete description of potentially phenotype-related properties of PrP^{Sc} in human prion diseases.

5.1.6 A proteolytic fragment of ~8 KDa in MV2 sCJD

When the thalamus from the MV2 case (MV2-2) showing atypical biochemical and neuropathological features was analysed by WB following proteolysis, a proteolytic fragment of ~8 KDa was detected in addition to the typical three bands of 21 - 30 KDa. The PrP^{res} profile seen in this case is closely similar to the profile reported in some GSS cases with P102L mutation, which have shown PK-resistant fragments of 21 to 30 KDa in addition to a proteolytic fragment of ~8 KDa (Parchi *et al.* 1998; Piccardo *et al.* 1998). The prevalence of this low molecular weight fragment in sCJD remains to be determined. However, small proteolytic fragments of PrP may not be so uncommon in sCJD (Kascsak *et al.* 1993; Krebs *et al.* 2007; Piccardo *et al.* 1998) and thus their presence may not be an absolute biochemical indicator for GSS, which is further supported by similar observation in a FFI case (Hill *et al.* 2006).

5.2 Outstanding questions and future research

This study focused on the analysis of vCJD, which is most important in public health terms in the UK, and MM1 subtype of sCJD which is the most frequently occurring form of human TSE. For a fuller understanding of prions in humans, it will be important to expand the novel biochemical approaches into other forms of human prion disease including untested subtypes of sCJD, FFI, GSS and the more recently described PSPr. It will be also important to investigate whether PrP^{Sc} complexity identified in this study can be related to biological properties such as disease infectivity or strain property. A comparative transmission study between CJD samples which have similar levels of total PrP^{Sc} but differ greatly in their PrP^{res} levels (for example, Cb3 and Th3 samples in MV2-3 [see section 2.3.2.2.5]) may give an insight into the biological significance of PK-sensitive isoform of PrP^{Sc} in human prion diseases. The relationship between the size of PrP^{Sc} aggregates and their pathological activities may be partly answered by comparing sucrose fractions containing PrP^{Sc} species that differ in their size and/or density. In addition to these outstanding questions, three more specific questions of future interest are discussed in detail.

5.2.1 Further analysis of size distribution of PrP^{Sc} in the thalamus of vCJD brains

When the thalamus tissues of vCJD were fractionated in the 10 - 60% sucrose step gradient, PrP^{Sc} was identified throughout the gradient and PK-resistant fraction of PrP^{Sc} was readily detectable even in the top first fraction. This is in sharp contrast to the results obtained from the two other regions (frontal cortex and cerebellum) of vCJD brains in which PrP^{Sc} was mainly recovered in the bottom three fractions. Currently, it is unclear whether the distribution profile of PrP^{Sc} molecules obtained from the thalamus of vCJD is directly related to aggregate sizes. A growing body of evidence supports the notion that small oligomeric species of PrP^{Sc} are more relevant to prion infectivity and neurotoxicity than large aggregates (Caughey and Lansbury 2003; Kristiansen *et al.* 2007; Silveira *et al.* 2005; Simoneau *et al.* 2007). Therefore,

it will be important to determine more precisely the size classes of PrP^{Sc} in the thalamus of vCJD, particularly when considering that severe neuronal loss with marked astrocytosis in this region is one of the diagnostic pathological features in vCJD (Ironside *et al.* 2000; Ironside *et al.* 2002). Traditional sizing methods such as size exclusion chromatography or filtration may be considered for further analysis of size classes of PrP^{Sc} (Caughey *et al.* 1995; Safar *et al.* 1990; Tzaban *et al.* 2002), however, their drawbacks in analysing large, insoluble PrP^{Sc} aggregates are also well recognized (Silveira *et al.* 2006). The techniques of field flow fractionation which are known to be capable of high-resolution separation over a wide size range of PrP aggregates may be more applicable in determining the size distribution of PrP^{Sc} in the thalamus of vCJD (Silveira *et al.* 2006; Silveira *et al.* 2005; Sklaviadis *et al.* 1992).

5.2.2 Further analysis of conformational stability of PrP^{Sc}

Although a limited number of cases were examined in this study, the results indicate that PrP^{Sc} from vCJD is more susceptible to GdnHCl-induced denaturation than PrP^{Sc} from the two most frequently occurring forms of sCJD (MM1 and VV2). In a recent study describing the stability of PrP^{res} in sCJD with MM genotype at codon 129, PrP^{res} from MM2 sCJD was shown to be significantly more sensitive to GdnHCl-induced denaturation than PrP^{res} from MM1 sCJD (Cali *et al.* 2009). One limitation of the stability assay performed by Cali and colleagues lies in that they relied on limited proteolysis in measuring the stability of PrP^{Sc}, which precluded the analysis of PK-sensitive isoform of PrP^{Sc}. In this context, it would be interesting to determine the conformational stability of PrP^{Sc} in MM2 sCJD using the CDI. Additionally, it would be of interest to compare the stability of PrP^{Sc} between MM2 sCJD and sFI. These two rare forms of human prion disease with MM genotype at *PRNP* codon 129 are not distinguishable by one-dimensional gel electrophoresis despite their significant difference in disease phenotypes (Parchi *et al.* 1999a; Parchi *et al.* 1999b). Although they were reported to be distinguishable by two-dimensional gel electrophoresis, questions still remain about whether differences in the glycans are

sufficient to explain the significant phenotypic difference between the two forms of disease (Pan *et al.* 2005b; Pan *et al.* 2001). In this context, it would be worthwhile to investigate whether the stability of PrP^{Sc} can distinguish the two rare phenotypes of human prion disease.

Conformational stability of PrP^{Sc} in individual prion strains was reported to correlate with their incubation periods (Legname *et al.* 2006). In a more recent study from the same group, synthetic prion strains with various incubation periods were produced by varying the conformational stability of recombinant PrP amyloids (Colby *et al.* 2009). Moreover, the stability of PrP^{Sc} from different forms of sCJD showed a good correlation with the stability of PrP^{Sc} from bank voles inoculated with sCJD materials (Pirisinu *et al.* 2009). Accordingly, it is of interest to investigate the stability of PrP^{Sc} in CJD inocula, in recipient mice of primary transmission and of subsequent passage, and then to analyse how the stability of PrP^{Sc} can be related to disease incubation periods in interspecies and intraspecies transmission of CJD.

5.2.3 Abnormal PrP species in FFI

It is well known that FFI has very low levels of PrP^{Sc} in the brain despite fatal clinical disease (Almer *et al.* 1999; Brown *et al.* 1995). Even when the case (and region) showing highest level of PrP^{res} accumulation was taken for comparison, the overall level of PrP^{res} was 5 to 10 times lower than that detected in sCJD (Parchi *et al.* 2000a). Furthermore, although FFI is pathologically characterized by thalamic degeneration accompanying marked neuronal loss and astrogliosis (Gambetti *et al.* 2003), the level of PrP^{res} in this region is similar to other brain areas or, in patients with longer disease duration, much lower than cerebral cortex (Parchi *et al.* 1995). The sporadic form of fatal insomnia (sFI), which shares similar clinical and pathological profiles with FFI, was also characterized by the accumulation of very low level of PrP^{res} in the brain (Parchi *et al.* 1999a). Therefore, it is thought that pathological changes of neuronal loss and gliosis in the thalamus of FFI brains may not be directly associated with the local burden of PrP^{res} (Collins *et al.* 2001; Parchi

et al. 2000a). In this context, it is of interest to investigate whether neuronal loss and astrogliosis observed in the thalamus of FFI can be associated with other forms of abnormal PrP species including:

1) PK-sensitive isoform of PrP^{Sc} (defined as PrP species which has buried 3F4 epitope but sensitive to proteolysis);
2) aggregated form(s) of PrP^{C} (defined as PrP species which has exposed 3F4 epitope but migrates to the heavier fractions of the 10 - 60% sucrose gradient);
3) topological variants of PrP^{C} such as cyPrP and ^{ctm}PrP (defined as PrP species whose 3F4 epitope is accessible but its ER-targeting signal peptide is not cleaved).

The identification of an abnormal PrP species which is more directly associated with the neuropathological changes seen in the thalamus of FFI may help answer why the selective vulnerability of a subpopulation of GABAergic neurons is significantly different between FFI and other types of human prion diseases (Guentchev *et al.* 1999).

5.3 Implications of this study

The accumulation of PrP^{Sc} is the only unambiguous marker of prion infection established to date and PrP^{Sc} is the only known component of the infectious prions. PrP^{Sc} has been operationally defined by its biochemical properties such as insolubility in non-denaturing detergents and/or resistance to proteolytic degradation (Meyer *et al.* 1986). The property of PK-resistance has been thoroughly exploited to the extent that the terms of protease-resistant prion protein (PrP^{res}) and disease-associated prion protein (PrP^{Sc}) are sometimes used interchangeably (Caughey *et al.* 2009). In the absence of a foreign nucleic acid genome associated with prion diseases, the strain phenomenon in prion diseases has been explained by the conformational difference of PrP^{Sc} according to the prion hypothesis (Prusiner 1998). Efforts to provide a molecular basis for the biological diversity of prions have focused on biochemical characterization of PrP^{Sc}. In human prion diseases including CJD, much evidence supporting conformation-based strain diversity has been gathered by Western blot analysis of PrP^{res}. Such assays produce information on core fragment size and glycosylation site occupancy of PrP^{res}. Variation in these parameters in combination with *PRNP* genotype has been invoked as the molecular basis to distinguish different disease phenotypes (Hill *et al.* 2003; Parchi *et al.* 1999b; Parchi *et al.* 1996). Considering recent findings on the complexity of PrP^{Sc} largely identified in laboratory prion strains, however, PrP^{res} analysis alone may not provide a complete description of PrP^{Sc} present in CJD brains. In that context, this study identifies previously unrecognised heterogeneity in PrP^{Sc} in CJD brains through the use of assays that differ in principle from conventional Western blot analysis of PrP^{res}. The novel biochemical approaches employed in this study have identified complexity of PrP^{Sc} in CJD brains, not only between different forms of human prion disease but also within individual cases of particular disease entities. Moreover, recent studies have reported that biochemical parameters such as PrP^{res} stability and the size of PrP^{res} aggregates can have significant effects on the biological properties of prions (Colby *et al.* 2009; Legname *et al.* 2006; Silveira *et al.* 2005). Therefore, the results from this study not only provide a more complete description of PrP^{Sc}

species occurring in CJD but also would contribute to a fuller understanding of the agents that cause the disease in humans. Understanding how the PrP^{Sc} complexity newly recognized in this study relates with the disease phenotypes and/or prion strains remains to be determined.

References

Aguzzi A., Baumann F. and Bremer J. (2008) The prion's elusive reason for being. *Annu. Rev. Neurosci.* **31,** 439-477.

Aguzzi A. and Calella A. M. (2009) Prions: protein aggregation and infectious diseases. *Physiol Rev.* **89,** 1105-1152.

Aguzzi A. and Haass C. (2003) Games played by rogue proteins in prion disorders and Alzheimer's disease. *Science* **302,** 814-818.

Aguzzi A., Heikenwalder M. and Polymenidou M. (2007) Insights into prion strains and neurotoxicity. *Nat. Rev. Mol. Cell Biol.* **8,** 552-561.

Aguzzi A. and Polymenidou M. (2004) Mammalian prion biology: one century of evolving concepts. *Cell* **116,** 313-327.

Almer G., Hainfellner J. A., Brucke T., Jellinger K., Kleinert R., Bayer G., Windl O., Kretzschmar H. A., Hill A., Sidle K., Collinge J. and Budka H. (1999) Fatal familial insomnia: a new Austrian family. *Brain* **122 (Pt 1),** 5-16.

Arsac J. N., Andreoletti O., Bilheude J. M., Lacroux C., Benestad S. L. and Baron T. (2007) Similar biochemical signatures and prion protein genotypes in atypical scrapie and Nor98 cases, France and Norway. *Emerg. Infect. Dis.* **13,** 58-65.

Atarashi R., Wilham J. M., Christensen L., Hughson A. G., Moore R. A., Johnson L. M., Onwubiko H. A., Priola S. A. and Caughey B. (2008) Simplified ultrasensitive prion detection by recombinant PrP conversion with shaking. *Nat. Methods* **5,** 211-212.

Barbanti P., Fabbrini G., Salvatore M., Petraroli R., Cardone F., Maras B., Equestre M., Macchi G., Lenzi G. L. and Pocchiari M. (1996) Polymorphism at codon 129 or codon 219 of PRNP and clinical heterogeneity in a previously unreported family with Gerstmann-Straussler-Scheinker disease (PrP-P102L mutation). *Neurology* **47,** 734-741.

Baron T., Biacabe A. G., Arsac J. N., Benestad S. and Groschup M. H. (2007) Atypical transmissible spongiform encephalopathies (TSEs) in ruminants. *Vaccine* **25,** 5625-5630.

Barria M. A., Mukherjee A., Gonzalez-Romero D., Morales R. and Soto C. (2009) De novo generation of infectious prions in vitro produces a new disease phenotype. *PLoS. Pathog.* **5,** e1000421.

Basler K., Oesch B., Scott M., Westaway D., Walchli M., Groth D. F., McKinley M. P., Prusiner S. B. and Weissmann C. (1986) Scrapie and cellular PrP isoforms are encoded by the same chromosomal gene. *Cell* **46,** 417-428.

Bellinger-Kawahara C. G., Kempner E., Groth D., Gabizon R. and Prusiner S. B. (1988) Scrapie prion liposomes and rods exhibit target sizes of 55,000 Da. *Virology* **164,** 537-541.

Bellon A., Seyfert-Brandt W., Lang W., Baron H., Groner A. and Vey M. (2003) Improved conformation-dependent immunoassay: suitability for human prion detection with enhanced sensitivity. *J. Gen. Virol.* **84,** 1921-1925.

Belt P. B., Muileman I. H., Schreuder B. E., Bos-de R. J., Gielkens A. L. and Smits M. A. (1995) Identification of five allelic variants of the sheep PrP gene and their association with natural scrapie. *J. Gen. Virol.* **76 (Pt 3),** 509-517.

Benestad S. L., Arsac J. N., Goldmann W. and Noremark M. (2008) Atypical/Nor98 scrapie: properties of the agent, genetics, and epidemiology. *Vet. Res.* **39,** 19.

Benestad S. L., Sarradin P., Thu B., Schonheit J., Tranulis M. A. and Bratberg B. (2003) Cases of scrapie with unusual features in Norway and designation of a new type, Nor98. *Vet. Rec.* **153,** 202-208.

Beringue V., Le D. A., Tixador P., Reine F., Lepourry L., Perret-Liaudet A., Haik S., Vilotte J. L., Fontes M. and Laude H. (2008) Prominent and persistent extraneural infection in human PrP transgenic mice infected with variant CJD. *PLoS. ONE.* **3,** e1419.

Bessen R. A., Kocisko D. A., Raymond G. J., Nandan S., Lansbury P. T. and Caughey B. (1995) Non-genetic propagation of strain-specific properties of scrapie prion protein. *Nature* **375,** 698-700.

Bessen R. A. and Marsh R. F. (1992a) Biochemical and physical properties of the prion protein from two strains of the transmissible mink encephalopathy agent. *J. Virol.* **66,** 2096-2101.

Bessen R. A. and Marsh R. F. (1992b) Identification of two biologically distinct strains of transmissible mink encephalopathy in hamsters. *J. Gen. Virol.* **73 (Pt 2),** 329-334.

Bessen R. A. and Marsh R. F. (1994) Distinct PrP properties suggest the molecular basis of strain variation in transmissible mink encephalopathy. *J. Virol.* **68,** 7859-7868.

Biacabe A. G., Laplanche J. L., Ryder S. and Baron T. (2004) Distinct molecular phenotypes in bovine prion diseases. *EMBO Rep.* **5,** 110-115.

Biasini E., Seegulam M. E., Patti B. N., Solforosi L., Medrano A. Z., Christensen H. M., Senatore A., Chiesa R., Williamson R. A. and Harris D. A. (2008) Non-infectious aggregates of the prion protein react with several PrP(Sc)-directed antibodies. *J. Neurochem.*

Bishop M. T., Hart P., Aitchison L., Baybutt H. N., Plinston C., Thomson V., Tuzi N. L., Head M. W., Ironside J. W., Will R. G. and Manson J. C. (2006) Predicting

susceptibility and incubation time of human-to-human transmission of vCJD. *Lancet Neurol.* **5,** 393-398.

Bishop M. T., Pennington C., Heath C. A., Will R. G. and Knight R. S. (2009) PRNP variation in UK sporadic and variant Creutzfeldt Jakob disease highlights genetic risk factors and a novel non-synonymous polymorphism. *BMC. Med. Genet.* **10,** 146.

Bishop M. T., Ritchie D. L., Will R. G., Ironside J. W., Head M. W., Thomson V., Bruce M. and Manson J. C. (2008) No major change in vCJD agent strain after secondary transmission via blood transfusion. *PLoS. ONE.* **3,** e2878.

Bocharova O. V., Breydo L., Salnikov V. V., Gill A. C. and Baskakov I. V. (2005) Synthetic prions generated in vitro are similar to a newly identified subpopulation of PrPSc from sporadic Creutzfeldt-Jakob Disease. *Protein Sci.* **14,** 1222-1232.

Bolton D. C., McKinley M. P. and Prusiner S. B. (1982) Identification of a protein that purifies with the scrapie prion. *Science* **218,** 1309-1311.

Bolton D. C., Seligman S. J., Bablanian G., Windsor D., Scala L. J., Kim K. S., Chen C. M., Kascsak R. J. and Bendheim P. E. (1991) Molecular location of a species-specific epitope on the hamster scrapie agent protein. *J. Virol.* **65,** 3667-3675.

Borchelt D. R., Scott M., Taraboulos A., Stahl N. and Prusiner S. B. (1990) Scrapie and cellular prion proteins differ in their kinetics of synthesis and topology in cultured cells. *J. Cell Biol.* **110,** 743-752.

Bossers A., Belt P. B. G. M., Raymond G. J., Caughey B., de Vries R. and Smits M. A. (1997) Scrapie susceptibility-linked polymorphisms modulate the in vitro conversion of sheep prion protein to protease-resistant forms. *Proc. Natl. Acad. Sci. U. S. A* **94,** 4931-4936.

Bouzamondo E., Milroy A. M., Ralston H. J., III, Prusiner S. B. and DeArmond S. J. (2000) Selective neuronal vulnerability during experimental scrapie infection: insights from an ultrastructural investigation. *Brain Res.* **874,** 210-215.

Brandel J. P., Heath C. A., Head M. W., Levavasseur E., Knight R., Laplanche J. L., Langeveld J. P., Ironside J. W., Hauw J. J., MacKenzie J., Alperovitch A., Will R. G. and Haik S. (2009) Variant Creutzfeldt-Jakob disease in France and the United Kingdom: Evidence for the same agent strain. *Ann. Neurol.* **65,** 249-256.

Brandner S., Isenmann S., Raeber A., Fischer M., Sailer A., Kobayashi Y., Marino S., Weissmann C. and Aguzzi A. (1996) Normal host prion protein necessary for scrapie-induced neurotoxicity. *Nature* **379,** 339-343.

Bremer J., Baumann F., Tiberi C., Wessig C., Fischer H., Schwarz P., Steele A. D., Toyka K. V., Nave K. A., Weis J. and Aguzzi A. (2010) Axonal prion protein is required for peripheral myelin maintenance. *Nat. Neurosci.*

Brown D. A. and Rose J. K. (1992) Sorting of GPI-anchored proteins to glycolipid-enriched membrane subdomains during transport to the apical cell surface. *Cell* **68,** 533-544.

Brown D. R. (2001) Copper and prion disease. *Brain Res. Bull.* **55,** 165-173.

Brown P., Brandel J. P., Preece M. and Sato T. (2006) Iatrogenic Creutzfeldt-Jakob disease: the waning of an era. *Neurology* **67,** 389-393.

Brown P., Cathala F., Raubertas R. F., Gajdusek D. C. and Castaigne P. (1987) The epidemiology of Creutzfeldt-Jakob disease: conclusion of a 15-year investigation in France and review of the world literature. *Neurology* **37,** 895-904.

Brown P., Gibbs C. J., Jr., Rodgers-Johnson P., Asher D. M., Sulima M. P., Bacote A., Goldfarb L. G. and Gajdusek D. C. (1994) Human spongiform encephalopathy: the National Institutes of Health series of 300 cases of experimentally transmitted disease. *Ann. Neurol.* **35,** 513-529.

Brown P., Kenney K., Little B., Ironside J., Will R., Cervenakova L., Bjork R. J., San Martin R. A., Safar J., Roos R. and . (1995) Intracerebral distribution of infectious amyloid protein in spongiform encephalopathy. *Ann. Neurol.* **38,** 245-253.

Brown P., Preece M., Brandel J. P., Sato T., McShane L., Zerr I., Fletcher A., Will R. G., Pocchiari M., Cashman N. R., d'Aignaux J. H., Cervenakova L., Fradkin J., Schonberger L. B. and Collins S. J. (2000) Iatrogenic Creutzfeldt-Jakob disease at the millennium. *Neurology* **55,** 1075-1081.

Bruce M., Chree A., McConnell I., Foster J., Pearson G. and Fraser H. (1994) Transmission of bovine spongiform encephalopathy and scrapie to mice: strain variation and the species barrier. *Philos. Trans. R. Soc. Lond B Biol. Sci.* **343,** 405-411.

Bruce M. E. (1993) Scrapie strain variation and mutation. *Br. Med. Bull.* **49,** 822-838.

Bruce M. E. (2003) TSE strain variation. *Br. Med. Bull.* **66,** 99-108.

Bruce M. E. and Fraser H. (1991) Scrapie strain variation and its implications. *Curr. Top. Microbiol. Immunol.* **172,** 125-138.

Bruce M. E., McConnell I., Fraser H. and Dickinson A. G. (1991) The disease characteristics of different strains of scrapie in Sinc congenic mouse lines: implications for the nature of the agent and host control of pathogenesis. *J. Gen. Virol.* **72 (Pt 3),** 595-603.

Bruce M. E., McConnell I., Will R. G. and Ironside J. W. (2001) Detection of variant Creutzfeldt-Jakob disease infectivity in extraneural tissues. *Lancet* **358,** 208-209.

Bruce M. E., Will R. G., Ironside J. W., McConnell I., Drummond D., Suttie A., McCardle L., Chree A., Hope J., Birkett C., Cousens S., Fraser H. and Bostock C. J.

(1997) Transmissions to mice indicate that 'new variant' CJD is caused by the BSE agent. *Nature* **389,** 498-501.

Budka H. (2003) Neuropathology of prion diseases. *Br. Med. Bull.* **66,** 121-130.

Budka H., Aguzzi A., Brown P., Brucher J. M., Bugiani O., Gullotta F., Haltia M., Hauw J. J., Ironside J. W., Jellinger K. and . (1995) Neuropathological diagnostic criteria for Creutzfeldt-Jakob disease (CJD) and other human spongiform encephalopathies (prion diseases). *Brain Pathol.* **5,** 459-466.

Budka H., Dormont D., Kretzschmar H., Pocchiari M. and van D. C. (2002) BSE and variant Creutzfeldt-Jakob disease: never say never. *Acta Neuropathol.* **103,** 627-628.

Bueler H., Aguzzi A., Sailer A., Greiner R. A., Autenried P., Aguet M. and Weissmann C. (1993) Mice devoid of PrP are resistant to scrapie. *Cell* **73,** 1339-1347.

Buschmann A., Biacabe A. G., Ziegler U., Bencsik A., Madec J. Y., Erhardt G., Luhken G., Baron T. and Groschup M. H. (2004) Atypical scrapie cases in Germany and France are identified by discrepant reaction patterns in BSE rapid tests. *J. Virol. Methods* **117,** 27-36.

Buschmann A., Gretzschel A., Biacabe A. G., Schiebel K., Corona C., Hoffmann C., Eiden M., Baron T., Casalone C. and Groschup M. H. (2006) Atypical BSE in Germany--proof of transmissibility and biochemical characterization. *Vet. Microbiol.* **117,** 103-116.

Buschmann A., Kuczius T., Bodemer W. and Groschup M. H. (1998) Cellular prion proteins of mammalian species display an intrinsic partial proteinase K resistance. *Biochem. Biophys. Res. Commun.* **253,** 693-702.

Cali I., Castellani R., Alshekhlee A., Cohen Y., Blevins J., Yuan J., Langeveld J. P., Parchi P., Safar J. G., Zou W. Q. and Gambetti P. (2009) Co-existence of scrapie prion protein types 1 and 2 in sporadic Creutzfeldt-Jakob disease: its effect on the phenotype and prion-type characteristics. *Brain* **132,** 2643-2658.

Cali I., Castellani R., Yuan J., Al Shekhlee A., Cohen M. L., Xiao X., Moleres F. J., Parchi P., Zou W. Q. and Gambetti P. (2006) Classification of sporadic Creutzfeldt-Jakob disease revisited. *Brain* **129,** 2266-2277.

Canello T., Engelstein R., Moshel O., Xanthopoulos K., Juanes M. E., Langeveld J., Sklaviadis T., Gasset M. and Gabizon R. (2008) Methionine sulfoxides on PrPSc: a prion-specific covalent signature. *Biochemistry* **47,** 8866-8873.

Capobianco R., Casalone C., Suardi S., Mangieri M., Miccolo C., Limido L., Catania M., Rossi G., Di F. G., Giaccone G., Bruzzone M. G., Minati L., Corona C., Acutis P., Gelmetti D., Lombardi G., Groschup M. H., Buschmann A., Zanusso G., Monaco S., Caramelli M. and Tagliavini F. (2007) Conversion of the BASE prion strain into the BSE strain: the origin of BSE? *PLoS. Pathog.* **3,** e31.

Casalone C., Zanusso G., Acutis P., Ferrari S., Capucci L., Tagliavini F., Monaco S. and Caramelli M. (2004) Identification of a second bovine amyloidotic spongiform encephalopathy: molecular similarities with sporadic Creutzfeldt-Jakob disease. *Proc. Natl. Acad. Sci. U. S. A* **101,** 3065-3070.

Castilla J., Gonzalez-Romero D., Saa P., Morales R., De Castro J. and Soto C. (2008a) Crossing the species barrier by PrP(Sc) replication in vitro generates unique infectious prions. *Cell* **134,** 757-768.

Castilla J., Morales R., Saa P., Barria M., Gambetti P. and Soto C. (2008b) Cell-free propagation of prion strains. *EMBO J.* **27,** 2557-2566.

Castilla J., Saa P., Hetz C. and Soto C. (2005a) In vitro generation of infectious scrapie prions. *Cell* **121,** 195-206.

Castilla J., Saa P., Morales R., Abid K., Maundrell K. and Soto C. (2006) Protein misfolding cyclic amplification for diagnosis and prion propagation studies. *Methods Enzymol.* **412,** 3-21.

Castilla J., Saa P. and Soto C. (2005b) Detection of prions in blood. *Nat. Med.* **11,** 982-985.

Caughey B. (2003) Prion protein conversions: insight into mechanisms, TSE transmission barriers and strains. *Br. Med. Bull.* **66,** 109-120.

Caughey B. (1993) Scrapie associated PrP accumulation and its prevention: insights from cell culture. *Br. Med. Bull.* **49,** 860-872.

Caughey B., Baron G. S., Chesebro B. and Jeffrey M. (2009) Getting a Grip on Prions: Oligomers, Amyloids, and Pathological Membrane Interactions. *Annu. Rev. Biochem.*

Caughey B., Kocisko D. A., Raymond G. J. and Lansbury P. T., Jr. (1995) Aggregates of scrapie-associated prion protein induce the cell-free conversion of protease-sensitive prion protein to the protease-resistant state. *Chem. Biol.* **2,** 807-817.

Caughey B. and Lansbury P. T. (2003) Protofibrils, pores, fibrils, and neurodegeneration: separating the responsible protein aggregates from the innocent bystanders. *Annu. Rev. Neurosci.* **26,** 267-298.

Caughey B., Race R. E. and Chesebro B. (1988) Detection of prion protein mRNA in normal and scrapie-infected tissues and cell lines. *J. Gen. Virol.* **69 (Pt 3),** 711-716.

Caughey B. and Raymond G. J. (1991) The scrapie-associated form of PrP is made from a cell surface precursor that is both protease- and phospholipase-sensitive. *J. Biol. Chem.* **266,** 18217-18223.

Caughey B., Raymond G. J. and Bessen R. A. (1998) Strain-dependent differences in beta-sheet conformations of abnormal prion protein. *J. Biol. Chem.* **273,** 32230-32235.

Caughey B. W., Dong A., Bhat K. S., Ernst D., Hayes S. F. and Caughey W. S. (1991) Secondary structure analysis of the scrapie-associated protein PrP 27-30 in water by infrared spectroscopy. *Biochemistry* **30,** 7672-7680.

Cervenakova L., Goldfarb L. G., Garruto R., Lee H. S., Gajdusek D. C. and Brown P. (1998) Phenotype-genotype studies in kuru: implications for new variant Creutzfeldt-Jakob disease. *Proc. Natl. Acad. Sci. U. S. A* **95,** 13239-13241.

Chakrabarti O. and Hegde R. S. (2009) Functional depletion of mahogunin by cytosolically exposed prion protein contributes to neurodegeneration. *Cell* **137,** 1136-1147.

Chandler R. L. (1961) Encephalopathy in mice produced by inoculation with scrapie brain material. *Lancet* **1,** 1378-1379.

Chaplin M. J., Barlow N., Ryder S., Simmons M. M., Spencer Y., Hughes R. and Stack M. J. (2002) Evaluation of the effects of controlled autolysis on the immunodetection of PrP(Sc) by immunoblotting and immunohistochemistry from natural cases of scrapie and BSE. *Res. Vet. Sci.* **72,** 37-43.

Chapman J., Ben-Israel J., Goldhammer Y. and Korczyn A. D. (1994) The risk of developing Creutzfeldt-Jakob disease in subjects with the PRNP gene codon 200 point mutation. *Neurology* **44,** 1683-1686.

Chen B., Morales R., Barria M. A. and Soto C. (2010) Estimating prion concentration in fluids and tissues by quantitative PMCA. *Nat. Methods* **7,** 519-520.

Chesebro B. (1998) BSE and prions: uncertainties about the agent. *Science* **279,** 42-43.

Chesebro B., Trifilo M., Race R., Meade-White K., Teng C., LaCasse R., Raymond L., Favara C., Baron G., Priola S., Caughey B., Masliah E. and Oldstone M. (2005) Anchorless prion protein results in infectious amyloid disease without clinical scrapie. *Science* **308,** 1435-1439.

Colby D. W., Giles K., Legname G., Wille H., Baskakov I. V., DeArmond S. J. and Prusiner S. B. (2009) Design and construction of diverse mammalian prion strains. *Proc. Natl. Acad. Sci. U. S. A* **106,** 20417-20422.

Colby D. W., Wain R., Baskakov I. V., Legname G., Palmer C. G., Nguyen H. O., Lemus A., Cohen F. E., DeArmond S. J. and Prusiner S. B. (2010) Protease-sensitive synthetic prions. *PLoS. Pathog.* **6,** e1000736.

Collinge J. (1997) Human prion diseases and bovine spongiform encephalopathy (BSE). *Hum. Mol. Genet.* **6,** 1699-1705.

Collinge J., Brown J., Hardy J., Mullan M., Rossor M. N., Baker H., Crow T. J., Lofthouse R., Poulter M., Ridley R. and . (1992) Inherited prion disease with 144 base pair gene insertion. 2. Clinical and pathological features. *Brain* **115 (Pt 3),** 687-710.

Collinge J., Palmer M. S. and Dryden A. J. (1991) Genetic predisposition to iatrogenic Creutzfeldt-Jakob disease. *Lancet* **337,** 1441-1442.

Collinge J., Sidle K. C., Meads J., Ironside J. and Hill A. F. (1996) Molecular analysis of prion strain variation and the aetiology of 'new variant' CJD. *Nature* **383,** 685-690.

Collinge J., Whitfield J., McKintosh E., Beck J., Mead S., Thomas D. J. and Alpers M. P. (2006) Kuru in the 21st century--an acquired human prion disease with very long incubation periods. *Lancet* **367,** 2068-2074.

Collinge J., Whitfield J., McKintosh E., Frosh A., Mead S., Hill A. F., Brandner S., Thomas D. and Alpers M. P. (2008) A clinical study of kuru patients with long incubation periods at the end of the epidemic in Papua New Guinea. *Philos. Trans. R. Soc. Lond B Biol. Sci.* **363,** 3725-3739.

Collinge J., Whittington M. A., Sidle K. C., Smith C. J., Palmer M. S., Clarke A. R. and Jefferys J. G. (1994) Prion protein is necessary for normal synaptic function. *Nature* **370,** 295-297.

Collins S., McLean C. A. and Masters C. L. (2001) Gerstmann-Straussler-Scheinker syndrome,fatal familial insomnia, and kuru: a review of these less common human transmissible spongiform encephalopathies. *J. Clin. Neurosci.* **8,** 387-397.

Collins S. J., Sanchez-Juan P., Masters C. L., Klug G. M., van D. C., Poleggi A., Pocchiari M., Almonti S., Cuadrado-Corrales N., de Pedro-Cuesta J., Budka H., Gelpi E., Glatzel M., Tolnay M., Hewer E., Zerr I., Heinemann U., Kretszchmar H. A., Jansen G. H., Olsen E., Mitrova E., Alperovitch A., Brandel J. P., MacKenzie J., Murray K. and Will R. G. (2006) Determinants of diagnostic investigation sensitivities across the clinical spectrum of sporadic Creutzfeldt-Jakob disease. *Brain* **129,** 2278-2287.

Colombo G., Meli M., Morra G., Gabizon R. and Gasset M. (2009) Methionine sulfoxides on prion protein Helix-3 switch on the alpha-fold destabilization required for conversion. *PLoS. ONE.* **4,** e4296.

Cook W. (2007) Nor98-like strain of scrapie found in Wyoming. Press release, Wyoming Livestock Board, 16 March, Available from:http://wlsb.state.wy.us/.

Cronier S., Gros N., Tattum M. H., Jackson G. S., Clarke A. R., Collinge J. and Wadsworth J. D. (2008) Detection and characterization of proteinase K-sensitive disease-related prion protein with thermolysin. *Biochem. J.* **416,** 297-305.

D'Alessandro M., Petraroli R., Ladogana A. and Pocchiari M. (1998) High incidence of Creutzfeldt-Jakob disease in rural Calabria, Italy. *Lancet* **352,** 1989-1990.

Dagdanova A., Ilchenko S., Notari S., Yang Q., Obrenovich M. E., Hatcher K., McAnulty P., Huang L., Zou W., Kong Q., Gambetti P. and Chen S. G. (2010) Characterization of the prion protein in human urine. *J. Biol. Chem.*

Deleault A. M., Deleault N. R., Harris B. T., Rees J. R. and Supattapone S. (2008) The effects of prion protein proteolysis and disaggregation on the strain properties of hamster scrapie. *J. Gen. Virol.* **89,** 2642-2650.

Deleault N. R., Harris B. T., Rees J. R. and Supattapone S. (2007) Formation of native prions from minimal components in vitro. *Proc. Natl. Acad. Sci. U. S. A* **104,** 9741-9746.

DeMarco M. L. and Daggett V. (2004) From conversion to aggregation: protofibril formation of the prion protein. *Proc. Natl. Acad. Sci. U. S. A* **101,** 2293-2298.

Dickinson A. G. (1976) Scrapie in sheep and goats. *Front Biol.* **44,** 209-241.

Doh-ura K., Tateishi J., Sasaki H., Kitamoto T. and Sakaki Y. (1989) Pro----leu change at position 102 of prion protein is the most common but not the sole mutation related to Gerstmann-Straussler syndrome. *Biochem. Biophys. Res. Commun.* **163,** 974-979.

Donne D. G., Viles J. H., Groth D., Mehlhorn I., James T. L., Cohen F. E., Prusiner S. B., Wright P. E. and Dyson H. J. (1997) Structure of the recombinant full-length hamster prion protein PrP(29-231): the N terminus is highly flexible. *Proc. Natl. Acad. Sci. U. S. A* **94,** 13452-13457.

Duffy P., Wolf J., Collins G., DeVoe A. G., Streeten B. and Cowen D. (1974) Letter: Possible person-to-person transmission of Creutzfeldt-Jakob disease. *N. Engl. J. Med.* **290,** 692-693.

Epstein V., Pointing S. and Halfacre S. (2005) Atypical scrapie in the Falkland Islands. *Vet. Rec.* **157,** 667-668.

Everest S. J., Thorne L., Barnicle D. A., Edwards J. C., Elliott H., Jackman R. and Hope J. (2006) Atypical prion protein in sheep brain collected during the British scrapie-surveillance programme. *J. Gen. Virol.* **87,** 471-477.

Ford M. J., Burton L. J., Morris R. J. and Hall S. M. (2002) Selective expression of prion protein in peripheral tissues of the adult mouse. *Neuroscience* **113,** 177-192.

Fraser H. and Dickinson A. G. (1968) The sequential development of the brain lesion of scrapie in three strains of mice. *J. Comp Pathol.* **78,** 301-311.

Gajdusek D. C. (1977) Unconventional viruses and the origin and disappearance of kuru. *Science* **197,** 943-960.

Gajdusek D. C., Gibbs C. J. and Alpers M. (1966) Experimental transmission of a Kuru-like syndrome to chimpanzees. *Nature* **209,** 794-796.

Gajdusek D. C., Gibbs C. J., Jr. and Alpers M. (1967) Transmission and passage of experimenal "kuru" to chimpanzees. *Science* **155,** 212-214.

Gajdusek D. C., Gibbs C. J., Jr., Asher D. M. and David E. (1968) Transmission of experimental kuru to the spider monkey (Ateles geoffreyi). *Science* **162,** 693-694.

Gajdusek D. C. and ZIGAS V. (1957) Degenerative disease of the central nervous system in New Guinea; the endemic occurrence of kuru in the native population. *N. Engl. J. Med.* **257,** 974-978.

Gajdusek D. C. and ZIGAS V. (1959) Kuru; clinical, pathological and epidemiological study of an acute progressive degenerative disease of the central nervous system among natives of the Eastern Highlands of New Guinea. *Am. J. Med.* **26,** 442-469.

Gambetti P., Dong Z., Yuan J., Xiao X., Zheng M., Alshekhlee A., Castellani R., Cohen M., Barria M. A., Gonzalez-Romero D., Belay E. D., Schonberger L. B., Marder K., Harris C., Burke J. R., Montine T., Wisniewski T., Dickson D. W., Soto C., Hulette C. M., Mastrianni J. A., Kong Q. and Zou W. Q. (2008) A novel human disease with abnormal prion protein sensitive to protease. *Ann. Neurol.* **63,** 697-708.

Gambetti P., Kong Q., Zou W., Parchi P. and Chen S. G. (2003) Sporadic and familial CJD: classification and characterisation. *Br. Med. Bull.* **66,** 213-239.

Gibbs C. J., Jr., Gajdusek D. C., Asher D. M., Alpers M. P., Beck E., Daniel P. M. and Matthews W. B. (1968) Creutzfeldt-Jakob disease (spongiform encephalopathy): transmission to the chimpanzee. *Science* **161,** 388-389.

Glatzel M., Ott P. M., Linder T., Gebbers J. O., Gmur A., Wust W., Huber G., Moch H., Podvinec M., Stamm B. and Aguzzi A. (2003) Human prion diseases: epidemiology and integrated risk assessment. *Lancet Neurol.* **2,** 757-763.

Glatzel M., Rogivue C., Ghani A., Streffer J. R., Amsler L. and Aguzzi A. (2002) Incidence of Creutzfeldt-Jakob disease in Switzerland. *Lancet* **360,** 139-141.

Goldfarb L. G. (2002) Kuru: the old epidemic in a new mirror. *Microbes. Infect.* **4,** 875-882.

Goldfarb L. G., Brown P., Mitrova E., Cervenakova L., Goldin L., Korczyn A. D., Chapman J., Galvez S., Cartier L., Rubenstein R. and . (1991) Creutzfeldt-Jacob disease associated with the PRNP codon 200Lys mutation: an analysis of 45 families. *Eur. J. Epidemiol.* **7,** 477-486.

Goldfarb L. G., Brown P., Vrbovska A., Baron H., McCombie W. R., Cathala F., Gibbs C. J., Jr. and Gajdusek D. C. (1992a) An insert mutation in the chromosome 20 amyloid precursor gene in a Gerstmann-Straussler-Scheinker family. *J. Neurol. Sci.* **111,** 189-194.

Goldfarb L. G., Cervenakova L. and Gajdusek D. C. (2004) Genetic studies in relation to kuru: an overview. *Curr. Mol. Med.* **4,** 375-384.

Goldfarb L. G., Petersen R. B., Tabaton M., Brown P., LeBlanc A. C., Montagna P., Cortelli P., Julien J., Vital C., Pendelbury W. W. and . (1992b) Fatal familial insomnia and familial Creutzfeldt-Jakob disease: disease phenotype determined by a DNA polymorphism. *Science* **258,** 806-808.

Gomori A. J., Partnow M. J., Horoupian D. S. and Hirano A. (1973) The ataxic form of Creutzfeldt-Jakob disease. *Arch. Neurol.* **29,** 318-323.

Gonzalez-Romero D., Barria M. A., Leon P., Morales R. and Soto C. (2008) Detection of infectious prions in urine. *FEBS Lett.* **582,** 3161-3166.

Govaerts C., Wille H., Prusiner S. B. and Cohen F. E. (2004) Evidence for assembly of prions with left-handed beta-helices into trimers. *Proc. Natl. Acad. Sci. U. S. A* **101,** 8342-8347.

Grassi J., Creminon C., Frobert Y., Fretier P., Turbica I., Rezaei H., Hunsmann G., Comoy E. and Deslys J. P. (2000) Specific determination of the proteinase K-resistant form of the prion protein using two-site immunometric assays. Application to the post-mortem diagnosis of BSE. *Arch. Virol. Suppl* 197-205.

Green R., Horrocks C., Wilkinson A., Hawkins S. A. and Ryder S. J. (2005) Primary isolation of the bovine spongiform encephalopathy agent in mice: agent definition based on a review of 150 transmissions. *J. Comp Pathol.* **132,** 117-131.

Guentchev M., Groschup M. H., Kordek R., Liberski P. P. and Budka H. (1998) Severe, early and selective loss of a subpopulation of GABAergic inhibitory neurons in experimental transmissible spongiform encephalopathies. *Brain Pathol.* **8,** 615-623.

Guentchev M., Hainfellner J. A., Trabattoni G. R. and Budka H. (1997) Distribution of parvalbumin-immunoreactive neurons in brain correlates with hippocampal and temporal cortical pathology in Creutzfeldt-Jakob disease. *J. Neuropathol. Exp. Neurol.* **56,** 1119-1124.

Guentchev M., Wanschitz J., Voigtlander T., Flicker H. and Budka H. (1999) Selective neuronal vulnerability in human prion diseases. Fatal familial insomnia differs from other types of prion diseases. *Am. J. Pathol.* **155,** 1453-1457.

Haik S., Peoc'h K., Brandel J. P., Privat N., Laplanche J. L., Faucheux B. A. and Hauw J. J. (2004) Striking PrPsc heterogeneity in inherited prion diseases with the D178N mutation. *Ann. Neurol.* **56,** 909-910.

Hainfellner J. A., Brantner-Inthaler S., Cervenakova L., Brown P., Kitamoto T., Tateishi J., Diringer H., Liberski P. P., Regele H., Feucht M. and . (1995) The original Gerstmann-Straussler-Scheinker family of Austria: divergent clinicopathological phenotypes but constant PrP genotype. *Brain Pathol.* **5,** 201-211.

Haraguchi T., Fisher S., Olofsson S., Endo T., Groth D., Tarentino A., Borchelt D. R., Teplow D., Hood L., Burlingame A. and . (1989) Asparagine-linked glycosylation of the scrapie and cellular prion proteins. *Arch. Biochem. Biophys.* **274,** 1-13.

Hayashi H., Takata M., Iwamaru Y., Ushiki Y., Kimura K. M., Tagawa Y., Shinagawa M. and Yokoyama T. (2004) Effect of tissue deterioration on postmortem BSE diagnosis by immunobiochemical detection of an abnormal isoform of prion protein. *J. Vet. Med. Sci.* **66,** 515-520.

Head M. W., Bunn T. J., Bishop M. T., McLoughlin V., Lowrie S., McKimmie C. S., Williams M. C., McCardle L., MacKenzie J., Knight R., Will R. G. and Ironside J. W. (2004a) Prion protein heterogeneity in sporadic but not variant Creutzfeldt-Jakob disease: UK cases 1991-2002. *Ann. Neurol.* **55,** 851-859.

Head M. W. and Ironside J. W. (2009) Sporadic Creutzfeldt-Jakob disease: discrete subtypes or a spectrum of disease? *Brain* **132,** 2627-2629.

Head M. W., Knight R., Zeidler M., Yull H., Barlow A. and Ironside J. W. (2009a) A case of protease sensitive prionopathy in a patient in the UK. *Neuropathol. Appl. Neurobiol.* **35,** 628-632.

Head M. W., Ritchie D., Smith N., McLoughlin V., Nailon W., Samad S., Masson S., Bishop M., McCardle L. and Ironside J. W. (2004b) Peripheral tissue involvement in sporadic, iatrogenic, and variant Creutzfeldt-Jakob disease: an immunohistochemical, quantitative, and biochemical study. *Am. J. Pathol.* **164,** 143-153.

Head M. W., Tissingh G., Uitdehaag B. M., Barkhof F., Bunn T. J., Ironside J. W., Kamphorst W. and Scheltens P. (2001) Sporadic Creutzfeldt-Jakob disease in a young Dutch valine homozygote: atypical molecular phenotype. *Ann. Neurol.* **50,** 258-261.

Head M. W., Yull H. M., Ritchie D. L., Bishop M. T. and Ironside J. W. (2009b) Pathological investigation of the first blood donor and recipient pair linked by transfusion-associated variant Creutzfeldt-Jakob disease transmission. *Neuropathol. Appl. Neurobiol.* **35,** 433-436.

Health Protection Agency. (2007) Fourth case of transfusion-associated variant CJD infection. Health Protection Report. Available at: http//www.hpa.org.uk/hpr/archives/2007/news2007/news0307.htm.

Hegde R. S., Mastrianni J. A., Scott M. R., DeFea K. A., Tremblay P., Torchia M., DeArmond S. J., Prusiner S. B. and Lingappa V. R. (1998) A transmembrane form of the prion protein in neurodegenerative disease. *Science* **279,** 827-834.

Hegde R. S. and Rane N. S. (2003) Prion protein trafficking and the development of neurodegeneration. *Trends Neurosci.* **26,** 337-339.

Hetz C., Russelakis-Carneiro M., Walchli S., Carboni S., Vial-Knecht E., Maundrell K., Castilla J. and Soto C. (2005) The disulfide isomerase Grp58 is a protective factor against prion neurotoxicity. *J. Neurosci.* **25,** 2793-2802.

Hetz C. A. and Soto C. (2006) Stressing out the ER: a role of the unfolded protein response in prion-related disorders. *Curr. Mol. Med.* **6,** 37-43.

Hill A. F., Desbruslais M., Joiner S., Sidle K. C., Gowland I., Collinge J., Doey L. J. and Lantos P. (1997) The same prion strain causes vCJD and BSE. *Nature* **389,** 448-50, 526.

Hill A. F., Joiner S., Beck J. A., Campbell T. A., Dickinson A., Poulter M., Wadsworth J. D. and Collinge J. (2006) Distinct glycoform ratios of protease resistant prion protein associated with PRNP point mutations. *Brain* **129,** 676-685.

Hill A. F., Joiner S., Wadsworth J. D., Sidle K. C., Bell J. E., Budka H., Ironside J. W. and Collinge J. (2003) Molecular classification of sporadic Creutzfeldt-Jakob disease. *Brain* **126,** 1333-1346.

Hilton D. A. (2006) Pathogenesis and prevalence of variant Creutzfeldt-Jakob disease. *J. Pathol.* **208,** 134-141.

Hilton D. A., Fathers E., Edwards P., Ironside J. W. and Zajicek J. (1998) Prion immunoreactivity in appendix before clinical onset of variant Creutzfeldt-Jakob disease. *Lancet* **352,** 703-704.

Hilton D. A., Ghani A. C., Conyers L., Edwards P., McCardle L., Ritchie D., Penney M., Hegazy D. and Ironside J. W. (2004) Prevalence of lymphoreticular prion protein accumulation in UK tissue samples. *J. Pathol.* **203,** 733-739.

Hope J., Wood S. C., Birkett C. R., Chong A., Bruce M. E., Cairns D., Goldmann W., Hunter N. and Bostock C. J. (1999) Molecular analysis of ovine prion protein identifies similarities between BSE and an experimental isolate of natural scrapie, CH1641. *J. Gen. Virol.* **80 (Pt 1),** 1-4.

Horiuchi M., Priola S. A., Chabry J. and Caughey B. (2000) Interactions between heterologous forms of prion protein: binding, inhibition of conversion, and species barriers. *Proc. Natl. Acad. Sci. U. S. A* **97,** 5836-5841.

Houston E. F., Halliday S. I., Jeffrey M., Goldmann W. and Hunter N. (2002) New Zealand sheep with scrapie-susceptible PrP genotypes succumb to experimental challenge with a sheep-passaged scrapie isolate (SSBP/1). *J. Gen. Virol.* **83,** 1247-1250.

Houston F., Foster J. D., Chong A., Hunter N. and Bostock C. J. (2000) Transmission of BSE by blood transfusion in sheep. *Lancet* **356,** 999-1000.

Houston F., McCutcheon S., Goldmann W., Chong A., Foster J., Siso S., Gonzalez L., Jeffrey M. and Hunter N. (2008) Prion diseases are efficiently transmitted by blood transfusion in sheep. *Blood* **112,** 4739-4745.

Hsiao K., Baker H. F., Crow T. J., Poulter M., Owen F., Terwilliger J. D., Westaway D., Ott J. and Prusiner S. B. (1989) Linkage of a prion protein missense variant to Gerstmann-Straussler syndrome. *Nature* **338,** 342-345.

Huang Z., Prusiner S. B. and Cohen F. E. (1995) Scrapie prions: a three-dimensional model of an infectious fragment. *Fold. Des* **1,** 13-19.

Hunter N. (2003) Scrapie and experimental BSE in sheep. *Br. Med. Bull.* **66,** 171-183.

Hunter N. (2007) Scrapie: uncertainties, biology and molecular approaches. *Biochim. Biophys. Acta* **1772,** 619-628.

Hunter N., Foster J., Chong A., McCutcheon S., Parnham D., Eaton S., MacKenzie C. and Houston F. (2002) Transmission of prion diseases by blood transfusion. *J. Gen. Virol.* **83,** 2897-2905.

Hunter N., Foster J. D., Goldmann W., Stear M. J., Hope J. and Bostock C. (1996) Natural scrapie in a closed flock of Cheviot sheep occurs only in specific PrP genotypes. *Arch. Virol.* **141,** 809-824.

Huzarewich R. L., Siemens C. G. and Booth S. A. (2010) Application of "omics" to prion biomarker discovery. *J. Biomed. Biotechnol.* **2010,** 613504.

Ironside J. W. (1998) Neuropathological findings in new variant CJD and experimental transmission of BSE. *FEMS Immunol. Med. Microbiol.* **21,** 91-95.

Ironside J. W., Bishop M. T., Connolly K., Hegazy D., Lowrie S., Le G. M., Ritchie D. L., McCardle L. M. and Hilton D. A. (2006) Variant Creutzfeldt-Jakob disease: prion protein genotype analysis of positive appendix tissue samples from a retrospective prevalence study. *BMJ* **332,** 1186-1188.

Ironside J. W., Ghetti B., Head M. W., Piccardo P. and Will R. G. (2008) Prion diseases, in *Greenfield's Neuropathology,* (Love S., Louis D.N. and Ellison D.W., eds), pp. 1197-1274.

Ironside J. W. and Head M. W. (2004) Neuropathology and molecular biology of variant Creutzfeldt-Jakob disease. *Curr. Top. Microbiol. Immunol.* **284,** 133-159.

Ironside J. W., Head M. W., Bell J. E., McCardle L. and Will R. G. (2000) Laboratory diagnosis of variant Creutzfeldt-Jakob disease. *Histopathology* **37,** 1-9.

Ironside J. W., Head M. W., McCardle L. and Knight R. (2002) Neuropathology of variant Creutzfeldt-Jakob disease. *Acta Neurobiol. Exp. (Wars.)* **62,** 175-182.

Ironside J. W., Ritchie D. L. and Head M. W. (2005) Phenotypic variability in human prion diseases. *Neuropathol. Appl. Neurobiol.* **31,** 565-579.

Jones M., Peden A. H., Head M. W. and Ironside J. W. (2010) The application of in vitro cell-free conversion systems to human prion diseases. *Acta Neuropathol.*

Jones M., Peden A. H., Prowse C. V., Groner A., Manson J. C., Turner M. L., Ironside J. W., Macgregor I. R. and Head M. W. (2007) In vitro amplification and detection of variant Creutzfeldt-Jakob disease PrPSc. *J. Pathol.* **213,** 21-26.

Jones M., Peden A. H., Wight D., Prowse C., Macgregor I., Manson J., Turner M., Ironside J. W. and Head M. W. (2008) Effects of human PrPSc type and PRNP genotype in an in-vitro conversion assay. *Neuroreport* **19,** 1783-1786.

Jones M., Peden A. H., Yull H., Wight D., Bishop M. T., Prowse C. V., Turner M. L., Ironside J. W., Macgregor I. R. and Head M. W. (2009a) Human platelets as a substrate source for the in vitro amplification of the abnormal prion protein (PrP) associated with variant Creutzfeldt-Jakob disease. *Transfusion* **49,** 376-384.

Jones M., Wight D., Barron R., Jeffrey M., Manson J., Prowse C., Ironside J. W. and Head M. W. (2009b) Molecular model of prion transmission to humans. *Emerg. Infect. Dis.* **15,** 2013-2016.

Jones M., Wight D., McLoughlin V., Norrby K., Ironside J. W., Connolly J. G., Farquhar C. F., Macgregor I. R. and Head M. W. (2009c) An antibody to the aggregated synthetic prion protein peptide (PrP106-126) selectively recognizes disease-associated prion protein (PrP) from human brain specimens. *Brain Pathol.* **19,** 293-302.

Kang S. W., Rane N. S., Kim S. J., Garrison J. L., Taunton J. and Hegde R. S. (2006) Substrate-specific translocational attenuation during ER stress defines a pre-emptive quality control pathway. *Cell* **127,** 999-1013.

Kanyo Z. F., Pan K. M., Williamson R. A., Burton D. R., Prusiner S. B., Fletterick R. J. and Cohen F. E. (1999) Antibody binding defines a structure for an epitope that participates in the PrPC-->PrPSc conformational change. *J. Mol. Biol.* **293,** 855-863.

Kascsak R. J., Rubenstein R., Merz P. A., Tonna-DeMasi M., Fersko R., Carp R. I., Wisniewski H. M. and Diringer H. (1987) Mouse polyclonal and monoclonal antibody to scrapie-associated fibril proteins. *J. Virol.* **61,** 3688-3693.

Kascsak R. J., Tonna-DeMasi M., Fersko R., Rubenstein R., Carp R. I. and Powers J. M. (1993) The role of antibodies to PrP in the diagnosis of transmissible spongiform encephalopathies. *Dev. Biol. Stand.* **80,** 141-151.

Kaski D., Mead S., Hyare H., Cooper S., Jampana R., Overell J., Knight R., Collinge J. and Rudge P. (2009) Variant CJD in an individual heterozygous for PRNP codon 129. *Lancet* **374,** 2128.

Kaylor J., Bodner N., Edridge S., Yamin G., Hong D. P. and Fink A. L. (2005) Characterization of oligomeric intermediates in alpha-synuclein fibrillation: FRET studies of Y125W/Y133F/Y136F alpha-synuclein. *J. Mol. Biol.* **353,** 357-372.

Kazlauskaite J., Sanghera N., Sylvester I., Venien-Bryan C. and Pinheiro T. J. (2003) Structural changes of the prion protein in lipid membranes leading to aggregation and fibrillization. *Biochemistry* **42,** 3295-3304.

Kim J. I., Cali I., Surewicz K., Kong Q., Raymond G. J., Atarashi R., Race B., Qing L., Gambetti P., Caughey B. and Surewicz W. K. (2010) Mammalian prions generated from bacterially expressed prion protein in the absence of any mammalian cofactors. *J. Biol. Chem.*

Kim S. J., Rahbar R. and Hegde R. S. (2001) Combinatorial control of prion protein biogenesis by the signal sequence and transmembrane domain. *J. Biol. Chem.* **276,** 26132-26140.

Kimberlin R. H. and Walker C. (1977) Characteristics of a short incubation model of scrapie in the golden hamster. *J. Gen. Virol.* **34,** 295-304.

Klein T. R., Kirsch D., Kaufmann R. and Riesner D. (1998) Prion rods contain small amounts of two host sphingolipids as revealed by thin-layer chromatography and mass spectrometry. *Biol. Chem.* **379,** 655-666.

Klingeborn M., Wik L., Simonsson M., Renstrom L. H., Ottinger T. and Linne T. (2006) Characterization of proteinase K-resistant N- and C-terminally truncated PrP in Nor98 atypical scrapie. *J. Gen. Virol.* **87,** 1751-1760.

Kocisko D. A., Come J. H., Priola S. A., Chesebro B., Raymond G. J., Lansbury P. T. and Caughey B. (1994) Cell-free formation of protease-resistant prion protein. *Nature* **370,** 471-474.

Kong Q., Zheng M., Casalone C., Qing L., Huang S., Chakraborty B., Wang P., Chen F., Cali I., Corona C., Martucci F., Iulini B., Acutis P., Wang L., Liang J., Wang M., Li X., Monaco S., Zanusso G., Zou W. Q., Caramelli M. and Gambetti P. (2008) Evaluation of the human transmission risk of an atypical bovine spongiform encephalopathy prion strain. *J. Virol.* **82,** 3697-3701.

Korth C., Kaneko K., Groth D., Heye N., Telling G., Mastrianni J., Parchi P., Gambetti P., Will R., Ironside J., Heinrich C., Tremblay P., DeArmond S. J. and Prusiner S. B. (2003) Abbreviated incubation times for human prions in mice expressing a chimeric mouse-human prion protein transgene. *Proc. Natl. Acad. Sci. U. S. A* **100,** 4784-4789.

Korth C., Stierli B., Streit P., Moser M., Schaller O., Fischer R., Schulz-Schaeffer W., Kretzschmar H., Raeber A., Braun U., Ehrensperger F., Hornemann S., Glockshuber R., Riek R., Billeter M., Wuthrich K. and Oesch B. (1997) Prion (PrPSc)-specific epitope defined by a monoclonal antibody. *Nature* **390,** 74-77.

Kovacs G. G. and Budka H. (2009) Molecular pathology of human prion diseases. *Int. J. Mol. Sci.* **10,** 976-999.

Kovacs G. G., Head M. W., Hegyi I., Bunn T. J., Flicker H., Hainfellner J. A., McCardle L., Laszlo L., Jarius C., Ironside J. W. and Budka H. (2002a) Immunohistochemistry for the prion protein: comparison of different monoclonal antibodies in human prion disease subtypes. *Brain Pathol.* **12,** 1-11.

Kovacs G. G., Puopolo M., Ladogana A., Pocchiari M., Budka H., van D. C., Collins S. J., Boyd A., Giulivi A., Coulthart M., asnerie-Laupretre N., Brandel J. P., Zerr I., Kretzschmar H. A., de Pedro-Cuesta J., Calero-Lara M., Glatzel M., Aguzzi A., Bishop M., Knight R., Belay G., Will R. and Mitrova E. (2005) Genetic prion disease: the EUROCJD experience. *Hum. Genet.* **118,** 166-174.

Kovacs G. G., Zerbi P., Voigtlander T., Strohschneider M., Trabattoni G., Hainfellner J. A. and Budka H. (2002b) The prion protein in human neurodegenerative disorders. *Neurosci. Lett.* **329,** 269-272.

Krebs B., Bader B., Klehmet J., Grasbon-Frodl E., Oertel W. H., Zerr I., Stricker S., Zschenderlein R. and Kretzschmar H. A. (2007) A novel subtype of Creutzfeldt-Jakob disease characterized by a small 6 kDa PrP fragment. *Acta Neuropathol.* **114,** 195-199.

Kretzschmar H. A., Honold G., Seitelberger F., Feucht M., Wessely P., Mehraein P. and Budka H. (1991) Prion protein mutation in family first reported by Gerstmann, Straussler, and Scheinker. *Lancet* **337,** 1160.

Kretzschmar H. A., Prusiner S. B., Stowring L. E. and DeArmond S. J. (1986) Scrapie prion proteins are synthesized in neurons. *Am. J. Pathol.* **122,** 1-5.

Kristiansen M., Deriziotis P., Dimcheff D. E., Jackson G. S., Ovaa H., Naumann H., Clarke A. R., van Leeuwen F. W., Menendez-Benito V., Dantuma N. P., Portis J. L., Collinge J. and Tabrizi S. J. (2007) Disease-associated prion protein oligomers inhibit the 26S proteasome. *Mol. Cell* **26,** 175-188.

Ladogana A., Puopolo M., Croes E. A., Budka H., Jarius C., Collins S., Klug G. M., Sutcliffe T., Giulivi A., Alperovitch A., Delasnerie-Laupretre N., Brandel J. P., Poser S., Kretzschmar H., Rietveld I., Mitrova E., Cuesta J. P., Martinez-Martin P., Glatzel M., Aguzzi A., Knight R., Ward H., Pocchiari M., van Duijn C. M., Will R. G. and Zerr I. (2005) Mortality from Creutzfeldt-Jakob disease and related disorders in Europe, Australia, and Canada. *Neurology* **64,** 1586-1591.

Langedijk J. P., Fuentes G., Boshuizen R. and Bonvin A. M. (2006) Two-rung model of a left-handed beta-helix for prions explains species barrier and strain variation in transmissible spongiform encephalopathies. *J. Mol. Biol.* **360,** 907-920.

Lasmezas C. I., Deslys J. P., Demaimay R., Adjou K. T., Lamoury F., Dormont D., Robain O., Ironside J. and Hauw J. J. (1996) BSE transmission to macaques. *Nature* **381,** 743-744.

Lau A. L., Yam A. Y., Michelitsch M. M., Wang X., Gao C., Goodson R. J., Shimizu R., Timoteo G., Hall J., Medina-Selby A., Coit D., McCoin C., Phelps B., Wu P., Hu C., Chien D. and Peretz D. (2007) Characterization of prion protein (PrP)-derived peptides that discriminate full-length PrPSc from PrPC. *Proc. Natl. Acad. Sci. U. S. A* **104,** 11551-11556.

Le D. A., Beringue V., Andreoletti O., Reine F., Lai T. L., Baron T., Bratberg B., Vilotte J. L., Sarradin P., Benestad S. L. and Laude H. (2005) A newly identified type of scrapie agent can naturally infect sheep with resistant PrP genotypes. *Proc. Natl. Acad. Sci. U. S. A* **102,** 16031-16036.

Lee H. S., Brown P., Cervenakova L., Garruto R. M., Alpers M. P., Gajdusek D. C. and Goldfarb L. G. (2001) Increased susceptibility to Kuru of carriers of the PRNP 129 methionine/methionine genotype. *J. Infect. Dis.* **183,** 192-196.

Lee H. S., Sambuughin N., Cervenakova L., Chapman J., Pocchiari M., Litvak S., Qi H. Y., Budka H., del S. T., Furukawa H., Brown P., Gajdusek D. C., Long J. C., Korczyn A. D. and Goldfarb L. G. (1999) Ancestral origins and worldwide distribution of the PRNP 200K mutation causing familial Creutzfeldt-Jakob disease. *Am. J. Hum. Genet.* **64,** 1063-1070.

Lee I. Y., Westaway D., Smit A. F., Wang K., Seto J., Chen L., Acharya C., Ankener M., Baskin D., Cooper C., Yao H., Prusiner S. B. and Hood L. E. (1998) Complete genomic sequence and analysis of the prion protein gene region from three mammalian species. *Genome Res.* **8,** 1022-1037.

Legname G., Baskakov I. V., Nguyen H. O., Riesner D., Cohen F. E., DeArmond S. J. and Prusiner S. B. (2004) Synthetic mammalian prions. *Science* **305,** 673-676.

Legname G., Nguyen H. O., Baskakov I. V., Cohen F. E., DeArmond S. J. and Prusiner S. B. (2005) Strain-specified characteristics of mouse synthetic prions. *Proc. Natl. Acad. Sci. U. S. A* **102,** 2168-2173.

Legname G., Nguyen H. O., Peretz D., Cohen F. E., DeArmond S. J. and Prusiner S. B. (2006) Continuum of prion protein structures enciphers a multitude of prion isolate-specified phenotypes. *Proc. Natl. Acad. Sci. U. S. A* **103,** 19105-19110.

Lehmann S. and Harris D. A. (1997) Blockade of glycosylation promotes acquisition of scrapie-like properties by the prion protein in cultured cells. *J. Biol. Chem.* **272,** 21479-21487.

Lewis V., Hill A. F., Klug G. M., Boyd A., Masters C. L. and Collins S. J. (2005) Australian sporadic CJD analysis supports endogenous determinants of molecular-clinical profiles. *Neurology* **65,** 113-118.

Liao Y. C., Lebo R. V., Clawson G. A. and Smuckler E. A. (1986) Human prion protein cDNA: molecular cloning, chromosomal mapping, and biological implications. *Science* **233,** 364-367.

Llewelyn C. A., Hewitt P. E., Knight R. S., Amar K., Cousens S., MacKenzie J. and Will R. G. (2004) Possible transmission of variant Creutzfeldt-Jakob disease by blood transfusion. *Lancet* **363,** 417-421.

Locht C., Chesebro B., Race R. and Keith J. M. (1986) Molecular cloning and complete sequence of prion protein cDNA from mouse brain infected with the scrapie agent. *Proc. Natl. Acad. Sci. U. S. A* **83,** 6372-6376.

Lugaresi E., Montagna P., Baruzzi A., Cortelli P., Tinuper P., Zucconi M., Gambetti P. L. and Medori R. (1986) [Familial insomnia with a malignant course: a new thalamic disease]. *Rev. Neurol. (Paris)* **142,** 791-792.

Lysek D. A., Schorn C., Nivon L. G., Esteve-Moya V., Christen B., Calzolai L., von S. C., Fiorito F., Herrmann T., Guntert P. and Wuthrich K. (2005) Prion protein NMR structures of cats, dogs, pigs, and sheep. *Proc. Natl. Acad. Sci. U. S. A* **102,** 640-645.

Ma J. and Lindquist S. (2001) Wild-type PrP and a mutant associated with prion disease are subject to retrograde transport and proteasome degradation. *Proc. Natl. Acad. Sci. U. S. A* **98,** 14955-14960.

Ma J. and Lindquist S. (2002) Conversion of PrP to a self-perpetuating PrPSc-like conformation in the cytosol. *Science* **298,** 1785-1788.

Mabbott N. A. and MacPherson G. G. (2006) Prions and their lethal journey to the brain. *Nat. Rev. Microbiol.* **4,** 201-211.

Makarava N., Kovacs G. G., Bocharova O., Savtchenko R., Alexeeva I., Budka H., Rohwer R. G. and Baskakov I. V. (2010) Recombinant prion protein induces a new transmissible prion disease in wild-type animals. *Acta Neuropathol.*

Mallucci G., Dickinson A., Linehan J., Klohn P. C., Brandner S. and Collinge J. (2003) Depleting neuronal PrP in prion infection prevents disease and reverses spongiosis. *Science* **302,** 871-874.

Mallucci G. R., Ratte S., Asante E. A., Linehan J., Gowland I., Jefferys J. G. and Collinge J. (2002) Post-natal knockout of prion protein alters hippocampal CA1 properties, but does not result in neurodegeneration. *EMBO J.* **21,** 202-210.

Manson J., West J. D., Thomson V., McBride P., Kaufman M. H. and Hope J. (1992) The prion protein gene: a role in mouse embryogenesis? *Development* **115,** 117-122.

Maple L., Lathrop R., Bozich S., Harman W., Tacey R., Kelley M. and nilkovitch-Miagkova A. (2004) Development and validation of ELISA for herceptin detection in human serum. *J. Immunol. Methods* **295,** 169-182.

Masters C. L., Gajdusek D. C. and Gibbs C. J., Jr. (1981) Creutzfeldt-Jakob disease virus isolations from the Gerstmann-Straussler syndrome with an analysis of the various forms of amyloid plaque deposition in the virus-induced spongiform encephalopathies. *Brain* **104,** 559-588.

Mastrianni J. A., Nixon R., Layzer R., Telling G. C., Han D., DeArmond S. J. and Prusiner S. B. (1999) Prion protein conformation in a patient with sporadic fatal insomnia. *N. Engl. J. Med.* **340,** 1630-1638.

McCutcheon S., Hunter N. and Houston F. (2005) Use of a new immunoassay to measure PrP Sc levels in scrapie-infected sheep brains reveals PrP genotype-specific differences. *J. Immunol. Methods* **298,** 119-128.

McKinley M. P., Bolton D. C. and Prusiner S. B. (1983) A protease-resistant protein is a structural component of the scrapie prion. *Cell* **35,** 57-62.

McKinley M. P., Meyer R. K., Kenaga L., Rahbar F., Cotter R., Serban A. and Prusiner S. B. (1991) Scrapie prion rod formation in vitro requires both detergent extraction and limited proteolysis. *J. Virol.* **65,** 1340-1351.

McLean C. A., Cherny R. A., Fraser F. W., Fuller S. J., Smith M. J., Beyreuther K., Bush A. I. and Masters C. L. (1999) Soluble pool of Abeta amyloid as a determinant of severity of neurodegeneration in Alzheimer's disease. *Ann. Neurol.* **46,** 860-866.

McLean C. A., Storey E., Gardner R. J., Tannenberg A. E., Cervenakova L. and Brown P. (1997) The D178N (cis-129M) "fatal familial insomnia" mutation associated with diverse clinicopathologic phenotypes in an Australian kindred. *Neurology* **49,** 552-558.

Mead S. (2006) Prion disease genetics. *Eur. J. Hum. Genet.* **14,** 273-281.

Medori R., Tritschler H. J., LeBlanc A., Villare F., Manetto V., Chen H. Y., Xue R., Leal S., Montagna P., Cortelli P. and . (1992) Fatal familial insomnia, a prion disease with a mutation at codon 178 of the prion protein gene. *N. Engl. J. Med.* **326,** 444-449.

Meier P., Genoud N., Prinz M., Maissen M., Rulicke T., Zurbriggen A., Raeber A. J. and Aguzzi A. (2003) Soluble dimeric prion protein binds PrP(Sc) in vivo and antagonizes prion disease. *Cell* **113,** 49-60.

Meyer N., Rosenbaum V., Schmidt B., Gilles K., Mirenda C., Groth D., Prusiner S. B. and Riesner D. (1991) Search for a putative scrapie genome in purified prion fractions reveals a paucity of nucleic acids. *J. Gen. Virol.* **72 (Pt 1),** 37-49.

Meyer R. K., Lustig A., Oesch B., Fatzer R., Zurbriggen A. and Vandevelde M. (2000) A monomer-dimer equilibrium of a cellular prion protein (PrPC) not observed with recombinant PrP. *J. Biol. Chem.* **275,** 38081-38087.

Meyer R. K., McKinley M. P., Bowman K. A., Braunfeld M. B., Barry R. A. and Prusiner S. B. (1986) Separation and properties of cellular and scrapie prion proteins. *Proc. Natl. Acad. Sci. U. S. A* **83,** 2310-2314.

Monari L., Chen S. G., Brown P., Parchi P., Petersen R. B., Mikol J., Gray F., Cortelli P., Montagna P., Ghetti B. and . (1994) Fatal familial insomnia and familial Creutzfeldt-Jakob disease: different prion proteins determined by a DNA polymorphism. *Proc. Natl. Acad. Sci. U. S. A* **91,** 2839-2842.

Moore R. C., Hope J., McBride P. A., McConnell I., Selfridge J., Melton D. W. and Manson J. C. (1998) Mice with gene targetted prion protein alterations show that Prnp, Sinc and Prni are congruent. *Nat. Genet.* **18,** 118-125.

Moroncini G., Kanu N., Solforosi L., Abalos G., Telling G. C., Head M., Ironside J., Brockes J. P., Burton D. R. and Williamson R. A. (2004) Motif-grafted antibodies containing the replicative interface of cellular PrP are specific for PrPSc. *Proc. Natl. Acad. Sci. U. S. A* **101,** 10404-10409.

Moser M., Colello R. J., Pott U. and Oesch B. (1995) Developmental expression of the prion protein gene in glial cells. *Neuron* **14,** 509-517.

Nicholson E. M., Brunelle B. W., Richt J. A., Kehrli M. E., Jr. and Greenlee J. J. (2008) Identification of a heritable polymorphism in bovine PRNP associated with genetic transmissible spongiform encephalopathy: evidence of heritable BSE. *PLoS. ONE.* **3,** e2912.

Nishida N., Tremblay P., Sugimoto T., Shigematsu K., Shirabe S., Petromilli C., Erpel S. P., Nakaoke R., Atarashi R., Houtani T., Torchia M., Sakaguchi S., DeArmond S. J., Prusiner S. B. and Katamine S. (1999) A mouse prion protein transgene rescues mice deficient for the prion protein gene from purkinje cell degeneration and demyelination. *Lab Invest* **79,** 689-697.

Nonno R., Di Bari M. A., Cardone F., Vaccari G., Fazzi P., Dell'Omo G., Cartoni C., Ingrosso L., Boyle A., Galeno R., Sbriccoli M., Lipp H. P., Bruce M., Pocchiari M. and Agrimi U. (2006) Efficient transmission and characterization of Creutzfeldt-Jakob disease strains in bank voles. *PLoS. Pathog.* **2,** e12.

Notari S., Capellari S., Langeveld J., Giese A., Strammiello R., Gambetti P., Kretzschmar H. A. and Parchi P. (2007) A refined method for molecular typing reveals that co-occurrence of PrP(Sc) types in Creutzfeldt-Jakob disease is not the rule. *Lab Invest* **87,** 1103-1112.

Notari S., Strammiello R., Capellari S., Giese A., Cescatti M., Grassi J., Ghetti B., Langeveld J. P., Zou W. Q., Gambetti P., Kretzschmar H. A. and Parchi P. (2008) Characterization of truncated forms of abnormal prion protein in Creutzfeldt-Jakob disease. *J. Biol. Chem.* **283,** 30557-30565.

Nurmi M. H., Bishop M., Strain L., Brett F., McGuigan C., Hutchison M., Farrell M., Tilvis R., Erkkila S., Simell O., Knight R. and Haltia M. (2003) The normal population distribution of PRNP codon 129 polymorphism. *Acta Neurol. Scand.* **108,** 374-378.

Oesch B., Westaway D., Walchli M., McKinley M. P., Kent S. B., Aebersold R., Barry R. A., Tempst P., Teplow D. B., Hood L. E. and . (1985) A cellular gene encodes scrapie PrP 27-30 protein. *Cell* **40,** 735-746.

Okamoto M., Furuoka H., Horiuchi M., Noguchi T., Hagiwara K., Muramatsu Y., Tomonaga K., Tsuji M., Ishihara C., Ikuta K. and Taniyama H. (2003) Experimental transmission of abnormal prion protein (PrPsc) in the small intestinal epithelial cells of neonatal mice. *Vet. Pathol.* **40,** 723-727.

Orru C. D., Wilham J. M., Hughson A. G., Raymond L. D., McNally K. L., Bossers A., Ligios C. and Caughey B. (2009) Human variant Creutzfeldt-Jakob disease and sheep scrapie PrP(res) detection using seeded conversion of recombinant prion protein. *Protein Eng Des Sel* **22,** 515-521.

Orsi A., Fioriti L., Chiesa R. and Sitia R. (2006) Conditions of endoplasmic reticulum stress favor the accumulation of cytosolic prion protein. *J. Biol. Chem.* **281,** 30431-30438.

Owen F., Poulter M., Lofthouse R., Collinge J., Crow T. J., Risby D., Baker H. F., Ridley R. M., Hsiao K. and Prusiner S. B. (1989) Insertion in prion protein gene in familial Creutzfeldt-Jakob disease. *Lancet* **1,** 51-52.

Palmer M. S., Dryden A. J., Hughes J. T. and Collinge J. (1991) Homozygous prion protein genotype predisposes to sporadic Creutzfeldt-Jakob disease. *Nature* **352,** 340-342.

Pan K. M., Baldwin M., Nguyen J., Gasset M., Serban A., Groth D., Mehlhorn I., Huang Z., Fletterick R. J., Cohen F. E. and . (1993) Conversion of alpha-helices into beta-sheets features in the formation of the scrapie prion proteins. *Proc. Natl. Acad. Sci. U. S. A* **90,** 10962-10966.

Pan T., Chang B., Wong P., Li C., Li R., Kang S. C., Robinson J. D., Thompsett A. R., Tein P., Yin S., Barnard G., McConnell I., Brown D. R., Wisniewski T. and Sy M. S. (2005a) An aggregation-specific enzyme-linked immunosorbent assay: detection of conformational differences between recombinant PrP protein dimers and PrP(Sc) aggregates. *J. Virol.* **79,** 12355-12364.

Pan T., Colucci M., Wong B. S., Li R., Liu T., Petersen R. B., Chen S., Gambetti P. and Sy M. S. (2001) Novel differences between two human prion strains revealed by two-dimensional gel electrophoresis. *J. Biol. Chem.* **276,** 37284-37288.

Pan T., Li R., Kang S. C., Pastore M., Wong B. S., Ironside J., Gambetti P. and Sy M. S. (2005b) Biochemical fingerprints of prion diseases: scrapie prion protein in human prion diseases that share prion genotype and type. *J. Neurochem.* **92,** 132-142.

Pan T., Li R., Kang S. C., Wong B. S., Wisniewski T. and Sy M. S. (2004) Epitope scanning reveals gain and loss of strain specific antibody binding epitopes associated with the conversion of normal cellular prion to scrapie prion. *J. Neurochem.* **90,** 1205-1217.

Pan T., Wong P., Chang B., Li C., Li R., Kang S. C., Wisniewski T. and Sy M. S. (2005c) Biochemical fingerprints of prion infection: accumulations of aberrant full-length and N-terminally truncated PrP species are common features in mouse prion disease. *J. Virol.* **79,** 934-943.

Paramithiotis E., Pinard M., Lawton T., LaBoissiere S., Leathers V. L., Zou W. Q., Estey L. A., Lamontagne J., Lehto M. T., Kondejewski L. H., Francoeur G. P., Papadopoulos M., Haghighat A., Spatz S. J., Head M., Will R., Ironside J., O'Rourke K., Tonelli Q., Ledebur H. C., Chakrabartty A. and Cashman N. R. (2003) A prion protein epitope selective for the pathologically misfolded conformation. *Nat. Med.* **9,** 893-899.

Parchi P., Capellari S., Chen S. G., Petersen R. B., Gambetti P., Kopp N., Brown P., Kitamoto T., Tateishi J., Giese A. and Kretzschmar H. (1997) Typing prion isoforms. *Nature* **386,** 232-234.

Parchi P., Capellari S., Chin S., Schwarz H. B., Schecter N. P., Butts J. D., Hudkins P., Burns D. K., Powers J. M. and Gambetti P. (1999a) A subtype of sporadic prion disease mimicking fatal familial insomnia. *Neurology* **52,** 1757-1763.

Parchi P., Capellari S. and Gambetti P. (2000a) Intracerebral distribution of the abnormal isoform of the prion protein in sporadic Creutzfeldt-Jakob disease and fatal insomnia. *Microsc. Res. Tech.* **50,** 16-25.

Parchi P., Castellani R., Capellari S., Ghetti B., Young K., Chen S. G., Farlow M., Dickson D. W., Sima A. A., Trojanowski J. Q., Petersen R. B. and Gambetti P. (1996) Molecular basis of phenotypic variability in sporadic Creutzfeldt-Jakob disease. *Ann. Neurol.* **39,** 767-778.

Parchi P., Castellani R., Cortelli P., Montagna P., Chen S. G., Petersen R. B., Manetto V., Vnencak-Jones C. L., McLean M. J., Sheller J. R. and . (1995) Regional distribution of protease-resistant prion protein in fatal familial insomnia. *Ann. Neurol.* **38,** 21-29.

Parchi P., Chen S. G., Brown P., Zou W., Capellari S., Budka H., Hainfellner J., Reyes P. F., Golden G. T., Hauw J. J., Gajdusek D. C. and Gambetti P. (1998) Different patterns of truncated prion protein fragments correlate with distinct phenotypes in P102L Gerstmann-Straussler-Scheinker disease. *Proc. Natl. Acad. Sci. U. S. A* **95,** 8322-8327.

Parchi P., Giese A., Capellari S., Brown P., Schulz-Schaeffer W., Windl O., Zerr I., Budka H., Kopp N., Piccardo P., Poser S., Rojiani A., Streichemberger N., Julien J., Vital C., Ghetti B., Gambetti P. and Kretzschmar H. (1999b) Classification of sporadic Creutzfeldt-Jakob disease based on molecular and phenotypic analysis of 300 subjects. *Ann. Neurol.* **46,** 224-233.

Parchi P., Notari S., Weber P., Schimmel H., Budka H., Ferrer I., Haik S., Hauw J. J., Head M. W., Ironside J. W., Limido L., Rodriguez A., Strobel T., Tagliavini F. and Kretzschmar H. A. (2009a) Inter-laboratory assessment of PrPSc typing in creutzfeldt-jakob disease: a Western blot study within the NeuroPrion Consortium. *Brain Pathol.* **19,** 384-391.

Parchi P., Strammiello R., Notari S., Giese A., Langeveld J. P., Ladogana A., Zerr I., Roncaroli F., Cras P., Ghetti B., Pocchiari M., Kretzschmar H. and Capellari S. (2009b) Incidence and spectrum of sporadic Creutzfeldt-Jakob disease variants with mixed phenotype and co-occurrence of PrP(Sc) types: an updated classification. *Acta Neuropathol.*

Parchi P., Zou W., Wang W., Brown P., Capellari S., Ghetti B., Kopp N., Schulz-Schaeffer W. J., Kretzschmar H. A., Head M. W., Ironside J. W., Gambetti P. and

Chen S. G. (2000b) Genetic influence on the structural variations of the abnormal prion protein. *Proc. Natl. Acad. Sci. U. S. A* **97,** 10168-10172.

Pastrana M. A., Sajnani G., Onisko B., Castilla J., Morales R., Soto C. and Requena J. R. (2006) Isolation and characterization of a proteinase K-sensitive PrPSc fraction. *Biochemistry* **45,** 15710-15717.

Pattison I. H. and Millson G. C. (1961) Scrapie produced experimentally in goats with special reference to the clinical syndrome. *J. Comp Pathol.* **71,** 101-109.

Peden A., McCardle L., Head M. W., Love S., Ward H. J., Cousens S. N., Keeling D. M., Millar C. M., Hill F. G. and Ironside J. W. (2010) Variant CJD infection in the spleen of a neurologically asymptomatic UK adult patient with haemophilia. *Haemophilia.*

Peden A. H., Head M. W., Ritchie D. L., Bell J. E. and Ironside J. W. (2004) Preclinical vCJD after blood transfusion in a PRNP codon 129 heterozygous patient. *Lancet* **364,** 527-529.

Peden A. H., Ritchie D. L., Head M. W. and Ironside J. W. (2006) Detection and localization of PrPSc in the skeletal muscle of patients with variant, iatrogenic, and sporadic forms of Creutzfeldt-Jakob disease. *Am. J. Pathol.* **168,** 927-935.

Peden A. H., Ritchie D. L., Uddin H. P., Dean A. F., Schiller K. A., Head M. W. and Ironside J. W. (2007) Abnormal prion protein in the pituitary in sporadic and variant Creutzfeldt-Jakob disease. *J. Gen. Virol.* **88,** 1068-1072.

Peretz D., Scott M. R., Groth D., Williamson R. A., Burton D. R., Cohen F. E. and Prusiner S. B. (2001) Strain-specified relative conformational stability of the scrapie prion protein. *Protein Sci.* **10,** 854-863.

Peretz D., Williamson R. A., Legname G., Matsunaga Y., Vergara J., Burton D. R., DeArmond S. J., Prusiner S. B. and Scott M. R. (2002) A change in the conformation of prions accompanies the emergence of a new prion strain. *Neuron* **34,** 921-932.

Peretz D., Williamson R. A., Matsunaga Y., Serban H., Pinilla C., Bastidas R. B., Rozenshteyn R., James T. L., Houghten R. A., Cohen F. E., Prusiner S. B. and Burton D. R. (1997) A conformational transition at the N terminus of the prion protein features in formation of the scrapie isoform. *J. Mol. Biol.* **273,** 614-622.

Pergami P., Jaffe H. and Safar J. (1996) Semipreparative chromatographic method to purify the normal cellular isoform of the prion protein in nondenatured form. *Anal. Biochem.* **236,** 63-73.

Piccardo P., Dlouhy S. R., Lievens P. M., Young K., Bird T. D., Nochlin D., Dickson D. W., Vinters H. V., Zimmerman T. R., Mackenzie I. R., Kish S. J., Ang L. C., De C. C., Pocchiari M., Brown P., Gibbs C. J., Jr., Gajdusek D. C., Bugiani O., Ironside J., Tagliavini F. and Ghetti B. (1998) Phenotypic variability of Gerstmann-Straussler-Scheinker disease is associated with prion protein heterogeneity. *J. Neuropathol. Exp. Neurol.* **57,** 979-988.

Piccardo P., Liepnieks J. J., William A., Dlouhy S. R., Farlow M. R., Young K., Nochlin D., Bird T. D., Nixon R. R., Ball M. J., DeCarli C., Bugiani O., Tagliavini F., Benson M. D. and Ghetti B. (2001) Prion proteins with different conformations accumulate in Gerstmann-Straussler-Scheinker disease caused by A117V and F198S mutations. *Am. J. Pathol.* **158,** 2201-2207.

Pirisinu L., Bari M. D., Fazzi P., Marcon S., D'Agostino C., Esposito E., Simon S., Frassanito P., Vaccari G., Agrimi U. and Nonno R. (2009) Biochemical characterization of animal and human strains in bank voles (Myodes glareolus), pp. 179 (Prion 2009 Abstract P.10.8).

Pocchiari M., Puopolo M., Croes E. A., Budka H., Gelpi E., Collins S., Lewis V., Sutcliffe T., Guilivi A., Delasnerie-Laupretre N., Brandel J. P., Alperovitch A., Zerr I., Poser S., Kretzschmar H. A., Ladogana A., Rietvald I., Mitrova E., Martinez-Martin P., Pedro-Cuesta J., Glatzel M., Aguzzi A., Cooper S., MacKenzie J., van Duijn C. M. and Will R. G. (2004) Predictors of survival in sporadic Creutzfeldt-Jakob disease and other human transmissible spongiform encephalopathies. *Brain* **127,** 2348-2359.

Polak M. P., Zmudzinski J. F., Jacobs J. G. and Langeveld J. P. (2008) Atypical status of bovine spongiform encephalopathy in Poland: a molecular typing study. *Arch. Virol.* **153,** 69-79.

Polymenidou M., Stoeck K., Glatzel M., Vey M., Bellon A. and Aguzzi A. (2005) Coexistence of multiple PrPSc types in individuals with Creutzfeldt-Jakob disease. *Lancet Neurol.* **4,** 805-814.

Pombo M., Berthold I., Gingrich E., Jaramillo M., Leef M., Sirota L., Hsu H. and Arciniega J. (2004) Validation of an anti-PA-ELISA for the potency testing of anthrax vaccine in mice. *Biologicals* **32,** 157-163.

Prusiner S. B. (1998) Prions. *Proc. Natl. Acad. Sci. U. S. A* **95,** 13363-13383.

Prusiner S. B. (1982) Novel proteinaceous infectious particles cause scrapie. *Science* **216,** 136-144.

Prusiner S. B., Garfin D. E., Cochran S. P., McKinley M. P., Groth D. F., Hadlow W. J., Race R. E. and Eklund C. M. (1980a) Experimental scrapie in the mouse: electrophoretic and sedimentation properties of the partially purified agent. *J. Neurochem.* **35,** 574-582.

Prusiner S. B., Groth D. F., Bildstein C., Masiarz F. R., McKinley M. P. and Cochran S. P. (1980b) Electrophoretic properties of the scrapie agent in agarose gels. *Proc. Natl. Acad. Sci. U. S. A* **77,** 2984-2988.

Prusiner S. B., Hadlow W. J., Garfin D. E., Cochran S. P., Baringer J. R., Race R. E. and Eklund C. M. (1978) Partial purification and evidence for multiple molecular forms of the scrapie agent. *Biochemistry* **17,** 4993-4999.

Prusiner S. B., McKinley M. P., Bowman K. A., Bolton D. C., Bendheim P. E., Groth D. F. and Glenner G. G. (1983) Scrapie prions aggregate to form amyloid-like birefringent rods. *Cell* **35,** 349-358.

Prusiner S. B., Scott M., Foster D., Pan K. M., Groth D., Mirenda C., Torchia M., Yang S. L., Serban D., Carlson G. A. and . (1990) Transgenetic studies implicate interactions between homologous PrP isoforms in scrapie prion replication. *Cell* **63,** 673-686.

Puoti G., Giaccone G., Rossi G., Canciani B., Bugiani O. and Tagliavini F. (1999) Sporadic Creutzfeldt-Jakob disease: co-occurrence of different types of PrP(Sc) in the same brain. *Neurology* **53,** 2173-2176.

Rambold A. S., Muller V., Ron U., Ben-Tal N., Winklhofer K. F. and Tatzelt J. (2008) Stress-protective signalling of prion protein is corrupted by scrapie prions. *EMBO J.* **27,** 1974-1984.

Rane N. S., Kang S. W., Chakrabarti O., Feigenbaum L. and Hegde R. S. (2008) Reduced translocation of nascent prion protein during ER stress contributes to neurodegeneration. *Dev. Cell* **15,** 359-370.

Rane N. S., Yonkovich J. L. and Hegde R. S. (2004) Protection from cytosolic prion protein toxicity by modulation of protein translocation. *EMBO J.* **23,** 4550-4559.

Raymond G. J., Bossers A., Raymond L. D., O'Rourke K. I., McHolland L. E., Bryant P. K., III, Miller M. W., Williams E. S., Smits M. and Caughey B. (2000) Evidence of a molecular barrier limiting susceptibility of humans, cattle and sheep to chronic wasting disease. *EMBO J.* **19,** 4425-4430.

Raymond G. J., Hope J., Kocisko D. A., Priola S. A., Raymond L. D., Bossers A., Ironside J., Will R. G., Chen S. G., Petersen R. B., Gambetti P., Rubenstein R., Smits M. A., Lansbury P. T., Jr. and Caughey B. (1997) Molecular assessment of the potential transmissibilities of BSE and scrapie to humans. *Nature* **388,** 285-288.

Riek R., Hornemann S., Wider G., Billeter M., Glockshuber R. and Wuthrich K. (1996) NMR structure of the mouse prion protein domain PrP(121-321). *Nature* **382,** 180-182.

Riek R., Hornemann S., Wider G., Glockshuber R. and Wuthrich K. (1997) NMR characterization of the full-length recombinant murine prion protein, mPrP(23-231). *FEBS Lett.* **413,** 282-288.

Riesner D. (2003) Biochemistry and structure of PrP(C) and PrP(Sc). *Br. Med. Bull.* **66,** 21-33.

Ritchie D. L., Boyle A., McConnell I., Head M. W., Ironside J. W. and Bruce M. E. (2009) Transmissions of variant Creutzfeldt-Jakob disease from brain and lymphoreticular tissue show uniform and conserved bovine spongiform encephalopathy-related phenotypic properties on primary and secondary passage in wild-type mice. *J. Gen. Virol.* **90,** 3075-3082.

Rogers M., Serban D., Gyuris T., Scott M., Torchia T. and Prusiner S. B. (1991) Epitope mapping of the Syrian hamster prion protein utilizing chimeric and mutant genes in a vaccinia virus expression system. *J. Immunol.* **147,** 3568-3574.

Saborio G. P., Permanne B. and Soto C. (2001) Sensitive detection of pathological prion protein by cyclic amplification of protein misfolding. *Nature* **411,** 810-813.

Safar J., Ceroni M., Gajdusek D. C. and Gibbs C. J., Jr. (1991) Differences in the membrane interaction of scrapie amyloid precursor proteins in normal and scrapie- or Creutzfeldt-Jakob disease-infected brains. *J. Infect. Dis.* **163,** 488-494.

Safar J., Roller P. P., Gajdusek D. C. and Gibbs C. J., Jr. (1993) Conformational transitions, dissociation, and unfolding of scrapie amyloid (prion) protein. *J. Biol. Chem.* **268,** 20276-20284.

Safar J., Wang W., Padgett M. P., Ceroni M., Piccardo P., Zopf D., Gajdusek D. C. and Gibbs C. J., Jr. (1990) Molecular mass, biochemical composition, and physicochemical behavior of the infectious form of the scrapie precursor protein monomer. *Proc. Natl. Acad. Sci. U. S. A* **87,** 6373-6377.

Safar J., Wille H., Itri V., Groth D., Serban H., Torchia M., Cohen F. E. and Prusiner S. B. (1998) Eight prion strains have PrP(Sc) molecules with different conformations. *Nat. Med.* **4,** 1157-1165.

Safar J. G., Geschwind M. D., Deering C., Didorenko S., Sattavat M., Sanchez H., Serban A., Vey M., Baron H., Giles K., Miller B. L., DeArmond S. J. and Prusiner S. B. (2005a) Diagnosis of human prion disease. *Proc. Natl. Acad. Sci. U. S. A* **102,** 3501-3506.

Safar J. G., Kellings K., Serban A., Groth D., Cleaver J. E., Prusiner S. B. and Riesner D. (2005b) Search for a prion-specific nucleic acid. *J. Virol.* **79,** 10796-10806.

Safar J. G., Scott M., Monaghan J., Deering C., Didorenko S., Vergara J., Ball H., Legname G., Leclerc E., Solforosi L., Serban H., Groth D., Burton D. R., Prusiner S. B. and Williamson R. A. (2002) Measuring prions causing bovine spongiform encephalopathy or chronic wasting disease by immunoassays and transgenic mice. *Nat. Biotechnol.* **20,** 1147-1150.

Safar J. G., Wille H., Geschwind M. D., Deering C., Latawiec D., Serban A., King D. J., Legname G., Weisgraber K. H., Mahley R. W., Miller B. L., DeArmond S. J. and Prusiner S. B. (2006) Human prions and plasma lipoproteins. *Proc. Natl. Acad. Sci. U. S. A* **103,** 11312-11317.

Sailer A., Bueler H., Fischer M., Aguzzi A. and Weissmann C. (1994) No propagation of prions in mice devoid of PrP. *Cell* **77,** 967-968.

Sasaki K., Minaki H. and Iwaki T. (2009) Development of oligomeric prion-protein aggregates in a mouse model of prion disease. *J. Pathol.* **219,** 123-130.

Schaller O., Fatzer R., Stack M., Clark J., Cooley W., Biffiger K., Egli S., Doherr M., Vandevelde M., Heim D., Oesch B. and Moser M. (1999) Validation of a western immunoblotting procedure for bovine PrP(Sc) detection and its use as a rapid surveillance method for the diagnosis of bovine spongiform encephalopathy (BSE). *Acta Neuropathol.* **98,** 437-443.

Schoch G., Seeger H., Bogousslavsky J., Tolnay M., Janzer R. C., Aguzzi A. and Glatzel M. (2006) Analysis of prion strains by PrPSc profiling in sporadic Creutzfeldt-Jakob disease. *PLoS. Med.* **3,** e14.

Schulz-Schaeffer W. J., Giese A., Windl O. and Kretzschmar H. A. (1996) Polymorphism at codon 129 of the prion protein gene determines cerebellar pathology in Creutzfeldt-Jakob disease. *Clin. Neuropathol.* **15,** 353-357.

Scott M. R., Will R., Ironside J., Nguyen H. O., Tremblay P., DeArmond S. J. and Prusiner S. B. (1999) Compelling transgenetic evidence for transmission of bovine spongiform encephalopathy prions to humans. *Proc. Natl. Acad. Sci. U. S. A* **96,** 15137-15142.

Servac V. C., Shi Y. Z., Bresjanac M., Popovic M., Pretnar H. K., Galvani V., Rupreht R., Cernilec M., Vranac T., Hafner I. and Jerala R. (2004) Monoclonal antibody against a peptide of human prion protein discriminates between Creutzfeldt-Jacob's disease-affected and normal brain tissue. *J. Biol. Chem.* **279,** 3694-3698.

Shibuya S., Higuchi J., Shin R. W., Tateishi J. and Kitamoto T. (1998) Codon 219 Lys allele of PRNP is not found in sporadic Creutzfeldt-Jakob disease. *Ann. Neurol.* **43,** 826-828.

Shindoh R., Kim C. L., Song C. H., Hasebe R. and Horiuchi M. (2009) The region approximately between amino acids 81 and 137 of proteinase K-resistant PrPSc is critical for the infectivity of the Chandler prion strain. *J. Virol.* **83,** 3852-3860.

Shirley B. A. (1995) Urea and guanidine hydrochloride denaturation curves. *Methods Mol. Biol.* **40,** 177-190.

Silveira J. R., Hughson A. G. and Caughey B. (2006) Fractionation of prion protein aggregates by asymmetrical flow field-flow fractionation. *Methods Enzymol.* **412,** 21-33.

Silveira J. R., Raymond G. J., Hughson A. G., Race R. E., Sim V. L., Hayes S. F. and Caughey B. (2005) The most infectious prion protein particles. *Nature* **437,** 257-261.

Simoneau S., Rezaei H., Sales N., Kaiser-Schulz G., Lefebvre-Roque M., Vidal C., Fournier J. G., Comte J., Wopfner F., Grosclaude J., Schatzl H. and Lasmezas C. I. (2007) In vitro and in vivo neurotoxicity of prion protein oligomers. *PLoS. Pathog.* **3,** e125.

Sklaviadis T., Dreyer R. and Manuelidis L. (1992) Analysis of Creutzfeldt-Jakob disease infectious fractions by gel permeation chromatography and sedimentation field flow fractionation. *Virus Res.* **26,** 241-254.

Solforosi L., Bellon A., Schaller M., Cruite J. T., Abalos G. C. and Williamson R. A. (2007) Toward molecular dissection of PrPC-PrPSc interactions. *J. Biol. Chem.* **282,** 7465-7471.

Solomon I. H., Schepker J. A. and Harris D. A. (2009) Prion Neurotoxicity: Insights from Prion Protein Mutants. *Curr. Issues Mol. Biol.* **12,** 51-62.

Soto C., Anderes L., Suardi S., Cardone F., Castilla J., Frossard M. J., Peano S., Saa P., Limido L., Carbonatto M., Ironside J., Torres J. M., Pocchiari M. and Tagliavini F. (2005) Pre-symptomatic detection of prions by cyclic amplification of protein misfolding. *FEBS Lett.* **579,** 638-642.

Soto C. and Castilla J. (2004) The controversial protein-only hypothesis of prion propagation. *Nat. Med.* **10 Suppl,** S63-S67.

Sparkes R. S., Simon M., Cohn V. H., Fournier R. E., Lem J., Klisak I., Heinzmann C., Blatt C., Lucero M., Mohandas T. and . (1986) Assignment of the human and mouse prion protein genes to homologous chromosomes. *Proc. Natl. Acad. Sci. U. S. A* **83,** 7358-7362.

Spudich S., Mastrianni J. A., Wrensch M., Gabizon R., Meiner Z., Kahana I., Rosenmann H., Kahana E. and Prusiner S. B. (1995) Complete penetrance of Creutzfeldt-Jakob disease in Libyan Jews carrying the E200K mutation in the prion protein gene. *Mol. Med.* **1,** 607-613.

Stack M. J., Chaplin M. J. and Clark J. (2002) Differentiation of prion protein glycoforms from naturally occurring sheep scrapie, sheep-passaged scrapie strains (CH1641 and SSBP1), bovine spongiform encephalopathy (BSE) cases and Romney and Cheviot breed sheep experimentally inoculated with BSE using two monoclonal antibodies. *Acta Neuropathol.* **104,** 279-286.

Stahl N., Baldwin M. A., Burlingame A. L. and Prusiner S. B. (1990) Identification of glycoinositol phospholipid linked and truncated forms of the scrapie prion protein. *Biochemistry* **29,** 8879-8884.

Stahl N., Baldwin M. A., Teplow D. B., Hood L., Gibson B. W., Burlingame A. L. and Prusiner S. B. (1993) Structural studies of the scrapie prion protein using mass spectrometry and amino acid sequencing. *Biochemistry* **32,** 1991-2002.

Stahl N., Borchelt D. R., Hsiao K. and Prusiner S. B. (1987) Scrapie prion protein contains a phosphatidylinositol glycolipid. *Cell* **51,** 229-240.

Stewart R. S., Drisaldi B. and Harris D. A. (2001) A transmembrane form of the prion protein contains an uncleaved signal peptide and is retained in the endoplasmic Reticulum. *Mol. Biol. Cell* **12,** 881-889.

Stewart R. S. and Harris D. A. (2003) Mutational analysis of topological determinants in prion protein (PrP) and measurement of transmembrane and cytosolic PrP during prion infection. *J. Biol. Chem.* **278,** 45960-45968.

Stewart R. S. and Harris D. A. (2005) A transmembrane form of the prion protein is localized in the Golgi apparatus of neurons. *J. Biol. Chem.* **280,** 15855-15864.

Stewart R. S., Piccardo P., Ghetti B. and Harris D. A. (2005) Neurodegenerative illness in transgenic mice expressing a transmembrane form of the prion protein. *J. Neurosci.* **25,** 3469-3477.

Tagliavini F., Lievens P. M., Tranchant C., Warter J. M., Mohr M., Giaccone G., Perini F., Rossi G., Salmona M., Piccardo P., Ghetti B., Beavis R. C., Bugiani O., Frangione B. and Prelli F. (2001) A 7-kDa prion protein (PrP) fragment, an integral component of the PrP region required for infectivity, is the major amyloid protein in Gerstmann-Straussler-Scheinker disease A117V. *J. Biol. Chem.* **276,** 6009-6015.

Tanford C. (1968) Protein denaturation. *Adv. Protein Chem.* **23,** 121-282.

Taraboulos A., Scott M., Semenov A., Avrahami D., Laszlo L. and Prusiner S. B. (1995) Cholesterol depletion and modification of COOH-terminal targeting sequence of the prion protein inhibit formation of the scrapie isoform. *J. Cell Biol.* **129,** 121-132.

Tateishi J., Brown P., Kitamoto T., Hoque Z. M., Roos R., Wollman R., Cervenakova L. and Gajdusek D. C. (1995) First experimental transmission of fatal familial insomnia. *Nature* **376,** 434-435.

Tateishi J., Kitamoto T., Doh-ura K., Sakaki Y., Steinmetz G., Tranchant C., Warter J. M. and Heldt N. (1990) Immunochemical, molecular genetic, and transmission studies on a case of Gerstmann-Straussler-Scheinker syndrome. *Neurology* **40,** 1578-1581.

Tateishi J., Kitamoto T., Hoque M. Z. and Furukawa H. (1996) Experimental transmission of Creutzfeldt-Jakob disease and related diseases to rodents. *Neurology* **46,** 532-537.

Telling G. C., Parchi P., DeArmond S. J., Cortelli P., Montagna P., Gabizon R., Mastrianni J., Lugaresi E., Gambetti P. and Prusiner S. B. (1996) Evidence for the conformation of the pathologic isoform of the prion protein enciphering and propagating prion diversity. *Science* **274,** 2079-2082.

Thackray A. M., Hopkins L. and Bujdoso R. (2007a) Proteinase K-sensitive disease-associated ovine prion protein revealed by conformation-dependent immunoassay. *Biochem. J.* **401,** 475-483.

Thackray A. M., Hopkins L., Klein M. A. and Bujdoso R. (2007b) Mouse-adapted ovine scrapie prion strains are characterized by different conformers of PrPSc. *J. Virol.* **81,** 12119-12127.

Tixador P., Herzog L., Reine F., Jaumain E., Chapuis J., Le D. A., Laude H. and Beringue V. (2010) The physical relationship between infectivity and prion protein aggregates is strain-dependent. *PLoS. Pathog.* **6,** e1000859.

Tobler I., Gaus S. E., Deboer T., Achermann P., Fischer M., Rulicke T., Moser M., Oesch B., McBride P. A. and Manson J. C. (1996) Altered circadian activity rhythms and sleep in mice devoid of prion protein. *Nature* **380,** 639-642.

Tremblay P., Ball H. L., Kaneko K., Groth D., Hegde R. S., Cohen F. E., DeArmond S. J., Prusiner S. B. and Safar J. G. (2004) Mutant PrPSc conformers induced by a synthetic peptide and several prion strains. *J. Virol.* **78,** 2088-2099.

Turk E., Teplow D. B., Hood L. E. and Prusiner S. B. (1988) Purification and properties of the cellular and scrapie hamster prion proteins. *Eur. J. Biochem.* **176,** 21-30.

Tzaban S., Friedlander G., Schonberger O., Horonchik L., Yedidia Y., Shaked G., Gabizon R. and Taraboulos A. (2002) Protease-sensitive scrapie prion protein in aggregates of heterogeneous sizes. *Biochemistry* **41,** 12868-12875.

Uro-Coste E., Cassard H., Simon S., Lugan S., Bilheude J. M., Perret-Liaudet A., Ironside J. W., Haik S., Basset-Leobon C., Lacroux C., Peoch' K., Streichenberger N., Langeveld J., Head M. W., Grassi J., Hauw J. J., Schelcher F., Delisle M. B. and Andreoletti O. (2008) Beyond PrP9res) type 1/type 2 dichotomy in Creutzfeldt-Jakob disease. *PLoS. Pathog.* **4,** e1000029.

Vey M., Pilkuhn S., Wille H., Nixon R., DeArmond S. J., Smart E. J., Anderson R. G., Taraboulos A. and Prusiner S. B. (1996) Subcellular colocalization of the cellular and scrapie prion proteins in caveolae-like membranous domains. *Proc. Natl. Acad. Sci. U. S. A* **93,** 14945-14949.

Viles J. H., Cohen F. E., Prusiner S. B., Goodin D. B., Wright P. E. and Dyson H. J. (1999) Copper binding to the prion protein: structural implications of four identical cooperative binding sites. *Proc. Natl. Acad. Sci. U. S. A* **96,** 2042-2047.

Voigtlander T., Kloppel S., Birner P., Jarius C., Flicker H., Verghese-Nikolakaki S., Sklaviadis T., Guentchev M. and Budka H. (2001) Marked increase of neuronal prion protein immunoreactivity in Alzheimer's disease and human prion diseases. *Acta Neuropathol.* **101,** 417-423.

Wadsworth J. D., Hill A. F., Beck J. A. and Collinge J. (2003) Molecular and clinical classification of human prion disease. *Br. Med. Bull.* **66,** 241-254.

Wadsworth J. D., Joiner S., Hill A. F., Campbell T. A., Desbruslais M., Luthert P. J. and Collinge J. (2001) Tissue distribution of protease resistant prion protein in variant Creutzfeldt-Jakob disease using a highly sensitive immunoblotting assay. *Lancet* **358,** 171-180.

Wadsworth J. D., Joiner S., Linehan J. M., Asante E. A., Brandner S. and Collinge J. (2008a) Review. The origin of the prion agent of kuru: molecular and biological strain typing. *Philos. Trans. R. Soc. Lond B Biol. Sci.* **363,** 3747-3753.

Wadsworth J. D., Joiner S., Linehan J. M., Cooper S., Powell C., Mallinson G., Buckell J., Gowland I., Asante E. A., Budka H., Brandner S. and Collinge J. (2006)

Phenotypic heterogeneity in inherited prion disease (P102L) is associated with differential propagation of protease-resistant wild-type and mutant prion protein. *Brain* **129,** 1557-1569.

Wadsworth J. D., Joiner S., Linehan J. M., Desbruslais M., Fox K., Cooper S., Cronier S., Asante E. A., Mead S., Brandner S., Hill A. F. and Collinge J. (2008b) Kuru prions and sporadic Creutzfeldt-Jakob disease prions have equivalent transmission properties in transgenic and wild-type mice. *Proc. Natl. Acad. Sci. U. S. A* **105,** 3885-3890.

Walsh D. M., Klyubin I., Fadeeva J. V., Cullen W. K., Anwyl R., Wolfe M. S., Rowan M. J. and Selkoe D. J. (2002) Naturally secreted oligomers of amyloid beta protein potently inhibit hippocampal long-term potentiation in vivo. *Nature* **416,** 535-539.

Wang F., Wang X., Yuan C. G. and Ma J. (2010) Generating a Prion with Bacterially Expressed Recombinant Prion Protein. *Science*.

Wang F., Yang F., Hu Y., Wang X., Wang X., Jin C. and Ma J. (2007) Lipid interaction converts prion protein to a PrPSc-like proteinase K-resistant conformation under physiological conditions. *Biochemistry* **46,** 7045-7053.

Ward H. J., Everington D., Cousens S. N., Smith-Bathgate B., Leitch M., Cooper S., Heath C., Knight R. S., Smith P. G. and Will R. G. (2006) Risk factors for variant Creutzfeldt-Jakob disease: a case-control study. *Ann. Neurol.* **59,** 111-120.

Watts J. C. and Westaway D. (2007) The prion protein family: diversity, rivalry, and dysfunction. *Biochim. Biophys. Acta* **1772,** 654-672.

Weissmann C. and Flechsig E. (2003) PrP knock-out and PrP transgenic mice in prion research. *Br. Med. Bull.* **66,** 43-60.

Westaway D., Goodman P. A., Mirenda C. A., McKinley M. P., Carlson G. A. and Prusiner S. B. (1987) Distinct prion proteins in short and long scrapie incubation period mice. *Cell* **51,** 651-662.

Westergard L., Christensen H. M. and Harris D. A. (2007) The cellular prion protein (PrP(C)): its physiological function and role in disease. *Biochim. Biophys. Acta* **1772,** 629-644.

Will R. G. (2003) Acquired prion disease: iatrogenic CJD, variant CJD, kuru. *Br. Med. Bull.* **66,** 255-265.

Will R. G., Ironside J. W., Zeidler M., Cousens S. N., Estibeiro K., Alperovitch A., Poser S., Pocchiari M., Hofman A. and Smith P. G. (1996) A new variant of Creutzfeldt-Jakob disease in the UK. *Lancet* **347,** 921-925.

Will R. G., Zeidler M., Stewart G. E., Macleod M. A., Ironside J. W., Cousens S. N., MacKenzie J., Estibeiro K., Green A. J. and Knight R. S. (2000) Diagnosis of new variant Creutzfeldt-Jakob disease. *Ann. Neurol.* **47,** 575-582.

Wille H., Michelitsch M. D., Guenebaut V., Supattapone S., Serban A., Cohen F. E., Agard D. A. and Prusiner S. B. (2002) Structural studies of the scrapie prion protein by electron crystallography. *Proc. Natl. Acad. Sci. U. S. A* **99,** 3563-3568.

Windl O., Dempster M., Estibeiro J. P., Lathe R., de Silva R., Esmonde T., Will R., Springbett A., Campbell T. A., Sidle K. C., Palmer M. S. and Collinge J. (1996) Genetic basis of Creutzfeldt-Jakob disease in the United Kingdom: a systematic analysis of predisposing mutations and allelic variation in the PRNP gene. *Hum. Genet.* **98,** 259-264.

Windl O., Giese A., Schulz-Schaeffer W., Zerr I., Skworc K., Arendt S., Oberdieck C., Bodemer M., Poser S. and Kretzschmar H. A. (1999) Molecular genetics of human prion diseases in Germany. *Hum. Genet.* **105,** 244-252.

Wopfner F., Weidenhofer G., Schneider R., von B. A., Gilch S., Schwarz T. F., Werner T. and Schatzl H. M. (1999) Analysis of 27 mammalian and 9 avian PrPs reveals high conservation of flexible regions of the prion protein. *J. Mol. Biol.* **289,** 1163-1178.

Wroe S. J., Pal S., Siddique D., Hyare H., Macfarlane R., Joiner S., Linehan J. M., Brandner S., Wadsworth J. D., Hewitt P. and Collinge J. (2006) Clinical presentation and pre-mortem diagnosis of variant Creutzfeldt-Jakob disease associated with blood transfusion: a case report. *Lancet* **368,** 2061-2067.

Xie Z., O'Rourke K. I., Dong Z., Jenny A. L., Langenberg J. A., Belay E. D., Schonberger L. B., Petersen R. B., Zou W., Kong Q., Gambetti P. and Chen S. G. (2006) Chronic wasting disease of elk and deer and Creutzfeldt-Jakob disease: comparative analysis of the scrapie prion protein. *J. Biol. Chem.* **281,** 4199-4206.

Xiong L. W., Raymond L. D., Hayes S. F., Raymond G. J. and Caughey B. (2001) Conformational change, aggregation and fibril formation induced by detergent treatments of cellular prion protein. *J. Neurochem.* **79,** 669-678.

Yedidia Y., Horonchik L., Tzaban S., Yanai A. and Taraboulos A. (2001) Proteasomes and ubiquitin are involved in the turnover of the wild-type prion protein. *EMBO J.* **20,** 5383-5391.

Yuan J., Dong Z., Guo J. P., McGeehan J., Xiao X., Wang J., Cali I., McGeer P. L., Cashman N. R., Bessen R., Surewicz W. K., Kneale G., Petersen R. B., Gambetti P. and Zou W. Q. (2008) Accessibility of a critical prion protein region involved in strain recognition and its implications for the early detection of prions. *Cell Mol. Life Sci.* **65,** 631-643.

Yuan J., Xiao X., McGeehan J., Dong Z., Cali I., Fujioka H., Kong Q., Kneale G., Gambetti P. and Zou W. Q. (2006) Insoluble aggregates and protease-resistant conformers of prion protein in uninfected human brains. *J. Biol. Chem.* **281,** 34848-34858.

Yull H. M., Ironside J. W. and Head M. W. (2009) Further characterisation of the prion protein molecular types detectable in the NIBSC Creutzfeldt-Jakob disease brain reference materials. *Biologicals* **37,** 210-215.

Yull H. M., Ritchie D. L., Langeveld J. P., van Zijderveld F. G., Bruce M. E., Ironside J. W. and Head M. W. (2006) Detection of type 1 prion protein in variant Creutzfeldt-Jakob disease. *Am. J. Pathol.* **168,** 151-157.

Zahn R., Liu A., Luhrs T., Riek R., von S. C., Lopez G. F., Billeter M., Calzolai L., Wider G. and Wuthrich K. (2000) NMR solution structure of the human prion protein. *Proc. Natl. Acad. Sci. U. S. A* **97,** 145-150.

Zanusso G., Righetti P. G., Ferrari S., Terrin L., Farinazzo A., Cardone F., Pocchiari M., Rizzuto N. and Monaco S. (2002) Two-dimensional mapping of three phenotype-associated isoforms of the prion protein in sporadic Creutzfeldt-Jakob disease. *Electrophoresis* **23,** 347-355.

Zarranz J. J., Digon A., Atares B., Rodriguez-Martinez A. B., Arce A., Carrera N., Fernandez-Manchola I., Fernandez-Martinez M., Fernandez-Maiztegui C., Forcadas I., Galdos L., Gomez-Esteban J. C., Ibanez A., Lezcano E., Lopez de M. A., Marti-Masso J. F., Mendibe M. M., Urtasun M., Uterga J. M., Saracibar N., Velasco F. and de Pancorbo M. M. (2005) Phenotypic variability in familial prion diseases due to the D178N mutation. *J. Neurol. Neurosurg. Psychiatry* **76,** 1491-1496.

Zeidler M., Sellar R. J., Collie D. A., Knight R., Stewart G., Macleod M. A., Ironside J. W., Cousens S., Colchester A. C., Hadley D. M. and Will R. G. (2000) The pulvinar sign on magnetic resonance imaging in variant Creutzfeldt-Jakob disease. *Lancet* **355,** 1412-1418.

Zeidler M., Stewart G. E., Barraclough C. R., Bateman D. E., Bates D., Burn D. J., Colchester A. C., Durward W., Fletcher N. A., Hawkins S. A., MacKenzie J. M. and Will R. G. (1997) New variant Creutzfeldt-Jakob disease: neurological features and diagnostic tests. *Lancet* **350,** 903-907.

Zerr I., Giese A., Windl O., Kropp S., Schulz-Schaeffer W., Riedemann C., Skworc K., Bodemer M., Kretzschmar H. A. and Poser S. (1998) Phenotypic variability in fatal familial insomnia (D178N-129M) genotype. *Neurology* **51,** 1398-1405.

Zou W. Q., Capellari S., Parchi P., Sy M. S., Gambetti P. and Chen S. G. (2003) Identification of novel proteinase K-resistant C-terminal fragments of PrP in Creutzfeldt-Jakob disease. *J. Biol. Chem.* **278,** 40429-40436.

Zou W. Q., Zheng J., Gray D. M., Gambetti P. and Chen S. G. (2004) Antibody to DNA detects scrapie but not normal prion protein. *Proc. Natl. Acad. Sci. U. S. A* **101,** 1380-1385.

Appendix 1. Neuropathology of CJD brains

In order to characterize more precisely the 15 CJD cases used for biochemical analysis in section 2.3.2, three brain regions (FC, Cb and Th) from each case were examined using histopathological and immunohistochemical techniques (Note: Microscopic examination of the CJD brains was carried out under the supervision of Prof. James Ironside. Some of the description of pathological change may paraphrase him or his diagnostic reports).

1.1 vCJD

Florid plaques, a characteristic pathological feature in vCJD brains (Ironside *et al.* 2000), were easily identifiable in frontal cortex and cerebellum in all three vCJD cases (Figure A1.1a). These florid plaques were composed of an eosinophilic dense core with radiating fibrils in the periphery and were surrounded by vacuoles (Ironside *et al.* 2000). In addition to florid plaques, spongiform degeneration was also present in all three regions.

Immunohistochemistry for abnormal PrP revealed strong staining of florid plaques in the cerebral and cerebellar cortex in addition to numerous pericellular deposits (Figures A1.1b and A1.1c). In the thalamus, a widespread reticular PrP immunoreactivity was present often in a liner and perineuronal pattern along with occasional plaques (Figure A1.1d).

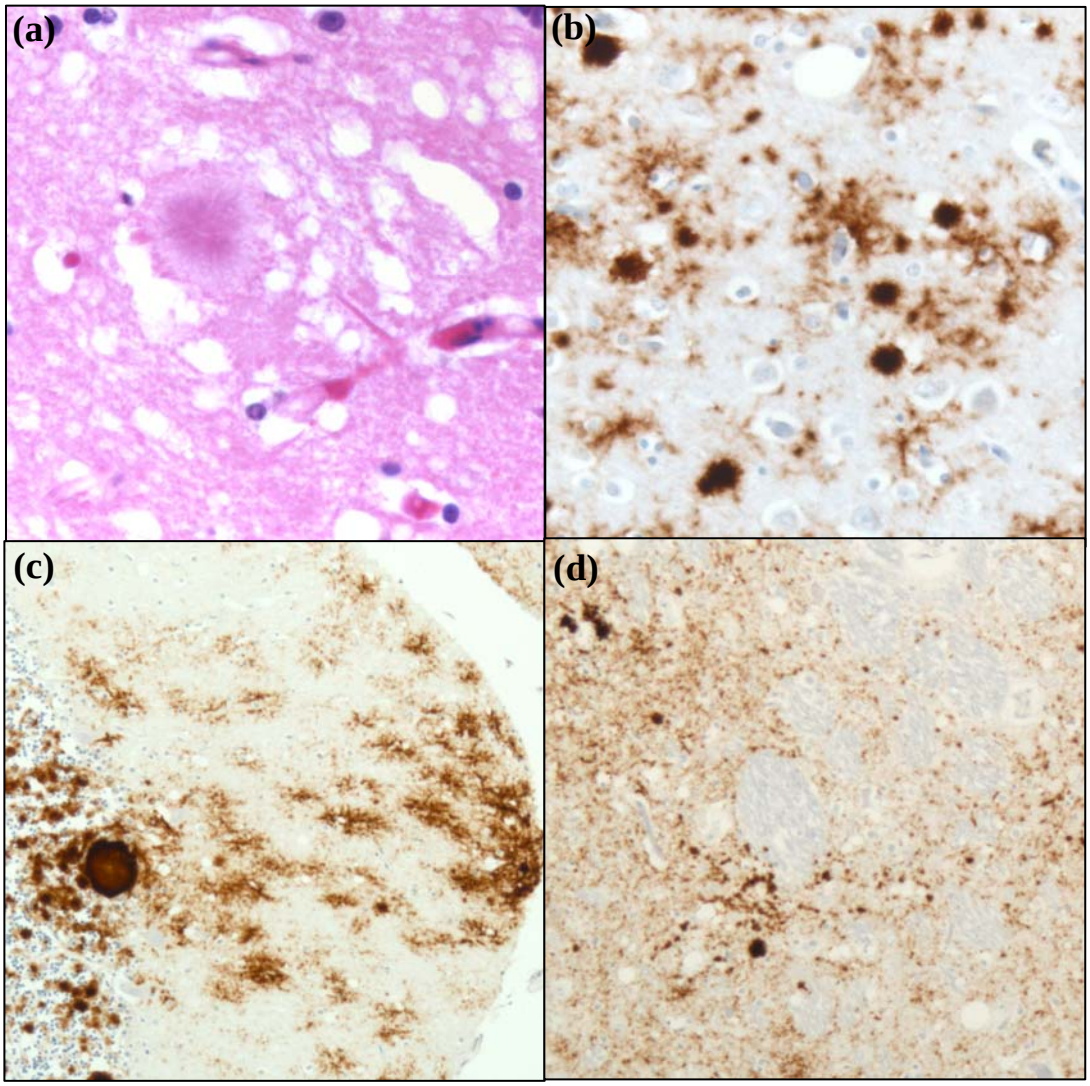

Figure A1.1 Neuropathology in vCJD. (a) Florid plaque in the frontal cortex from vCJD2 (hematoxylin and eosin). Original magnification: x400. (b) Immunohistochemistry for PrP in the frontal cortex from vCJD2 shows intense labelling of plaques and pericellular deposits. Original magnification: x200. (c) Immunohistochemistry for PrP in the cerebellar cortex from vCJD3 shows intense staining of florid plaques and smaller plaques in the granular layer and pericellular deposits in the molecular layer. Original magnification: x200. (d) Immunohistochemistry for PrP in the thalamus of vCJD1 shows a widespread reticular staining often in a liner and perineuronal distribution. Original magnification: x200. In all immunostained sections, PrP was labelled with the monoclonal antibody 3F4 with a hematoxylin counterstain.

1.2 MM1 sCJD

Previous studies reported that the spongiform change in MM1 subtype of sCJD was characterized by microvacuolation (Cali *et al.* 2009; Parchi *et al.* 1999b; Parchi *et al.* 2009a). Similar to these observations, the three MM1 subjects analysed in this study also showed microvacuolar spongiform degeneration (Figure A1.2a). However, in one of the three cases (MM1-2), confluent type of spongiform change was also focally identified in the thalamus. Whilst the frontal cortex in MM1-1 and MM1-3 showed a widespread severe spongiform change, the frontal cortex in the MM1-2 was largely spared. Both the cerebellum and thalamus in the three cases showed mild to moderate fine spongiform changes.

As reported previously (Parchi *et al.* 1999b; Parchi *et al.* 1996), the immunohistochemistry of the three MM1 sCJD cases was characterized by punctuate or synaptic pattern of PrP immunostaining (Figure A1.2c); in the granular layer of cerebellum, a rather coarser staining of PrP was present in a patchy pattern (Figure A1.2b). In the MM1-2 case which showed confluent type of vacuoles focally in the thalamus, a coarse/perivacuolar pattern of immunostaining was observed in the frontal cortex and thalamus (Figure A1.2d). In MM1-1, PrP deposits were demonstrated in the cerebellum and thalamus in which abnormal PrP was not reliably detectable by Western blot or CDI.

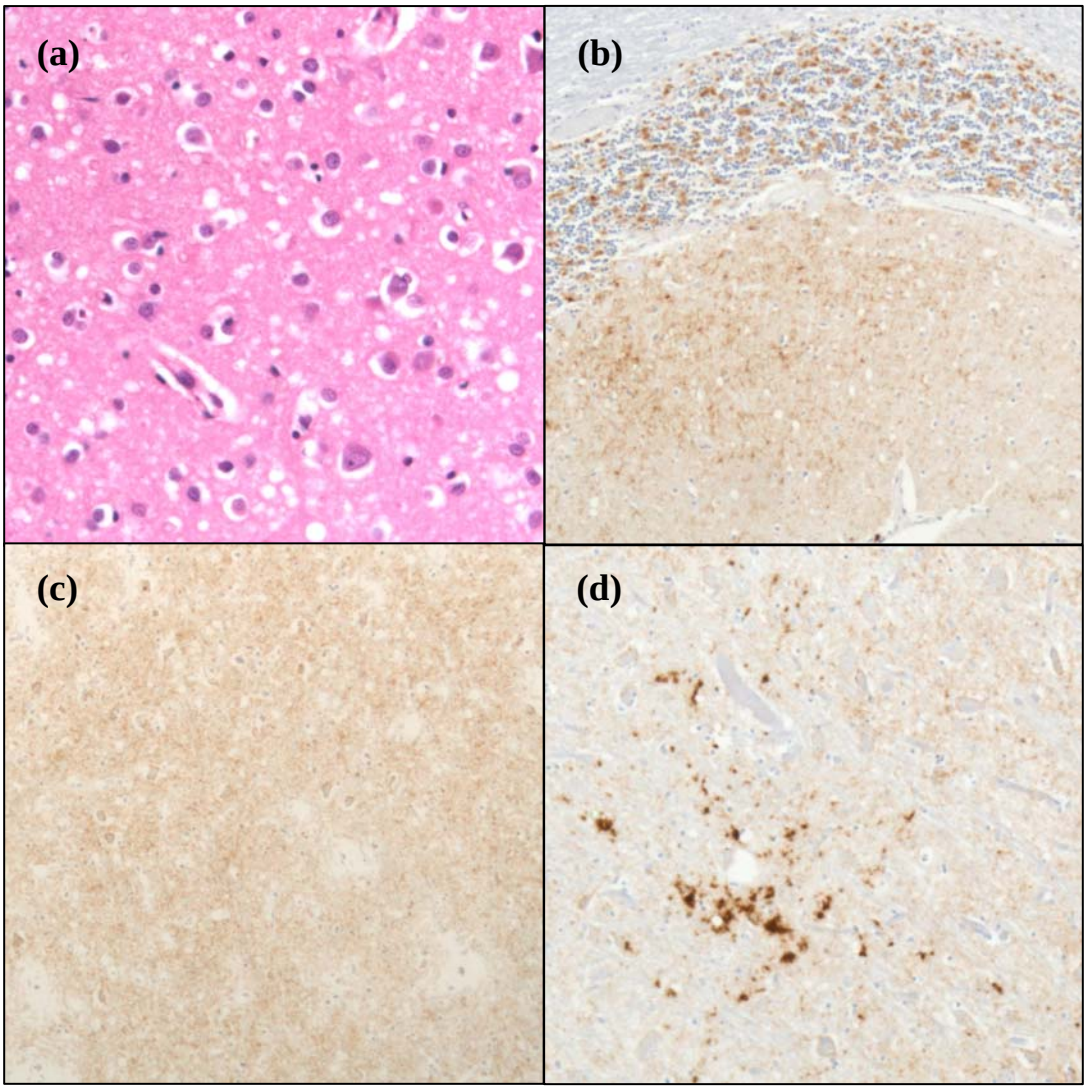

Figure A1.2 Neuropathology in MM1 sCJD. (a) Microvacuolar spongiform change in the frontal cortex from MM1-6 (hematoxylin and eosin). Original magnification: x200. (b) Synaptic staining for PrP in the molecular layer of the cerebellum (bottom) with coarser positivity in the granular layer of MM1-1. Original magnification: x100. (c) Widespread synaptic positivity in the thalamus from MM1-6. Original magnification: x100. (d) A coarse and perivacuolar pattern of PrP deposition in the thalamus from MM1-2. Original magnification: x100. In all immunostained sections, PrP was labelled with the mAb 3F4 with a hematoxylin counterstain.

1.3 MM2 sCJD

In MM2 subtype of sCJD, the spongiform change was characterized by confluent vacuoles in addition to fine spongiform degeneration (Cali *et al.* 2009; Parchi *et al.* 1999b; Parchi *et al.* 2009a). Although the three MM2 cases analysed in this study demonstrated confluent vacuolation, their pathological characteristics were more variable than those described in a previous study (Parchi *et al.* 1999b). In the case of MM2-1, mild confluent vacuolation was seen in the frontal cortex and thalamus. In the frontal cortex of MM2-2, there was marked cortical atrophy characterised by a severe loss of neurons and astrocytosis and there was also widespread spongiform change in this region which consisted of fine vacuoles with the occasional larger confluent vacuoles (Figure A1.3a). In the thalamus of MM2-2, there was mild vacuolation of predominantly microvacuolar type in addition to severe neuronal loss and gliosis. In MM2-3, the widespread spongiform degeneration in the frontal cortex was a mixture of both microvacuolation and the confluent larger vacuolation. The thalamus also demonstrated mild vacuolation. In all three cases, the cerebellum was mostly spared.

In all three cases examined in this study, positive PrP staining was seen only in the frontal cortex. In MM2-1, PrP deposits were focally present in a perivacuolar pattern against a synaptic background (Figure A1.3c). In MM2-2, there was a diffuse/synaptic pattern of staining with occasionally enhanced signals around vacuoles; intriguingly, PrP immunostaining emerged in a predominantly synaptic pattern even in an area showing dominantly larger/confluent vacuolation (Figure A1.3b). In MM2-3, the PrP immunostaining showed a widespread, predominantly synaptic pattern of positivity, but enhanced PrP staining around vacuoles was also easily recognizable (Figure A1.3d).

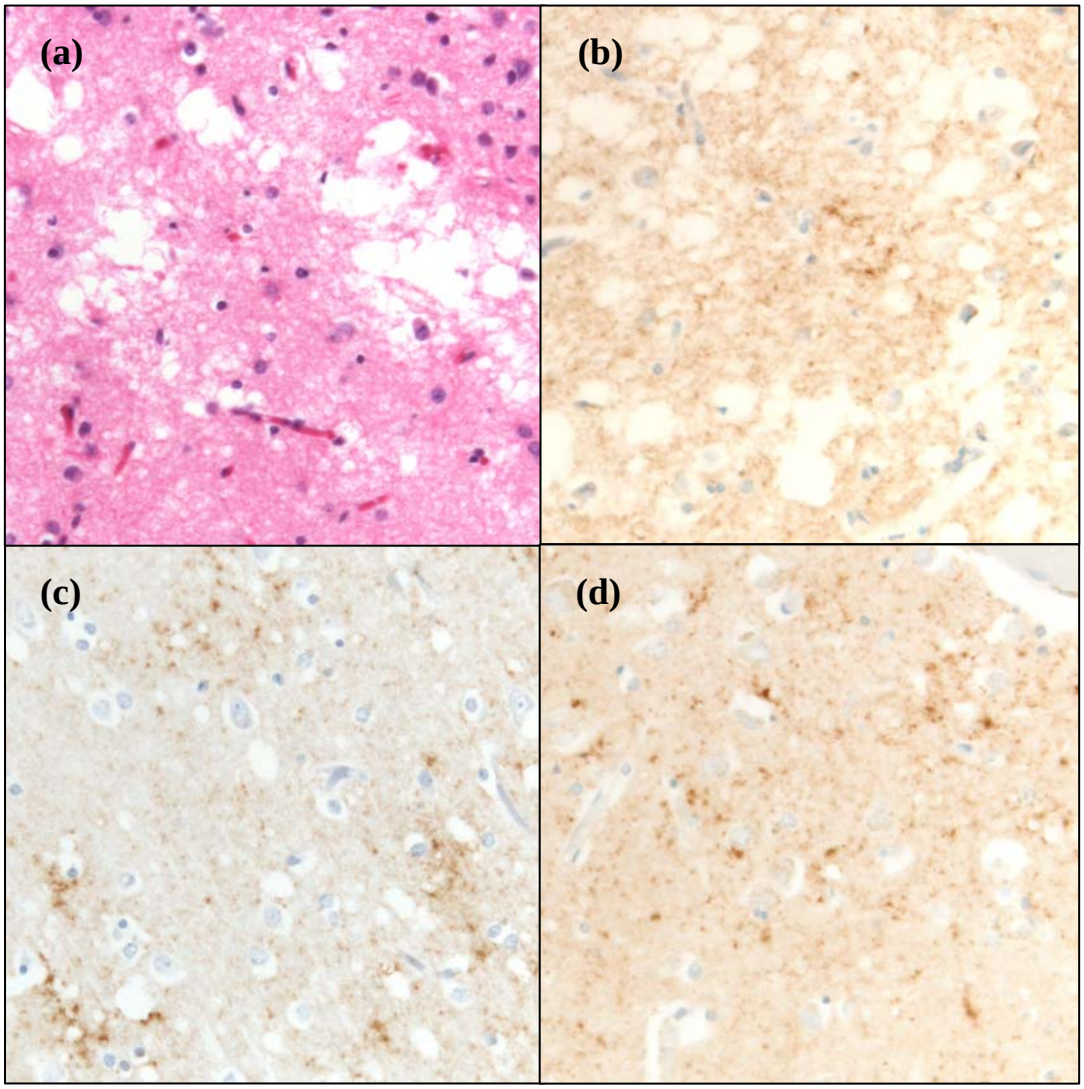

Figure A1.3 Neuropathology in MM2 sCJD. (a) Spongiform change composed of large confluent vacuoles in the frontal cortex from MM2-2 (hematoxylin and eosin). Original magnification: x200. (b) Synaptic pattern of PrP immunoreactivity in the frontal cortex from MM2-2. Original magnification: x200. (c) Focal perivacuolar staining surrounded by mild synaptic PrP immunoreactivity in the frontal cortex from MM2-1. Original magnification: x200. (d) Coarse and perivacuolar PrP immunoreactivity against widespread synaptic PrP staining in the frontal cortex from MM2-3. Original magnification: x200. The immunolabelling of PrP was performed using the mAbs KG9 (sections b and c) or 3F4 (section d). All immunostained sections were counterstained with hematoxylin.

1.4 MV1 sCJD

In the three MV1 patients, the histopathological changes in the three brain regions were overall similar to those seen in the MM1 patients. The spongiform change was characterized by microvacuoles (Figure A1.4a), but the larger, confluent type of vacuoles was also evident in the MV1-1 and MV1-2 cases (Figure A1.4b). Whilst the frontal cortex in MV1-1 and MV1-3 showed the appearance of widespread severe spongiform degeneration, the spongiform change in the frontal cortex of MV1-2 was relatively moderate. There was a variable degree of spongiform change in the thalamus and cerebellar cortex of the three MV1 patients.

In all three cases, immunohistochemical staining for abnormal PrP demonstrated a positive reaction with a predominantly synaptic pattern of staining; in the granular layer of the cerebellum, a rather coarse distribution of PrP staining was observed. Additionally, the perivacuolar accumulation of abnormal PrP was also evident around the regions of confluent spongiform change in the frontal cortex of both MV1-1 and MV1-2 (Figure A1.4c). Moreover, the thalamus of MV1-2 had focally plaque-like dense deposits against a widespread synaptic positivity (Figure A1.4d). In MV1-2, a mild degree of PrP deposition was detected in the cerebellum in which abnormal PrP was not identifiable by Western blot or CDI.

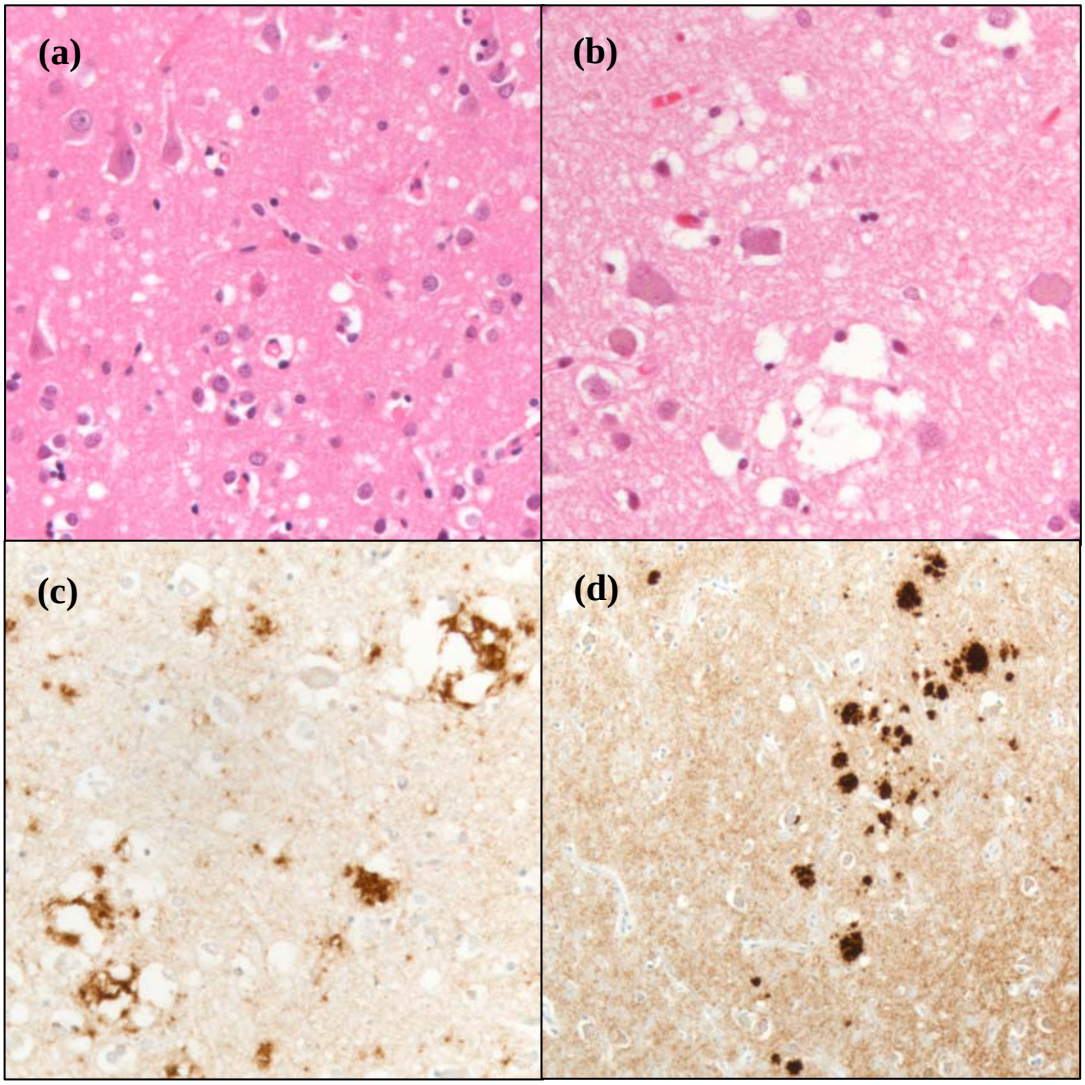

Figure A1.4 Neuropathology in MV1 sCJD. (a) Widespread microvacuolar spongiform degeneration in the frontal cortex from MV1-3 (hematoxylin and eosin). Original magnification: x200. (b) A focus showing large confluent vacuoles in the frontal cortex from MV1-1 (hematoxylin and eosin). Original magnification: x200. (c) Perivacuolar deposition of PrP around areas of confluent spongiform change in the frontal cortex from MV1-1. Original magnification: x200. (d) Plaque-like deposits against synaptic background in the thalamus from MV1-2. In all immunostained sections, PrP was labelled with the mAb 3F4 with a hematoxylin counterstain.

1.5 MV2 sCJD

On microscopic examination, the histopathological changes observed in MV2-1 and MV2-3 cases were noticeably distinguishable from that of MV2-2. In both MV2-1 and MV2-3 cases, the cerebellum showed kuru plaques predominantly present in the granular layer in addition to mild vacuolation in the molecular layer (Figure A1.5a). Widespread microvacuolar spongiform change was present in FC of MV2-1, whereas mild patchy spongiform change was identified in the FC of MV2-3. In both cases, severe spongiform degeneration was also evident in the thalamus. In MV2-2, the histopathological features were clearly different from the two other cases and appeared rather similar to typical MM2 cases. The widespread spongiform change in FC of MV2-2 was predominantly present in the form of "graph-like" confluent foci (Figure A1.6a) and severe confluent spongiform change was also observed in the thalamus. The cerebellum in this case was largely spared and no kuru plaques were detected.

An immunohistochemical staining pattern for abnormal PrP was similar between MV2-1 and MV2-3, and readily distinguishable from that of MV2-2. In the cerebellum of the two former cases, kuru plaques against coarse immunoreactivity were present predominantly in the granular layer in addition to mild synaptic staining in the molecular layer (Figure A1.5b). In the frontal cortex of these two cases, there was a synaptic pattern of PrP accumulation with occasional plaque-like dense deposits and perineuronal staining (Figure A1.5c). In comparison with MV2-1, the frontal cortex of MV2-3 in which abnormal PrP was not reliably detectable by CDI and WB was largely spared with mild positivity in limited microscopic areas. In the thalamus, plaque-like dense deposits were seen against synaptic and coarser granular patterns of PrP staining (Figure A1.5d).

In sharp contrast to these two cases, PrP immunostaining in MV2-2 showed strong positive reaction with a predominantly perivacuolar pattern of accumulation in the frontal cortex and thalamus (Figures A1.6b and A1.6d). The cerebellum of MV2-2

was largely spared showing no kuru plaques or plaque-like deposits; the focal deposition of PrP in the molecular layer was demonstrated in a coarse/perivacuolar pattern, the same as the two other regions (Figure A1.6c).

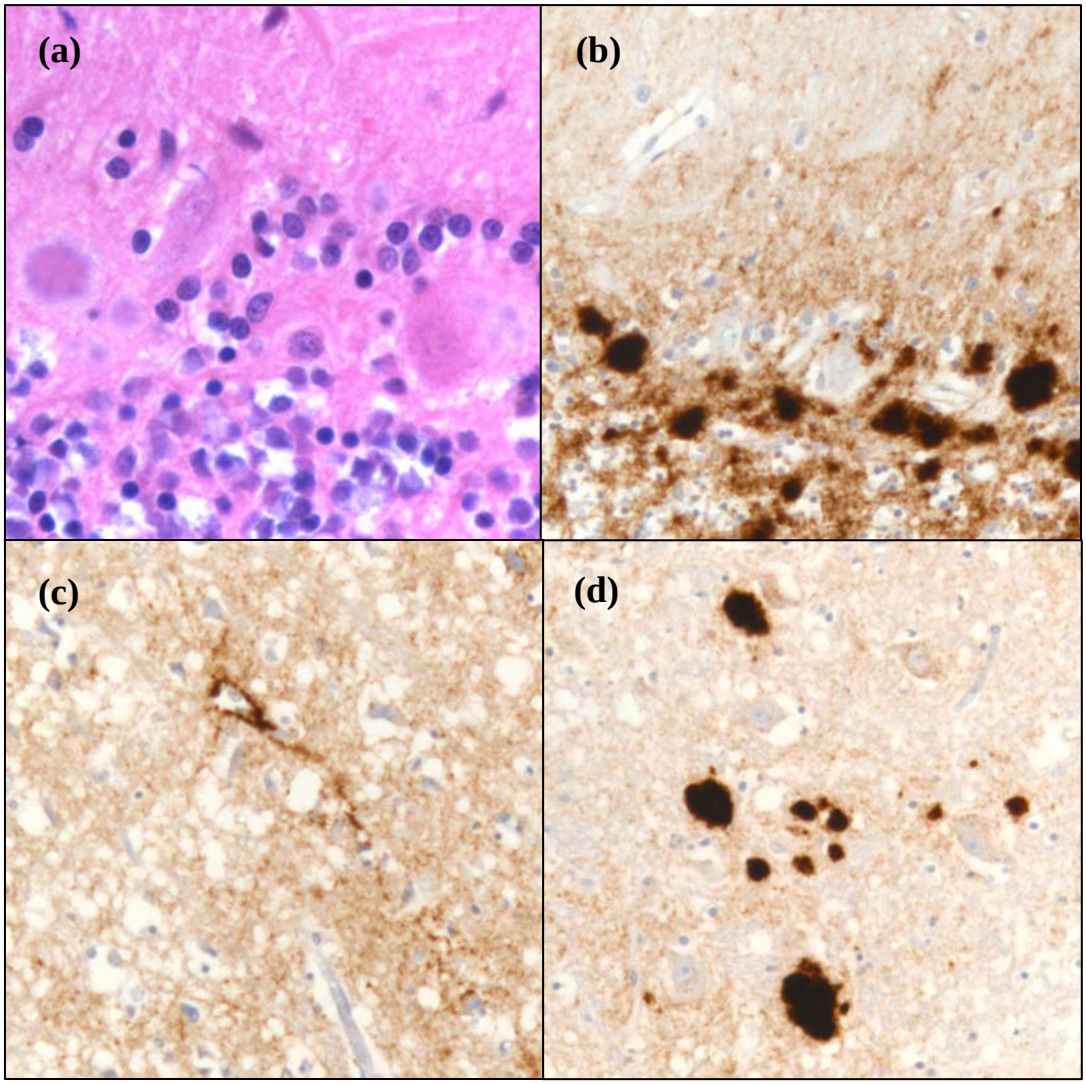

Figure A1.5 Neuropathology in MV2 sCJD. (a) Kuru plaques located in the granular layer of cerebellum from MV2-3 (hematoxylin and eosin). Original magnification: x400. (b) Intense staining of kuru plaques at the interface between the molecular layer and granular layer in the cerebellum from MV2-3. There is also synaptic immunoreactivity in the molecular layer. Original magnification: x200. (c) Widespread synaptic immunoreactivity along with the perineuronal staining in the frontal cortex from MV2-1. Original magnification: x200. (d) Plaque-like dense deposits against widespread mild synaptic immunostaining in the thalamus of MV2-1. Original magnification: x200. In all immunostained sections, PrP was labelled with the mAb 3F4 with a hematoxylin counterstain.

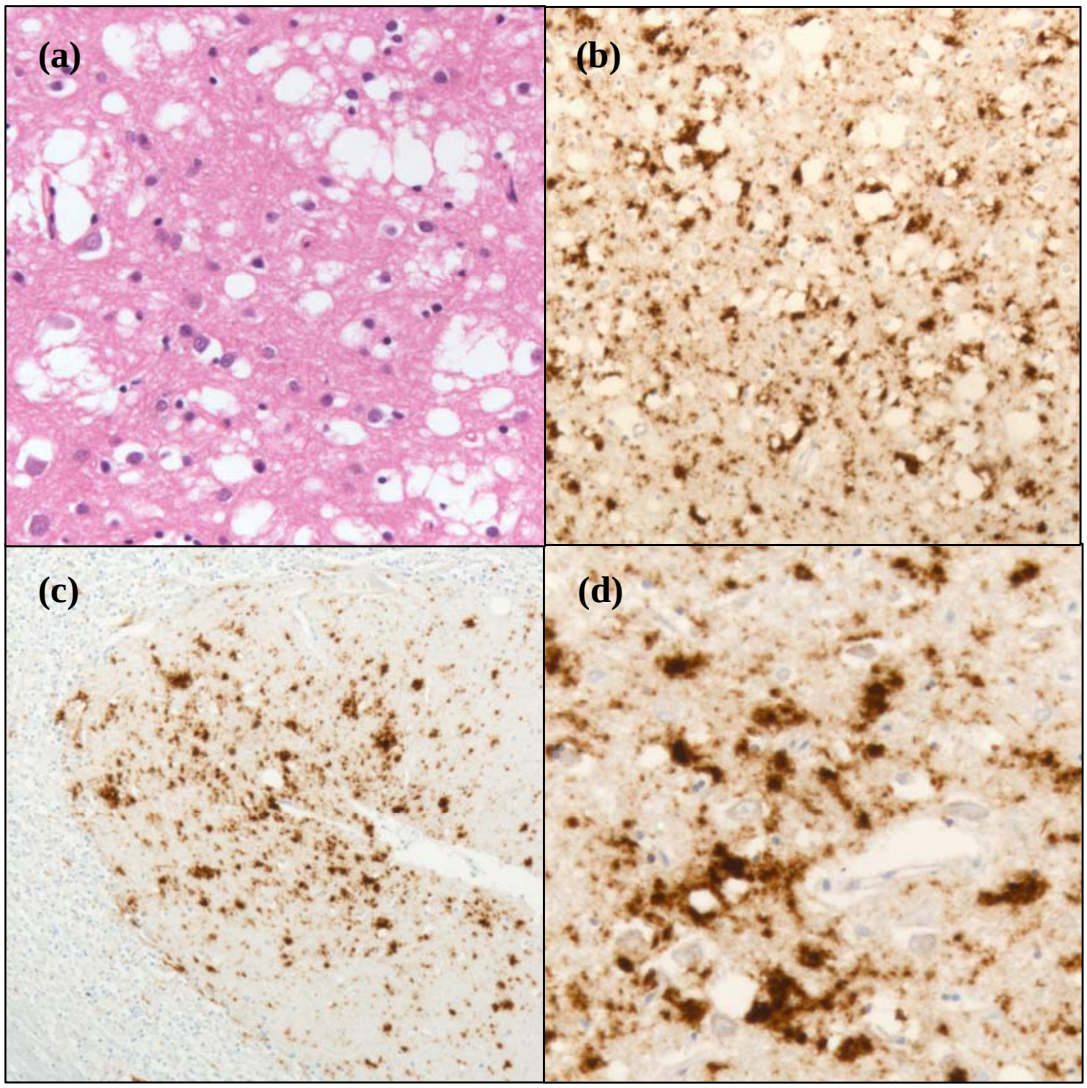

Figure A1.6 Neuropathology in a MV2 sCJD case with atypical pathological features. (a) Spongiform degeneration composed of large confluent vacuoles in the frontal cortex of MV2-2 (hematoxylin and eosin). Original magnification: x200. (b) Widespread intense perivacuolar PrP immunoreactivity in the frontal cortex from MV2-2. Original magnification: x100. (c) Coarse and perivacuolar immuostaining in the molecular layer of cerebellum from MV2-2. Original magnification: x100. (d) Intense perivacuolar deposition of PrP in the thalamus of MV2-2. Original magnification x200. In all immunostained sections, PrP was labelled with the mAb 3F4 with a hematoxylin counterstain.

1.6 Summary

In the three cases of vCJD, the neuropathological features were similar to those described previously (Ironside *et al.* 2000). The pathological features of MM1/MV1 cases were characterized by fine spongiform degeneration and synaptic PrP immunostaining, as described previously (Parchi *et al.* 1999b). Some of the MM1/MV1 cases showed focally confluent type of vacuoles along with perivacuolar PrP staining, in line with recent reports describing the mixed phenotypes in sCJD brains (Cali *et al.* 2009; Parchi *et al.* 2009b)(Table A1.1). The three MM2 sCJD cases also showed a mixture of both types of pathological features, but in the MM2-2 case, abnormal PrP was detected predominantly in a synaptic pattern even in a region dominated by larger/confluent vacuolation (Table A1.1).

Of the three MV2 cases, two cases (MV2-1 and MV2-3) showed typical neuropathology of MV2 subtype, which were characterized by the presence of kuru plaques in the cerebellum (Table A1.1). In contrast, the remaining case (MV2-2) did not show any kuru plaques or plaque-like PrP deposits in the cerebellum and this region was also largely spared from PrP immunostaining. The pathological change in the MV2-2 case was characterized by confluent vacuolation and perivacuolar PrP staining in the frontal cortex and thalamus; in this case, the cerebellum was largely spared except for focal distribution of coarse immunostaining in molecular layer. Collectively, the pathological changes observed in this MV2-2 case were somewhat similar to those of the MM2 subtype of sCJD described by Parchi et al (Parchi *et al.* 1999b). (Given the suspicion that this might indicate an error in genotyping, the genotype in this MV2-2 case was checked and confirmed by Genetics Laboratory in NSCJDU).

Table A1.1 Neuropathological features in different subtypes of sporadic CJD

sCJD subtype	ID	Neuropathological features		Remarks
		predominant	minor	
MM1	MM1-1	microvacuolation synaptic PrP staining	----------	
	MM1-2	microvacuolation synaptic PrP staining	confluent vacuoles perivacuolar PrP deposits	
	MM1-6	microvacuolation synaptic PrP staining	----------	
MM2	MM2-1	cluster of vacuoles mixture of synaptic and perivacuolar staining	----------	- Cb is mostly spared - Th shows mild vacuolation - No PrP staining in Cb and Th
	MM2-2	microvacuolation diffuse/synaptic PrP staining	confluent vacuoles perivacuolar staining	
	MM2-3	mixture of microvacuoles and confluent vacuoles; mixture of synaptic and perivacuolar staining	----------	
MV1	MV1-1	microvacuolation synaptic PrP staining	confluent vacuoles perivacuolar staining	
	MV1-2	microvacuolation synaptic PrP staining	confluent vacuoles perivacuolar staining	- plaque-like deposits in Th
	MV1-3	microvacuolation synaptic PrP staining	----------	
MV2	MV2-1	kuru plaques plaque-like PrP deposits synaptic PrP staining	----------	
	MV2-2	confluent vacuoles perivacuolar PrP deposits	----------	- No detectable kuru plaques - Cb is largely spared
	MV2-3	kuru plaques plaque-like PrP deposits synaptic PrP staining	----------	

Appendix 2. Papers submitted for publication

Status: Accepted subject to minor revision

Journal: Journal of Virology

Title: Distinct stability states of disease-associated prion protein (PrP^{Sc}) identified by conformation dependent immunoassay

Authors: Young Pyo Choi, Alexander H. Peden, Albrecht Gröner, James W. Ironside, and Mark W. Head

Abstract

The phenotypic and strain-related properties of human prion diseases are, according to the prion hypothesis, proposed to reside in the physico-chemical properties of the conformationally altered, disease-associated isoform of the prion protein (PrP^{Sc}), which accumulates in the brains of patients suffering from Creutzfeldt-Jakob disease and related conditions such as Gerstmann Straussler-Scheinker disease. Molecular strain typing of human prion diseases has focussed extensively on differences in the fragment size and glycosylation site occupancy of protease resistant prion protein (PrP^{res}) in conjunction with the presence of mutations and polymorphisms in the prion protein gene (*PRNP*). Here we report the results of employing an alternative strategy that specifically addresses the conformational stability of PrP^{Sc} and that has been used previously to characterise animal prion strains transmitted to rodents. The results show that there are at least two distinct conformation stability states in human prion diseases, neither of which appears to correlate fully with PrP^{res} type as judged by fragment size or glycosylation, the *PRNP* codon 129 status or the presence or absence of mutations in *PRNP*. These results suggest that conformational stability represents a further dimension to a complete description of potentially phenotype-related properties of PrP^{Sc} in human prion diseases.

Status: Accepted subject to minor revision

Journal: Brain Pathology

Title: Correlation of polydispersed prion protein and characteristic pathology in the thalamus in variant Creutzfeldt-Jakob disease: implication of small oligomeric species

Authors: Young Pyo Choi, Albrecht Gröner, James W. Ironside, and Mark W. Head

Abstract

The vacuolation, neuronal loss and gliosis that characterise human prion disease pathology are accompanied by the accumulation of an aggregated, insoluble and protease-resistant form (termed PrP^{Sc}) of a host-encoded protein (PrP^{C}). In variant Creutzfeldt-Jakob disease the frontal cortex and cerebellum exhibit intense vacuolation and the accumulation of PrP^{Sc} in the form of amyloid plaques and plaque-like structures. In contrast the posterior thalamus is characterised by intense gliosis and neuronal loss, but PrP^{Sc} plaques are rare and vacuolation is patchy. We have used sucrose density gradient centrifugation coupled with conformation dependent immunoassay to examine the biochemical properties of the PrP^{Sc} that accumulates in these different brain regions. The results show a greater degree of PrP^{Sc} polydisperal in thalamus compared to frontal cortex or cerebellum, including a subpopulation PrP^{Sc} molecules in the thalamus that have sedimentation properties resembling those of PrP^{C}. Much effort has focussed on identifying aspects of PrP^{Sc} biochemistry that distinguish between different forms of human prion disease and contribute to differential diagnosis. Here we show that PrP^{Sc} sedimentation properties, which can depend on aggregation state, correlate with, and may underlie the distinct neurodegenerative processes occurring in different regions of the variant Creutzfeldt-Jakob disease brain.